FACULTY OF SCIENCE
UNIVERSITY OF COPENHAGEN

δ^{13}C-CH_4 in ice core samples: Analyses, referencing and data interpretation approaches

Ph.D. thesis

Peter Sperlich

Supervisor:

Thomas Blunier
Centre for Ice and Climate, Niels Bohr Institute
University of Copenhagen

December 3, 2013

This thesis has been submitted to the PhD School of The Faculty of Science, University of Copenhagen

Abstract

Methane is an important greenhouse gas, knowledge of its isotopic composition constrains possible sink and source processes that caused the observed mixing ratio variability. Despite of the importance of methane research, only a small number of analytical systems existed that performed routine measurements when I started my PhD project. Because measurement standards for methane isotopes are not available, operating systems rely on individual rather than standardized access to the international isotope reference scales. Analytical and referencing artefacts impose problems when records of different laboratories are merged for interpretation. A methane carbon isotope record covering the last 160.000 years has recently been published (Möller et al., 2013) with the suggestion that the knowledge concerning methane source processes on glacial-interglacial time scales is too small to analyse such data using simplifying box models.

1) In my PhD study, I (together with Myriam Guillevic) built a system as tool to precisely reference the isotopic composition of methane to the international isotope scales in order to produce standard gases that the community is currently lacking. Large methane samples of ∼120 mL are combusted and afterwards, the produced carbon dioxide and water are cryogenically separated for isotopic analysis. We used methane gases which largely differ in their isotopic composition to mix a suite of synthetic standard gases in which methane is diluted to mixing ratios typical for ice core samples. The systhetic standards are accurately referenced to the international isotope scales and were intercallibrated with two collaborating laboratories. This work has been published by Sperlich et al. (2012). The calibration of these gases was meanwhile confirmed. Today, our pure methane gases represent the base of an international referencing effort that was initiated to provide such gases to other laboratories in future.

2) I (in collaboration with Christo Buizert) have built a complex setup to measure the methane carbon isotopic composition in ice core samples with high precision and accuracy. This setup allows routine measurements of methane carbon isotopes and produced the first dataset that is free from recently described artefacts based on Krypton interferences. After data of other laboratories are corrected for this effect, external data and our data are in excellent agreement. The setup comprises several features that contribute to the high measurement precision. These include an optimized melt-extraction unit, a chromatographical unit with high temperature and separation control, a combustion unit with permanent oxygen supply for constant oxidation conditions as well as a new gold catalyst for the oxidation of carbon monoxide at ambient temperatures (I use 60 °C). The system is furthermore configured to measure the isotopic composition of nitrous oxide in the same sample, making it the first system to measure the isotopic composition of both gases in an online mode using one mass spectrometer. This work has been published by Sperlich et al.

(2013).
3) The interpretation of the data represents the last step of my PhD thesis and is particularly challenged by the finding that the "traditional" analysis of methane carbon isotope data by box models is inaccurate (Möller et al., 2013). To test further analytical methods, I applied the Keeling Plot Analysis (KPA) to interpret methane isotope data from a very rapid DO-21 precursor event. The results suggest that the rapid methane concentration increase during the rapid warming event 85.000 years ago was caused by enhanced methane emissions from tropical wetlands, which seems plausible. A manuscript on this topic is drafted. Furthermore, I found a strong correlation between methane carbon isotope data I measured and reconstructions of global monsoon system strength on orbital time scales. This correlation also holds for the last 160.000 years as the analysis of the recently published record from Möller et al. (2013) shows. I investigate further geological records to analyse a possible climatic link between monsoon system strength, vegetation variability and the carbon isotopic composition of emitted methane. This represents the final chapter of my thesis and is intended to be submitted soon.

Resumé

Metan er en vigtig drivhusgas, kendskab om dens isotopsammensætning afgrænser mulige processer for kilder og dræn, der giver den observerede variabilitet i blandingsforholdet. På trods af betydningen af forskning i metan fandtes der ved begyndelsen af mit PhD-projekt kun et fåtal af analytiske systemer, der rutinemæssigt foretog målinger. Fordi målestandarder for metan-isotoper ikke er tilgængelige hviler operativsystemer på individuel, snarere end standardiseret, adgang til de internationale isotop-referenceskalaer. Analytiske eller referencemæssige fejl i målinger giver problemer når måleserier fra forskellige laboratorier fortolkes samlet. En metan-isotop måleserie, dækkende der sidste 160,000 år, er fornyeligt blevet udgivet (Möller et al., 2013) med udsagnet om at viden om metan kildeprocesser på istid-mellemistids tidsskalaer er for begrænset til at anvende simple box-modeller til at analyser sådanne data.

1) Under mit PhD-studier har jeg, sammen med Myriam Guillevic, bygget et system der præcist refererer den isotopiske sammensætning af metan til de internationale isotopskalaer for at fremstille standard gasarter som fællesskabet under tiden mangler. Store metan prøver af 120 mL forbrændes og efterfølgende separeres den herved producerede kuldioxid til isotopanalyse. Vi anvendte metan gasser som har store forskelle i deres isotopsammensætning for a blande en række af syntetiske standarder, hvori metan fortyndes til blandingsforhold der er typiske for iskerneprøver. De syntetiske standarder refererer præcist til de internationale isotopskalaer og er interkalibrerede i samarbejde med to andre laboratorier. Dette arbejder er udgivet af Sperlich et al. (2013). Kalibreringen af disse gasser er i mellemtiden blevet bekræftet. I dag repræsenterer vores rene metangasser basis for et international reference tiltag, der blev påbegyndt for at gøre sådanne gasser tilgængelige for fremtidigt laboratoriearbejde.

2) I samarbejde med Christo Buizert har jeg opbygget et komplekst system til at måle isotopsammensætningen af kulstof fra metan i iskerneprøver med høj præcision og nøjagtighed. Dette system tillader rutinemæssige målinger af isotopsammensætningen af kulstof fra metan ofg har produceret det første datasæt fri for de nyligt beskrevne målefejl baseret på krypton-interferens. Efter korrektion for denne effekt stemmer data fra andre laboratorier godt overens med vore data. Systemet indeholder en række funktioner der bidrager til høj målenøjagtighed. Dette omfatter en optimeret smelte udvindings-enhed, en kromatografisk enhed med høj temperatur -og separationskontrol, en forbrændingsenhed med permanent iltforsyning for konstante iltningsforhold, samt en ny guldkatalysator til iltning af kulilte ved omgivelsestemperaturen (jeg anvender 60°C). Systemet er viderer konfigureret til at måle isotopsammensætningen af kvælstofforilte (lattergas) i samme prøve, hvilket gør systemet til det første der online kan måle begge gasser med ét massespektrometer. Dette arbejder er udgivet af Sperlich et al. (2013).

3) Fortolkning af data er den sidste del af min PhD-afhandling. Dette er specielt udfordrende siden "traditionel" analyse af isotopsammensætningen af kulstof fra metan med box-modeller har vist sig at være unøjagtigt (Möller et al., 2013). For at afprøve andre analytiske metoder anvendte jeg Keeling Plot Analysis (KPA) til at fortolke metan-isotop data fra den meget abrupte begivenhed der er forstadie til DO-21. Resultaterne peger på at den hurtige forøgelse af metan koncentrationen under opvarmningen for 85,000 år siden var forårsaget af øget metanudleding fra tropiske vådområder, hvilket forekommer sandsynligt. Et udkast til et manuskript om dette emne er udarbejdet. Endvidere fandt jeg en stærk korrelation mellem den isotopsammensætning af kulstof fra metan jeg målte og rekonstruktioner af monsunintensitet på orbitale tidsskalaer. Som Möller et al. (2013) viser, gælder denne korrelation også for de sidste 160,000 år. Jeg undersøgte andre geologiske serier for at analysere en mulig klimatisk forbindelse mellem monsunintensitet, vegetations variabilitet og isotopsammensætningen af kulstof fra udledt metan. Dette udgør det sidste kapitel af min afhandling og er bestemt til snart at indsendes til udgivelse.

Preface

This thesis is structured in three main parts. The first part introduces the fields of ice core and analytical science that are relevant to this topic. In the second part, two publications present analytical methods for δ^{13}C-CH_4 referencing and δ^{13}C-CH_4 measurements in ice core samples, respectively. These two publications result from a small time fraction out of almost four years, when my learning and working in the gaslab was actually successful. I am grateful and happy that I could enjoy the freedom to experiment and to develop my own ideas in Thomas' gaslab group. And of course, for all the great people I met during my time at the Centre for Ice and Climate that were part of achieving this goal. At this place, I would like to especially thank the groups in Bern (Michael Bock, Jochen Schmitt), Utrecht (Thomas Röckmann, Célia Sapart, Guillaume Monteil at IMAU), Penn. State University (Todd Sowers), Wellington (Hinrich Schaefer, Gordon Brailsford, Katja Riedel, Keith Lassey at NIWA) and Jena (Willi Brand, Jürgen Richter und Michael Rothe, at MPI-BGC) for helpful discussions and support. The third and last part of this thesis is about the interpretation of δ^{13}C-CH_4 data and presents two new approaches as preliminary manuscripts. I intend to develop them further in order to submit them soon. At this point, I would like to thank Ed Brook, Martin Heimann and Anders Svensson for their generous willingness to join the evaluation committee and to read this thesis of which I hope it won't ruin the Christmas holidays.

Contents

List of Figures

List of Tables

List of abbreviations

IRMS	isotope ratio mass spectrometer
Gt	Giga tonnes, 1×10^9 tonnes
Tg	Terra gram, 1×10^{12} gram
Ga	Giga years, 1×10^9 years
Ma	Mega years, 1×10^6 years
ka	kilo years, 1×10^3 years
BP	before present, present defined as year 2000
GHG	greenhouse gas
CH_4	methane
pCH_4	atmospheric mixing ratio of methane
CO_2	carbon dioxide
pCO_2	atmospheric mixing ratio of carbon dioxide
CO	carbon monoxide
O_2	molecular oxygen
N_2	molecular nitrogen
H_2O	water
VOC	volatile organic carbon
NH	Northern Hemisphere
SH	Southern Hemisphere
SSA	singular spectrum analysis
KPA	Keeling plot analysis

Chapter 1

Introduction

Big bang and elements/isotopes on Earth

The "disintegration of this primeval atom" (Lemaitre, 1931) better known as "big-bang theory" provides a suitable point to begin this dissertational thesis with, as it explains the advent of time, space and matter. It is believed that the "big-bang" and the impact of consecutive supernova explosions gave birth to atoms and their stable isotopes in the universe and how they can be found on Earth since (e.g., Clayton, 2003; Broecker, 1988; Wayne, 2009). Isotopes are atoms of identical elements with identical numbers of electrons and protons but an element specific range of neutrons and hence atomic weight. While there are radioactive isotopes of some elements that are instable and decay according to their specific radioactive half-life, the absolute abundance of the so called stable isotopes is constant.

As an example, there are the two stable carbon isotopes ^{12}C and ^{13}C with 6 and 7 neutrons and an absolute abundance of 98.89 and 1.11 %, respectively. Furthermore, there is the instable, radioactive ^{14}C with a relative abundance of $\sim 1 \times 10^{-12}$. In short, most of ^{14}C is produced in the lower stratosphere by the impact of cosmic radiation while 50 % of it will be decayed after a half-life time of 5730 $\pm$ 40 years (Godwin, 1962). The abundance of the stable isotopes on Earth is shown in the periodic table of the isotopes, (Fig. 1.1). Despite their different numbers of neutrons, isotopes of the elements behave almost identical. However, it is the very small additional mass of one or several extra neutrons that creates a measurable fractionation effect that occurs when "heavy" and "light" isotopes of elements are cycled through environmental and biogeochemical systems. Isotope fractionation occurs, when α_i, which is defined as the ratio of the kinetic reaction rates (k) for the light (e.g. ^{12}C) and the heavy isotope (e.g. ^{13}C) in process (i)

$$\alpha_i = \frac{^{12}k_i}{^{13}k_i} \tag{1.1}$$

is different from one. The Kinetic Isotope Effect (KIE) then quantifies the isotope fractionation of a particular process

$$KIE = (\alpha_i - 1) \tag{1.2}$$

(Frey, 2006). The KIE is expressed in [‰] and is indicated as ε when referring to the isotope fractionation e.g. of atmospheric sink processes. This effect is better understood when looking at relative difference in atomic weights, where the difference between ^{1}H and ^{2}H or ^{12}C and ^{13}C accounts for $\sim$50 and $\sim$8 %, respectively. In general, heavier isotopes react slower in kinetic reactions, and they accumulate in exchange reactions where the bonds are strongest (Frey, 2006). These two fundamental laws of isotope chemistry are appreciated by a large scientific community studying biogeochemical cycles ranging from molecular processes to quantifications of element cycles on global and geological scales.

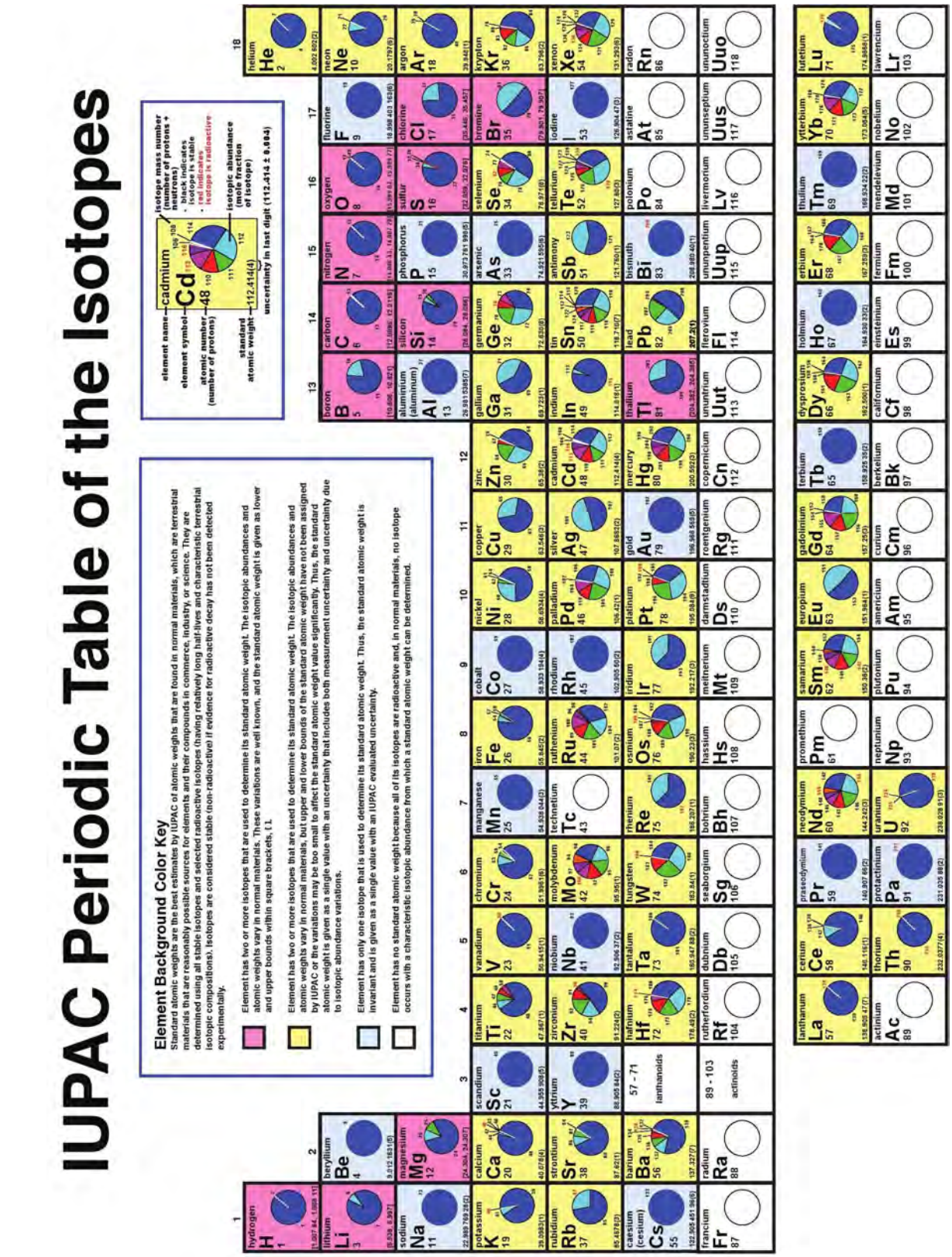

Figure 1.1: Periodic table of the isotopes.(IUPAC, 2013).

From early mass spectrometry to isotopic measurements of CH_4 in ice

The early days of isotope geochemistry have undoubtedly been extremely exciting times. By means of his custom made "mass spectrograph", Francis William Aston proved the existence of isotopes in neon (Aston, 1920) for which he was awarded the Nobel Prize for chemistry in 1922, (Nobelprize, 2013). Within 20 years, about 5 Nobel Prizes were granted to isotope researchers and soon the technical advancement allowed isotope geochemists to study small differences in samples that could be extrapolated to global scale phenomena.

In 1951, Epstein et al. (1951) establish an isotope thermometry and report the $\delta^{18}O$ of marine carbonates as function of ocean water temperature and salinity. Also in 1951, Urey et al. (1951) reported $\delta^{18}O$ in marine carbonate deposits and inferred palaeo-temperatures from the Cretaceous period. In 1959, Rosenfeld and Silverman (1959) presented their work on carbon isotope fractionation during microbial CH_4 formation. A few years later, Dansgaard (1964) published his study on the variability of water isotopes during condensation-evaporation processes in the atmosphere and its spatio-temporal significance. Based on these results, the analysis of polar ice core samples revolutionized the understanding of Earth's glacial-interglacial cycles and allowed for the quantification of glacial-interglacial temperature variability on the ice sheets (e.g., Johnsen et al., 1972; Jouzel et al., 2007).

The advancing isotope ratio mass spectrometry (IRMS) techniques (e.g., Brand, 2004) offered a powerful tool to a growing number of environmental research laboratories. The first $\delta^{13}C$-CH_4 measurements in ice core samples were reported in 1988, (Craig et al., 1988). However, it took almost another 20 years until measurement systems for routine ice core sample measurements were published (e.g., Ferretti et al., 2005; Sowers et al., 2005; Schaefer and Whiticar, 2007; Behrens et al., 2008; Bock et al., 2010a; Melton et al., 2011b; Sapart et al., 2011; Sperlich et al., 2013). While the analytical system of Craig et al. (1988) required 25 kg of ice, which is equivalent to full ice core size over 4 m length, the new techniques use between 200 - 700 g of ice and allow for a high temporal resolution measurements while being economical with ice consumption.

Outlook on technical development, new science

- "Clumped isotopes" investigate the abundance of two or more of the rare isotopes in one molecule as the deviation from the statistically expected value (Eiler, 2007). Since anomalies in the formation of clumped isotopes are chiefly temperature dependent, a temperature dependence model allows for example for the reconstruction paleo-temperatures from carbonate rocks and proved the close correlation between $p\mathrm{CO}_2$ on Earth's temperature around 300 and 440 million years ago (e.g., Came et al., 2007). A newly developed mass spectrometer, the "MAT Finnigan 253 Ultra" (Eiler et al., 2013) can be expected to boost isotope geochemistry science for the upcoming years. This system has a maximum mass resolution of about 25000 and is in that respect orders of magnitudes better than almost all commercial isotope ratio mass spectrometers (IRMS). In other words, the "MAT 253 Ultra" distinct the molecular masses 25000 and 25001. Of course molecules with masses that high are not frequently measured but the power of this technology is evident when shifting the resolving power by some orders of magnitude e.g. to 25.000 and 25.001. As an example for its biogeochemical application, the MAT 253 Ultra was recently shown to be capable of measuring clumped isotopes in pure CH_4 where it distinguishes between $^{13}\mathrm{CH}_3\mathrm{D}^+$ and $^{13}\mathrm{CH}_5^+$ ions (Eiler et al., 2013), which in the understanding of common IRMS have both the molecular masses of 18. This technology can thus provide important information that was previously not possible to observe. From an atmospheric methane point of view, it could be applied to quantify the amount of atmospheric CH_4 that stems from biomass burning and hence to find answers to open questions that concern the calculation of the global atmospheric CH_4 budget.

- Analytical systems measuring gas and isotopologue specific absorption of (near-) infrared radiation can be classified as "optical methods" as compared to IRMS. There are several different methods which shall not be discussed here; the interested reader is referred to reviewing literature on the principle analytical technology (e.g., Curl et al., 2010; McManus et al., 2010; Paldus and Kachanov, 2005) and to application examples (e.g., Mohn et al., 2010; Steen-Larsen et al., 2013). The great potential of this technology is the short analytical time and the mobility of these instruments that allow taking them into the field to do real time measurements, enabling isotope measurements in a continuous monitoring fashion even in extreme environments (e.g., Steen-Larsen et al., 2013). With respect to isotope measurements of atmospheric CH_4 and CO_2, the precision of these instruments (δ^{13}C-CH_4 = 0.5 ‰, (Picarro, 2013b) and δ^{13}C-CO_2 < 0.1 ‰, (Picarro, 2013a)), δ^{13}C-CH_4 = 0.21 ‰ (Witinski et al., 2011) is currently not precise enough to replace IRMS based instrumentation (precision for δ^{13}C-CH_4 = 0.04 ‰, (Lowe et al., 1994) and δ^{13}C-CO_2 = 0.03 ‰ and δ^{18}O-CO_2 = 0.05 ‰, (Trolier et al., 1996)) within the atmospheric monitoring network.

CH_4 as GHG

The solar radiation that reaches the top of the daytime atmosphere is called solar constant and has an energy of 1370 Wm^2. By assuming Earth is a perfect sphere, the average incoming radiation per m^2 of Earth's surface equals 342 Wm^2, which is derived by dividing the solar constant by 4 (the ratio of a sphere's surface to a sphere's cross section). Figure 1.2 shows a schematic of Earth's radiative budget. About 30 % of the incoming radiation is reflected back into space, either by clouds, aerosols or gases in the atmosphere or by Earth's surface. About 20 % of the incoming radiation is absorbed within the Atmosphere, while approximately 50 % reaches Earth's surface.

As the Earth surface heats, it emits infrared radiation as function of surface temperature. GHG absorb this infrared radiation and scatter it in random direction, where the energy flux that is redirected to Earth's surface equals ∼90 % of the long wave radiation flux that was previously emitted. Heat energy is thus retained as a function of GHG mixing ratio (Fig. 1.2). After CO_2, CH_4 is the second most important long-lived GHG, accounting for 20 % of the radiative effect which caused by long-lived GHG's in the contemporary atmosphere (Kirschke et al., 2013).

With the onset of the industrialization, human activities caused GHG's to increase. In case of CH_4, this has more than doubled the pre-industrial atmospheric mixing ratios (e.g., Blunier et al., 1993; Etheridge et al., 1998; MacFarling Meure et al., 2006). The future change in GHG mixing ratios is a crucial factor in anticipated global warming scenarios and inferred consequences on sea-level, precipitation and temperature change (e.g., Trenberth et al., 2007; Bindoff et al., 2007). It is therefore of utmost importance to study GHG's and Earth's climate system in great detail in order to identify biogeochemical feedbacks and to be able to make informed estimations and decisions for the future.

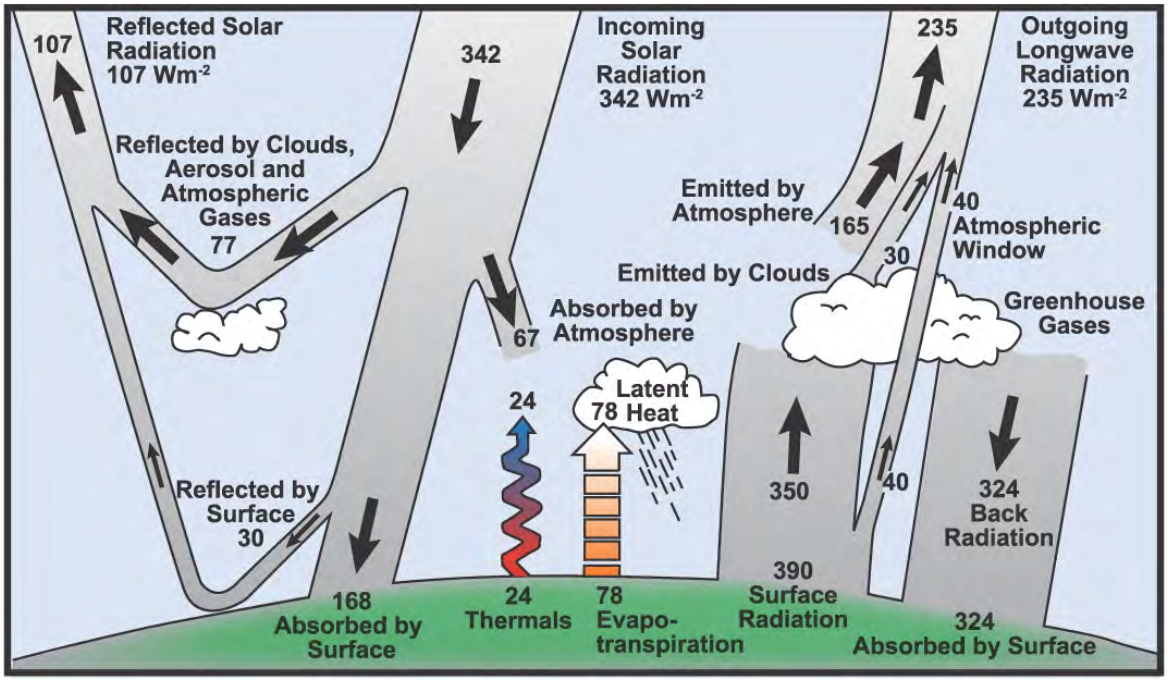

Figure 1.2: Shown is the radiative budget of the Earth. The incoming solar radiation is reflected and absorbed by atmospheric components and Earth's. Absorbed heat is emitted and can be back radiated or transported as latent heat within the atmosphere. The role of GHG is indicated by the branch of back radiation. The figure is taken from Le Treut et al. (2007).

Biogeochemical CH_4 formation

Five principle processes are associated with CH_4 formation: 1) Anaerobic digestion of organic matter by methanogenic microorganisms, 2) thermogenic reduction of organic matter to CH_4, 3) abiotic CH_4 formation from mantle carbon, 4) incomplete combustion of organic matter, 5) aerobic CH_4 formation in plants.

1) Microbial CH_4 is formed during the degradation of organic matter by methanogenic archaea (methanogens) in anaerobic conditions. Typical landscapes associated with microbial CH_4 formation are seasonally inundated wetlands, rice paddies, tundra, swamps, marshes, bogs, as well as marine and freshwater sediments (Breas et al., 2002). The formation of wetland CH_4 is dependent on both temperature and water saturation of soils. While water table changes exert the strongest control on CH_4 production in tropical wetlands, boreal CH_4 emissions are more sensitive to temperature (Bloom et al., 2010; Guo et al., 2012). The habitat of methanogenic archaea includes extreme environments, such as the acidic gastrointestinal tract of ruminants and termites as well as shallow and deeper ocean sediments up to several hundred meters below sea floor (Floodgate and Judd, 1992; Lipp et al., 2008). The substrate of methanogens is very limited. Hydrogenotrophic CH_4 is generated according to reaction 1.3

$$CO_2 + 4\,H_2 \longrightarrow CH_4 + 2\,H_2O \tag{1.3}$$

while aceticlastic methanogenesis is limited to acetate reduction following reaction 1.4

$$CH_3COO^- + H^+ \longrightarrow CH_4 + CO_2 \tag{1.4}$$

Hydrogenotrophic and aceticlastic methanogenesis often occur synchronously, however, their relative contribution to the total CH_4 production may vary depending on time (Angel et al., 2012) and nutrient supply (Holmes et al., 2013). Reaction 1.3 and 1.4 show that methanogens cannot decompose organic matter directly. Methanogenic CH_4 formation requires a complex microbial ecosystem involving other micro-organisms to break down organic matter into the limited range of molecules that methanogens can convert to CH_4 (Boone, 2000).

2) Thermogenic CH_4 is formed by degradation of sedimentary organic substrate in regimes of high temperatures and pressure. The typical environment for thermogenic CH_4 generation is fine-grained sediment, often at depths greater than 1000 m (below sea-floor). The degradation process from organic matter to thermogenic CH_4 takes place without any microbial activity and leads to more mature gases that are characterized by higher CH_4 concentrations with greater depths (Floodgate and Judd, 1992) and at temperatures exceeding 200 °C (Whiticar, 2000). Most of the CH_4 that is extracted as fossil energy source is thermogenically formed while microbial CH_4 accounts for ∼20 % within natural gases (Whiticar, 2000), which is reflected in their carbon and hydrogen isotope ratios (Floodgate and Judd, 1992). The estimated contribution of geological CH_4 to total CH_4 emissions ranges from 15 % (Denman et al., 2007) to 30 % (Etiope et al., 2008).

3) Abiotic CH_4 is formed in specific geological settings (Fig. 1.3) through distinct chemical reactions that don't require the presence of organic material (Abrajano et al., 1988; Schoell, 1988; Etiope and Lollar, 2013). Though, the carbon that is converted in this process can be a degradation product of organic matter such as graphite. In short, abiotic CH_4 4 is formed through the following pathways: Magmatic CH_4 forms in Earth's mantle from metal carbides, carbonate rocks or in specific CO_2-H_2O-rock systems at high pressure and temperatures (Abrajano et al., 1988; Etiope and Lollar, 2013). In temperatures as low as 200 °C, abiotic CH_4 is generated in aqueous solutions through gas-H_2O-rock reactions. Probably the most important pathways are "Fischer-Tropsch Type Reactions" (Etiope and Lollar, 2013). Here, abiotic CH_4 is created from CO_2, CO and H_2 in the presence of catalytic metals at temperatures below 200 °C (Etiope and Lollar, 2013). The consumed H_2 can be derived from serpentinization of mafic (magnesium and iron rich) rocks, where temperatures as low as 40 °C are reported for abiotic CH_4 formation (Etiope and Lollar, 2013).

4) Incomplete combustion of organic matter. Laboratory experiments were designed to study the emission spectra of biomass combustion under controlled conditions (Yokelson et al., 1997). Biomass burning is source to a variety of gases including CH_4. The ratio of CH_4 emissions was found largest during smoldering combustion, without visible flames (Yokelson et al., 1997). Natural wild fires comprise uncontrolled combustion over large areas where smoldering combustion and open flame combustion with higher temperatures take place simultaneously (van Leeuwen and van der Werf, 2011). The ratio of smoldering combustion compared to open flame combustion is an important measure for the emission

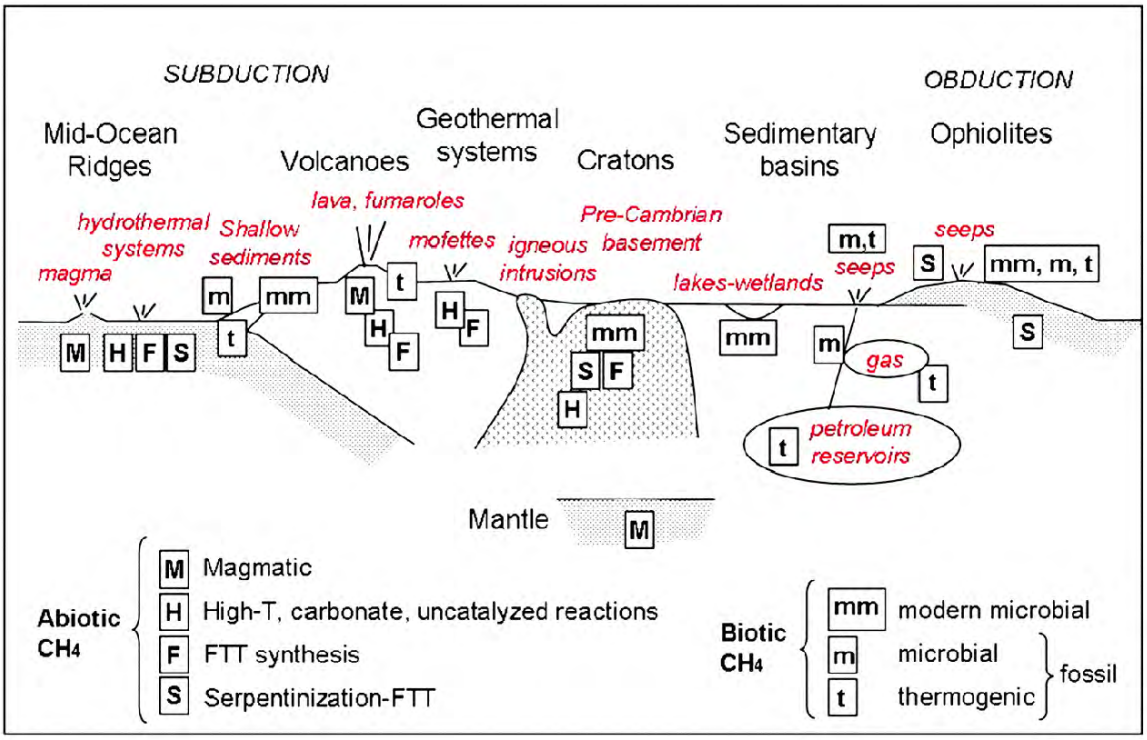

Figure 1.3: Schematic distribution of CH_4 formation processes with respect to the geological environment. Figure taken from Etiope and Lollar (2013), with courtesy of John Wiley and Sons, license number 3255991063670.

of CH_4 during biomass burning events. This ratio varies with the combusted vegetation types (Yokelson et al., 1997) and furthermore with plant H_2O content, temperature, wind and precipitation conditions as well as with the open space between trees (van Leeuwen and van der Werf, 2011). Commonly defined measures to quantify pyrogenic CH_4 emissions are CH_4 emission factors, which is the ratio of CH_4/CO_2 emissions. Ross et al. (2013) determined CH_4 emission factors based on satellite measurements and found the highest values for boreal forests (0.00603 mol/mol) followed by tropical forest (0.00527 mol/mol) and savanna fires (0.00395 mol/mol). Furthermore, van der Werf et al. (2010) reported CH_4 emission factors of 0.0088 and 0.0208 mol/mol for agricultural waste burning and peat fires, respectively. Per unit biomass, pyrogenic CH_4 (and CO) emissions are largest from fires associated with deforestation, forest- and peat degradation while savanna and grassland fires are most relevant to pyrogenic CO_2 emissions (van der Werf et al., 2010). Figure 1.4 shows the relative contribution of different geographical source areas to the total emissions.

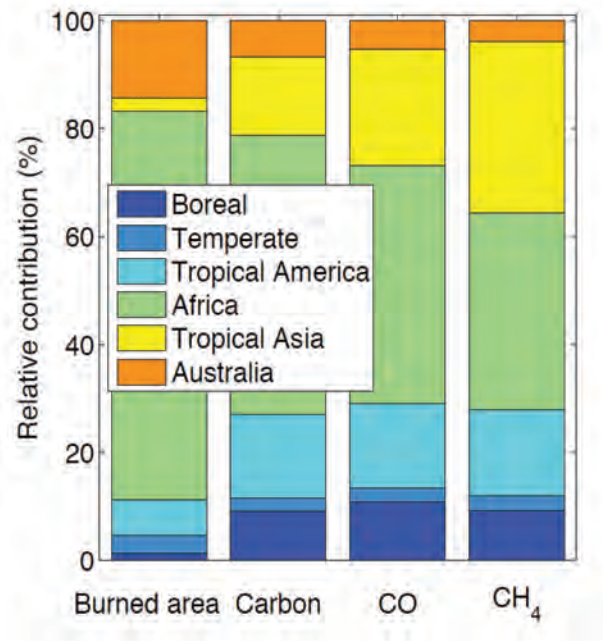

Figure 1.4: Relative contributions from CH_4 source regions to global CH_4 emissions from biomass burning between 1997 and 2009. The figure summarizes both natural and anthropogenic emissions. The Figure is taken from van der Werf et al. (2010).

5) Aerobic CH_4 formation in plants. For the first time, biogenic CH_4 formation has been observed in aerobic conditions by Keppler et al. (2006). Living plants and disconnected leaves were found to emit CH_4 in laboratory and field experiments. Initial up scaling to the global scale suggested the hitherto unrecognized aerobic CH_4 formation was one of the major global CH_4 sources (Keppler et al., 2006). This finding was controversially discussed and stimulated further research. While some authors did not find evidence for aerobic CH_4 formation (e.g., Beerling et al., 2008; Dueck et al., 2007; Nisbet et al., 2009), other experimentalists observed aerobic CH_4 formation and found environmental parameters such temperature, drought and UV-B radiation as controlling factor (e.g., Bruhn et al., 2009; McLeod et al., 2008; Vigano et al., 2008, 2009b). Aerobic CH_4 formation from six crop types (all C3 plants) increased in response to modified temperature- and H_2O stress, while it was reduced when atmospheric CO_2 was increased from present day to doubled concentrations (Qaderi and Reid, 2011).

Atmospheric CH_4 sources

A schematic of atmospheric CH_4 sources is shown in Figure 1.5. Atmospheric CH_4 mixing rations represent the integral of CH_4 source and sink fluxes over a given time. A recent review paper reports the sum of global CH_4 source fluxes between 548 and 678 Tg $CH_4 a^{-1}$ for the period 2000-2009 (Kirschke et al., 2013). The different estimates represent averages from multiple studies applying top-down or bottom-up techniques. For example, inverse models that suggest sink and source fluxes as "perfect solution" to match observations are top-down approaches (e.g., Hein et al., 1997), while bottom-up techniques simulate the entity of all processes and integrate sink and source fluxes (e.g., Olivier and Berdowski, 2001; van Aardenne et al., 2001). Top-down approaches assign about 70 % of the total CH_4 emissions to wetland sources, which represent the most important singe source category (Denman et al., 2007).

About 70 % of the total wetland CH_4 is emitted from tropical and southern hemispheric wetland sources (Walter et al., 2001). The global CH_4 sources can also be differentiated into those that occur naturally (e.g. natural wetlands, geological sources and wildfires), and those that are due to anthropogenic activity (e.g. emissions from fossil fuel production, agriculture, livestock and waste treatment). For the years 2000 to 2009, natural sources of 218 Tg $CH_4 a^{-1}$ were outweighed by anthropogenic sources of 335 Tg $CH_4 a^{-1}$. Generally, the estimations of natural sources contain typical uncertainties from 50 % for wetlands and about 100 % for other natural source processes while the uncertainty for anthropogenic sources is lower (Kirschke et al., 2013). Detailed CH_4 source fluxes are presented in table 1.1. It is noteworthy, that the aerobic CH_4 formation (Keppler et al., 2009) is not yet represented in global source estimations (Kirschke et al., 2013).

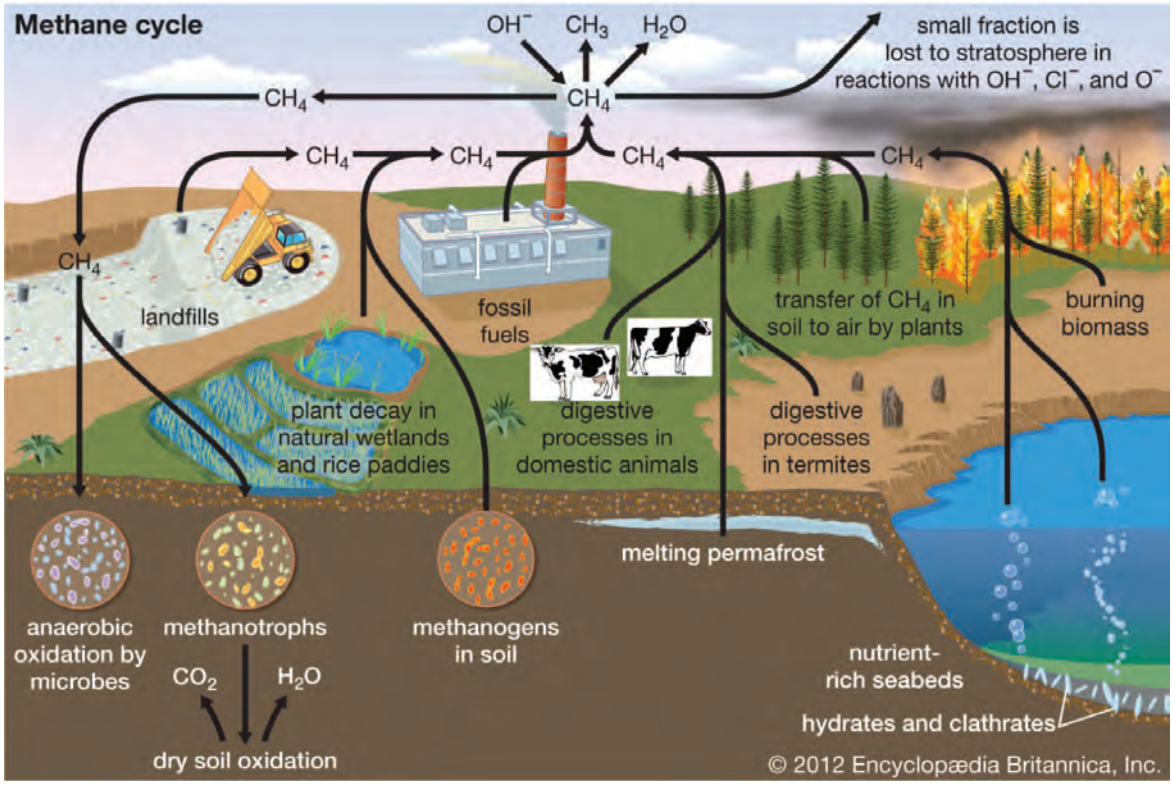

Figure 1.5: Schematic of CH_4 cycle. Shown are bot natural and anthropogenic CH_4 source processes as well as the destruction of CH_4 by the OH^- radical which is the major sink for atmospheric CH_4. Note even though it is commonly referred to as "CH_4 cycle" this rather refers to the sum of most important processes in CH_4 formation and destruction as part of the global carbon cycle. Modified version from Encyclopaedia (2013).

Table 1.1: CH_4 sources and sinks. Source categories and data taken from Denman et al. (2007). Source strength data are averages of references in Denman et al. (2007) with range in brackets. [a] indicates value from Gupta et al. (1996) which is also refernced to in literature. [b] highlights a recent values from Kirschke et al. (2013). [c] shows that all sink data are after Lassey (2007) while [d] indicates more recent value from Mischler et al. (2009). ϵ indicates the source specific KIE.

Category	**[Tg CH_4 a^{-1}]**	δ^{13}**C [‰]**
Natural sources		
Narural wetlands	174 [100-231]	-58
Termites	22 [20-29]	-70, -57 [a]
Ocean	10 [4-15]	-60
Hydrates	5 [4-5]	-60
Geological	9 [4-14], 54[33-75][b]	-40
Wild animals	15	-60
Wild fires	4 [2-5]	-25
Anthropogenic sources		
Energy	75 [74-77]	
Coal mining	38 [30-48]	-37
Gas, oil, industry	56 [36-68]	-44
Landfills and waste	54 [35-69]	-55
Ruminants	99 [76-189]	-60
Rice agriculture	62 [31-112]	-63
Biomass burning	47 [14-88]	-25
C3 cegetation	27	-25
C4 cegetation	9	-12
Sinks [c]		ϵ **[‰]**
OH	490±85	-4.65±0.75
Soils	30±15	-20±2
Stratosphere	40±8	-3±3, -15.3±4.7 [d]
Chlorine	25±12	-60±1

Atmospheric CH_4 sinks

There are four pathways that remove CH_4 from the troposphere. The major tropospheric CH_4 sink is photochemical oxidation by the OH radical, accounting for about 88 % of the total CH_4 removal (Denman et al., 2007). The OH reaction is described by Hein et al. (1997).

$$CH_4 + OH \longrightarrow CH_3 + H_2O \tag{1.5}$$

OH has a short atmospheric lifetime ($\sim$1 s) and it is involved in complex processes of atmospheric chemistry. It is known that its concentration is highest in low latitudes (Hein et al., 1997; Mikaloff Fletcher et al., 2004b) but its direct quantification remains difficult (Kirschke et al., 2013) and has a high uncertainty with $\sim$20 % (e.g., Mikaloff Fletcher et al., 2004b; Denman et al., 2007). The OH sink is indirectly quantified using chemistry-climate-models (Kirschke et al., 2013). Further sink processes include CH_4 consumption in dry soil layers by methanotrophic bacteria and CH_4 loss to the stratosphere, accounting for $\sim$5 % and 7 % of the overall sink, respectively (Denman et al., 2007). In the stratosphere, CH_4 is oxidized by OH, $O(^1D)$ and Cl (e.g., Khalil et al., 2000; Mikaloff Fletcher et al., 2004a). Both soil and stratospheric sink have an uncertainty of 50 % and 20 %, respectively. The combined uncertainty of the sink term propagates into the uncertainty of atmospheric lifetime, which was estimated at 8.7 $\pm$ 1.3 years (Denman et al., 2007). An overview of CH_4 sinks is presented in table 1.1. CH_4 oxidation by chlorine the in the marine boundary layer represents an additional CH_4 sink which might account for $\sim$4 % of the total sink term (Kirschke et al., 2013). However, the uncertainty of this process is very high (Quay et al., 1999) which is probably the reason why it is not fully included into the CH_4 budget presented by Denman et al. (2007).

Carbon isotope ratios of atmospheric CH_4

Carbon isotopes are the most frequently measured isotope ratios in atmospheric CH_4 and are the focus of this work. They are expressed as the relative deviation against the VPDB (Vienna Pee Dee Belemnite) reference material according to:

$$\delta^{13}C_{(VPDB)} = \frac{{}^{13}C_{sample}/{}^{12}C_{sample}}{{}^{13}C_{std}/{}^{12}C_{std}} - 1 \tag{1.6}$$

Average δ^{13}C-CH_4 values of the contemporary atmosphere range about -47.5 ‰ (e.g., Quay et al., 1999). Figure 1.6 shows monthly δ^{13}C-CH_4 averages from six monitoring stations from May 2008 to November 2011. The locations of the monitoring stations cover a meridional gradient that nearly reaches from pole-to-pole (79°N to 90°S). The annual cycle and the interhemispheric gradient of δ^{13}C-CH_4 are distinctly visible in Figure 1.6.

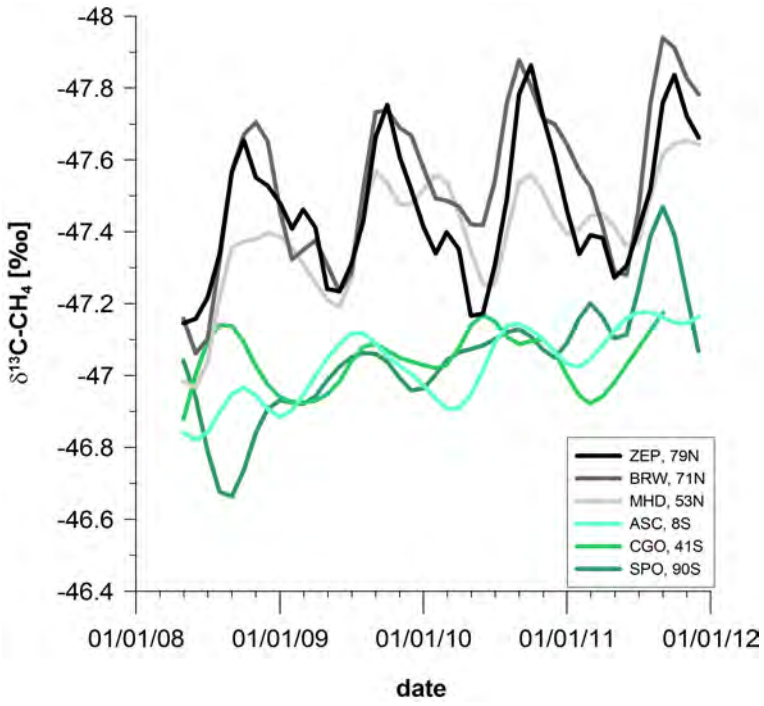

Figure 1.6: Seasonal variability from selected NOAA stations. Mean monthly δ^{13}C-CH_4 of six monitoring stations from the NOAA network. Mean values are calculated from flask sample data. Note the inverse y-axis. The legend abbreviates station names and indicates the latitude of the station. Abbreviations denote: ZEP = Zeppelin Station, Ny Alesund, Svalbard, Norway and Sweden, BRW = Barrow, Alaska, USA, MHD = Mace Head, County Galway, Ireland, ASC = Ascension Island, UK, CGO = Cape Grimm Observatory, Australia, SPO = South Pole Observatory, Antarctica, USA. Data taken from NOAA (2013).

Both features result from the spatio-temporal distribution of sinks and sources and atmospheric transport (e.g., Hein et al., 1997; Quay et al., 1999). CH_4 formation and removal processes have specific KIE's. Therefore, CH_4 sources have specific isotope ratios while the sink terms cause a known specific isotope fractionation. Table 1.1 shows typical ranges of

$\delta^{13}C$ of CH_4 sources and of the KIE from the CH_4 sinks. For example, the $\delta^{13}C$-CH_4 of wetland or biomass burning CH_4 ranges between -60$\pm$5 and -24$\pm$ 3 ‰, respectively (Quay et al., 1999). Exotically high $\delta^{13}C$-CH_4 values of -7 ‰ were measured in abiotic CH_4 (Abrajano et al., 1988). This source specific isotope variability is exploited when the CH_4 budget is constrained by inverse mass balance calculations that reproduce isotope and mixing ratio data by calculation CH_4 emission scenarios (e.g., Lassey, 2007; Sapart et al., 2012).

CH_4 in atmospheric chemistry

CH_4 plays an important role in Earth's atmospheric chemistry. It is shown in reaction 1.5 that the photochemical oxidation of CH_4 produces H_2O (e.g., Hein et al., 1997) which makes CH_4 a major H_2O source in the stratosphere (e.g., Seidel et al., 2001; Mikaloff Fletcher et al., 2004a). As a main sink for OH radicals (Mikaloff Fletcher et al., 2004a), CH_4 is in direct competition with other molecules for OH, such as VOC's or CO. This is an example how CH_4 impacts the oxidation capacity of the atmosphere and thus the lifetime of further atmospheric compounds (e.g., Kaplan et al., 2006). Furthermore, CH_4 is associated with tropospheric ozone formation (Fiore et al., 2002).

CH_4 observations

"You cannot manage what you don't measure" is a statement that was often quoted by speakers of the atmospheric monitoring community during the ICDC-2013 conference in Beijing. However, I cannot recall who this quote originated from. To monitor the atmospheric composition, a range of atmospheric observation systems and networks are installed. The monitoring systems comprise a variety of platforms in order to maximize the spatio-temporal data resolution. For example, GHG are permanently observed from satellites (e.g. Envisat, Sciamachi, (ESA, 2013)), during aeroplane flights (CARIBIC,(MPI-C, 2013)) as well as terrestrial observation stations and networks (AGAGE, NOAA, ICOS, TCCON) including tall tower stations (e.g. Zotto, (MPI-BGC, 2013)). These platforms measure in situ or sample air for GHG mixing- and isotope ratio analysis, some of them for more than 40 years (e.g. Mauna Loa, see NOAA (2013) or Baring Head, see NIWA (2013)) Figure 1.7.

Other strategies of GHG observations allow studying vertical profiles through the atmosphere by discrete sampling (Röckmann et al., 2011) or air core sampling (Karion et al., 2010) during balloon flights. Large horizontal transect can be covered by train- and shipboard sampling (e.g., Bergamaschi et al., 1998; Umezawa et al., 2009). The combined efforts allow for a high data density that can be interpreted in conjunction with atmospheric circulation data to disentangle GHG sink, source and transport processes (e.g., Dlugokencky et al., 2009).

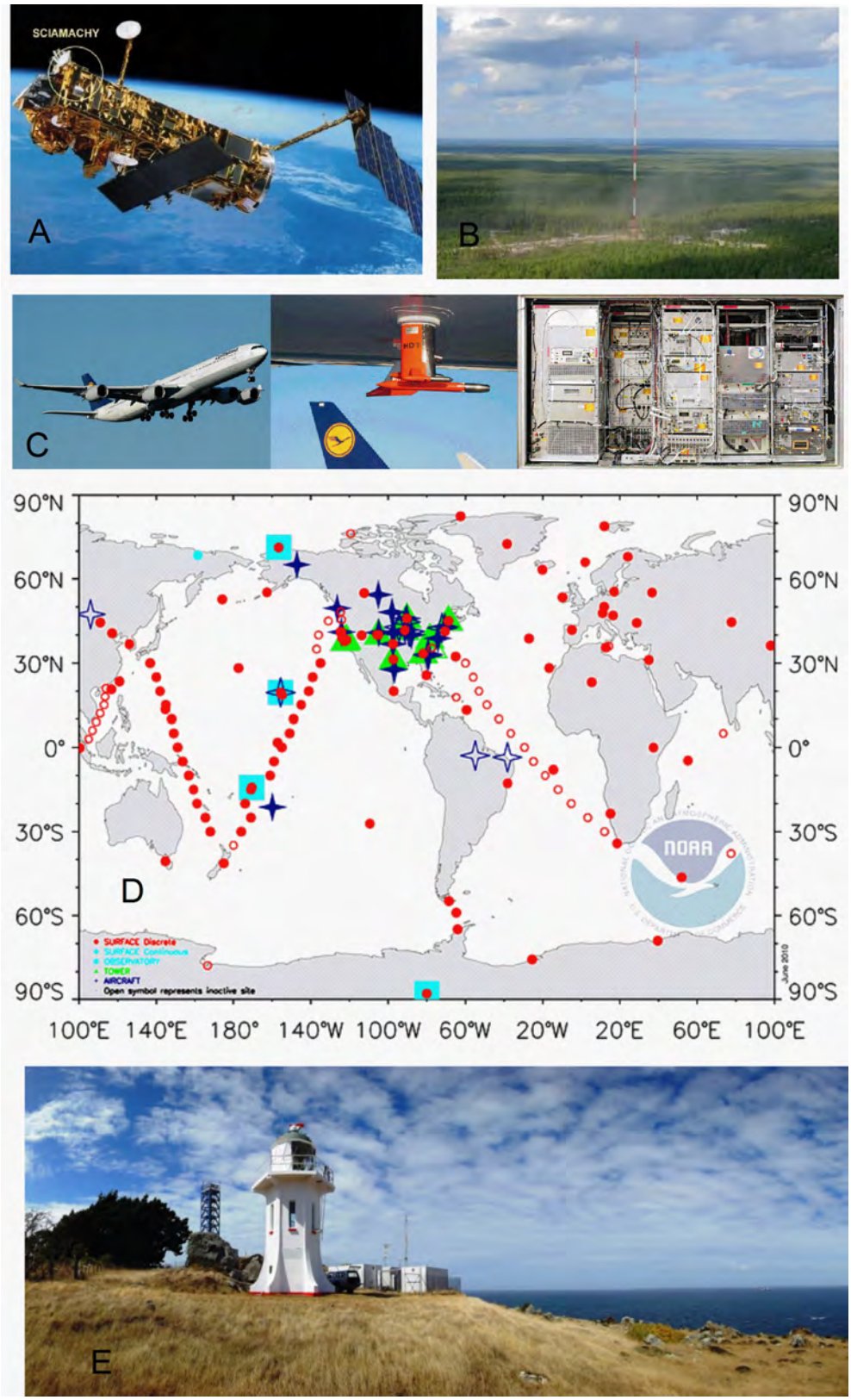

Figure 1.7: Atmospheric observation platforms. (A) Sciamachy module on ENVISAT satellite, (ESA, 2013). (B) ZOTTO tower, (MPI-BGC, 2013). (C) CARIBIC system, (MPI-C, 2013). (D) NOAA observation network, (NOAA, 2013). (E) Baring Head observatory, (NIWA, 2013)

CH_4 model studies

Computer models that simulate atmospheric chemistry and transport, climate dynamics and biogeochemical feedbacks are essential tools to investigate the CH_4 cycle (e.g., Martinerie et al., 1995; Hein et al., 1997; Mikaloff Fletcher et al., 2004a,b; Kaplan et al., 2006). The complexity of the models reach from "simple box models" (e.g., Tans, 1997) to complex models that include wetland and climate dynamics (see Melton et al. (2013) for a comprehensive model comparison study).

Accurately reconstructing or even forecasting the CH_4-cycle in the light of a changing climate is a delicate task. A recent study compared ten models used to simulate wetland-extend and wetland CH_4 emissions and found an inter-model variability in reproducing CH_4 emissions of 40 % (Melton et al., 2013). To improve the model agreement, it is necessary to reduce the uncertainty in global wetland extent, improve parameterisation (e.g. pCO_2 dependence of modelled CH_4 sources) and to increase the observations to test the modelled results (Melton et al., 2013).

Simple box models are commonly used in studies on palaeoatmospheric CH_4 mixing ratios (e.g., Chappellaz et al., 1997; Brook et al., 2000) and isotope ratios (e.g., Ferretti et al., 2005; Schaefer et al., 2006; Sowers, 2006; Fischer et al., 2008; Mischler et al., 2009; Bock et al., 2010a; Sapart et al., 2012). On glacial-interglacial time scales, Möller et al. (2013) discuss that box model calculations require under constrained assumptions and may thus produce misleading emission scenarios. Möller et al. (2013) conclude that complex models are needed to accurately simulate wetland and vegetation dynamics on glacial-interglacial time scales.

Hints from recent research for palaeo studies on atmospheric CH_4

Dlugokencky et al. (2009) combined satellite data with records from 46 stations in the global observation network to investigate the increasing CH_4 mixing ratios during 2007 and 2008 that followed puzzling pause on CH_4 growth between 1999 and 2006. Variations in the geographical pattern of CH_4 mixing ratios led to the suggestion that positive anomalies in Arctic temperatures and tropic precipitation were responsible for the CH_4 increase while satellite and CO data disproved extra CH_4 from biomass burning sources (Dlugokencky et al., 2009) . The conclusions were supported by a greater than usual depletion in δ^{13}C-CH_4 during the summer of 2007, which supports the hypothesis of increased wetland emissions.

In what way are these findings relevant for studies on palaeoatmospheric CH_4? Assuming the suggestions of Dlugokencky et al. (2009) are accurate, interannual pCH_4 increases of $\sim$8 ppb were due to changes in the natural system while anthropogenic emissions played an inferior role to this interannual increase. Hence, the interpretation of Dlugokencky et al. (2009) indicates the sensitivity of CH_4 emissions to temperature and precipitation changes and furthermore partitions the relative role of temperature and precipitation for Arctic and tropical CH_4 sources, respectively. These findings are in line with later observations of Bloom et al. (2010) that boreal and tropical CH_4 sources are most sensitive to temperature and water table, respectively.

It is of utmost importance to note, that the present day variability of CH_4 biogeochemistry doesn't allow for extrapolation to centennial or glacial-interglacial time scales. This is because processes can be non-linear (Chadwick et al., 2013) and because even remote tropical and Arctic ecosystems are anthropogenically modified and might thus respond differently to temperature and precipitation changes than the Eemian (previous interglacial period, 115-130 ka BP) ecosystems did. Furthermore, unidentified mechanisms might have played an important role in past changes that preclude present variability to serve as analogue. However, the above mentioned present day sensitivities might hint towards processes that are relevant for palaeo interpretations. In this particular case, it might be worth consulting palaeo reconstructions of Arctic temperatures and tropical precipitation for the interpretation of palaeoatmospheric CH_4 records.

Link to palaeoclimate

Throughout its entire history, Earth's climate and atmosphere were subject to radical changes (e.g., Manhes et al., 1980; Wayne, 2009). Studying the palaeoclimate system, might therefore allow learning about complex climate and atmospheric processes. For example, the palaeoatmosphere changed from a reducing to an oxidizing atmosphere, which is due to the accumulation of iron in Earth's inner core and the initiation of photosynthesis (Catling and Claire, 2005). The absence of mass-independent isotope fractionation in pyrite FeS_2 deposits gives evidence that atmospheric oxygen increased around 2.32 Ga ago (Bekker et al., 2004).

As another example, Ghosh and Bhattacharya (2001) reconstructed atmospheric CO_2 concentrations of 2225 $\pm$ 500 ppm about 200 Ma before present based on $\delta^{13}C$ measurements in soil carbonate deposits. Even though this might be an overestimation (Retallack, 2009), we know that at times when Earth's climate was much warmer than it is now (Ruddiman, 2001), the atmospheric CO_2 mixing ratio was a multiple of what it is today and probably in the range of those predicted for 2100 (e.g., Retallack, 2009; Breecker et al., 2010).

Just as these two examples of Bekker et al. (2004) and Ghosh and Bhattacharya (2001) show, palaeoatmospheric reconstructions are based on indirect "proxy" measurements for most of Earth's history. For the last 800 ka BP, atmospheric reconstructions can be made by direct measurements of historic air included in small bubbles within the polar ice sheets (e.g., Blunier et al., 1993, 1995; Brook et al., 1996b, 2000; Etheridge et al., 1998; Chappellaz et al., 1990, 1993a, 1997; MacFarling Meure et al., 2006; Loulergue et al., 2008; Schilt et al., 2010a,b). To create a continuous record, ice core measurements can be linked to direct atmospheric observations through overlapping measurements of firn air samples (e.g., MacFarling Meure et al., 2006; Ferretti et al., 2005).

Firn and ice as air archive

Polar snow and ice contain historic air that can be measured to study the history of the atmosphere. For the interpretation of ice core air measurements, it is important to understand the process of how the air was trapped in each sample. Figure 1.8 shows a schematic of the snow-firn-ice matrix. Obviously, the age of deposited snow and ice increases with increasing depth. While the air within the firn column is in exchange with the atmosphere, it gets irrevocably trapped in the close-off zone, when small bubbles are clipped from the tortuous pore space (Schwander et al., 1993). The close-off process occurs in site dependent depth ranges between 51 and 112 m and was probably deeper during glacial periods (Sowers et al., 1992). Therefore, air in the bubble has a younger age than the surrounding ice which is more pronounced during glacial periods. The age difference is referred to as Δage (Schwander and Stauffer, 1984) and ranges from $\sim$200 to 2000 years in the NEEM core (Rasmussen et al., 2013) and from 2000 to 6000 years in the DOME C core (Schwander et al., 2001), for recent and glacial periods, respectively. A precise knowledge of the gas age scale is a prerequisite for the analysis of atmospheric reconstructions from ice core air samples.

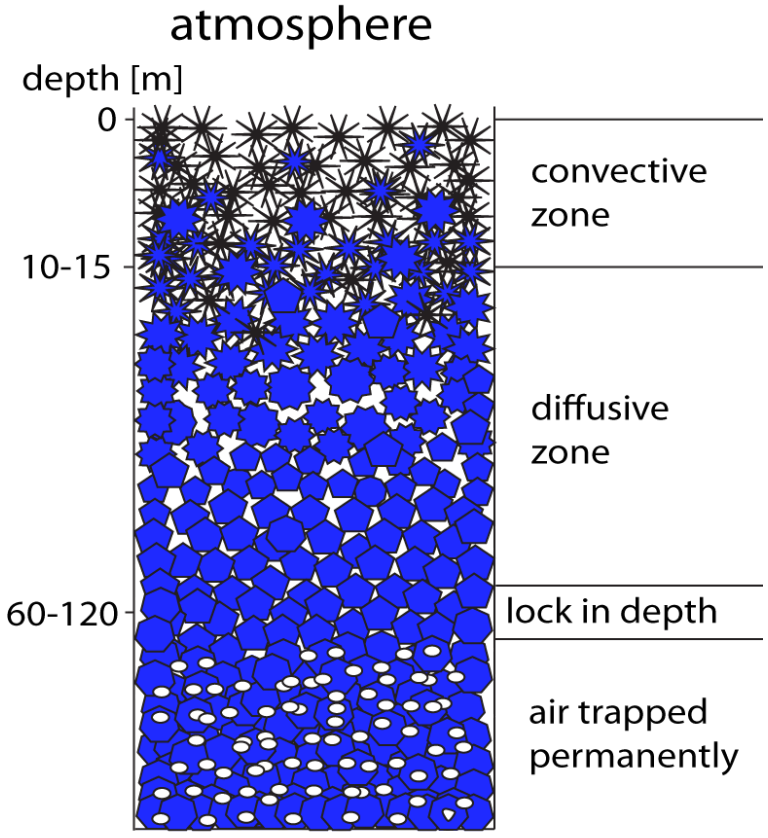

Figure 1.8: Firnification. Fresh snow and density firn contain air within the matrix. Air in the convective zone is in exchange with the atmosphere while it is subject to diffusion processes in deeper layers until air diffusion stops and air bubbles are permanently closed off.

Reconstructions of CH_4 mixing ratios

Analysis of CH_4 mixing ratios in ice core samples has provided deep insights into Earth's biogeochemistry since this possibility has been first reported in 1973 (Robbins et al., 1973). Blunier et al. (1993), Etheridge et al. (1998) and MacFarling Meure et al. (2006) show the rapid increase in pCH_4 since the onset of the industrialization. Chappellaz et al. (1990) found the pCH_4 variability over the last 160 ka to be associated with orbital parameters and suggested the radiative feedback of increased CH_4 has contributed to the climate changes, as was confirmed for the last 800 ka BP by Loulergue et al. (2008) (Figure 1.9). High resolution measurements carved out rapid changes in pCH_4 that have been unresolved before (e.g., Chappellaz et al., 1993a; Brook et al., 1996b). The newly observed millennial scale pCH_4 variability has a striking correspondence with rapid Greenland temperature variations (Brook et al., 1996b) as recorded by $\delta^{18}O_{(ice)}$, known as Dansgaard-Oeschger cycles (DO-cycles, (e.g., Johnsen et al., 2001)). It was suggested that the magnitude of millennial scale pCH_4 variability is furthermore modified by NH summer insulation (e.g., Brook et al., 1996b). This suggests that NH temperature is the primary control of millennial to glacial-interglacial scale pCH_4 variability and that -in consideration of the large NH ice sheets and its dampening effect on high latitude NH sources-, the pCH_4 variability was largely caused by tropical CH_4 sources (e.g., Chappellaz et al., 1993a; Brook et al., 1996b, 2000). Comparing $\delta^{15}N$ of N_2 as a proxy for air temperature with parallel pCH_4 measurements shows indeed that temperature variability is leading pCH_4 variability by 0-50 years (Severinghaus et al., 1998; Severinghaus and Brook, 1999; Huber et al., 2006; Grachev et al., 2007, 2009).

In a recent publication, Mitchell et al. (2011) showed that between 1000 and 1800, pCH_4 show little correlation with global temperature on decadal time scales. They also report a weak correlation with regional temperature reconstructions from high Eurasian latitudes and drought in headwater areas of rivers within the Asian monsoon region. Because of the geographical distribution of terrestrial landmasses, most relevant CH_4 sources are in the tropics and in the northern hemisphere (e.g., Hein et al., 1997; Mikaloff Fletcher et al., 2004b). High resolution CH_4 measurements on Antarctic and Greenlandic ice cores covering identical time periods can therefore provide insights into the spatio-temporal variability of CH_4 sources (e.g., Chappellaz et al., 1997; Dällenbach et al., 2000; Baumgartner et al., 2012).

A puzzling millennial scale feature of the Holocene pCH_4 record is the dip around 5ka BP during stable Greenlandic temperatures (Blunier et al., 1995). While Blunier et al. (1995) assigned this variability to a drying of tropical wetlands and consequently lower CH_4 emissions, Ruddiman (2003) argued the decrease was a natural phenomenon and interpreted the consecutive as the beginning of human impact. Based on the interhemispheric gradient, Chappellaz et al. (1997) confirm a weakening of tropical CH_4 sources as reason for the observed pCH_4 dip at 5 ka BP, which was recently supported by Singarayer et al. (2011) who assigned reduced CH_4 emissions to reduced precipitation in southern hemisphere tropical wetlands at 5 ka BP.

High resolution CH_4 measurements allow for synchronization between ice cores (e.g., Blunier et al., 2007; Schüpbach et al., 2011). CH_4 was used to match bi-hemispheric ice core

records that highlighted asynchronous pattern of interhemispheric climate dynamics (e.g., Blunier et al., 1998; Blunier and Brook, 2001) that is also known as "bipolar seesaw" (Broecker, 1998; Stocker and Johnsen, 2003). The latest technical development allows connecting optical instruments to measure $p\mathrm{CH}_4$ in continuously melted ice core samples (Stowasser et al., 2012). This technique features the highest reported precision and enables the best possible temporal resolution so far and was used to create a new "land mark" $p\mathrm{CH}_4$ record from the NH NEEM ice core (Chappellaz et al., 2013). This new dataset tremendously reduces the uncertainty in $p\mathrm{CH}_4$ variability and highlights features such as the magnitude of rapid $p\mathrm{CH}_4$ variations and their temporal gradient that have previously been suffering from lower temporal resolution and precision (Chappellaz et al., 2013).

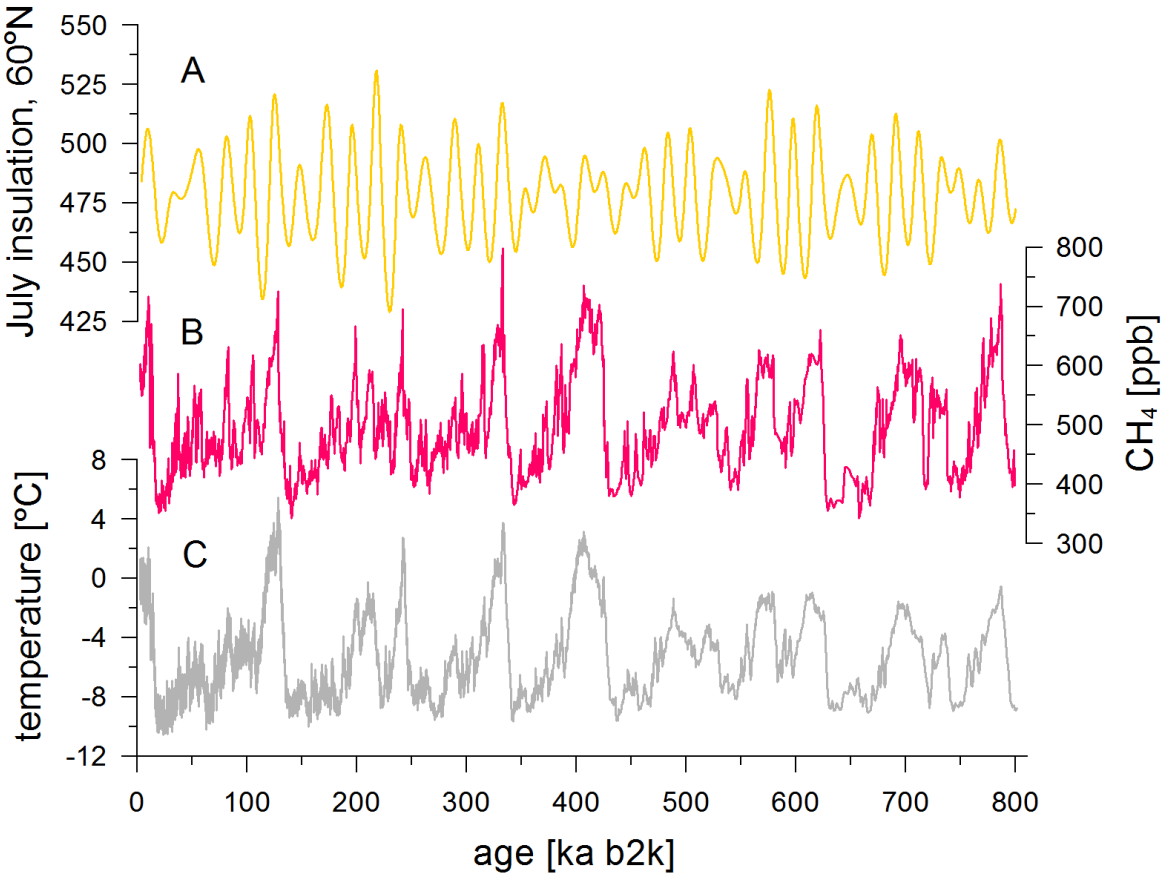

Figure 1.9: (A) mean solar insulation for July at 60 °N, (Laskar et al., 2004) in comparisson to (B) $p\mathrm{CH}_4$ over 800 ka BP, (Loulergue et al., 2008) and (C) reconstruction of relative temperature variability at Dome-C, (Jouzel et al., 2007).

Reconstructions of CH_4 carbon isotope ratios

The first palaeoatmospheric δ^{13}C-CH_4 record was measured in the Greenlandic Crete and Dye 3 ice cores and was dated to 350-100 years before 1988, where the age was referenced to the ice age scale because the Δage was unknown Craig et al. (1988). Surprisingly, it took another 17 years until further δ^{13}C-CH_4 ice core records were published (e.g., Ferretti et al., 2005; Sowers et al., 2005). Since, replicate δ^{13}C-CH_4 records have been measured in both Antarctic (Ferretti et al., 2005; Mischler et al., 2009) and Greenlandic ice cores (Sapart et al., 2012) resolving the last $\sim$1500 years (Figure 1.10).

Interestingly, the δ^{13}C-CH_4 measurements reveal some unexpected variability between 0 and 1750 AD (Ferretti et al., 2005), as δ^{13}C-CH_4 varied by 2 permil while $p$$CH_4$ was constant (Etheridge et al., 1998). By utilizing top-down approaches in simple box models, Ferretti et al. (2005); Mischler et al. (2009); Sapart et al. (2012) provide details on human impact to atmospheric CH_4 as early as 2000 years before present. However, the conclusions are based on a number of assumptions, such as stable atmospheric sink (Levine et al., 2011a,b) and transport terms, fixed geological CH_4 emissions and constant δ^{13}C values of all sources throughout the entire study period. Generally, the sources are categorised and either more or less depleted than atmospheric δ^{13}C-CH_4. Variations in source strength are balanced to meet δ^{13}C-CH_4 and $p$$CH_4$ reconstructions (Sapart et al., 2012).

In comparison, bottom-up model approaches indicate the necessity of appropriately chosen -and possibly climate-coupled- CH_4 sink terms, in order to consolidate bottom-up scenarios with observations (Lassey, 2007; Houweling et al., 2008). In particular, Houweling et al. (2008) refer to the aerobic CH_4 formation that is not yet sufficiently known and to the possibility of changing OH sink terms throughout the climate variation known as little ice age. Lassey (2007) estimate that omitting Cl sink terms will lead to mismatches in bottom-up studies by 2 permil, which, however, is still within the uncertainty range due to the uncertainty associated with δ^{13}C estimates of the CH_4 sources. Likewise, the uncertainty of δ^{13}C source values propagates within top-down scenarios.

Reconstructions of δ^{13}C-CH_4 extend through the entire Holocene (Sowers, 2009), the last deglaciation (Schaefer et al., 2006; Fischer et al., 2008; Melton et al., 2011a) and most recently to full glacial-interglacial cycles (Möller et al., 2013). Rapid $p$$CH_4$ variations (Brook et al., 1996b) create a diffusion based artefact in δ^{13}C-CH_4 that can be corrected for (e.g., Trudinger et al., 1997; Buizert et al., 2013). On millennial to glacial-interglacial time scales, the uncertainty of the data interpretation increases as a consequence of the uncertainty in determining biogeochemical processes that control the δ^{13}C of CH_4 sources (e.g., Möller et al., 2013). For example, Sowers (2009) discuss variations in tropical/boreal source ratios, C3/C4 plant ratio in CH_4 source ecosystems, different CH_4 formation pathways as well as CH_4 hydrate emissions to allow for the Holocene CH_4 variability. However, Sowers (2009) concluded that a number of processes is required to match CH_4, δ^{13}C-CH_4 and δ^{2}H-CH_4 observations and that the most likely explanation is that all processes were in place. Melton et al. (2011a) analyzed triple isotope measurements (δ^{13}C, δ^{2}H, δ^{14}C) of CH_4 that cover the transition from the Younger Dryas into the Pre-Boreal period ($\sim$11.4 to 11.6 ka BP) and suggest that biomass burning and recently discussed thermokarst sources (Walter et al.,

2006) might have caused the 250 ppb increase in CH_4. However, the less robust $\delta^{14}C$ data (Petrenko et al., 2009) are the only analytical means to distinguish between $\delta^{14}C$ depleted thermokarst CH_4 sources and the group of boreal wetlands, termites and aerobic CH_4, all of which could substitute thermokarst CH_4 sources in the budget to explain CH_4, $\delta^{13}C$-CH_4 and $\delta^{2}H$-CH_4 observations.

The uncertainty becomes even larger on glacial-interglacial time scales which is why Möller et al. (2013) refrain from calculating CH_4 emission scenarios to prevent over interpretation and misleading conclusions. Interestingly, Möller et al. (2013) found that $\delta^{13}C$-CH_4 and pCH_4 are weakly correlated and can even be decoupled during periods of significant variability. However, they found a strong correlation between $\delta^{13}C$-CH_4 and pCO_2 (Ahn and Brook, 2008; Bereiter et al., 2012) and sea-level (Rohling et al., 2009a) variability on glacial-interglacial time scales. This relation raises new questions on the mechanisms driving pCH_4 and $\delta^{13}C$-CH_4. Their data are unambiguous and robust, as they cover a period of 160 ka and include measurements made in several laboratories on two different ice cores.

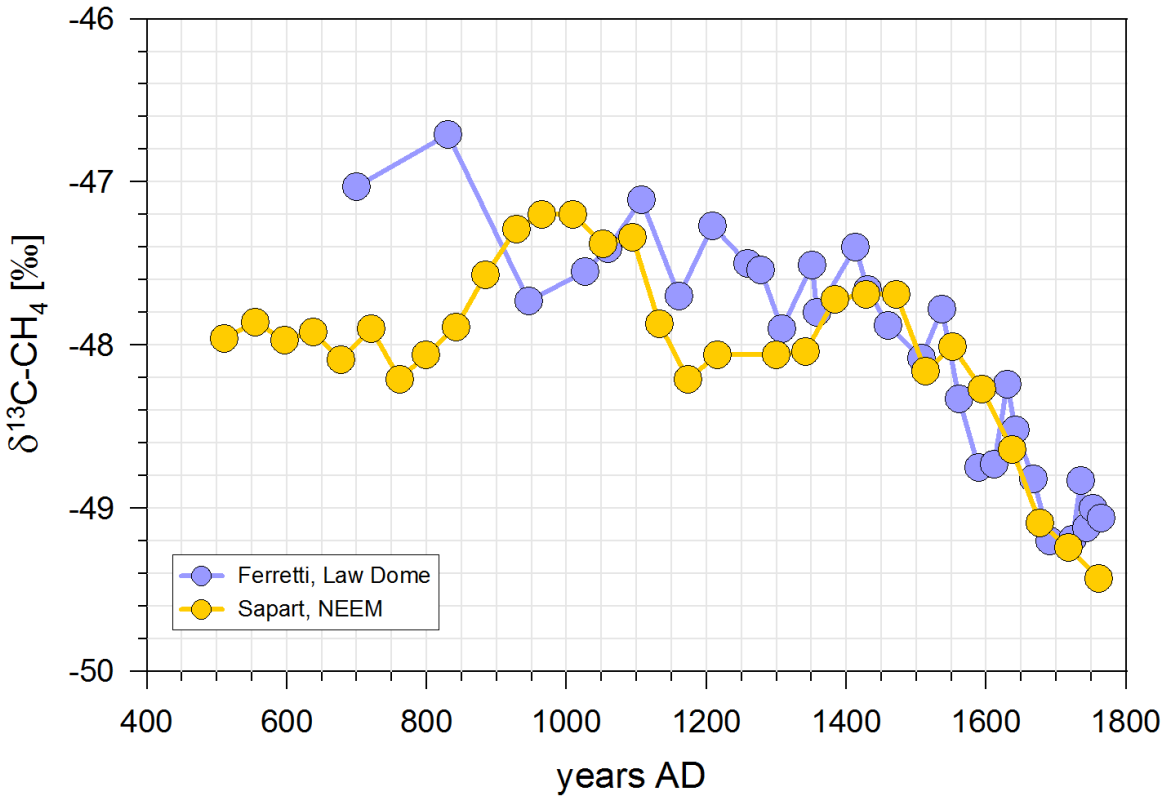

Figure 1.10: CH_4 carbon isotopes from 500 - 1800 AD. Orange circles represent Greenlandic $\delta^{13}C$-CH_4 from the recently drilled NEEM core (Sapart et al., 2012), blue circles represent Antarctic $\delta^{13}C$-CH_4 data from the Law-Dome ice core by Ferretti et al. (2005).

Chapter 2

Producing a CH_4 isotope standard

Atmos. Meas. Tech., 5, 2227–2236, 2012
www.atmos-meas-tech.net/5/2227/2012/
doi:10.5194/amt-5-2227-2012

Atmospheric Measurement Techniques

A combustion setup to precisely reference $\delta^{13}C$ and δ^2H isotope ratios of pure CH_4 to produce isotope reference gases of $\delta^{13}C$-CH_4 in synthetic air

P. Sperlich[1,*,], M. Guillevic[1,2,**], C. Buizert[1], T. M. Jenk[1], C. J. Sapart[3], H. Schaefer[4], T. J. Popp[1], and T. Blunier[1]**

[1]Centre for Ice and Climate, University of Copenhagen (CIC), Copenhagen, Denmark
[2]Laboratoire des Sciences du Climat et de l'Environment (LSCE), Gif sur Yvette, France
[3]Institute for Marine and Atmospheric Research Utrecht (IMAU), Utrecht University, Utrecht, The Netherlands
[4]National Institute for Water and Atmospheric Research (NIWA), Wellington, New Zealand
[*]now at: Max-Planck-Institute for Biogeochemistry (MPI-BGC), Jena, Germany
[**]These authors contributed equally to this work.

Correspondence to: P. Sperlich (psperl@bgc-jena.mpg.de)

Received: 17 March 2012 – Published in Atmos. Meas. Tech. Discuss.: 11 May 2012
Revised: 2 September 2012 – Accepted: 3 September 2012 – Published: 18 September 2012

Abstract. Isotope records of atmospheric CH_4 can be used to infer changes in the biogeochemistry of CH_4. One factor currently limiting the quantitative interpretation of such changes are uncertainties in the isotope measurements stemming from the lack of a unique isotope reference gas, certified for $\delta^{13}C$-CH_4 or δ^2H-CH_4. We present a method to produce isotope reference gases for CH_4 in synthetic air that are precisely anchored to the VPDB and VSMOW scales and have $\delta^{13}C$-CH_4 values typical for the modern and glacial atmosphere. We quantitatively combusted two pure CH_4 gases from fossil and biogenic sources and determined the $\delta^{13}C$ and δ^2H values of the produced CO_2 and H_2O relative to the VPDB and VSMOW scales within a very small analytical uncertainty of 0.04 ‰ and 0.7 ‰, respectively. We found isotope ratios of −39.56 ‰ and −56.37 ‰ for $\delta^{13}C$ and −170.1 ‰ and −317.4 ‰ for δ^2H in the fossil and biogenic CH_4, respectively. We used both CH_4 types as parental gases from which we mixed two filial CH_4 gases. Their $\delta^{13}C$ was determined to be −42.21 ‰ and −47.25 ‰ representing glacial and present atmospheric $\delta^{13}C$-CH_4. The δ^2H isotope ratios of the filial CH_4 gases were found to be −193.1 ‰ and −237.1 ‰, respectively. Next, we mixed aliquots of the filial CH_4 gases with ultrapure N_2/O_2 ($CH_4 \leq 2$ ppb) producing two isotope reference gases of synthetic air with CH_4 mixing ratios near atmospheric values. We show that our method is reproducible and does not introduce isotopic fractionation for $\delta^{13}C$ within the uncertainties of our detection limit (we cannot conclude this for δ^2H because our system is currently not prepared for δ^2H-CH_4 measurements in air samples). The general principle of our method can be applied to produce synthetic isotope reference gases targeting δ^2H-CH_4 or other gas species.

1 Introduction

Methane is a powerful greenhouse gas and therefore of major interest when studying the climate system. Records of CH_4 in the recent atmosphere exhibit small changes in seasonal and spatial patterns (e.g. Dlugokencky et al., 2009; Tyler et al., 2007). In contrast, ice core records of CH_4 mixing and isotope ratios show much stronger variability on decadal to glacial time scales (e.g., Bock et al., 2010; Ferretti et al., 2005; Fischer et al., 2008; Loulergue et al., 2008; Sowers, 2006). The isotopic composition of atmospheric CH_4 is a function of the relative strengths of its sinks and sources, which are themselves characterized by distinct signatures of the carbon and hydrogen isotope ratios (e.g. Quay et al., 1999), see Fig. 1. Therefore, changes in the biogeochemistry of CH_4 can be inferred by analyzing the CH_4 mixing ratio and isotope records. Isotope ratios are reported using the delta notation according to Eq. (1):

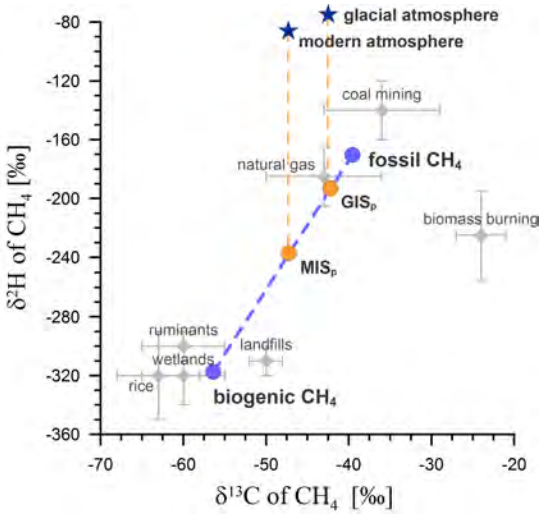

Fig. 1. Dual isotope signatures of CH_4 for $\delta^{13}C$ and δ^2H. Grey diamonds mark the field of $\delta^{13}C$ and δ^2H isotopes of CH_4 according to its source (Quay et al., 1999). Blue circles indicate $\delta^{13}C$ and δ^2H pairs of the parental CH_4 gases (fossil and biogenic CH_4). Based on our fossil and biogenic CH_4, we can produce filial CH_4 mixtures with $\delta^{13}C$ and δ^2H isotope values that fall on the dashed blue mixing line. The two filial CH_4 gas mixtures are indicated by orange circles where GIS_p and MIS_p represent the $\delta^{13}C$ of glacial and modern atmospheric samples, respectively. Isotope signatures of glacial and modern atmospheric CH_4 are indicated by the dark blue stars.

$$\delta = \left(\frac{R_{\text{sample}}}{R_{\text{standard}}}\right) - 1, \quad (1)$$

where R denotes the ratio of the heavy over the light isotope in the sample and the standard, respectively. Dual inlet-isotope ratio mass spectrometry (DI-IRMS) and gas-chromatography coupled isotope ratio mass spectrometry (GC-IRMS) are commonly applied to measure the isotope ratios of atmospheric CH_4 (Merritt et al., 1995b; Rice et al., 2001), following the principle of identical treatment (Werner and Brand, 2001). Isotope reference gases are used to anchor the sample to the international isotope scales, which is VPDB for $\delta^{13}C$-CH_4 and VSMOW for δ^2H-CH_4. Ideally, the isotope reference gas is similar in mixing ratio and isotopic composition to the measurand (Werner and Brand, 2001; Brand et al., 2009) to allow for the highest analytical precision and accuracy. Accurate referencing is vital. This becomes particularly obvious when datasets from different laboratories are merged for the interpretation of spatial atmospheric processes (Levin et al., 2012). It is essential to unambiguously determine whether different observations are due to natural variability or analytical offsets. Even very small offsets in isotope values can have a large impact on the quantification of sink and source budgets (Mikaloff Fletcher et al., 2004). One limitation to the accuracy of CH_4 isotope measurements is the accuracy to which the true isotope value of the isotope reference gas is known. Laboratories can increase their compatibility by circulating a suite of isotope reference gases in so called round-robins. Round-robins have been conducted for more than 14 yr and included several measurands, e.g. CH_4 mixing ratios and CO_2 isotopes in air to highlight accuracy offsets and to identify scale contraction effects (Brand, 2011). However, the comparison is limited as the flasks are not permanently available to each laboratory. To our knowledge, round-robin results for CH_4 isotopes in air have not been published yet. The compatibility of measurements on CH_4 isotopes in air could be achieved by establishing a suite of unique isotope reference gases that are available to all laboratories, as it is done for CH_4 mixing ratios (Dlugokencky et al., 2005) and CO_2 isotopes (Ghosh et al., 2005), respectively. An ideal suite of isotope reference gases would cover the isotope and mixing ratio variability of modern and glacial atmospheres. Despite the obvious demand, such a suite of unique isotope reference gases is currently not available for isotopes of CH_4. Even pure CH_4 gases with certified isotope ratios are currently not available from recognized authorities (such as the International Atomic Energy Agency, IAEA, or the National Institute of Standards and Technology, NIST). Here, we present a method that can potentially be used to produce large amounts of isotope reference gases for atmospheric CH_4 with targeted and precisely referenced isotope ratios.

2 Methods

2.1 Method overview

This method is designed to produce atmospheric isotope reference gases for CH_4, based on a suite of initial gases that are needed for the process. All standards and gases employed are listed in Table 1, using the terminology of Coplen (2011). Figure 2 illustrates the relationship of the measured gases to the VPDB and VSMOW isotope scales. We prepared two pure CH_4 gases that are referred to as fossil and biogenic CH_4, respectively, with regards to their origin. Next, we determined the isotopic composition of the fossil and biogenic CH_4 versus VPDB and VSMOW for $\delta^{13}C$ and δ^2H, respectively. This was achieved with a pure, referenced CO_2 gas (referred to as CO_2-40339) and three isotope reference waters (named DC′02, NM′09 and −15). The mentioned isotope reference materials are calibrated versus international measurement standards, specified by Verkouteren (1999) for CO_2 and IAEA (2009) for H_2O. From the parental fossil and biogenic CH_4, we mixed two filial CH_4 gases. We matched the $\delta^{13}C$ value of the filial mixtures to atmospheric values reported for the present day and the last glacial maximum

Table 1. Overview of gases and waters. All gases used for measuring, mixing and referencing are mentioned in the top panel, the bottom panel displays all waters that were used to reference the δ^2H-CH_4. The application and reference path of each measure are described in the second column while the third column informs on material type and purity level if applicable. The fourth column shows the relevant isotope ratios of applied reference material, the fifth column identifies the distributor of materials or specifies the origin of the measure if not commercially purchased.

Gas name	Application	Gas type, purity	δ^{13}C [‰]	Origin
RM 8563	international measurement standard	CO_2	−41.56	IAEA
CO_2-40339	isotope reference gas	CO_2, 99.998 Vol. %	−35.41	Air Liquide, Denmark
fossil CH_4	parental gas, CH_4 mixing	CH_4, 99.995 Vol. %		Air Liquide, Denmark
biogenic CH_4	parental gas, CH_4 mixing	CH_4		biogas plant, northern Germany
GIS_p	pure CH_4, glacial δ^{13}C	mixed CH_4		fossil and biogenic CH_4
MIS_p	pure CH_4, modern δ^{13}C	mixed CH_4		fossil and biogenic CH_4
GIS	synthetic isotope reference gas, glacial δ^{13}C	CH_4 in air		GIS_p with CH_4-free air
MIS	synthetic isotope reference gas, modern δ^{13}C	CH_4 in air		MIS_p with CH_4-free air
NEEM	sample, referenced with GIS and MIS	atmospheric air		NEEM camp, Greenland
CH_4-free air	matrix air for gas mixing	N_2/O_2, labline 5.0		Strandmøllen, Denmark
O_2	oxidation combustion ractor	O_2, 99.995 mol %		Air Liquide, Denmark
Water name	**Application**	**Type**	**δ^2H [‰]**	**Origin**
VSMOW-2	international measurement standard	H_2O	0.0	IAEA
SLAP-2	international measurement standard	H_2O	-427.5	IAEA
DC′02	isotope reference material	H_2O	−427.6	Dome C, Antarctica
NM′09	isotope reference material	H_2O	−257.3	NEEM camp, Greenland
−15	isotope reference material	H_2O	−111.1	internally produced

(Quay et al., 1999; Fischer et al., 2008). The filial CH_4 mixtures will hereafter be referred to as the glacial isotope standard (GIS_p) and the modern isotope standard (MIS_p), respectively, where the index "p" specifies a pure CH_4 gas. Both δ^{13}C-CH_4 and δ^2H-CH_4 isotope ratios of GIS_p and MIS_p were precisely referenced versus CO_2-40339 and the isotope reference waters, see Fig. 1 and section 2.2. Next, aliquots of GIS_p and MIS_p were blended with CH_4-free air, until atmospheric mixing ratios of CH_4 were reached. This resulted in two synthetic isotope reference gases containing CH_4 with δ^{13}C values akin to the glacial and modern atmosphere which will be referred to as GIS and MIS, respectively. We then used GIS and MIS as isotope reference gas to reference a tank of atmospheric air (taken at a clean air site in Northwest Greenland (77.45° N, 51.06° W) in July 2008, hereafter referred to as NEEM) according to the principle of identical treatment (Werner and Brand, 2001). Finally, our results for δ^{13}C-CH_4 of NEEM were compared to the results that two external laboratories found for NEEM (not for δ^2H-CH_4 because our setup is currently not equipped for such measurement).

2.2 Calibration of pure CH_4

Figure 3a shows a schematic of the setup used to quantitatively combust pure CH_4 to CO_2 and H_2O, which were subsequently trapped for consecutive isotope analysis. This procedure will hereafter be referred to as the offline combustion method. The combustion unit is a vacuum system consisting of two quartz glass tubes of 10 and 12 mm inner diameter (ID) and 350 mm in length. Both are routed through a tube furnace (300 mm heated length, 60 mm ID) and are filled with copper oxide (61205-100G, Sigma-Aldrich, Denmark) throughout the heated zone. The copper oxide is held in place by quartz glass frits to one side and with quartz wool to the other side. Tubes outside the furnace are made of borosilicate glass. Figure 3a shows the H_2O section to the right side and the CO_2 section with the gas inlet to the left side of the furnace. The H_2O section is made of a glass tube with 10 mm outer diameter (OD). It consists of a double loop used as a continuous H_2O trap which leads into a 250 ml bottle trap. The tear-shaped bottle bottom enables focusing the H_2O in a narrow, well defined spot for easy pipetting of the sample into a septum-sealed sample vial for subsequent δ^2H analysis. The tubes in the CO_2 section are of 12 mm OD, only the branch to the gas inlet is of 6 mm OD so it can be connected to a 1/4″ stainless steel T-piece. A 250 ml cylindrical trap with a stopcock is connected with a 1/2″ Ultra-Torr connector. It can be removed to transfer the CH_4-derived CO_2 for subsequent analysis. Figure 3b displays the gas manifold, which represents the interface between the combustion unit and all peripheral units such as the pump, gas tanks and sample cylinders. Manifold and combustion unit are connected via a flexible stainless steel tube that prevents the propagation of vibrations from the pump to the glass system. A pressure gauge (2 bar max) between combustion unit and flexible tube is used to quantify the amount of introduced sample gas

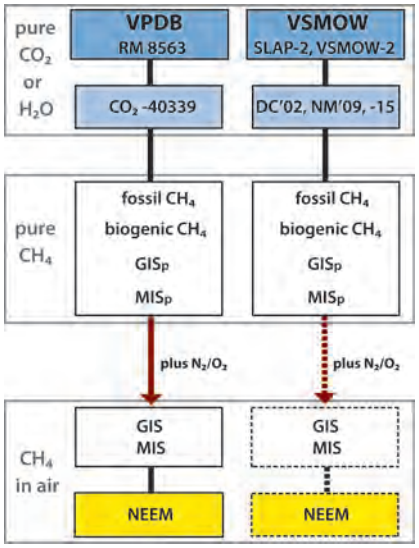

Fig. 2. Shown are the relations of measurements to the VPDB and VSMOW isotope scales in a top-down hierarchy. The dark blue boxes represent the isotope scales and name the international measurement standard used to reference our isotope reference materials, shown in light blue boxes. These isotope reference materials were used to reference the pure CH_4 gases to the respective isotope scale. The red arrows indicate the step where GIS and MIS are produced by diluting the referenced GIS_p and MIS_p with CH_4 free air, respectively. The yellow boxes in the bottom line represent the sample level. NEEM was referenced according to this reference scheme and is thus anchored to the isotope scales via the respective hierarchy of isotope reference materials. GIS, MIS and NEEM could not be referenced to the VSMOW scale because the GC-IRMS setup is not prepared for isotope measurements of δ^2H on CH_4 in air (therefore indicated by arrows and boxes in dashed lines). Grey boxes group the type of measurement standards, isotope reference materials and gas mixtures.

and to indicate pressure changes inside the combustion unit. The pressure in the mixing part of the manifold is measured by a second pressure gauge (60 bar max). Two 1 l sample cylinders in the high pressure part of the manifold are used as reservoirs to mix and store pure CH_4 gases. The copper inside the combustion unit is oxidized with O_2 (Table 1) at temperatures of 600 °C according to Reaction (R1):

$$2Cu + O_2 \rightleftharpoons 2CuO, \quad \text{(R1)}$$

O_2 is released during the combustion by the reverse reaction of (R1) when the furnace is heated to 850 °C. The copper either serves as a reducing or oxidizing agent (O_2 acceptor or donor) depending on the furnace temperature setting (Merritt et al., 1995a). In the beginning of a combustion process, the continuous H_2O trap was cooled to −78 °C. Aliquots of 120–160 ml CH_4 were injected into the evacuated combustion reactor at ambient temperatures, resulting in pressures of about 200 mbar. Subsequently, the oven was heated to 850 °C so that the copper oxide in the combustion unit released the oxygen for the CH_4 oxidation (Merritt et al., 1995a).

The combustion process is accelerated by submerging either the CO_2 or the H_2O trap in liquid nitrogen (−196 °C), while the respective other trap is heated to room temperature. Alternately, cooling the CO_2 or the H_2O trap to liquid nitrogen temperatures forces the CO_2 and H_2O back and forth through the system and thereby transports the CH_4 through the combustion reactor. This process is hereafter referred to as cryo-transfer, where each cryo-transfer lasted approximately 10 min. Each cryo-transfer cycle generates more CO_2 and H_2O until the CH_4 is quantitatively combusted. While the CO_2 is driven back and forth through the combustion reactor, the H_2O accumulates in the continuous H_2O trap. Whenever the CO_2 trap is cooled for a cryo-transfer, the newly produced H_2O first freezes in the CO_2 trap along with the CO_2 and is then transferred to the continuous H_2O trap during the following cooling of the final H_2O trap with liquid nitrogen. The transfer of H_2O into the continuous H_2O trap was accelerated by heating the CO_2 trap and the glass lines with a heat gun.

The number of cryo-transfer cycles is critical as isotope fractionation occurs during the combustion process. Incomplete oxidation leads to an offset between the $\delta^{13}C$ of the initial CH_4 and the $\delta^{13}C$ of the CO_2 derived from it (described in detail by Merritt et al., 1995a, and Zeng et al., 1994). Tests showed reproduced $\delta^{13}C$ values when the samples were quantitatively combusted. This was the case after 25 cryo-transfer cycles for test with sample sizes between 115 and 160 ml and combustion temperatures between 840 and 860 °C (Fig. 4). Higher temperatures in the combustion unit increase the equillibium pressure of oxygen over the copper and thereby the oxidation rate, thus, requiring less cryo-transfers for a complete combustion. However, we chose to limit the oxidation temperature to 850 °C in order to increase the life-time of the combustion reactor, following Merritt et al. (1995a) and Zeng et al. (1994).

N_2O might form from traces of N_2 and O_2 in the oxidation reactor (Vaughn et al., 2004) and must be eliminated to avoid mass interferences with CO_2 in the DI-IRMS (Ghosh and Brand, 2004). Therefore, we reduced N_2O to N_2 and O_2 in the reduction reactor (Fig. 3a) according to the following Reaction (R2):

$$N_2O + Cu \rightarrow N_2 + CuO \quad \text{(R2)}$$

First, we freeze all sample gas by cooling the traps to liquid nitrogen temperatures and thereby cryo-focus the samples in the traps before we close the trap valves. Next, the reduction unit is evacuated while held at a constant temperature of 850 °C. This step liberates any O_2 in the reduction unit according to Reaction (R1), thereby increasing the reduction capacity of the copper in preparation for the following reduction process (Kapteijn et al., 1996). Afterwards, the oven

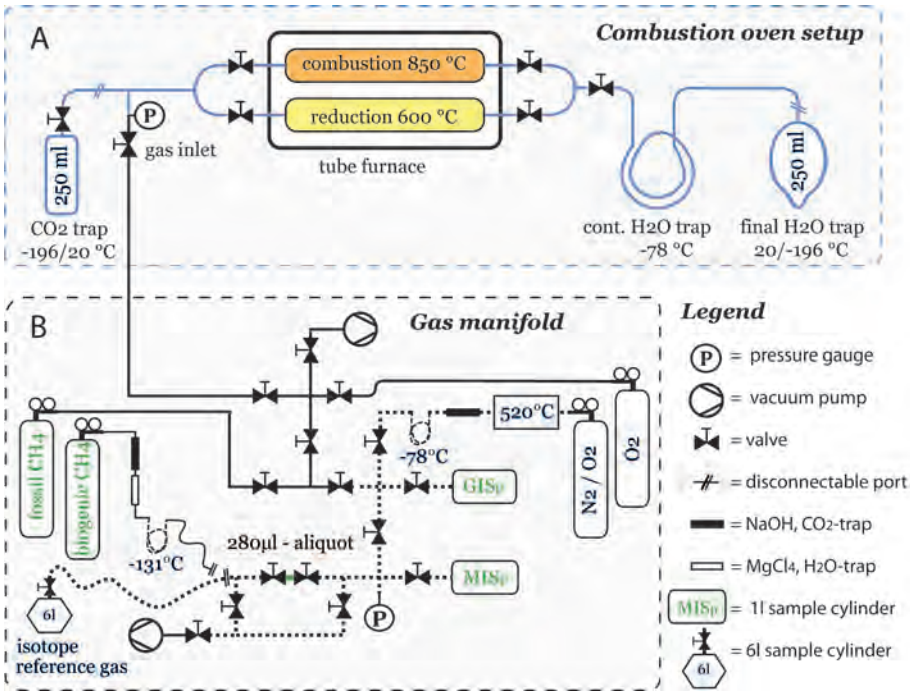

Fig. 3. Schematic figure of the setup. The top panel **(A)** illustrates the combustion and reduction reactors as well as the CO_2 and the two H_2O traps. The blue lines indicate the glass parts of this vacuum component. The diagonal parallel lines indicate the disconnection ports, where the CO_2 trap and the H_2O trap can be removed to transfer the sample. The bottom panel **(B)** shows the gas manifold that facilitates mixing and aliquoting the samples. Solid black lines represent the brass components used for gas introduction and evacuation. Dotted black lines indicate stainless steel components that take pressures of up to 60 bars. Diagonal parallel lines show the disconnection port that either connects the tank of biogenic CH_4 or the reservoir for the isotope reference gas. The aliquot volume of 280 µl is indicated by the green line between the valves

temperature is decreased to 600 °C and we cryo-transfer the sample gas 10 times through the reduction unit, where N_2O is reduced according to Reaction (R2). While O_2 is absorbed by the copper, N_2 remains in the sample gas (Kapteijn et al., 1996). The CO_2 does not react with the copper at 600 °C. This way, N_2O is quantitatively eliminated from the sample gas. Subsequently, the CO_2 trap is submerged in liquid nitrogen for four minutes until all CO_2 is trapped. Extending the CO_2 trapping time to 20 min showed no effect on the $\delta^{13}C$ values. The CO_2 trap is closed and disconnected for subsequent analysis. The continuous H_2O trap is heated and all H_2O focussed in the bottom of the tear-drop-shaped H_2O trap by submerging the latter in liquid nitrogen. Afterwards, the H_2O is melted within the small tear and the H_2O trap is disconnected to transfer the H_2O with a pipette into a 0.7 ml glass vial (548-0036, VWR International, Denmark) for subsequent δ^2H analysis. The glass vial is crimp-sealed with a septum to prevent loss through evaporation.

The combustion unit gets re-oxidized with pure O_2 at 600 °C in preparation for the consecutive sample. The O_2 absorption time depends on the oxidation level of the copper. We re-oxidized the combustion reactor after each sample by maintaining a constant O_2 pressure of 900 mbar for 10 min. It takes one day to prepare and combust one sample including the time to prepare the setup for the consecutive experiment.

We measured the $\delta^{13}C$ of CO_2 produced from the CH_4 combustion by DI-IRMS (Delta V Plus, Thermo Finnigan, Germany). For δ^2H in H_2O, we used commercial instruments, either a high Temperature Conversion/Elemental Analyser coupled to an IRMS (TC/EA-IRMS, Thermo Finnigan, Delta V Advantage) or laser spectroscopy (Picarro Inc. USA) as described by Gkinis et al. (2010).

We performed a sensitivity test for the effect of laboratory air leakage on the measured $\delta^{13}C$-CH_4 and monitored the variability of laboratory air in all combusted samples. We conclude that leakage or system blanks have no significant effect on our results (detailed information in the Supplement).

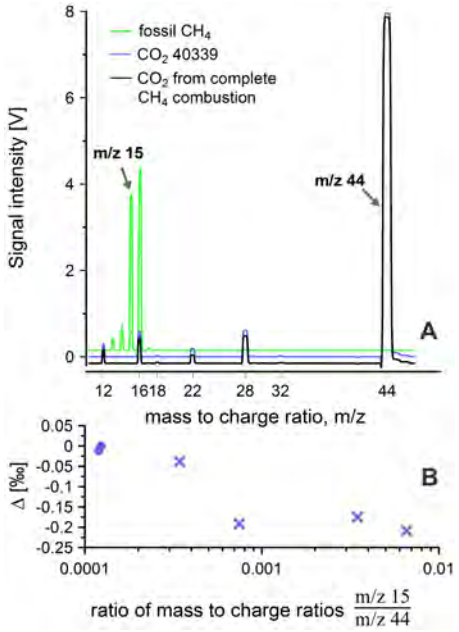

Fig. 4. Assessment of the completeness of the combustion of pure CH_4 gases. **(A)** Shown are three scans of mass abundances, each resulting from the injection of one gas into the ion source of the dual inlet IRMS. The lines result from pure CH_4 (green line), the pure CO_2-40339 (blue line) and CO_2 derived from a completely combusted CH_4 sample (black line). Because all measurements have the same background signal and would overlap, the green and the black line are artificially offset by 0.15 V and −0.15 V, respectively, to highlight the details. Both CH_4^+ and CO_2^+ decompose in the source, but a signal on mass to charge ratio m/z 15 can only result from injection of CH_4, while only injected CO_2 produces a signal on m/z 44. The ratio of m/z 15 over m/z 44 can therefore be used to quantify the remaining fraction of CH_4 within the CO_2 of a combusted sample. A high ratio of m/z 15 over m/z 44 indicates a large fraction of CH_4 in the CO_2 gas, hence an incomplete combustion. **(B)** The difference between measured and expected δ^{13}C-CH_4 (Δ) in dependence on the completeness of combustion. CO_2 from completely combusted CH_4 gas shows ratios of m/z 15 over m/z 44 of ≤ 0.0002 (blue circles), indicating absence of CH_4. Incomplete CH_4 combustion produces offsets in normalised δ^{13}C-CH_4 (blue crosses). Complete combustion is reached after 25 cryo-transfers when m/z 15 over m/z 44 in the CH_4 derived CO_2 is ≤ 0.0002 and the δ^{13}C-CH_4 offset becomes negligible.

2.3 Preparation of pure CH_4 gases and mixing of GIS_p and MIS_p

We mixed fossil and biogenic CH_4 to obtain GIS_p and MIS_p (Fig. 1). The fossil CH_4 was commercially purchased and has a high purity level of 99.995 %. The biogenic CH_4 was taken from a biogas reactor in northern Germany (Table 1) and needed purification prior to its use. Biogenic CH_4 is produced when methanogenic bacteria ferment organic material in anaerobic conditions. This process is commercially used to generate biogenic CH_4 as a green fuel from agricultural products with CH_4 contents of up to ∼ 95 %. The remaining 5 % mostly constist of atmospheric air but also of traces of CO_2, H_2O and H_2S that are also generated during the biogas production. We received a 50 l tank of biogenic CH_4 and removed CO_2, H_2O and H_2S while a CH_4 aliquot was transferred from the source tank to a 1 l sample cylinder at the manifold (Fig. 3b). A 1.5 m long, 1/4″ OD tube was filled with sodium hydroxide and magnesium perchlorate hydrate to absorb CO_2 and H_2O, respectively. Subsequently, a coiled 1/8″ tube (2 m long) submerged in a liquid nitrogen/n-Pentane slush froze out H_2S and residual H_2O at −131 °C. Aliquots of purified biogenic CH_4 could then be introduced into the combustion unit from the 1 l sample cylinder for analysis as described in Sect. 2.2. We introduced biogenic CH_4 into both 1 l sample cylinders shown in Fig. 3b. Afterwards, we added fossil CH_4 and controlled the mixing ratio between biogenic and fossil CH_4 in each mixture by terminating the flow of fossil CH_4 when the pressure indicated that the desired mixing ratio was reached. We produced GIS_p and MIS_p with biogenic CH_4 contents of 15 % and 52 % , respectively, and analysed their isotopic composition using the offline combustion method (Sect. 2.2). Detailed information on the determination of the purity level of the purified biogenic CH_4 is available in the Supplement.

2.4 Producing and measuring synthetic isotope reference gases GIS and MIS

The N_2/O_2 mixture that we used for mixing the synthetic isotope reference gases consisted of N_2 and O_2 in atmospheric mixing ratios but additionally contained 2 ppmv of CH_4. This CH_4 fraction needed to be removed prior to blending. Therefore, the N_2/O_2 mixture was routed through a combustion furnace built from a 60 cm long piece of 1/2″ OD seamless stainless steel tube. The central 20 cm of this tube is filled with a catalyst (SF-PH-102S-1008201, PureSphere, South Korea) and heated to 520 ± 1 °C. Downstream of the oven, two traps in series removed H_2O from the air flow. The first trap is a 1 m long, 1/4″ OD line filled with magnesium perchlorate, which is followed by a 2 m coil of 1/8″ OD tube submerged in ethanol-dry ice (−78 °C). The furnace is efficiently removing CH_4 from the N_2/O_2 mixture to ≤ 2 ppbv, i.e. the detection limit of the laser spectrometer used to monitor the CH_4 fraction (Picarro Inc, USA). The process steps applied for the purification are shown in Fig. 3b. The purified N_2/O_2 mixture is hereafter referred to as CH_4-free air (Table 1).

The produced isotope reference gases based on GIS_p and MIS_p will be referred to as GIS and MIS, respectively. We started preparing the mixing of the synthetic isotope reference gas by transferring an aliquot of GIS_p or MIS_p to the designated aliquot volume of 280 ± 1 µl (Fig. 3b) while

Table 2. Mean δ^{13}C and δ^2H isotope values of pure CH_4 gases (top panel) and of NEEM, measured with the produced isotope reference gases (bottom panel). The calculations of the uncertainties are explained in Sect. 3 and are based on n repetitive measurements. "oc" denotes the offline combustion method, DI-IRMS refers to Dual Inlet IRMS and laser spec. indicates δ^2H measurements by laser spectroscopy. The * indicates the δ^2H measurements that needed correction for a 4.4 ‰ system offset (Sect. 3). The indices GIS and MIS indicate the applied isotope reference gas for the measurement of NEEM. The laboratory agreement shows the difference between the referencing of NEEM with our GC-IRMS setup and our produced isotope reference gases compared to the mean value of the two external laboratories. Our GC-IRMS system can currently not measure δ^2H-CH_4.

Measurand	δ^{13}C [‰]	δ^{13}C method	δ^2H [‰]	δ^2H method	n
fossil CH_4	-39.56 ± 0.04	oc, DI-IRMS	-170.1 ± 0.7	oc, TC/EA-IRMS	4
biogenic CH_4	-56.37 ± 0.04	oc, DI-IRMS	-317.4 ± 0.7	oc, TC/EA-IRMS	4
GIS_p	-42.21 ± 0.04	oc, DI-IRMS	-193.1 ± 0.7	oc, TC/EA-IRMS	3
MIS_p	-47.25 ± 0.04	oc, DI-IRMS	-237.1 ± 0.7	oc, laser spec.*	2
Measurand	δ^{13}C [‰]	δ^{13}C method	Daily system error [‰]	Laboratory agreement [‰]	n
$NEEM_{GIS}$	-47.29 ± 0.06	GC-IRMS	-0.29 ± 0.04	0.02	3
$NEEM_{MIS}$	-47.32 ± 0.06	GC-IRMS	-0.34 ± 0.06	-0.01	6

measuring the pressure within this section. We used two 6 l air sample flasks (SilcoCan, Restek, USA) to mix and store the synthetic isotope reference gases. Each flask was flushed with CH_4-free air and evacuated 3 times prior to the mixing to remove residual air. We first filled the evacuated target flask with CH_4-free air through a line bypassing the aliquot (Fig. 3b). This was to introduce CH_4-free air into the target flask so potential adsorption effects between gas and flask-wall could take place with CH_4-free air rather than with CH_4 to minimise potential isotope fractionation of CH_4. At a pressure of 1 bar, the CH_4-free air flow was re-routed through the aliquot volume to inject the CH_4 into the flask. We continued filling the flask with CH_4-free air until we reached the calculated pressure to obtain the desired CH_4 mixing ratio. We produced one mixture of MIS and one of GIS. The determined CH_4 mixing ratio for MIS was 1800 ± 20 ppb and for GIS 1420 ± 20 ppb (the large error bars result from the GC-IRMS system that is not optimised for high precision measurements of CH_4 mixing ratios). GIS exceeded the CH_4 mixing ratio reported for the glacial atmosphere by a factor of ~ 4, which is due to our limitation to further dilute GIS_p, given the maximum pressure of the sample flask of 2.8 bar. A larger mixing reservoir would avoid this limitation.

We used a GC-IRMS setup designed for measurements of atmospheric samples to test the produced isotope reference gases. Our GC-IRMS system and data analysis is similar to the method described by Sapart et al. (2011) where CH_4 is pre-concentrated, cryo-focussed and chromatographically separated from other sample components before it is combusted to CO_2 and H_2O within a He carrier gas flow. In a first step, the isotope ratios of the CH_4 derived CO_2 of standards and samples are referenced via the flat-topped peaks of our pure, referenced CO_2-40339, which is injected into the IRMS through the reference open split. In the consecutive data processing, the measurements of the samples are referenced to the VPDB scale by applying a simple correction algorithm that accounts for the systematic errors as determined by blocks of 3 standard measurements that bracket blocks of 3 sample measurements according to Werner and Brand (2001).

For the following tests, we assumed that the δ^{13}C values of GIS and MIS are identical to those of GIS_p and MIS_p and that our gas-mixing method does not cause isotopic fractionation. The deviation between GC-IRMS measurements of GIS or MIS and the respective DI-IRMS measurements of GIS_p or MIS_p then represents the quantity of the daily system offset of the GC-IRMS setup and could then be used in the data correction algorithm. Thereby, GIS and MIS serve as standards to anchor the δ^{13}C-CH_4 in NEEM to the VPDB isotope scale. In order to validate our method to produce isotope reference gases, we compare our final results for NEEM to the δ^{13}C-CH_4 values that two external laboratories have reported for NEEM. These are the Institute for Marine and Atmospheric Research in Utrecht (IMAU), University of Utrecht, the Netherlands, using the system described by Sapart et al. (2011) and the Institute for Climate and Environmental Physics (Bern), University of Bern, Switzerland. IMAU measured NEEM with -47.31 ± 0.05 ‰ (Sapart et al., 2012) and Bern with -47.30 ± 0.11 ‰ (J. Schmitt, personal communication, 2011), respectively.

3 Results and discussion

All results of CH_4 isotope ratios measured by DI-IRMS, TC/EA-IRMS, laser spectroscopy and GC-IRMS, respectively, are summarized in Table 2. Based on the pooled standard deviation of 13 samples (fossil and biogenic CH_4, GIS_p and MIS_p) the precision of the offline combustion method for pure CH_4 gases is 0.04 ‰ for δ^{13}C and 0.7 ‰ for δ^2H. Two of those samples were measured for δ^2H using laser spectroscopy as part of a larger batch of measurements which

needed correction for a 4.4‰ offset of unknown origin. We speculate this offset resulted from isotope fractionation due to evaporation/condensation processes within the sample vials when an autosampler failure caused a significantly longer storage time at room temperature.

We found $\delta^{13}C$ and $\delta^{2}H$ values of -39.56 ± 0.04‰ and -170.1 ± 0.7‰ in our fossil CH_4 and -56.37 ± 0.04‰ and -317.4 ± 0.7‰ in our biogenic CH_4 in line with values reported by Quay et al. (1999) for those sources. We mixed these CH_4 gases and matched the $\delta^{13}C$ values in the filial mixtures to glacial and present atmospheric values. GIS_p and MIS_p show $\delta^{13}C$ values of -42.21 ± 0.04‰ and -47.25 ± 0.04‰, respectively. Resulting $\delta^{2}H$ values for GIS_p and MIS_p are -193.1 ± 0.7‰ and -237.1 ± 0.7‰, respectively. The $\delta^{2}H$ values do not correspond to atmospheric values. Atmospheric $\delta^{2}H$-CH_4 is so strongly enriched in ^{2}H due to sink fractionation (Quay et al., 1999) that it cannot be realised by mixing of CH_4 from commonly available sources (Fig. 1). Repeated referencing of the produced isotope reference gases GIS and MIS versus CO_2-40339 in our GC-IRMS system revealed (i) an offset of the measured versus the true value and (ii) a day to day variability of the offset. The observed systematic offset in our GC-IRMS system shows a typical variability between 0 and 0.05‰ throughout one day and a maximum variability of 0.4‰ between different days. The propagated uncertainties of the day to day variability ranges between 0.04‰ and 0.06‰. The variation of the uncertainty demonstrates the importance of measuring isotope reference gases and samples following the principle of identical treatment. We repeatedly measured NEEM against GIS and MIS, applied the offset corrections and obtained -47.29 ± 0.06‰ and -47.32 ± 0.06‰, respectively. All uncertainties of the GC-IRMS measurements on atmospheric samples shown in Table 2 are independently calculated by propagating the standard errors of the mean (because we produced one mixture of each GIS and MIS, uncertainties based on the gas mixing are not included). The NEEM air was also measured at IMAU and Bern, both partners in the NEEM project. We found a difference of 0.02‰ and -0.01‰ between our NEEM results being referenced versus GIS and MIS, respectively, and the mean of IMAU and Bern. The results agree well within the uncertainty of the measurements. Our results show that our method to produce isotope reference gases is reproducible and does not introduce significant isotopic fractionation.

4 Conclusions

We developed a high precision method to reference the $\delta^{13}C$ and $\delta^{2}H$ isotopic composition of pure CH_4 samples on the VPDB or VSMOW scale, respectively. Based on the pooled standard deviation, we estimate the reproducibility of our offline combustion method to 0.04 ‰ and 0.7‰ for $\delta^{13}C$ and $\delta^{2}H$, respectively. Referenced parental CH_4 gases were mixed to obtain pure CH_4 gases with precisely referenced isotopic composition of $\delta^{13}C$ near atmospheric values. Based on these CH_4 mixtures, we created synthetic isotope reference gases with atmospheric CH_4 concentrations and $\delta^{13}C$-CH_4 isotope values. The synthetic reference gases allow us to detect and correct for system drifts and offsets in our GC-IRMS setup for atmospheric samples demonstrating the importance of our effort to produce atmospheric reference gases. We measured an air sample from a Greenland clean air site and found our results as determined with our produced isotope reference gases to be in excellent agreement with the results from partner laboratories. Isotope measurements are becoming increasingly precise. Therefore, it is important to establish a suite of isotope reference gases for $\delta^{13}C$ in CH_4 covering the whole range of investigated $\delta^{13}C$ and CH_4 mixing ratios, as was done for CH_4 mixing ratios (Dlugokencky et al., 2005) and for CO_2 isotope ratios (Ghosh et al., 2005). Our method can be used to produce synthetic isotope reference gases for $\delta^{13}C$-CH_4 in air at various mixing ratios. The system can be adapted for mixing isotope reference gases in large tanks with pressures of up to 60 bar, requiring additional tests on the stability of large volume mixtures. With a source gas that is more enriched in $\delta^{2}H$, the suite could be extended to atmospheric values of $\delta^{2}H$-CH_4. Further, additional components (e.g. N_2O, CO_2, CO) can potentially be added, which would be beneficial for new analytical systems, which are measuring multiple components in one sample. However, we feel that it is important to complement multi-component isotope reference gas mixtures with single-component isotope reference gases because the combination of the two enables to identify analytical interferences with other trace gases present. Most important for the future would be to initialise a program to produce and maintain such isotope reference gases in order to provide them to the community in a long term perspective, thereby fulfilling the requirements of the WMO-GAW.

Supplementary material related to this article is available online at: http://www.atmos-meas-tech.net/5/2227/2012/amt-5-2227-2012-supplement.pdf.

Acknowledgements. We would like to thank the field team that took the gas samples during the field season 2008 at NEEM. NEEM is directed and organized by the Center for Ice and Climate at the Niels Bohr Institute and US NSF, Office of Polar Programs. It is supported by funding agencies and institutions in Belgium (FNRS-CFB and FWO), Canada (GSC), China (CAS), Denmark (FIST), France (IPEV, CNRS/INSU, CEA and ANR), Germany (AWI), Iceland (RannIs), Japan (NIPR), Korea (KOPRI), The Netherlands (NWO/ALW), Sweden (VR), Switzerland (SNF), United Kingdom (NERC) and the USA (US NSF, Office of Polar Programs). Furthermore, we would like to thank Jörg Polzer and HAASE Energietechnik AG for kindly providing the biogenic

CH_4 as well as Michael Bock, Barbara Seth and Jochen Schmitt for measuring δ^{13}C-CH_4 in "NEEM" air. Many thanks also to Mads Dam Ellehøj, Henriette Lerche and Bo Vinther for the δ^2H measurements, to Colleen Templeton and furthermore to Pantmann Labglass for Danish Design glass-blowing. Furthermore, we would like to thank the three anonymous reviewers for their constructive comments that helped improve the manuscript.

Edited by: A. C. Manning

References

Bock, M., Schmitt, J., Möller, L., Spahni, R., Blunier, T., and Fischer, H.: Hydrogen Isotopes Preclude Marine Hydrate CH_4 Emissions at the Onset of Dansgaard-Oeschger Events, Science, 328, 1686–1689, 2010.

Brand, W. A.: GAW Report No. 194, 15th WMO/IAEA Meeting of Experts on Carbon Dioxide, Other Greenhouse Gases and Related Tracers Measurements Techniques, Jena, Germany, 7–10 September 2009, 2011.

Brand, W. A., Coplen, T. B., Aerts-Bijma, A. T., Bohlke, J. K., Gehre, M., Geilmann, H., Groning, M., Jansen, H. G., Meijer, H. A. J., Mroczkowski, S. J., Qi, H. P., Soergel, K., Stuart-Williams, H., Weise, S. M., and Werner, R. A.: Comprehensive inter-laboratory calibration of reference materials for δ^{18}O versus VSMOW using various on-line high-temperature conversion techniques, Rapid Commun. Mass Sp., 23, 999–1019, 2009.

Coplen, T. B.: Guidelines and recommended terms for expression of stable-isotope-ratio and gas-ratio measurement results, Rapid Commun. Mass Sp., 25, 2538–2560, 2011.

Dlugokencky, E. J., Myers, R. C., Lang, P. M., Masarie, K. A., Crotwell, A. M., Thoning, K. W., Hall, B. D., Elkins, J. W., and Steele, L. P.: Conversion of NOAA atmospheric dry air CH_4 mole fractions to a gravimetrically prepared standard scale, J. Geophys. Res.-Atmos., 110, D18306, doi:10.1029/2005JD006035, 2005.

Dlugokencky, E. J., Bruhwiler, L., White, J. W. C., Emmons, L. K., Novelli, P. C., Montzka, S. A., Masarie, K. A., Lang, P. M., Crotwell, A. M., Miller, J. B., and Gatti, L. V.: Observational constraints on recent increases in the atmospheric CH_4 burden, Geophys. Res. Lett., 36, L18803, doi:10.1029/2009GL039780, 2009.

Ferretti, D. F., Miller, J. B., White, J. W. C., Etheridge, D. M., Lassey, K. R., Lowe, D. C., Meure, C. M. M., Dreier, M. F., Trudinger, C. M., van Ommen, T. D., and Langenfelds, R. L.: Unexpected changes to the global methane budget over the past 2000 years, Science, 309, 1714–1717, 2005.

Fischer, H., Behrens, M., Bock, M., Richter, U., Schmitt, J., Loulergue, L., Chappellaz, J., Spahni, R., Blunier, T., Leuenberger, M., and Stocker, T. F.: Changing boreal methane sources and constant biomass burning during the last termination, Nature, 452, 864–867, 2008.

Ghosh, P. and Brand, W. A.: The effect of N_2O on the isotopic composition of air$-CO_2$ samples, Rapid Commun. Mass Sp., 18, 1830–1838, 2004.

Ghosh, P., Patecki, M., Rothe, M., and Brand, W. A.: Calcite-CO_2 mixed into CO_2-free air: a new CO_2-in-air stable isotope reference material for the VPDB scale, Rapid Commun. Mass Sp., 19, 1097–1119, 2005.

Gkinis, V., Popp, T. J., Johnsen, S. J., and Blunier, T.: A continuous stream flash evaporator for the calibration of an IR cavity ring-down spectrometer for the isotopic analysis of water, Isotopes in Environmental and Health Studies, 46, 463–475, doi:10.1080/10256016.2010.538052, 2010.

IAEA: Reference Sheet for International Measurement Standards, The International Atomic Energy Agency in cooperation with the National Institute for Science and Technology (NIST), 5 May 2009, 2009.

Kapteijn, F., RodriguezMirasol, J., and Moulijn, J. A.: Heterogeneous catalytic decomposition of nitrous oxide, Appl. Catal. B-Environ., 9, 25–64, 1996.

Levin, I., Veidt, C., Vaughn, B., Brailsford, G., Bromley, T., Heinz, R., Lowe, D., Miller, J. B., Poß, C., and White, J.: No inter-hemispheric $\delta^{13}CH_4$ trend observed, Nature, 486, E3–E4, 2012.

Loulergue, L., Schilt, A., Spahni, R., Masson-Delmotte, V., Blunier, T., Lemieux, B., Barnola, J. M., Raynaud, D., Stocker, T. F., and Chappellaz, J.: Orbital and millennial-scale features of atmospheric CH_4 over the past 800,000 years, Nature, 453, 383–386, 2008.

Merritt, D. A., Freeman, K. H., Ricci, M. P., Studley, S. A., and Hayes, J. M.: Performance and Otpimization of a Combustion Interface for Isotope Ratio Monitoring Gas-Chromatography Mass-Spectrometry, Anal. Chem., 67, 2461–2473, 1995a.

Merritt, D. A., Hayes, J. M., and Marias, D. J. D.: Carbon Isotopic Analysis of Atmospheric Methane by Isotope-Ratio-Monitoring Gas-Chromatography Mass-Spectrometry, J. Geophys. Res.-Atmos., 100, 1317–1326, 1995b.

Mikaloff Fletcher, S. E., Tans, P. P., Bruhwiler, L. M., Miller, J. B., and Heimann, M.: CH_4 sources estimated from atmospheric observations of CH_4 and its $^{13}C/^{12}C$ isotopic ratios: 2. Inverse modeling of CH_4 fluxes from geographical regions, Global Biogeochem. Cy., 18, 15, GB4005, doi:10.1029/2004GB002224, 2004.

Quay, P., Stutsman, J., Wilbur, D., Snover, A., Dlugokencky, E., and Brown, T.: The isotopic composition of atmospheric methane, Global Biogeochem. Cy., 13, 445–461, 1999.

Rice, A. L., Gotoh, A. A., Ajie, H. O., and Tyler, S. C.: High-precision continuous-flow measurement of δC^{13} and δD of atmospheric CH_4, Anal. Chem., 73, 4104–4110, 2001.

Sapart, C. J., van der Veen, C., Vigano, I., Brass,, M., van de Wal, R. S. W., Bock, M., Fischer, H., Sowers, T., Buizert, C., Sperlich, P., Blunier, T., Behrens, M., Schmitt, J., Seth, B., and Röckmann, T.: Simultaneous stable isotope analysis of methane and nitrous oxide on ice core samples, Atmos. Meas. Tech., 4, 2607–2618, doi:10.5194/amt-4-2607-2011, 2011.

Sapart, C. J., Martinerie, P., Chappellaz, J., van de Wal, R. S. W., Sperlich, P., van der Veen, C., Bernard, S., Sturges, W. T., Blunier, T., Witrant, E., Schwander, J., Etheridge, D., and Röckmann, T.: Reconstruction of the carbon isotopic composition of methane over the last 50 yr based on firn air measurements at 11 polar sites, Atmos. Chem. Phys. Discuss., 12, 9587–9619, doi:10.5194/acpd-12-9587-2012, 2012.

Sowers, T.: Late quaternary atmospheric CH_4 isotope record suggests marine clathrates are stable, Science, 311, 838–840, 2006.

Tyler, S. C., Rice, A. L., and Ajie, H. O.: Stable isotope ratios in atmospheric CH_4: Implications for seasonal sources and sinks, J. Geophys. Res.-Atmos., 112, D03303, doi:10.1029/2006JD007231, 2007.

Vaughn, B., Miller, J., Ferretti, D. F., and White, J. W. C.: Stable isotope measurements of atmospheric CO_2 and CH_4, in: Handbook of Stable Isotope Analytical Techniques, edited by: Groot, P. A., Vol. 1, 272–304, Elsevier B.V., 2004.

Verkouteren, R. M.: Preparation, characterization, and value assignment of carbon dioxide isotopic reference materials: RMs 8562, 8563, and 8564, Anal. Chem., 71, 4740–4746, 1999.

Werner, R. A. and Brand, W. A.: Referencing strategies and techniques in stable isotope ratio analysis, Rapid Commun. Mass Sp., 15, 501–519, 2001.

Zeng, Y. Q., Mukai, H., Bandow, H., and Nojiri, Y.: Application of gas-chromatography combustion-isotope ratio mass-spectrometry to carbon isotopic analysis of methane and carbon-monoxide in environmental-samples, Anal Chim. Acta, 289, 195–204, doi:10.1016/0003-2670(94)80103-7, 1994.

Manuscript prepared for Atmos. Meas. Tech.
with version 4.2 of the LaTeX class copernicus.cls.
Date: 18 September 2012

Supplementary information to: A combustion setup to precisely reference $\delta^{13}C$ and $\delta^{2}H$ isotope ratios of pure CH_4 to produce isotope reference gases of $\delta^{13}C-CH_4$ in synthetic air

Sperlich, P.[1, *, **], **Guillevic, M.**[1, 2, **], **Buizert, C.**[1], **Jenk, T.M.**[1], **Sapart, C.J.**[3], **Schaefer, H.**[4], **Popp, T.J.**[1], **and Blunier, T.**[1]

[1]Centre for Ice and Climate, University of Copenhagen (CIC), Copenhagen, Denmark
[2]Laboratoire des Sciences du Climat et de l'Environnement (LSCE), Gif sur Yvette, France
[3]Institute for Marine and Atmospheric Research Utrecht (IMAU), Utrecht University, Utrecht, The Netherlands
[4]National Institute for Water and Atmospheric Research (NIWA), Wellington, New Zealand
[*]now at: Max-Planck-Institute for Biogeochemistry (MPI-BGC), Jena, Germany
[**]These authors contributed equally to this work.

1 Purity of biogenic CH_4

1.1 Impurity quantification in biogenic CH_4

The biogenic CH_4 was sampled at a biogas power plant in northern Germany that uses agricultural crops to produce CH_4 which is pumped into the local gas grid. This requires a high purity level of the CH_4 which is achieved by coupling the biogas plant to an industrial purification reactor that increases the CH_4 content to about 95% by removing H_2S, H_2O and CO_2. The remaining 5% comprise mostly N_2, O_2, CO_2 and traces of H_2S. For our purposes, the biogenic CH_4 needed further purification. Non-CH_4 carbon containing molecules that could impact on the isotope measurements were removed. H_2S, which possibly degrades the analytical systems was furthermore reduced.

To assess the composition and purity of the gases, mass abundance scans were performed by dual-inlet IRMS analysis for high purity fossil CH_4, biogenic CH_4 as well as purified biogenic CH_4. The mass abundance scans were then compared to analyze their content of non-CH_4 components. In general, mass abundance scans of a pure CH_4 show diverse spectra of masses because certain fractions of CH_4 molecules decompose and/or re-combine to secondary molecules within the ion source, as a result of the electron bombardment (Brunnée and Voshage, 1964). Ions producing these spectra can therefore be an artefact, suggesting the abundance of non existing gas species in the sample gas. Converting mass abundances to gas compositions therefore introduces an error. The mass abundance scans are thus not the most accurate method to quantify impurities within a CH_4 gas. However, we will show that comparing mass abundance scans of CH_4 with different purity level allows for a sufficient estimate.

Correspondence to: P. Sperlich
(psperl@bgc-jena.mpg.de)

1.2 Carbon containing impurities

The performed mass abundance scans were evaluated by ISODAT 3.0, the software used to control the mass spectrometer. The results for the purified biogenic CH_4 are shown in Table 1 and Figure 1, indicating very small signals on m/z 26, 29, 30 and 44 which are caused by non-CH_4 hydrocarbon ions. We allocated molecules with their chemical formulas to the peaks: $C_2H_2^+$,$C_2H_5^+$,$C_2H_6^+$,$C_3H_8^+$ and CO_2^+, thus containing one to three carbon atoms per molecule.

We assume that mass abundance signals on m/z 12, 13, 14, 15, 16 and 17 are caused by CH_4-derived ions containing one carbon and variable numbers of hydrogen atoms. The sum of peak areas from mass abundances that derive from CH_4 molecules was compared to the sum of peak areas from mass abundances that possibly results of non-CH_4 hydrocarbons (m/z 26, 29, 30, 44) which were weighted for the maximum number of carbon atoms. This is based on the assumption that the entire signal on m/z 26, 29, 30 and 44 is derived from hydrocarbons and that all ions causing the peak on m/z 44 comprised of $C_3H_8^+$ with three carbon atoms instead of CO_2^+. This is important because one molecule of C_3H_8 produces 3 molecules of CO_2 in the combusted sample. Therefore, one molecule of $C_3H_8^+$ contributes three times stronger to the signal on m/z 44 than one molecule of CO_2. We also assume that non-CH_4 hydrocarbons are stable in the ionization chamber and do not contribute to signals m/z 12 to m/z 17.

In this most conservative scenario, a maximum of about 0.55% of the carbon that was detected in the ion source resulted from an ion containing more than one carbon atom. A similar analysis of our high purity fossil CH_4 reveals that about 0.67% of the detected ions were derived from ions containing at least two carbon atoms. The company providing the high purity fossil CH_4 specifies the purity level of its CH_4 N45 with 99.995% with a mixing ratio of non-CH_4 hydrocarbons ≤ 20 ppmv. Therefore, we conclude that

the scan procedure over-estimates the content of non-CH_4 hydrocarbons by two orders of magnitude due to processes inside the ion source. Based on the comparison of the mass abundance scans from purified biogenic CH_4 and fossil CH_4, we can assume a similar purity level.

A simple mass balance calculation based on the assumption of a 99.995 % purity level shows, that the average $\delta^{13}C$ isotope ratio of the impurities would have to be higher than 744 ‰ or lower than -856 ‰ to affect the determined carbon isotope ratios of the biogenic CH_4 by more than the given uncertainty. Because these extreme carbon isotope ratios are highly unlikely in naturally occurring gases, we conclude that our biogenic CH_4 is sufficiently purified from non-CH_4 hydrocarbons.

1.3 H_2S

The low H_2S content of both purified and unpurified biogenic CH_4 samples could only be detected by the most sensitive Faraday cup detector of the IRMS. Because this detector was saturated for the very abundant CH_4 ions, we related the H_2S signal on m/z 34 to the O_2 signal on m/z 32 which is constant in both the purified and un-purified biogenic CH_4. The purification step decreased the H_2S by 75%. However, this is at a very low concentration levels where the evaluation of the H_2S peaks is unreliable. Given that H_2S was reduced to prevent degradation of the analytical system and is not expected to alter the measurements on CH_4 isotope ratios we consider the observed reduction as sufficient.

2 Effect of system leakage

2.1 Monitoring Argon in the sample

Mass abundance scans using dual-inlet IRMS were performed on each combusted CH_4 sample. Any leakage of laboratory air into the offline combustion setup would increase the relative abundance of Argon (Ar) compared to the mass abundance of CO_2. We interpreted the ratio of the peak heights of Ar (m/z 40) to CO_2 (m/z 44) as indicator for laboratory air leakage into the offline combustion setup during a combustion process. To increase the sensitivity of this comparison, we used the Ar signal of a Faraday cup with a 100 times stronger. The resulting ratio is 0.006 +/- 0.0003 for the pure CO_2-40339. We found the same ratio in the combusted samples stemming from fossil CH_4. We found a ratio of 0.03 in the biogenic CH_4 which is higher due to the containing 5% of atmospheric air. We found these ratios to be stable for the respective CH_4 type. These measurements give us confidence that the measurements were not affected by leakage into the system during the aliquotation, the combustion or the sample transfer into the dual-inlet IRMS.

2.2 Sensitivity test for laboratory-air leakage

The effect of an undetected CO_2 blank can be estimated with the following sensitivity test. The offline combustion system was evacuated, closed off and tested for leaks in over-night test prior to each measurement. A sample would only be introduced if the pressure increase overnight stayed below the detection limit of our piezoelectric pressure gauge (1 mbar precision). We give a conservative estimate of the maximum effect an undetected leak would have as blank contribution. We assume a pressure increase of 1 mbar in the system of $\sim$ 600 ml volume, which corresponds to a leakage of 0.6 ml. If we conservatively assume 1 part per thousand of the leakage is CO_2 with a $\delta^{13}C$ isotope ratio of -7 ‰ a small biogenic CH_4 sample with a $\delta^{13}C$ of -56 ‰ would be most affected. A mass balance calculation shows that the maximum possible blank contribution would affect a 120 ml sample of biogenic CH_4 with -56 ‰ by 0.0002 ‰ which is by two orders of magnitude lower than the precision of our method. We conclude that any undetected potential blank has no significant effect on our results. The blank contribution is most likely even lower because most of the combusted samples were about 50% larger than anticipated in the calculation. Also, the lab air contains more depleted CO_2 from human breath which is more depleted in ^{13}C. Any additional CH_4 leakage would furthermore reduce this blank effect due to its lower isotopic leverage.

References

References

Brunnée, C. and Voshage, H.: Massenspektrometrie, Teil 1, Verlag Karl Thiemig KG, München, 12 edn., 1964.

Table 1. Table S1: Mass abundances in the purified biogenic CH_4 as evaluated by ISODAT 3.0. The evaluation parameters were extremely tuned to be able to capture very small abundances and therefore compromising the accuracy of the quantification. Hence, peak numbers 8 and 9 show opposing sizes in peak area and height. The CH_4-derived ions were identified following Brunnée and Voshage (1964).

number of identified peak	magnetic field [steps]	m/z	ion	peak height [mV]	peak area [mV * steps]
1	5385	12	C^+	648	1964
2	5665	13	CH^+	1842	5837
3	5935	14	CH_2^+	3855	12182
4	6190	15	CH_3^+	22075	74717
5	6450	16	CH_4^+	25370	78391
6	6690	17	CH_5^+ or $^{13}CH_4^+$	485	1673
7	6920	18	H_2O^+	823	2760
8	7365	20	$H_2^{18}O^+$	4	22
9	8630	26	$C_2H_2^+$	2	25
10	9020	28	N_2^+	795	3249
11	9210	29	$C_2H_5^+$	15	86
12	9400	30	$C_2H_6^+$	10	65
13	9765	32	O_2^+	221	995
14	10120	34	H_2S^+	not evaluated	not evaluated
15	11140	40	Ar^+	19	128
16	11795	44	$C_3H_8^+$ or CO_2^+	33	202

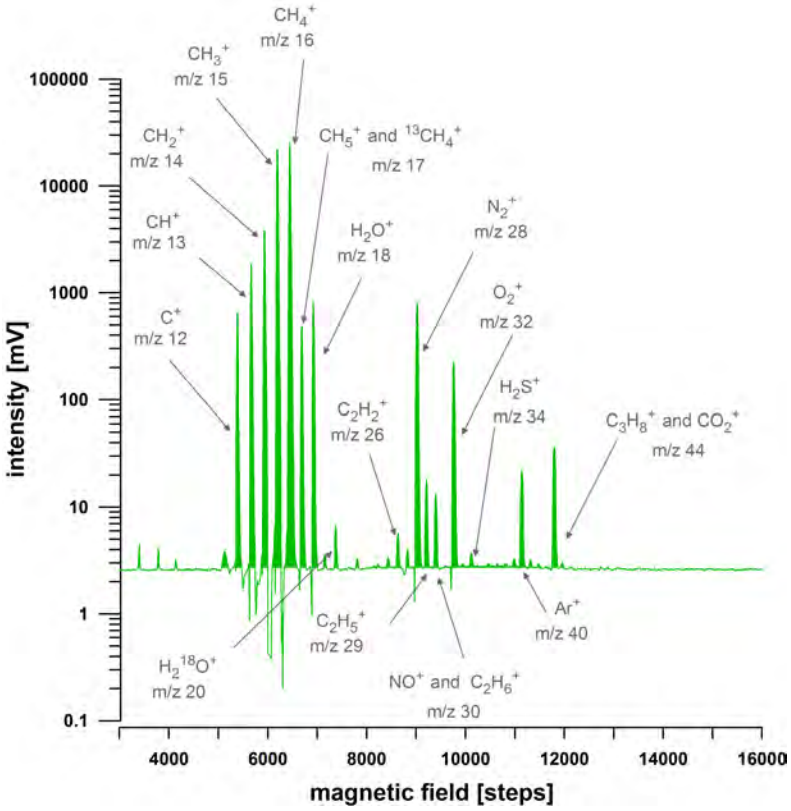

Fig. 1. Figure S1: Shown is a scan of mass abundances between m/z 5 and m/z 60 when purified bio-methane is introduced into the ion source of the dual inlet IRMS. The y-axis is set to logarithmic scale to better visualize the low abundances. Chemical formulas and m/z ratios identify the respective peaks, indicated by the arrows.

Chapter 3

Measuring CH_4 carbon isotopes in ice core samples

Atmos. Meas. Tech., 6, 2027–2041, 2013
www.atmos-meas-tech.net/6/2027/2013/
doi:10.5194/amt-6-2027-2013

Atmospheric Measurement Techniques Open Access

An automated GC-C-GC-IRMS setup to measure palaeoatmospheric δ^{13}C-CH_4, δ^{15}N-N_2O and δ^{18}O-N_2O in one ice core sample

P. Sperlich[1,*], C. Buizert[1,], T. M. Jenk[1,***], C. J. Sapart[2], M. Prokopiou[2], T. Röckmann[2], and T. Blunier[1]**

[1]Centre for Ice and Climate (CIC), Niels Bohr Institute, University of Copenhagen, Copenhagen, Denmark
[2]Institute for Marine and Atmospheric Research in Utrecht (IMAU), University of Utrecht, Utrecht, The Netherlands
[*]now at: Max-Planck-Institute for Biogeochemistry (MPI-BGC), Jena, Germany
[**]now at: College of Earth, Ocean and Atmospheric Sciences, Oregon State University, Corvallis, USA
[***]now at: Paul Scherrer Institute, Villigen, Switzerland

Correspondence to: P. Sperlich (sperlich@nbi.ku.dk)

Received: 27 January 2013 – Published in Atmos. Meas. Tech. Discuss.: 28 February 2013
Revised: 26 June 2013 – Accepted: 6 July 2013 – Published: 13 August 2013

Abstract. Air bubbles in ice core samples represent the only opportunity to study the mixing ratio and isotopic variability of palaeoatmospheric CH_4 and N_2O. The highest possible precision in isotope measurements is required to maximize the resolving power for CH_4 and N_2O sink and source reconstructions. We present a new setup to measure δ^{13}C-CH_4, δ^{15}N-N_2O and δ^{18}O-N_2O isotope ratios in one ice core sample and with one single IRMS instrument, with a precision of 0.09, 0.6 and 0.7 ‰, respectively, as determined on 0.6–1.6 nmol CH_4 and 0.25–0.6 nmol N_2O. The isotope ratios are referenced to the VPDB scale (δ^{13}C-CH_4), the N_2-air scale (δ^{15}N-N_2O) and the VSMOW scale (δ^{18}O-N_2O). Ice core samples of 200–500 g are melted while the air is constantly extracted to minimize gas dissolution. A helium carrier gas flow transports the sample through the analytical system. We introduce a new gold catalyst to oxidize CO to CO_2 in the air sample. CH_4 and N_2O are then separated from N_2, O_2, Ar and CO_2 before they get pre-concentrated and separated by gas chromatography. A combustion unit is required for δ^{13}C-CH_4 analysis, which is equipped with a constant oxygen supply as well as a post-combustion trap and a post-combustion GC column (GC-C-GC-IRMS). The post-combustion trap and the second GC column in the GC-C-GC-IRMS combination prevent Kr and N_2O interferences during the isotopic analysis of CH_4-derived CO_2. These steps increase the time for δ^{13}C-CH_4 measurements, which is used to measure δ^{15}N-N_2O and δ^{18}O-N_2O first and then δ^{13}C-CH_4. The analytical time is adjusted to ensure stable conditions in the ion source before each sample gas enters the IRMS, thereby improving the precision achieved for measurements of CH_4 and N_2O on the same IRMS. The precision of our measurements is comparable to or better than that of recently published systems. Our setup is calibrated by analysing multiple reference gases that were injected over bubble-free ice samples. We show that our measurements of δ^{13}C-CH_4 in ice core samples are generally in good agreement with previously published data after the latter have been corrected for krypton interferences.

1 Introduction

Methane (CH_4) and nitrous oxide (N_2O) are important long-lived greenhouse gases that play a significant role in Earth's radiative budget (Solomon et al., 2007). The analysis of ancient air as archived in air bubbles within the polar ice sheets has significantly improved the understanding of Earth's atmospheric and biogeochemical variability. Especially CH_4 records have been used as proxy on the extension of wetlands on the stability of marine clathrates as CH_4 source. On glacial timescales, periods of warmer climate in the Northern Hemisphere correlated with increased concentrations of CH_4 and N_2O in the atmosphere (Flückiger et al., 2004; Loulergue et al., 2008; Schilt et al., 2010). Moreover, the mixing

ratios of both gases have significantly increased during industrialization, largely due to human activities (Solomon et al., 2007). Atmospheric mixing ratios of 1774 and 319 ppb have been published in the last IPCC report for CH_4 and N_2O, respectively (Solomon et al., 2007). With the prospect of even further increasing mixing ratios and their impact on future climate, it is important to thoroughly understand the biogeochemical processes related to both gases.

Brenninkmeijer et al. (2003) describe how the isotope fractionation of specific source and sink processes affect the integrated isotopic composition of the respective trace gases in the atmosphere. In an inverse approach, ice core isotope records of CH_4 and N_2O provide distinct constraints on biogeochemical processes that can be linked to the variability observed in the CH_4 and N_2O mixing ratios on decadal to millennial timescales (Sowers et al., 2003, 2005; Sowers, 2006, 2009; Ferretti et al., 2005; Schaefer et al., 2006; Fischer at al., 2008; Bock et al., 2010b; Melton et al., 2011a; Sapart et al., 2012). Because ice core records of CH_4 and N_2O isotopic composition indicate the natural response of specific greenhouse gas sinks and sources to palaeoclimate changes, this information is of great interest to global warming predictions.

Here, we present a method to simultaneously measure $\delta^{13}C$ isotope ratios of CH_4 as well as $\delta^{15}N$ and $\delta^{18}O$ isotope ratios of N_2O in a single ice core, firn gas or atmospheric sample. By melting ice core samples under vacuum, between 20 and 50 mL STP (standard temperature and pressure) of air can be extracted from 200–500 g of ice for isotopic analysis. Alternatively, atmospheric samples and reference gases can be injected into the system. The system is highly automated and comprises custom made units to separate CH_4 and N_2O from the main air components (N_2, O_2, Ar) and other trace gases (CO_2, CO) before using a modified gas-chromatography combustion unit coupled to a single isotope ratio mass spectrometer (GC-C-IRMS) in continuous-flow mode for isotope ratio determination. The combustion unit converts CH_4 to CO_2 so that the $\delta^{13}C$-CH_4 is measured as $\delta^{13}C$-CO_2 on the triple collector system of a mass spectrometer (Merritt et al., 1995). Our system includes permanent oxidation, a post-combustion cryo-trap and a second GC column, similar to Melton et al. (2011b). This GC-C-GC-IRMS method ensures a stable oxidation of the combustion reactor with minimized oxygen load into the IRMS, and it excludes interferences of the $\delta^{13}C$-CH_4 measurement with Kr inside the IRMS (Schmitt et al., 2013). The system is anchored to the international isotope scales using reference gases that were synthesized after Sperlich et al. (2012) for $\delta^{13}C$-CH_4 or calibrated by intercomparison measurements with two external laboratories for $\delta^{15}N$-N_2O and $\delta^{18}O$-N_2O. A novelty of this system is the isotope analysis of two isobaric gas species (CH_4-derived CO_2 and N_2O) from one ice core sample using one mass spectrometer in an online measurement mode. Furthermore, we introduce a gold catalyst for quantitative oxidation of CO which – to our knowledge – has hitherto not been used in setups for atmospheric measurements. We suggest the presented system as a powerful tool to provide high-precision isotopic analysis of palaeoatmospheric CH_4 and N_2O.

2 Methods

2.1 Extraction system

The extraction unit (Fig. 1) represents the interface for sample and reference gas introduction into the analytical setup and it includes the first step to separate the analytes from the main air components (N_2, O_2 and Ar). The sample lines of the extraction system are made of 1/4″ stainless steel (SST) tubes and Swagelok components (Swagelok, USA) except for the two six-port valves (V1 and V2) that are manufactured by VICI (VICI, USA) and connected to 1/16″ SST tubing. All connections are either welded or sealed with metal gaskets to exclude artefacts due to out-gassing of polymer gaskets (Sturm et al., 2004). All analytical lines are either continuously flushed by helium (He, 99.9995 %, Air Liquide, Denmark) or permanently evacuated by the turbo-pump (Pfeiffer, Germany).

The gas manifold enables the injection of gas from up to four different gas tanks or sample flasks into the extraction unit via a mass flow controller (referred to as MFC, manufactured by MKS, model 1179A, specified for N_2, 200 mL min^{-1}). A 100 mL sample volume parallel to the MFC enables aliquotation by expansion of gases from the gas manifold into the volume. The pressure reading of gauge "P1" (Keller, 21Y, max. 2 bar) is used to calculate the amount of air in the sample volume. We use two principle methods to introduce samples:

1. Ice core samples are placed in the 1.25 L melt vessel (SST glass adapter, DN 100, MDC vacuum, UK). Reference gases or air from flask samples can also be introduced into the melt vessel or into the water trap (T1) using manual valves and either the MFC or the sample volume. T1 comprises a 20 cm DN 50 SST tube that is welded to a quick flange connector and sealed with an aluminium gasket. Both 1/4″ tubes connecting the water trap are welded onto the opposing quick flange cap. The water trap is filled with glass beads of 3 mm diameter and cooled with a dry-ice/ethanol bath to −78 °C. The second pressure gauge "P2" (Edwards APG100-LC, minimum pressure 10^{-4} mbar) is mounted between T1 and the air-extraction trap (T2) to monitor vacuum and extraction efficiency. The gases can be extracted from the vacuum-extraction line by adsorbing the gases into T2 holding 1.5 g Hayesep D (60/80 mesh, Sigma-Aldrich) when submerged in liquid nitrogen (LN_2). Intensive extraction tests using several charcoal adsorbents (e.g. Norit RO and Fluka 05112, both from Sigma-Aldrich) in T2 showed additional CH_4

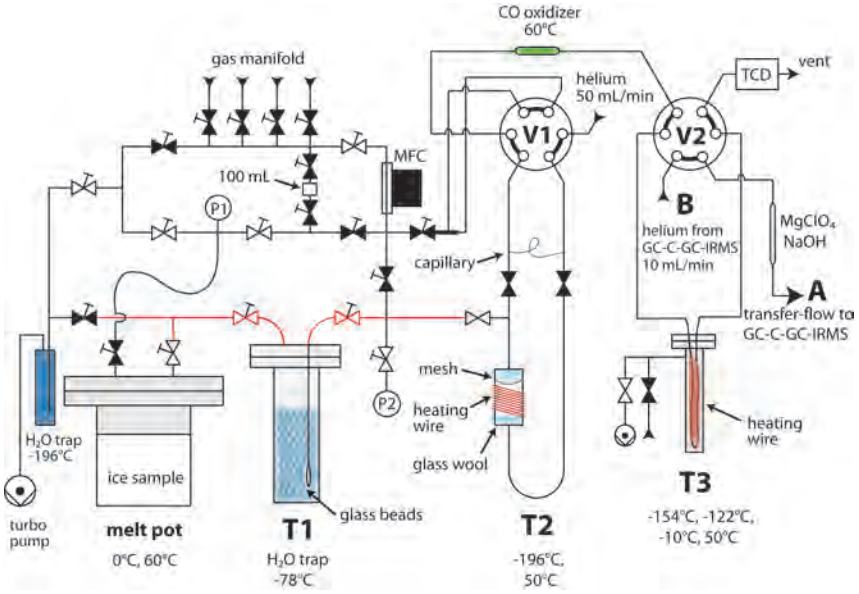

Fig. 1. Extraction unit design and flow scheme. Valve symbols with a handle symbolize manually operated valves, while symbols without a handle indicate automatically actuated valves. Filled valve symbols indicate closed valves; open symbols represent open valves. The figure shows the valve positioning of the extraction line during the melt extraction of an ice core sample. The red lines mark the section of the extraction unit which is thermally insulated and heated to 55 °C. The letters A and B identify the ports of V2 that are connected to the respective port A at V5 and port B at V4 of the GC-C-GC-IRMS setup (Fig. 2). Port A transfers the sample to the GC-C-GC-IRMS unit, while port B receives the carrier-gas flow for A.

contribution and high δ^{13}C-CH_4 variability. We also found that the speed of adsorption can be increased by a factor of 10 when the diameter of the adsorbing trap is increased from 6 to 15 mm. T2 is therefore built from a SST housing (ID $\sim$ 15 mm, F-type filter, Swagelok) welded to a U-shaped 1/4″ SST tube. A concave-shaped SST mesh doubles the area cross section of Hayesep D. Glass-wool plugs on top of the mesh and below the Hayesep D hold the adsorbent in place. T2 adsorbs about 200 mL air (STP) from the extraction line in less than 15 min, and has a maximum absorption capacity of $\sim$ 1.5 L (STP). The trap is equipped with a PID-controlled (proportional-integral-derivative) heating wire (4 m, 12.5 Ω m^{-1}, Type 1 NC 1, Thermocoax) that heats the trap to 50 °C when an automated lift removes the LN_2 Dewar from T2. The air sample is then transported by the extraction flow (50 mL min^{-1} He). A capillary above T2 maintains a He flush flow of 2 mL min^{-1} when the valves of T2 towards V1 are closed (Fig. 1). The SST line and the valves that connect the melt vessel with T1 and T2 are thermally insulated and constantly held at 55 °C with a PID-controlled heating wire.

2. Alternatively, the MFC can inject gas from pressurized tanks into the extraction flow directly when V1 and the manual valves are set accordingly (Fig. 1).

For both sample introduction methods, the sample gas is transported by the extraction flow through the CO oxidizer. Our CO oxidizer is comprised of a 10 cm 1/4″ SST tube holding a gold catalyst over a length of 5 cm (Aurolite™, Au/TiO_2, Strem Chemicals) between two glass-wool plugs that are kept in place by SST meshes at both ends. The CO-oxidizer column is held at 60 °C by a PID-controlled heating wire. The CO oxidizer is followed by the separation trap (T3), which is a modification of the principle described by DesMarais (1978). Thirty centimetres of a 1/8″ SST tube are filled with Hayesep D (80/100 mesh, Sigma-Aldrich, Switzerland) and temperature-controlled to −153, −122, −10 and 50 °C (all ± 0.4 °C) using a PID-controlled heating wire and a Pt-1000 temperature sensor. This 1/8″ tube is routed through an airtight DN 40 SST-cylinder, which can be evacuated or filled with helium. The lower part of the DN 40 tube is submerged in LN_2. To cool T3, the heat conductivity between the Hayesep D-filled 1/8″ tube and the LN_2-cooled DN 40 tube is increased by pressurizing the latter with helium to 2.5 bar. When the trap is heated to −10 or 50 °C, the space between 1/8″ and DN 40 tube is evacuated. T3 retains CH_4, N_2O, CO_2 and Kr at temperatures

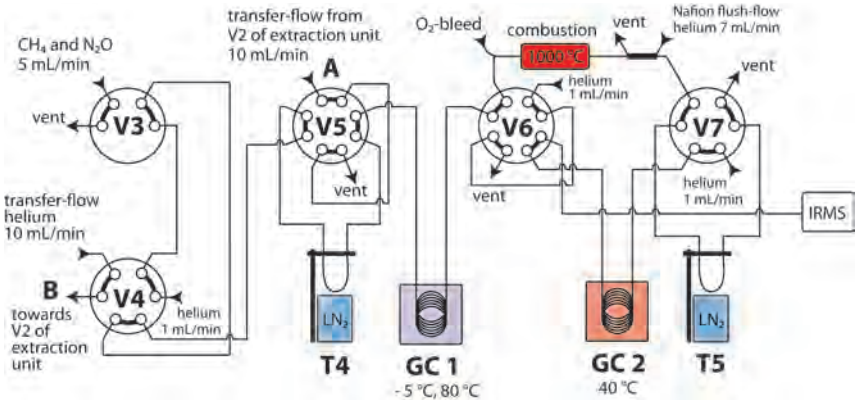

Fig. 2. Flow scheme of the GC-C-GC-IRMS unit. The letters A and B show the valve ports that connect to the ports A and B of the ice extraction unit, respectively. The CH_4 and N_2O sample is delivered to port A of the GC-C-GC-IRMS unit by the helium stream that flows out of the GC-C-GC-IRMS unit at port B.

$\leq -122\,°C$, while most N_2, O_2 and Ar pass through. The effluent of T3 is monitored with a thermal conductivity detector (micro-TCD, VICI) to enable CH_4 and N_2O mixing ratio analysis from TCD and IRMS peak areas. From T3, the sample is transported through a glass tube of 6 mm outer diameter (OD) and 600 mm length that holds Ascarite™ (NaOH, Sigma-Aldrich) to remove CO_2 and $Mg(ClO_4)_2$ (Merck) to remove H_2O.

2.2 GC-C-GC-IRMS system

The final purification and analysis of the air samples occurs via a combined GC-C-GC-IRMS setup (Fig. 2) after the ice core and air extraction unit. All valves are two-position VICI valves, and all tubing either 1/16″ SST tubes or fused silica capillaries. Valve V4 provides the transfer flow (10 mL min^{-1} He) and the analytical flow (1 mL min^{-1} He). Coming from T3, the sample is cryo-focussed on T4, a 55 cm section of GC-column (PoraBOND Q, 0.25 mm ID, Agilent) that can be submerged in LN_2. V4 allows for routing of either the transfer or the analytical flow through the injector valve V3 (2 µL, VICI, USA) for ∼ 1 nmol sized injections of pure CH_4 and N_2O into T3 or T4. These injections were used to tune the timing of the sequences and to monitor the reproducibility and drift during the test phase of the setup. The transfer flow from V4 to the ice extraction unit returns to valve V5 of the GC-C-GC-IRMS section (Fig. 2). This helium flow cryo-focuses the purified CH_4 and N_2O samples in T4. V5 then routes the analytical flow through T4 to introduce the sample gases into GC 1 (PoraBOND Q, 0.25 mm ID, 25 m length, Agilent). GC 1 is submerged in an ethanol bath at −5 °C to increase the chromatographic separation between CH_4 and N_2O to ∼ 160 s. GC 1 can be heated to 80 °C for desorption of H_2O. While it is possible to measure $\delta^{15}N$ and $\delta^{18}O$ in N_2O directly using GC-IRMS, CH_4 samples need to be combusted to CO_2 for $\delta^{13}C$ analysis (Merritt et al., 1995). The CH_4 elutes from GC 1 before N_2O and is routed to the combustion unit via V6. The combustion reactor contains three Ni wires (99.994 %), three Cu wires (99.9999 %) to store and provide oxygen during combustion and two Pt wires (99.997 %) to catalyse the combustion, (all wires are 0.1 mm OD, Alfa Aesar, UK). A small flow of oxygen is constantly added to guarantee maximum oxidation of the combustion reactor at all times in order to ensure a high CH_4 combustion rate (Cullis and Willatt, 1983). Water originating from the combustion process is removed by a Nafion membrane (60 cm length, TT-020, Perma Pure, USA) and a helium counter-flow of 7 mL min^{-1} at −5 °C. The eluting CH_4-derived CO_2 is trapped on T5 comprising of a fused silica capillary (350 µm ID, 55 cm length) submerged in LN_2. To increase the trapping efficiency and to prevent CO_2 loss, the capillary trap T5 contains a Ni wire (99.994 % Ni, 100 µm OD, Alfa Aesar), (e.g. Brand, 1995; Behrens et al., 2008). When the CH_4-derived CO_2 is trapped in T5, V6 redirects the GC flow to analyse the N_2O first. V6 and V7 are then switched, and T5 is removed from the LN_2 bath to pass the CH_4-derived CO_2 through GC 2, which is held at 40 °C (PoraBOND Q, 0.25 mm ID, 25 m length, Agilent) prior to measuring the CH_4-derived CO_2. Helium-flushed purge housings are used on valves V3–V6. The sample gases enter the IRMS (Delta V Plus, Thermo Fisher, Germany) through the open-split interface (ConFlo IV, Thermo Fisher, Germany). Before the N_2O- and CH_4-derived CO_2 samples are introduced into the IRMS, multiple "on/off" peaks of pure N_2O and CO_2 reference gases are applied to stabilize the IRMS (Sect. 3.2).

Table 1. Applied gases. Reference gas names are listed in column 1. Column 2, 3 and 4 show the calibration path for δ^{13}C-CH_4, the determined δ^{13}C and the mixing ratio of CH_4, respectively. The referencing path for N_2O is mentioned in column 5, while column 6, 7, and 8 indicate the δ^{15}N, the δ^{18}O and the mixing ratio of N_2O, respectively. The standard deviation for the isotopic composition of N_2O in GIS is larger compared to the other gases due to the calibration with two gases during measurements that were optimized to measure δ^{13}C-CH_4. The larger scatter results from the measurement of small N_2O amounts. Note that the mean value of the QCS measurements for the isotopic composition of N_2O proves very good accuracy for the calibration of GIS (Fig. 7).

Gas	referencing $[CH_4]$	δ^{13}C-CH_4 [‰]	$[CH_4]$ [ppb]	referencing $[N_2O]$	δ^{15}N-N_2O [‰]	δ^{18}O-N_2O [‰]	$[N_2O]$ [ppb]
GIS	RM-8563	-42.21 ± 0.04[a]	429	NEEM/AL	-1.05 ± 0.6	40.09 ± 0.5	345
NEEM	IMAU/Bern	-47.30 ± 0.01	1839	IMAU/[b]	6.49 ± 0.04	44.58 ± 0.06	322
AL	NEEM/GIS	-49.55 ± 0.16	716	IMAU/NEEM	1.01 ± 0.15	38.8 ± 0.4	272
NOAA	NEEM	-38.57 ± 0.05	1642	IMAU/NEEM	-0.46 ± 0.15	41.06 ± 0.4	332

The uncertainty estimates are based on the standard deviation (1σ) apart from [a], which is described by Sperlich et al. (2012). The [b] indicates when the referencing method of NEEM for the isotopic composition of N_2O is explained by Sapart et al. (2011).

2.3 Referencing to the isotope scales

We used four different reference gases in the described setup (Table 1). GIS (glacial isotope standard) refers to a synthetic air mixture that was prepared after Sperlich et al. (2012) with additional N_2O. An atmospheric air tank was sampled in the year 2008 at a clean-air site of the NEEM camp in northwest Greenland and is hereafter referred to as NEEM. Furthermore, we use two synthetic air mixtures called AL and NOAA that were provided by Air Liquide (Teknisk Luft, Air Liquide, Denmark) and the National Oceanic and Atmospheric Administration (NOAA, Boulder, USA), respectively.

The isotope ratios of all gas standards are referenced to the VPDB isotope scale for δ^{13}C-CH_4 and to the δ^{15}N scale of N_2 air and the δ^{18}O VSMOW scale for N_2O, respectively. The isotopic composition of N_2O in NEEM is prescribed by extrapolating the atmospheric trend between 1990 and 2002 (Röckmann and Levin, 2005) to July 2008, which is the sampling time of the NEEM cylinder. The integrity of our calibration scale for N_2O isotopic composition was tested by inter-calibration measurements of NEEM, AL and NOAA by the Institute for Marine and Atmospheric Research in Utrecht (IMAU), the Netherlands (published in Sapart et al., 2011). The isotopic composition of N_2O in GIS was referenced on the setup described in this paper by calibrating against NEEM and AL. The δ^{13}C-CH_4 in NEEM was calibrated by IMAU and the Institute for Climate and Environmental Physics at the University of Bern, Switzerland (Bern), (Jochen Schmitt, personal communication, 2011). GIS was independently referenced for δ^{13}C-CH_4 against RM 8563 (Verkouteren, 1999) with the δ^{13}C-CO_2 of RM 8563 assigned by Coplen et al. (2006). GIS was previously shown to be in excellent agreement with the externally calibrated NEEM air (Sperlich et al., 2012). AL was referenced for δ^{13}C-CH_4 on the described setup based on NEEM and GIS, while NOAA was calibrated for δ^{13}C-CH_4 by NEEM only. The mixing ratios of CH_4 and N_2O in GIS, NEEM and AL were measured at the Max-Planck-Institute for Biogeochemistry (Armin Jordan and Bert Steinberg, personal communication, 2012), while NOAA was provided with certificates. GIS was chosen as working standard for ice core measurements due to the similar mixing ratio of CH_4. Air samples with higher CH_4 mixing ratios, atmospheric samples such as NOAA, firn air or atmospheric samples, were referenced against NEEM.

2.4 Measurement correction and referencing protocol

The ice core measurement routine is shown in Table 2 and the routine for atmospheric gases from air tanks is shown in Table 3. Blocks of three GIS measurements are bracketing the ice core sample and the quality control standard (QCS) measurements. For each reference gas measurement, 40 mL (STP) of GIS were extracted from T1. The offset between the average isotope ratio determined for each block, and the target isotope ratio assigned to GIS is considered to indicate the daily offset of the system to the international isotope scales, including the system drift between the beginning and the end of the measurement day. The isotope ratio measurements of the ice core samples and the quality control standards are corrected for the sample size offset (Sect. 3.7) first, and then for the system offset as determined by GIS according to Werner and Brand (2001).

2.5 Ice core sample and system preparation

Measurements of ice samples begin with cooling of the H_2O trap T1 in a dry-ice/ethanol bath. To increase the heat conduction within the glass bead bed, T1 is pressurized with helium to ~ 1500 mbar for ~ 2 h. GC 1 is placed in the ethanol bath at $-5\,^{\circ}$C if it has previously been heated to $80\,^{\circ}$C. Meanwhile, ice core samples which are stored at $-25\,^{\circ}$C are prepared in the cold room at $-15\,^{\circ}$C. All surfaces of ice core samples are cleaned by removing the top 3–5 mm with a bandsaw. Attached saw dust is then removed with a scalpel

Table 2. Measurement sequence for ice core samples. A sequence for two ice core sample measurements comprises 11 extraction measurements. Column 2 describes the function of each extraction. Column 3 and 4 show the name and amount of the extracted sample, while column 5 specifies the way the samples are introduced and column 6 shows from which analytical component the respective sample is extracted, where MV stands for melt vessel.

extraction	function	name	amount	introduction	extracted from
1	reference gas	GIS	40 mL	MFC	T1
2	reference gas	GIS	40 mL	MFC	T1
3	reference gas	GIS	40 mL	MFC	T1
4	ice core sample	[...]	200–500 g	manual	MV
5	blank test	blank	–	–	MV
6	QCS	AL	30–50 mL	MFC	T1
7	ice core sample	[...]	200–500 g	manual	MV
8	blank test	blank	–	–	MV
9	reference gas	GIS	40 mL	MFC	T1
10	reference gas	GIS	40 mL	MFC	T1
11	reference gas	GIS	40 mL	MFC	T1

or brushed off while the ice sample is carefully checked for anomalous features. To prevent contamination by laboratory air and/or drill-fluid intrusion, cracked parts are removed from each sample. Also, layers with exceptionally high content of dust or soot particles were cut out to prevent artefacts (Rhodes et al., 2013). On average, 30 % is removed from each sample. The decontaminated ice sample and a glass-coated magnet stir bar are then placed inside the melt vessel, which is sealed with a copper gasket and fastened with 16 bolts to 25 Nm torque. Two samples are prepared and stored in a −20 °C chest freezer to be analysed the same day. The analytical system is finally prepared by evacuating T1 as well as all lines and pressure regulators of the atmospheric reference gases connected to the gas manifold (Fig. 1). The measurement routine is started when the pressure inside the extraction system reaches 10^{-3} mbar, indicating the system is sufficiently leak-tight and dried after previous analysis.

After every day of ice core measurements, the melt vessel is cleaned with ultra-pure water and detergent soap for laboratory glassware (Alconox™, USA), as suggested by Mitchell et al. (2011), before it is dried at 80 °C overnight. To remove trapped water from T1, it is heated to 150 °C with a PID-controlled heating sleeve. The elevated temperature of the extraction line (55 °C, Fig. 1) promotes the drying efficiency of the whole extraction line. Under vacuum, any water is rapidly transferred from the heated parts into the water trap (LN_2 cooled) close to the turbo-pump. This water trap can easily be opened to remove the water. With this method, we avoid opening the connectors in the extraction line.

Table 3. Measurement sequence for air samples from flasks or tanks. The presented sequence is used for triplet measurements of two samples, bracketed by reference gas triplets. Column 2 describes the function of the measured gas, which is described and quantified in column 3 and 4, respectively. Column 5 indicates that all samples are injected through the mass flow controller (MFC) directly into T3 or to be extracted from T1, as indicated in column 6.

extraction	function	name	amount	introduction	extracted from
1	reference gas	NEEM	40 mL	MFC	T1/T3
2	reference gas	NEEM	40 mL	MFC	T1/T3
3	reference gas	NEEM	40 mL	MFC	T1/T3
4	air sample 1	[...]	40 mL	MFC	T1/T3
5	air sample 1	[...]	40 mL	MFC	T1/T3
6	air sample 1	[...]	40 mL	MFC	T1/T3
7	reference gas	NEEM	40 mL	MFC	T1/T3
8	reference gas	NEEM	40 mL	MFC	T1/T3
9	reference gas	NEEM	40 mL	MFC	T1/T3
10	air sample 2	[...]	40 mL	MFC	T1/T3
11	air sample 2	[...]	40 mL	MFC	T1/T3
12	air sample 2	[...]	40 mL	MFC	T1/T3
13	reference gas	NEEM	40 mL	MFC	T1/T3
14	reference gas	NEEM	40 mL	MFC	T1/T3
15	reference gas	NEEM	40 mL	MFC	T1/T3

2.6 Measurement procedure

2.6.1 Ice core samples

In order to minimize the time between the measurements, samples are introduced into the extraction unit while the previous sample is analysed in the GC-C-GC-IRMS section of the setup. This results in a sample interval of only 42 min. Ice core samples and reference gases are treated as similar as possible in order to balance analytical effects during analysis, following the principle of identical treatment (Werner and Brand, 2001). However, one difference exists in the application and extraction of ice core and reference gas sample: the MFC is used to inject reference gas into T1, from where it is extracted into T2. In contrast, ice core samples release the air during melting inside the melt vessel from where the gas is continuously cryo-pumped through T1 into T2. This is the only gas-handling difference between ice core sample and reference gas. We tested for isotope fractionation effects based on the different gas handling but found no significant isotope fractionation in our setup (see Sect. 3.7). The continuous extraction technique minimizes the pressure and the time the gas is in contact with the melt water as to reduce gas dissolution.

Every analysis begins with the evacuation of the extracting unit. The thoroughly cooled T1 represents the cavity for reference gas extractions, and is evacuated for 6 min prior to reference gas introduction. To measure an ice core sample, the melt vessel is attached during the previous reference gas measurement so it can be evacuated for 20–30 min without

delaying the measurement routine. During this time, the melt vessel is cooled in an ice water bath to prevent the sample from melting ahead of schedule. The measurement routine then continues with cooling T2 in LN_2 for 8 min in preparation for the extraction of ice core air or reference gases. Towards the end of cooling T2, reference gases are injected into T1, or the ice bath under the melt vessel is replaced by a hot water bath (60 °C) to start melting the ice. When T2 has cooled for 8 min, the air extraction is started by opening the valve between T1 and T2 and the melt vessel for ice extractions. After 40 mL (STP) of reference gas have been extracted for 13 min, the pressure within the extraction unit (P2) decreased from 14 mbar to 0.07 mbar, indicating 99.5 % extraction efficiency. The pressure decrease during extractions is very reproducible, and only varies with the amount of air and the variable melting time of ice core samples. By ensuring that reference gas and ice core samples are extracted to similar pressures, isotope fractionation effects based on variable completeness of extraction cancel out. The IRMS operating software (ISODAT) is started as soon as the pressure in the extraction system is lower than 0.11 mbar (P2), thereby ensuring identical extraction efficiency for all samples.

When the extraction has ended, reference gases and samples are subject to identical analytical procedures, precisely timed by the ISODAT script. First, T3 is cooled to −154 °C within 1 min and is held constant by the PID controller. After T3 has cooled for 4 min, the extraction is stopped. T2 gets heated from −196 to 50 °C in less than 1 min, thereby desorbing the sample within the extraction flow and transferring the sample from T2 through the CO oxidizer to T3. T3 separates N_2, O_2 and Ar from the sample gas mixture and retains CH_4, N_2O, CO_2 and Kr on the Hayesep D. At the same time, the temperature of T3 is increased to −122 °C to improve the separation performance of T3 (Umezawa et al., 2009). Residual N_2, O_2 and Ar will be separated later in the GC-C-GC-IRMS section. The TCD signal to measure the amount of N_2, O_2 and Ar is recorded using a LabView script. The separation in T3 is completed after 400 s. V2 is then switched and T3 heated to −10 °C so the transfer flow can carry the desorbing trace gases through the chemical trap into the capillary trap T4, which was submerged in LN_2 10 s before. CH_4 and N_2O are focussed in T4 after 360 s, V2 is then switched and T3 heated to 50 °C to vent residual water. Next, V5 is switched and the analytical flow transports both sample gases from T4 through GC 1 as T4 gets lifted from the LN_2 bath. It takes about 220 s for the CH_4 to pass through GC 1 and to enter the combustion oven. After 200 s, the post-combustion trap T5 is lowered into a LN_2 bath to trap the CH_4-derived CO_2.

After 80 s of post-combustion trapping, all CH_4-derived CO_2 is trapped in T5, and V6 gets switched to route the analytical flow directly to the open split and the IRMS for the isotopic measurement of N_2O. Meanwhile, V7 gets switched to a pure helium flow of 1 mL min^{-1} to remove the oxygen from T5. When the N_2O measurement is completed, V6 gets switched to route the CH_4-derived CO_2 from T5 through GC 2 into the open split for isotopic analysis in the IRMS. In the mean time, T1 and T2 are evacuated in preparation for the following sample.

2.6.2 Air samples

The analysis of air samples is similar to the analysis of ice core samples, and differs only in the fully automated introduction of air samples if the samples are applied from pressurized vessels. Air tanks can be connected to the gas manifold where the MFC introduces the samples through V1 into the extraction flow (Fig. 1). A sample flow time of 90 s allows for the sample and helium flows to equilibrate before V2 is switched to direct the sample into the pre-cooled T3. After this point, the analysis is exactly the same as described in Sect. 2.6.1; however, only one sample is introduced and analysed at a time. If the air samples are at sub-ambient pressures, they are introduced to T2 through the sample volume to be extracted like the reference gases during ice core measurements.

2.6.3 Sampling for system blank

System blank tests are determined after every ice core sample extraction (Table 2). For this purpose, the valves of the extraction line get closed when the ice extraction is completed. The sample vessel with the extracted sample is thereby kept under vacuum, but it can collect air from potential leakage into the extraction unit. The extraction volume is then extracted for 5 min and processed as a regular sample.

3 Results and discussion

3.1 CO oxidizer

Using the post-combustion trap strictly requires the elimination of any potential interference of non-CH_4 gases (CO and CO_2) with the CH_4-derived CO_2 in the mass spectrometer. To exclude any spurious CO contribution, CO is quantitatively oxidized to CO_2 and then removed by the Ascarite trap (Fig. 1). Schütze reagent is often used in analytical setups to oxidize CO to CO_2 at room temperatures when the CO is to be analysed for its isotopic composition of $\delta^{13}C$ and $\delta^{18}O$ (e.g. Brenninkmeijer, 1993). Alternatively, Sofnocat or hopcalite can be applied as oxidation catalyst (e.g. Kato et al., 1999). However, the CO-oxidation efficiency of both catalysts decreases with increasing moisture content (McPherson et al., 2009). To our awareness, this is the first system described for atmospheric measurements using Aurolite as catalyst to oxidize CO to CO_2. The efficiency of Aurolite is reported to even improve with increasing moisture content in the sample gas stream (e.g. Date et al., 2002; McPherson et al., 2009), making it particular suitable for CO elimination in air extracted from melted ice core samples. Our CO oxidizer is heated to 60 °C to increase the CO oxidation

efficiency (Date et al., 2002), while the oxidation of CH_4 can be ruled out at temperatures below 130 °C (Walther et al., 2009). We chose Aurolite on TiO_2 support because of its superior conversion efficiency and gold particle stability compared to Al_2O_3 and ZnO (Walther et al., 2009).

To test the system, synthetic CH_4- and CO_2-free air with a CO mixing ratio of 350 ppb was mixed in the setup described by Sperlich et al. (2012). This air mixture was applied to the system with and without the CO oxidizer as well as with a trap holding Schütze reagent (iodine pentoxide, 99.99 %, Sigma-Aldrich) inside a 6 mm OD glass tube over a length of 150 mm. The timing of the GC-C-GC-IRMS system was adjusted to fully combust, trap and analyse the residual CO that eluted from GC 1. Note that the CO that was oxidized in the CO oxidizer or in the Schütze reagent was chemically trapped on the Ascarite trap (Fig. 1) and therefore not detected. A series of experiments with Aurolite showed no CO-derived CO_2 peak that exceeded the normal blank peak, while up to 90 % of the CO passed through the Schütze reagent unoxidized. Our tests suggest that Aurolite quantitatively oxidizes CO in atmospheric samples and is significantly more reliable to oxidize CO than commercial Schütze reagent, and it also has the benefit of being immune to moisture. Based on the gold nanoparticle size stability reported by Date et al. (2002) and Walther et al. (2009), and the fact that our CO oxidizer is in contact with far less than 1 L of air per measurement day, we expect the CO oxidizer to be stable for many years.

3.2 Preparing the IRMS for measurement of two different gases

While only a small fraction of the analyte molecules that enter the ion source of an IRMS get ionized and reach the detector, other sample molecules can be subject not only to unintended physical and chemical interactions with the analytical system itself but also with molecules of other gas species present in the analyser. Potential effects include system memory, adsorption and desorption of gases altering the background levels, ion reactions (Anicich, 1993), reactions enabled by the hot filament and a combination of all (Brand, 2004). Measuring two isobaric gases such as N_2O and CO_2 in the same sample on the same IRMS can reduce the precision significantly if the conditions inside the IRMS vary throughout the measurements (Carter and Barwick, 2011). To increase the stability of our analyser, we inject a large pulse of pure reference gas into the ion source for 1 min before the start of each measurement sequence. The following measurement sequences are comprised of 10 or 12 flat-topped peaks of pure CO_2 or N_2O reference gas for CH_4-derived CO_2 and the N_2O measurement, respectively (Fig. 3). This enables simultaneous improvement and monitoring of the reproducibility before the sample peak enters the IRMS. The standard deviation of the three flat-topped reference gas peaks preceding the sample is 0.029 ‰ for

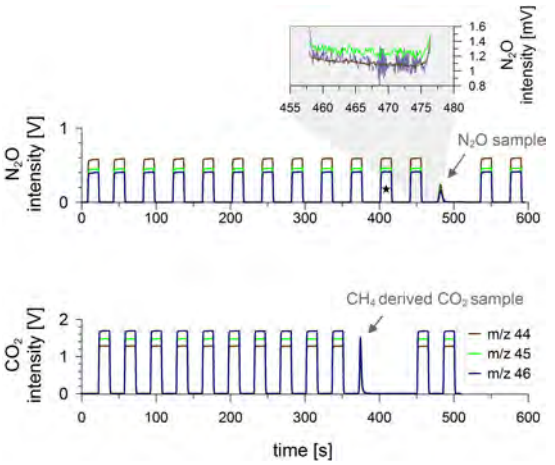

Fig. 3. Chromatograms with the three *m/z* 44, 45 and 46 traces for CH_4 (bottom panel) and of N_2O (top panel) measurements. The enlargement in the top panel shows the background before the N_2O sample peak in detail (units in mV). The flat-topped peaks in the main chromatograms are "on/off" peaks from pure N_2O and CO_2 reference gases. The chromatograms show the measurement of an ice core sample with low N_2O and CH_4 mixing ratios, typical for glacial periods. Reference gas peak 11 of the N_2O measurement (marked with star) includes a very small CO_2 remainder (not visible) stemming from system blank and incomplete CO_2 removal by the Ascarite. We use its isotopic composition to monitor the performance of the Ascarite trap (Fig. 1).

δ^{13}C-CO_2, 0.061 ‰ for δ^{15}N-N_2O and 0.086 ‰ for δ^{18}O-N_2O, respectively (average of 66 measurement sequences). These values refer to reference gas peak 8, 9 and 10 in the CH_4-derived CO_2 sequence and 9, 10 and 12 in the N_2O sequence (peak number 11 in the N_2O sequence is not considered due to the small contribution of CO_2 (caption of Fig. 3). The traces show baseline separation for ≥ 5 s between reference gas and sample peaks in all chromatograms, which is the time interval used for baseline determination as part of the peak integration parameters. Measurements of atmospheric and synthetic air mixtures with precisely referenced δ^{13}C-CH_4 (Sperlich et al., 2012) suggest this conditioning method of the IRMS showed no significant η effect (Brand, 2004) over δ^{13}C-CH_4 range of 5 ‰, reflecting the magnitude of δ^{13}C-CH_4 variability in firn and ice core samples (e.g. Fischer et al., 2008).

3.3 Excluding krypton interference

Krypton – which is abundant in the atmosphere at ~ 1 ppm (Aoki and Makide, 2005) – was found to co-elute from the GC column with CH_4 and interfere with the analysis of CH_4-derived CO_2 (Schmitt et al., 2013). The system described here deploys a post-combustion cryo-trap followed by a second GC column (Fig. 2). This combination ensures cryogenic

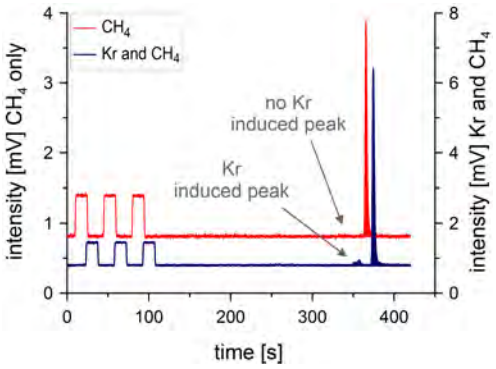

Fig. 4. A small krypton signal is visible when comparing the *m/z* 43 traces of δ^{13}C-CH_4 measurements in an atmospheric air mixture (dark-blue line, right axis) and in a pure CH_4 gas (red line, left axis), where the latter contains no Kr. Both peaks of CH_4 occur on *m/z* 43, while the baseline separated peak induced by remnant Kr occurs only in the atmospheric sample. To avoid an overlap of the displayed peaks, the chromatogram of the pure CH_4 is shifted by 15 s.

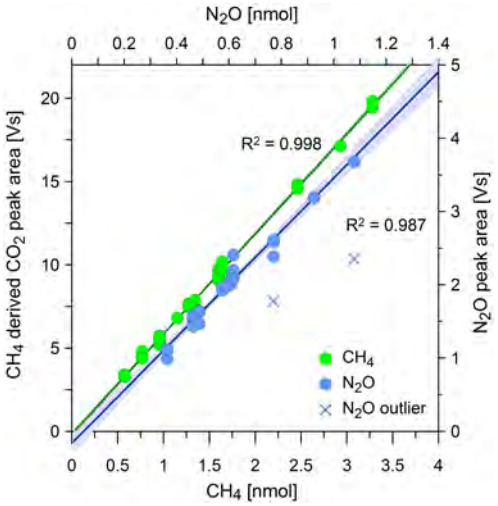

Fig. 5. Sample recovery. Green circles show the injected CH_4 amount [nmol] and the resulting IRMS peak area [Vs] as detected during bubble-free ice measurements with the injection of four different air mixtures in variable amounts. Blue circles display analogue information for N_2O. The two blue crosses show outliers of N_2O that suffered from a loss of IRMS peak area for unknown reasons. Both outliers are therefore not included in the calculation of the regression, which are shown with 95 % confidence interval.

separation of CH_4-derived CO_2 and Kr in T5 as only fractions of the Kr get trapped in T5 at LN_2 temperature. After the cryogenic separation, GC 2 ensures chromatographic separation of CH_4-derived CO_2 and remaining Kr. To test the Kr impact, the CO_2 gas configuration was modified to monitor the mass triplet *m/z* 43/44/45 during a CH_4 measurement instead of *m/z* 44/45/46 (Fig. 4). This test showed a crippled peak from $^{86}Kr^{++}$ on *m/z* 43 which precedes the δ^{13}C-CH_4 measurement of atmospheric air with baseline separation of 10 s between Kr- and the CH_4-derived CO_2 peak on *m/z* 43 (Fig. 4). In this case, the sample peak produced a small signal on *m/z* 43, as can also be seen for the three reference gas peaks (pure CO_2) at the beginning of both sequences. In comparison, injections of pure CH_4 via V3 into T4 underwent exactly the same analytical steps in the GC-C-GC-IRMS section but did not show the crippled $^{86}Kr^{++}$ peak on *m/z* 43 at all (Fig. 4). This test identifies the crippled peak from $^{86}Kr^{++}$ in the air sample and proves that our δ^{13}C-CH_4 measurements are not affected by Kr interferences.

3.4 Shot noise

We apply the approach of Merritt et al. (1994) to calculate the shot noise for the different analytes and the average peak areas of reference gases and samples. We calculated a shot-noise range on the 1-σ level of 0.04–0.05 ‰ for δ^{13}C-CH_4, 0.11–0.17 ‰ for δ^{15}N-N_2O and 0.15–0.22 ‰ for δ^{18}O-N_2O. The calculated shot-noise ratio may therefore explain between 40 and 50 % of the measurement uncertainty for δ^{13}C-CH_4 and between 20 and 29 % and 21–31 % of the uncertainty of the δ^{15}N and δ^{18}O measurements of N_2O, respectively. The remaining uncertainty is most likely based on the variability of the sample preparation. Generally, the shot-noise ratio is larger for N_2O than for CO_2 due to the lower abundances of the rare isotope (1.1 % ^{13}C, 0.37 % ^{15}N and 0.201 % ^{18}O, e.g. Sessions, 2006) and the signal intensity of N_2O as compared to CH_4-induced CO_2, due to lower mixing ratios (e.g. Schilt et al., 2010) and ionization efficiency (Friedli and Siegenthaler, 1988; Ghosh and Brand, 2004).

3.5 Sample recovery of injected air standards

Figure 5 shows the sample recovery as the response of the system to sample size variations between 0.5 and 3.2 nmol CH_4 and 0.3 and 1.1 nmol N_2O. The measurements are based on the extractions of air samples between 20 and 70 mL, respectively (Sect. 3.7). Since the valves to route the MFC injection of reference gases into the extraction line were manually controlled, a small variability of the applied volume and hence in IRMS peak area of CH_4-induced CO_2 and N_2O could not be avoided. The linear regression of the average IRMS peak area over the injected sample size shows an R^2 of 0.998 and 0.987 for CH_4 and N_2O, respectively. We therefore conclude the extraction unit and the components of the GC-C-GC-IRMS system responded linearly to sample size variability, indicating appropriate system design and timing steps enabling quantitative analysis within the expected sample size range.

3.6 System blank tests

The detected system blanks represent an integrated signal of system leakage and contamination within the analytical gas streams, but more importantly, they represent ice-sample-specific leakage through the melt vessel gasket as well as sample remnants from incomplete extractions. Another theoretical source of N_2O blank peaks is the microbial production of N_2O from NO_3 and NH_4. This N_2O production might take place after the ice core extraction, while the melted sample remains in the melt vessel (Jochen Schmitt, personal communication, 2013). However, we have no evidence for this process and cannot distinguish between all contributing sources.

We compared the IRMS peak areas of each blank test to the IRMS peak areas of the preceding ice core sample for 35 ice core measurements, and found blank peak areas with an average size of 1.5 and 3.0 % of the preceding CH_4 and N_2O sample, respectively. The N_2O blank size neither correlates with the CH_4 blank nor could any anomalous signal be detected on the TCD, precluding leakage from laboratory air. We speculate that the higher N_2O blank values resulted from ice core air remnants due to higher solubility as compared to CH_4 or in situ production during melting. In fact, 12 out of 35 blank tests showed a peak area that exceeded 5 % of the peak area of the preceding N_2O sample. The blank tests of the other 23 ice core samples averaged to 1.1 % of the sample peak area. These tests might indicate limitations in the extraction efficiency for N_2O during the melt extraction as compared to the extraction efficiency of CH_4. Because the isotope ratios of such small peaks are not unambiguously detectable, we do not apply blank corrections to our isotope measurements.

During the test phase of the setup, we installed a helium flow of 200 mL min^{-1} to strip dissolved gases from the melted ice core sample after the majority of the gases have been extracted as described in Sect. 2.6.1. Unlike Behrens et al. (2008) and Bock et al. (2010a), we pumped on the extraction line at the downstream end of T2 to absorb the sample gases on T2 while removing the helium for 5–10 min. Measurements of ice core samples that were extracted with the stripping method did not show a significant blank reduction or a reduced variability of isotopic analysis for CH_4 and N_2O, and did not conclude a more efficient extraction method. The stripping technique was thus excluded from the setup.

3.7 System calibration with bubble-free ice measurements

We follow the approach of Sowers and Jubenville (2000), Bock et al. (2010a) and Sapart et al. (2011) to calibrate our ice core extraction systems using artificial, bubble-free ice (BFI). We measured a total number of 35 air standard extractions over eight BFI samples. The first air standard was injected over the frozen BFI sample in the evacuated melt vessel. The BFI was then melted completely before the extraction was started. After the first extraction, the melted BFI sample was kept in the melt vessel under vacuum. Air standards were then injected over the melted BFI sample and the extraction started after 2 min. The air standards were taken from four different air mixtures (GIS, AL, NEEM, NOAA, Table 1), each with different isotopic composition and different mixing ratios of CH_4 and N_2O, respectively. By analysing between 20 and 70 mL (STP) of the air standards, the calibration experiments covered a large range of sample sizes including the amount of sample air to be expected from the extraction of 200 to 500 g of glacial and interglacial ice core samples (Fig. 6).

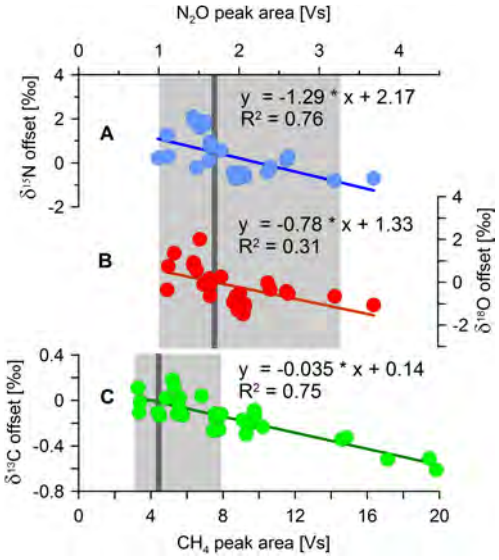

Fig. 6. Impact of sample size variability on the isotopic composition of δ^{15}N-N_2O **(A)**, δ^{18}O-N_2O **(B)** and δ^{13}C-CH_4 **(C)**. The offsets in isotopic composition of CH_4 and N_2O were determined in 33 and 26 BFI extractions, respectively. The dark-grey lines indicate the IRMS peak area of the reference gas measurements (GIS), which were used to reference the BFI samples to the respective isotope scales. The shaded zones indicate the IRMS peak area range of ice core sample measurements. Coloured lines display the linear regressions that are used to correct the isotopic composition of sample measurements for the difference in IRMS peak area between sample and reference gas.

Two BFI samples that were produced in the same BFI batch contained dissolved gases that only affected their first BFI measurement that included their melt process. This observation is in line with the description of Bock et al. (2010a), who found dissolved gases in BFI samples even though the BFI contained no visible gas inclusions. The stability of the consecutive extractions over melted BFI showed that a melted sample was completely degassed by the previous air extraction. Changing the air standards of two

consecutive injections showed no memory effect in the isotope ratios of CH_4 or N_2O, highlighting quantitative extraction. A significantly increased variability in both N_2O isotope ratios occurred during two days of BFI measurements. The data of these measurements were excluded, resulting in less N_2O data of BFI measurements as compared to CH_4 (Fig. 6). We speculate that this effect is based on disequilibration effects inside the Hayesep D in trap T2 after longer standby times. Regular use of T2 or pre-conditioning it with adsorption–desorption cycles in case T2 has not been used for a while stabilized the N_2O isotope ratios. However, CH_4 measurements were unaffected. The system returned to stable analysis the following day.

The isotope ratio of the BFI measurements was referenced via reference gas injections of 40 mL (GIS) to the respective international isotope scales. The linear regression of the isotope ratio offset versus the sample peak size is used to correct for differences in analyte amount of ice-core-air extractions from the melt vessel and reference gas extractions from T1 (Fig. 6). We find no significant isotope fractionation between the extractions from T1 and from the melt vessel for experiments with identical amounts of analytes. We therefore conclude that there is no significant offset between the extraction of reference gases from T1 and ice core samples from the melt vessel, and that the occurring fractionation is only based on the analyte amount. The correction according to the linear regression (Fig. 6) therefore covers the necessary corrections that relate all samples to the isotope scales as defined by 40 mL of the reference gas (Sect. 2.3). The sample-size-corrected BFI measurements show a standard deviation (1σ) of 0.09 ‰ for δ^{13}C-CH_4, 0.5 ‰ for δ^{15}N-N_2O and 0.7 ‰ for δ^{18}O-N_2O.

3.8 Quality control standard measurements

One QCS measurement was included in each routine for ice core measurements (Table 2). The QCS were varied in size and evaluated as an unknown sample with corrections for size- and system variability (Sect. 3.7). The results of 17 QCS measurements for δ^{13}C-CH_4, δ^{15}N-N_2O and δ^{18}O-N_2O of the QCS from an ice core measurement campaign are plotted in the performance chart (Fig. 7). Because the BFI tests showed no detectable isotope fractionation between the BFI extractions from the melt vessel and the reference gas extractions from T1, we consider the QCS measurements representative to indicate the magnitude of the measurement uncertainty that is inherent to the analysis of ice core samples. The standard deviation of the QCS measurements is therefore an important measure for the precision of the system. The estimated measurement uncertainty for δ^{13}C-CH_4 is 0.08 ‰ and 0.6 ‰ for both δ^{15}N-N_2O and δ^{18}O-N_2O, based on the 1σ standard deviation of the QCS measurements.

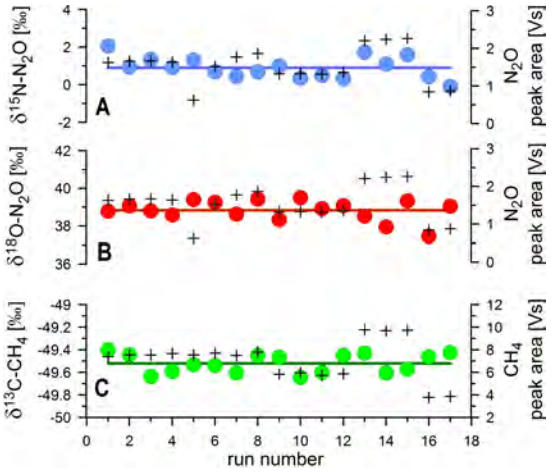

Fig. 7. Results of QCS measurements. The circles of the performance chart display the isotope ratio measurements of δ^{15}N-N_2O **(A)**, δ^{18}O-N_2O **(B)** and δ^{13}C-CH_4 **(C)** as determined during the QCS measurements by injecting variable amounts of AL. The crosses relate to the y axis on the right-hand side and indicate the IRMS peak area of the respective measurement. The lines show the average δ values of the measurements.

3.9 Reproducibility of ice core measurements

We measured 13 ice core samples (200–500 g) from the EUROCORE and NEEM ice core (gas age 657–1766 AD) to compare the performance of the setup with published δ^{13}C-CH_4 data (Fig. 8). Eleven of these samples are measured as replicates that are divided into four groups of 2–4 samples with a maximum age difference within each group of less than 14 yr. These sample groups can be assumed to contain air of similar composition (Buizert et al., 2012). The pooled standard deviation for δ^{13}C-CH_4 in these 11 samples of 0.07 ‰ is a representative measure for the reproducibility of ice core measurements. Unfortunately, we cannot provide the corresponding N_2O data of these samples as the measurement routine for N_2O measurements was not fully developed at the time these ice core measurements were done.

3.10 Precision of the setup

Multiple gases which differ in the isotopic composition as well as in the mixing ratio of CH_4 and N_2O were injected over BFI to calibrate the system. One measurement of AL in variable amounts was included as QCS measurement during every day of ice core measurements to monitor the performance of the analytical setup including the data processing. Finally, we showed the reproducibility for the δ^{13}C-CH_4 measurements of the setup by the pooled standard deviation of 11 pre-industrial ice core samples between 200 and 500 g. We find the uncertainty estimate based on the analysis of ice

core samples most representative. However, its comparability is restricted because each ice core sample represents a unique air mixture that may be affected by atmospheric variability and the stochastic nature of bubble trapping. Therefore, even two adjacent ice core samples are not necessarily 100 % identical. This problem of system calibration can be circumvented by repeated analysis of reference gases from pressurized tanks. For the δ^{13}C-CH_4 measurement, the uncertainty estimates as derived from the BFI measurements, the QCS measurements and the pooled standard deviation of ice core sample measurements are in good agreement, suggesting that a realistic measurement uncertainty is estimated by all three methods. For the isotopic analysis of N_2O, the uncertainty estimate of the BFI and the QCS measurements also agree well. Based on the good match of the uncertainty estimates discussed for δ^{13}C-CH_4, we suggest that the uncertainty of N_2O measurements can reliably be estimated from the BFI and QCS measurements. For all measured parameters, we chose to state the uncertainty with the highest value, independent of the method from which it was derived. We therefore conclude a measurement uncertainty of 0.09 ‰ for δ^{13}C-CH_4 (BFI), 0.6 ‰ for δ^{15}N-N_2O (QCS) and 0.7 ‰ for δ^{18}O-N_2O (BFI), which is comparable to or better than those of Sowers et al. (2003), Ferretti et al. (2005), Schaefer and Whiticar (2007), Behrens et al. (2008), Sowers (2009), Sapart et al. (2011) and Melton et al. (2011b).

3.11 Comparison to published ice core data and established systems

3.11.1 δ^{13}C-CH_4

We measured a total of 13 EUROCORE and NEEM ice core samples for δ^{13}C-CH_4 and compared our results with NEEM ice core data that were recently published by Sapart et al.(2012) as shown in Fig. 8. The data from Sapart et al. (2012) were corrected for the Kr effect, which was not known at the time of publication. The Kr-corrected IMAU data are between 0.15 and 0.88 ‰ more depleted in δ^{13}C-CH_4, depending on the CH_4 mixing ratio, where the highest correction was applied to the samples from the industrial period. Our data and the Kr-corrected data from Sapart et al. (2012) will be referred to as CIC and $IMAU_{Kr}$, respectively. We selected six data points of the $IMAU_{Kr}$ dataset between 677 and 1757 AD and measured between one and four samples per $IMAU_{Kr}$ data point on our setup. The mean gas age of the CIC and the respective $IMAU_{Kr}$ samples differed between 1 and 24 yr. Greenland ice core samples have been shown to integrate the atmospheric variability over a period of about 35 yr (Buizert et al., 2012). We therefore consider the compared samples to represent similar air samples.

CIC and $IMAU_{Kr}$ data show excellent agreement during five time intervals that cover a δ^{13}C-CH_4 range of nearly 2 ‰ (Fig. 8). However, we found a disagreement between $IMAU_{Kr}$ and the mean of four CIC samples (three Eurocore, one NEEM) during the δ^{13}C-CH_4 excursion reported by Sapart et al. (2012) at 964 AD, where the $IMAU_{Kr}$ sample is more enriched in δ^{13}C-CH_4 by $\sim$ 1 ‰. Between 900 and 1000 AD, three $IMAU_{Kr}$ samples agree well, which rules out that the disagreement is based on one outlier. Since we can exclude Kr interference as the reason for the offset, we speculate that the differences between CIC and $IMAU_{Kr}$ are due to differences in the ice core samples, the sample preparation or the ice extraction technique.

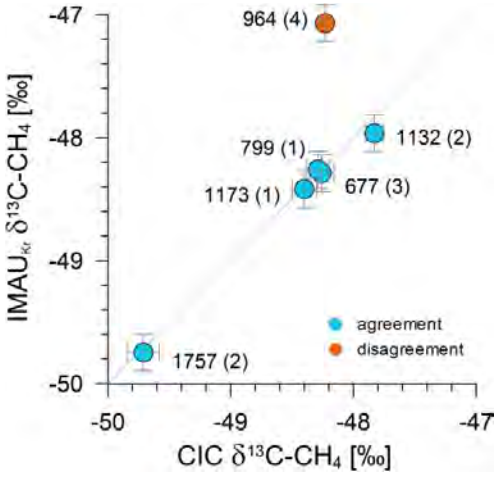

Fig. 8. Comparison of CIC and $IMAU_{Kr}$ δ^{13}C-CH_4 ice core data (the index in $IMAU_{Kr}$ indicates the data have been corrected for the Kr effect). Blue circles indicate data comparison of time sections where good agreement was found. The orange circle indicates the comparison where CIC and $IMAU_{Kr}$ found a disagreement of $\sim$ 1 ‰. Error bars indicate the measurement uncertainty or the average of the measurements used for the laboratory comparison. Bracketed numbers indicate the numbers of samples measured at CIC for the respective comparison, while numbers without brackets display the time (AD) of the $IMAU_{Kr}$ samples.

At about 950 and 1000 AD, Rhodes et al. (2013) show several spikes of excess CH_4, measured on a shallow NEEM ice core. The strongest of these CH_4 artefacts (+78 ppb) was detected in a depth of 272.1 m, which is close to the samples of Sapart et al. (2012) from 964 and 1009 AD (269.5 m and 278.3 m, respectively) but even closer to the depth of the one NEEM sample that was measured at CIC for this intercomparison (272.8 m). Note that the samples of Rhodes et al. (2013) were taken from a shallow core at NEEM, while the discussed NEEM samples are taken from the main core. The age–depth relation may vary slightly between the two cores, which hampers drawing unambiguous conclusions.

One hypothesis is that impurities in the ice are related to excess CH_4 (Rhodes et al., 2013) and thus possibly caused the disagreement between CIC and $IMAU_{Kr}$. While ice core layers that contained visible particles were removed during

sample preparation at CIC, small particles were observed and retained within one $IMAU_{Kr}$ sample that shows the disagreement. However, adjacent $IMAU_{Kr}$ samples with and without visible particles agree well in δ^{13}C-CH_4, as is confirmed from other depth ranges, thereby questioning the hypothesis that particles in the ice necessarily create artefacts in δ^{13}C-CH_4. Thus, the link between particles and δ^{13}C-CH_4 offset remains speculative.

One analytical difference between CIC and $IMAU_{Kr}$ is the technique to extract air from ice core samples. While a continuous melt-extraction technique is used at CIC, $IMAU_{Kr}$ data are based on a dry-extraction technique (Sapart et al., 2011). Both techniques are optimized for high extraction efficiency, and both techniques are shown to produce very similar results. It is therefore unlikely that conceptual differences of the extraction techniques alone caused the observed disagreement in δ^{13}C-CH_4.

Because the data comparison between CIC and $IMAU_{Kr}$ shows excellent agreement during all other time intervals, we find our setup suitable for δ^{13}C-CH_4 measurements in ice core samples. A δ^{13}C-CH_4 record of firn air samples was measured on our setup and also shows very good agreement with the results from other systems as published by Sapart et al. (2013).

3.11.2 δ^{15}N-N_2O and δ^{18}O-N_2O

A flask intercomparison study for N_2O isotope ratios in three different gas mixtures was conducted to compare our setup to the setup described by Sapart et al. (2011). The air mixtures used for this test varied by ~ 7 and ~ 6 ‰ in δ^{15}N and δ^{18}O, respectively (Table 1). The results for all gases showed excellent agreement within the uncertainty of the measurements and were published earlier (Sapart et al., 2011).

So far, intercomparison measurements on isotope ratios of N_2O ice core samples have not been made in the ice core community, and data for the time period of our δ^{13}C-CH_4 comparison measurements (657–1766 AD) are lacking. We therefore cannot give an ice core intercomparison at this stage but emphasize the need for such a study in the future.

4 Summary and conclusions

We introduced Aurolite as reliable catalyst for the oxidation of CO. Based on our test we conclude that Aurolite is useful to produce CO-free air for reference gas mixing purposes. We expect that Aurolite could also be used to analyse δ^{14}C-CO; however, more tests would be required to prove this hypothesis. We described our setup to measure δ^{13}C-CH_4, δ^{15}N-N_2O and δ^{18}O-N_2O isotope ratios in air- and ice core samples and thoroughly discussed its performance and measurement uncertainty based on bubble-free ice and quality control standard measurements. We proved the reproducibility of the analytical system and the suggested data-processing method based on detailed experiments with sample amounts that can be expected in 200–500 g of glacial and interglacial ice core samples. We furthermore compared our ice core measurement for δ^{13}C-CH_4 with published data which prove that our setup is capable of highlighting small yet significant isotope variations with excellent precision. A previously published intercomparison of isotope measurements of N_2O in reference gases proved the described setup to be in very good agreement with established systems. A high-resolution dataset of δ^{15}N-N_2O and δ^{18}O-N_2O measurements from ice core samples between 657 and 1766 AD is not available for intercomparison. However, we discussed measurement control strategies analogue to our δ^{13}C-CH_4 measurements that suggest our setup is suitable to reliably measure the isotopic composition of N_2O in ice core samples. We conclude that the precision of our setup for δ^{13}C-CH_4, δ^{15}N-N_2O and δ^{18}O-N_2O measurements is 0.09, 0.6 and 0.7 ‰, respectively. Especially the excellent precision of our setup for δ^{13}C-CH_4 and its independence of Kr interference make our setup suitable to analyse the variability of the interhemispheric gradient of CH_4 and of small changes of δ^{13}C-CH_4 in high temporal resolution. The described setup enables measurement of two samples per day, which allows production of large datasets in future. Upcoming work should also include the harmonization of similar analytical systems and sample preparation protocols to minimize interlaboratory offsets as well as the investigation of measurement artefacts.

Acknowledgements. We would like to thank the field teams that took the EUROCORE and NEEM samples. NEEM is directed and organized by the Centre for Ice and Climate at the Niels Bohr Institute and the US NSF, Office of Polar Programs. It is supported by funding agencies and institutions in Belgium (FNRS-CFB and FWO), Canada (NRCan/GSC), China (CAS), Denmark (FIST), France (IPEV, CNRS/INSU, CEA and ANR), Germany (AWI), Iceland (RannIs), Japan (NIPR), Korea (KOPRI), the Netherlands (NWO/ALW), Sweden (VR), Switzerland (SNF), the United Kingdom (NERC) and the United States (US NSF, Office of Polar Programs). We greatly appreciated helpful discussions with Hinrich Schaefer, Katja Riedel, Peter Franz and Gordon Brailsford from NIWA and with Willi Brand from the MPI-BGC. We are grateful for the support of Colleen Templeton, and would like to acknowledge the two referees Jochen Schmitt and Jochen Rudolph for their valuable contributions, which considerably improved the manuscript.

Edited by: R. Koppmann

References

Anicich, V. G.: Evaluated bimolecular ion-molecule gas-phase kinetics of positive-ions for use in modeling planetary-atmospheres, cometary comae, and interstellar clouds, J. Phys. Chem. Ref. Data, 22, 1469–1569, 1993.

Aoki, N. and Makide, Y.: The concentration of krypton in the atmosphere – its revision after half a century, Chem. Lett., 34, 1396–1397, doi:10.1246/cl.2005.1396, 2005.

Behrens, M., Schmitt, J., Richter, K. U., Bock, M., Richter, U. C., Levin, I., and Fischer, H.: A gas chromatography/combustion/isotope ratio mass spectrometry system for high-precision $\delta^{13}C$ measurements of atmospheric methane extracted from ice core samples, Rapid Commun. Mass Sp., 22, 3261–3269, doi:10.1002/rcm.3720, 2008.

Bock, M., Schmitt, J., Behrens, M., Möller, L., Schneider, R., Sapart, C., and Fischer, H.: A gas chromatography/pyrolysis/isotope ratio mass spectrometry system for high-precision δD measurements of atmospheric methane extracted from ice cores, Rapid Commun. Mass Sp., 24, 621–633, doi:10.1002/rcm.4429, 2010a.

Bock, M., Schmitt, J., Möller, L., Spahni, R., Blunier, T., and Fischer, H.: Hydrogen isotopes preclude marine hydrate CH_4 emissions at the onset of Dansgaard-Oeschger events, Science, 328, 1686–1689, doi:10.1126/science.1187651, 2010b.

Brand, W. A.: Precon: A fully automated interface for the pre-GC concentration of trace gases in air for isotopic analysis, Isot. Environ. Healt. S., 31, 277–284, doi:10.1080/10256019508036271, 1995.

Brand, W. A.: Mass spectrometer hardware for analyzing stable isotope ratios, in: Handbook of stable isotope analytical techniques, Vol. 1, edited by: Groot, P. A., Elsevier B. V., Amsterdam, 835–856, 2004.

Brenninkmeijer, C. A. M.: Measurement of the abundance of ^{14}CO in the atmosphere and the $^{13}C/^{12}C$ and $^{18}O/^{16}O$ ratio of atmospheric CO with applications in New-Zealand and Antarctica, J. Geophys. Res.-Atmos., 98, 10595–10614, doi:10.1029/93jd00587, 1993.

Brenninkmeijer, C. A. M., Janssen, C., Kaiser, J., Rockmann, T., Rhee, T. S., and Assonov, S. S.: Isotope effects in the chemistry of atmospheric trace compounds, Chem. Rev., 103, 5125–5161, doi:10.1021/cr020644k, 2003.

Buizert, C., Martinerie, P., Petrenko, V. V., Severinghaus, J. P., Trudinger, C. M., Witrant, E., Rosen, J. L., Orsi, A. J., Rubino, M., Etheridge, D. M., Steele, L. P., Hogan, C., Laube, J. C., Sturges, W. T., Levchenko, V. A., Smith, A. M., Levin, I., Conway, T. J., Dlugokencky, E. J., Lang, P. M., Kawamura, K., Jenk, T. M., White, J. W. C., Sowers, T., Schwander, J., and Blunier, T.: Gas transport in firn: Multiple-tracer characterisation and model intercomparison for NEEM, Northern Greenland, Atmos. Chem. Phys., 12, 4259–4277, doi:10.5194/acp-12-4259-2012, 2012.

Carter, J. F. and Barwick, V. J.: Good practice guide for isotope ratio mass spectrometry, 1st Edn., 1–48, ISBN 978-0-948926-31-0, 2011.

Coplen, T. B., Brand, W. A., Gehre, M., Groning, M., Meijer, H. A. J., Toman, B., and Verkouteren, R. M.: After two decades a second anchor for the VPDB $\delta^{13}C$ scale, Rapid Commun. Mass Sp., 20, 3165–3166, doi:10.1002/rcm.2727, 2006.

Cullis, C. F. and Willatt, B. M.: Oxidation of methane over supported precious metal-catalysts, J. Catal., 83, 267–285, doi:10.1016/0021-9517(83)90054-4, 1983.

Date, M., Ichihashi, Y., Yamashita, T., Chiorino, A., Boccuzzi, F., and Haruta, A.: Performance of Au/TiO_2 catalyst under ambient conditions, Catal. Today, 72, 89–94, doi:10.1016/s0920-5861(01)00481-3, 2002.

DesMarais, D. J.: Variable-temperature cryogenic trap for separation of gas-mixtures, Anal. Chem., 50, 1405–1406, doi:10.1021/ac50031a056, 1978.

Ferretti, D. F., Miller, J. B., White, J. W. C., Etheridge, D. M., Lassey, K. R., Lowe, D. C., Meure, C. M. M., Dreier, M. F., Trudinger, C. M., van Ommen, T. D., and Langenfelds, R. L.: Unexpected changes to the global methane budget over the past 2000 years, Science, 309, 1714–1717, doi:10.1126/science.1115193, 2005.

Fischer, H., Behrens, M., Bock, M., Richter, U., Schmitt, J., Loulergue, L., Chappellaz, J., Spahni, R., Blunier, T., Leuenberger, M., and Stocker, T. F.: Changing boreal methane sources and constant biomass burning during the last termination, Nature, 452, 864–867, doi:10.1038/nature06825, 2008.

Flückiger, J., Blunier, T., Stauffer, B., Chappellaz, J., Spahni, R., Kawamura, K., Schwander, J., Stocker, T. F., and Dahl-Jensen, D.: N_2O and CH_4 variations during the last glacial epoch: Insight into global processes, Global Biogeochem. Cy., 18, 14, Gb1020, doi:10.1029/2003gb002122, 2004.

Friedli, H. and Siegenthaler, U.: Influence of N_2O on isotope analyses in CO_2 and mass-spectrometric determination of N_2O in air samples, Tellus B, 40, 129–133, 1988.

Ghosh, P. and Brand, W. A.: The effect of N_2O on the isotopic composition of air-CO_2 samples, Rapid Commun. Mass Sp., 18, 1830–1838, doi:10.1002/rcm.1560, 2004.

Kato, S., Akimoto, H., Braunlich, M., Röckmann, T., and Brenninkmeijer, C. A. M.: Measurements of stable carbon and oxygen isotopic compositions of CO in automobile exhausts and ambient air from semi-urban Mainz, Germany, Geochem. J., 33, 73–77, 1999.

Loulergue, L., Schilt, A., Spahni, R., Masson-Delmotte, V., Blunier, T., Lemieux, B., Barnola, J. M., Raynaud, D., Stocker, T. F., and Chappellaz, J.: Orbital and millennial-scale features of atmospheric ch4 over the past 800,000 years, Nature, 453, 383–386, doi:10.1038/nature06950, 2008.

McPherson, J., Thompson, D., Pattrick, G., Holliday, R., Ramdayal, D., Khumalo, T., and Van der Lingen, E.: Commercial opportunities for gold catalysts, World Gold Conference 2009, Johannesburg, South Africa, 2009.

Melton, J. R., Schaefer, H., and Whiticar, M. J.: Enrichment in ^{13}C of atmospheric CH_4 during the younger dryas termination, Clim. Past., 8, 1177–1197, doi:10.5194/cp-8-1177-2012, 2011a.

Melton, J. R., Whiticar, M. J., and Eby, P.: Stable carbon isotope ratio analyses on trace methane from ice samples, Chem. Geol., 288, 88–96, doi:10.1016/j.chemgeo.2011.03.003, 2011b.

Merritt, D. A., Brand, W. A., and Hayes, J. M.: Isotope-ratio-monitoring gas-chromatography mass-spectrometry – methods for isotopic calibration, Org. Geochem., 21, 573–583, 1994.

Merritt, D. A., Freeman, K. H., Ricci, M. P., Studley, S. A., and Hayes, J. M.: Performance and optimization of a combustion interface for isotope ratio monitoring gas-chromatography mass-spectrometry, Anal. Chem., 67, 2461–2473, 1995.

Mitchell, L. E., Brook, E. J., Sowers, T., McConnell, J. R., and Taylor, K.: Multidecadal variability of atmospheric methane,

1000–1800 ce, J. Geophys. Res.-Biogeosci., 116, G02007, doi:10.1029/2010jg001441, 2011.

Rhodes, R. H., Faïn, X., Stowasser, C., Blunier, T., Chappellaz, J., McConnell, J., Romanini, D., Mitchell, L. E., and Brook, E. J.: Continuous methane measurements from a late holocene greenland ice core: Atmospheric and in-situ signals, Earth Planet. Sc. Lett., 368, 9–19, doi:10.1016/j.epsl.2013.02.034, 2013.

Röckmann, T. and Levin, I.: High-precision determination of the changing isotopic composition of atmospheric N_2O from 1990 to 2002, J. Geophys. Res.-Atmos., 110, D21304, doi:10.1029/2005jd006066, 2005.

Sapart, C. J., van der Veen, C., Vigano, I., Brass, M., van de Wal, R. S. W., Bock, M., Fischer, H., Sowers, T., Buizert, C., Sperlich, P., Blunier, T., Behrens, M., Schmitt, J., Seth, B., and Röckmann, T.: Simultaneous stable isotope analysis of methane and nitrous oxide on ice core samples, Atmos. Meas. Tech., 4, 2607–2618, doi:10.5194/amt-4-2607-2011, 2011.

Sapart, C. J., Monteil, G., Prokopiou, M., van de Wal, R. S. W., Kaplan, J. O., Sperlich, P., Krumhardt, K. M., van der Veen, C., Houweling, S., Krol, M. C., Blunier, T., Sowers, T., Martinerie, P., Witrant, E., Dahl-Jensen, D., and Röckmann, T.: Natural and anthropogenic variations in methane sources during the past two millennia, Nature, 490, 85–88, doi:10.1038/nature11461, 2012.

Sapart, C. J., Martinerie, P., Witrant, E., Chappellaz, J., van de Wal, R. S. W., Sperlich, P., van der Veen, C., Bernard, S., Sturges, W. T., Blunier, T., Schwander, J., Etheridge, D., and Röckmann, T.: Can the carbon isotopic composition of methane be reconstructed from multi-site firn air measurements?, Atmos. Chem. Phys., 13, 6993–7005, doi:10.5194/acp-13-6993-2013, 2013.

Schaefer, H. and Whiticar, M. J.: Measurement of stable carbon isotope ratios of methane in ice samples, Org. Geochem., 38, 216–226, doi:10.1016/j.orggeochem.2006.10.006, 2007.

Schaefer, H., Whiticar, M. J., Brook, E. J., Petrenko, V. V., Ferretti, D. F., and Severinghaus, J. P.: Ice record of $\delta^{13}C$ for atmospheric CH_4 across the younger dryas-preboreal transition, Science, 313, 1109–1112, doi:10.1126/science.1126562, 2006.

Schilt, A., Baumgartner, M., Schwander, J., Buiron, D., Capron, E., Chappellaz, J., Loulergue, L., Schupbach, S., Spahni, R., Fischer, H., and Stocker, T. F.: Atmospheric nitrous oxide during the last 140,000 years, Earth Planet. Sc. Lett., 300, 33–43, doi:10.1016/j.epsl.2010.09.027, 2010.

Schmitt, J., Seth, B., Bock, M., Fischer, H., Möller, L., Sapart, C. J., Prokopiou, M., Van der Veen, C., Röckmann, T., and Sowers, T.: On the interference of Kr during carbon isotope analysis of atmospheric methane using continuous flow combustion-isotope ratio mass spectrometry, Atmos. Meas. Tech., 6, 1425–1445, doi:10.5194/amt-6-1425-2013, 2013.

Sessions, A. L.: Isotope-ratio detection for gas chromatography, J. Sep. Sci., 29, 1946–1961, doi:10.1002/jssc.200600002, 2006.

Solomon, S., Qin, D., Manning, M., Alley, R. B., Berntsen, T., Bindoff, N. L., Chen, Z., Chidthaisong, A., Gregory, J. M., Hegerl, G. C., Heimann, M., Hewitson, B., Hoskins, B. J., Joos, F., Jouzel, J., Kattsov, V., Lohmann, U., Matsuno, T., Molina, M. J., Nicholls, N., Overpeck, J., Raga, G., Ramaswamy, V., Ren, J., Rusticucci, M., Somerville, R., Stocker, T. F., Whetton, P., Wood, R. A., and Wratt, D.: Climate change 2007: The physical science basis. Contribution of working group i to the fourth assessment report of the intergovernmental panel on climate change, 2007.

Sowers, T.: Late quaternary atmospheric CH_4 isotope record suggests marine clathrates are stable, Science, 311, 838–840, doi:10.1126/science.1121235, 2006.

Sowers, T.: Atmospheric methane isotope records covering the holocene period, Quaternary Sci. Rev., 29, 213–221, doi:10.1016/j.quascirev.2009.05.023, 2009.

Sowers, T. and Jubenville, J.: A modified extraction technique for liberating occluded gases from ice cores, J. Geophys. Res.-Atmos., 105, 29155–29164, 2000.

Sowers, T., Alley, R. B., and Jubenville, J.: Ice core records of atmospheric N_2O covering the last 106,000 years, Science, 301, 945–948, 2003.

Sowers, T., Bernard, S., Aballain, O., Chappellaz, J., Barnola, J. M., and Marik, T.: Records of the $\delta^{13}C$ of atmospheric CH_4 over the last 2 centuries as recorded in antarctic snow and ice, Global Biogeochem. Cy., 19, Gb2002, doi:10.1029/2004gb002408, 2005.

Sperlich, P., Guillevic, M., Buizert, C., Jenk, T. M., Sapart, C. J., Schaefer, H., Popp, T. J., and Blunier, T.: A combustion setup to precisely reference $\delta^{13}C$ and $\delta^{2}H$ isotope ratios of pure CH_4 to produce isotope reference gases of $\delta^{13}C$-CH_4 in synthetic air, Atmos. Meas. Tech., 5, 2227–2236, doi:10.5194/amt-5-2227-2012, 2012.

Sturm, P., Leuenberger, M., Sirignano, C., Neubert, R. E. M., Meijer, H. A. J., Langenfelds, R., Brand, W. A., and Tohjima, Y.: Permeation of atmospheric gases through polymer o-rings used in flasks for air sampling, J. Geophys. Res.-Atmos., 109, D04309, doi:10.1029/2003jd004073, 2004.

Umezawa, T., Aoki, S., Nakazawa, T., and Morimoto, S.: A high-precision measurement system for carbon and hydrogen isotopic ratios of atmospheric methane and its application to air samples collected in the western pacific region, J. Meteorol. Soc. Jpn., 87, 365–379, doi:10.2151/jmsj.87.365, 2009.

Verkouteren, R. M.: Preparation, characterization, and value assignment of carbon dioxide isotopic reference materials: Rms 8562, 8563, and 8564, Anal. Chem., 71, 4740–4746, doi:10.1021/ac990233c, 1999.

Walther, G., Cervera-Gontard, L., Quaade, U. J., and Horch, S.: Low temperature methane oxidation on differently supported 2 nm au nanoparticles, Gold Bull., 42, 13–19, doi:10.1007/BF03214901, 2009.

Werner, R. A. and Brand, W. A.: Referencing strategies and techniques in stable isotope ratio analysis, Rapid Commun. Mass Sp., 15, 501–519, 2001.

Chapter 4

CH_4 carbon isotopes during DO events 21 and 22

Methods: CH_4 carbon isotopes from NGRIP and NEEM samples from 75-95 ka BP

A total of 34 ice core samples were analyzed for δ^{13}C-CH_4 that represent the period 75 to 95 ka BP with a mean sample resolution of one sample in 590 years. The analytical setup for the measurements is described by Sperlich et al. (2013). All δ^{13}C-CH_4 data are referenced to the international VPDB scale using a referencing technique that is described by Sperlich et al. (2012). The δ^{13}C-CH_4 data have been corrected for isotope fractionation due to diffusion processes in the firn column (Buizert et al., 2013). The highest applied correction accounted for 0.35 ‰ in two samples and ranged below 0.05 ‰ in all other samples, which is about 50 % of the measurement uncertainty of 0.09 ‰ (Sperlich et al., 2013). For consistence, all samples are corrected for the firn fractionation. The determination of the firn fractionation requires $p$$CH_4$ data from both NGRIP and NEEM ice cores that have recently been published by Baumgartner et al. (2013) and Chappellaz et al. (2013), respectively. Furthermore, δ^{15}N and diffusive column hight data that are essential to calculate the firn diffusion fractionation that were kindly provided by M. Guillevic pers. comm. 2013 or were published by Kindler et al. (2013).

The new δ^{13}C-CH_4 record significantly increases the temporal resolution of $\sim$ 10 existing δ^{13}C-CH_4 datapoints from this period of time (Möller et al., 2013). We analyzed 19 samples from the NGRIP (e.g., NGRIP community members et al., 2004) and 15 samples from the NEEM (e.g., NEEM community members et al., 2013) core, respectively. The samples from both ice cores show excellent agreement which suggests ice core specific artefacts as were reported for deeper parts of the NEEM core (NEEM community members et al., 2013) can be excluded for both records. Both NGRIP and NEEM δ^{13}C-CH_4 data are presented on the GICC05_modelext time scale (Andersen et al., 2006; Wolff et al., 2010; Kindler et al., 2013) in this chapter (Fig. 4.1) and are shown in table 4.1.

Table 4.1: δ^{13}C-CH_4 data from NGRIP and NEEM core between 75-95 ka BP. The first column shows the bag # as identifier of each sample. Column 2 denotes to the depth of each bag top and the age in column 3 the mean gas age on the GICC05_modelext time scale. The δ^{13}C-CH_4 results as referenced on the VPDB scale and after correction for firn diffusion are shown in column 4 and 5, respectively. [a] indicates one rejected sample which showed twice the expected CH_4 peak size and suffered from contamination or in situ CH_4 production during analysis.

bag #	**depth [m]**	**gas age [ka BP]**	δ^{13}**C-CH_4** [‰]	δ^{13}**C-CH_4** [‰]
NGRIP				
4666	2565.75	75.086	-49.11	-49.15
4692	2580.05	76.059	-48.90	-48.94
4706	2587.75	76.599	-48.17	-48.15
4728	2599.85	77.979	-48.54	-48.56
4775	2625.70	80.118	-48.83	-48.82
4801	2640.00	81.199	-48.99	-48.94
4828	2654.85	82.173	-49.04	-49.01
4856	2670.25	83.223	-48.51	-48.50
4882	2684.55	84.173	-48.00	-47.99
4904	2696.65	85.015	-48.42	-48.09
4924	2707.65	86.044	-46.85	-46.85
4940	2716.45	86.934	-47.10	-47.09
4962	2728.55	88.177	-46.73	-46.68
4984	2740.65	89.202	-48.26	-48.26
5004	2751.65	89.989	-48.54	-48.49
5022	2761.55	91.032	-48.88	-48.85
5040	2771.45	92.086	-48.53	-48.55
5056	2780.25	93.072	-49.29	-49.33
5074	2790.15	94.137	-49.65	-49.68
NEEM				
3691	2029.5	75.987	-48.18	[a]
3703	2036.10	77.054	-48.54	-48.54
3715	2042.70	78.407	-48.69	-48.70
3727	2049.30	79.445	-48.69	-48.71
3740	2056.45	80.557	-49.09	-49.12
3754	2064.15	81.611	-48.72	-48.73
3770	2072.95	82.719	-49.19	-49.20
3786	2081.75	83.815	-48.41	-48.41
3804	2091.65	84.974	-47.49	-47.83
3820	2100.45	86.045	-46.87	-46.84
3836	2109.25	87.264	-46.79	-46.77
3852	2118.05	88.383	-47.31	-47.31
3863	2124.10	89.060	-48.11	-48.12
3895	2141.70	91.621	-48.88	-48.88
3909	2149.40	92.968	-49.29	-49.29
3923	2157.10	94.285	-49.91	-49.93

To compare the δ^{13}C-CH_4 data to further geological records, all data need to be on the same time scale. The fast changes in $p\mathrm{CH}_4$ represent a global signal and can therefore be used to bring atmospheric reconstructions from ice core measurements on a common relative time scale (Blunier et al., 2007). In this case, $p\mathrm{CH}_4$ from the Antarctic EDML ice core (Schilt et al., 2010b) was matched to the NGRIP and NEEM $p\mathrm{CH}_4$ data by transferring GICC05_modelext ages to the EDML-1 time scale at 10 match points and linear interpolation in between (table 4.2). Thereby, EDML gas records can be transferred onto GICC05_modelext, allowing to compare our NGRIP and NEEM δ^{13}C-CH_4 record to EDML $p\mathrm{CO}_2$ data (Bereiter et al., 2012). Applying the same matching method, relative sea-level (RSL) reconstructions (Rohling et al., 2009a) could be synchronized to GICC05_modelext through 8 match points linking $p\mathrm{CO}_2$ reconstructions by Bereiter et al. (2012); Rohling et al. (2009a) (table 4.2). While the dating uncertainty for EDML-1 to GICC05_modelext is probably less than 150 years, the uncertainty in the dating of the RSL data is expected to be larger since the $p\mathrm{CO}_2$ record from Rohling et al. (2009a) is a smoothed fit that does not include small variability and even smoothes the $p\mathrm{CO}_2$ variability assiciated with DO-19 and DO-20 into one single peak. The combined data set will be shown in Figure 4.1 including the three $p\mathrm{CH}_4$ records from NGRIP, NEEM and EDML records on GICC05_modelext.

Table 4.2: Matchpoints for gas age scales. The first and second column show the GICC05_modelext age that was transferred to the respective gas age of EDML-1 (Bereiter et al., 2012). EDML-1 gas ages older than 87.964 ka remained unaffected. Likewise, column 3 shows the EDML-1 gas age that replaced the gas age shown in column 4 from the time scale of Rohling et al. (2009a).

GICC05	**EDML-1**	**EDML-1**	**Rohling**
75.064	72.650	73.346	71.184
76.296	74.430	74.463	73.342
76.470	74.793	77.112	77.059
77.963	76.268	83.454	82.736
78.747	76.961	86.428	85.673
79.197	77.525	87.009	86.069
84.655	83.408	87.604	87.562
84.997	83.858	95.093	94.221
87.773	87.414		
87.964	87.999		

Results: CH_4 carbon isotopes from NGRIP and NEEM samples from 75-95 ka BP

NGRIP and NEEM δ^{13}C-CH_4 data are shown in Figure 4.1 and are compared to $p$$CH_4$ (Chappellaz et al., 2013) and δ^{18}O, where the latter is a proxy for Greenlandic temperature (NGRIP community members et al., 2004). At a first look, one can see little shared variance between δ^{13}C-CH_4 and CH_4, as has been recently suggested by Möller et al. (2013). Through the period between 95 and 90 ka BP, δ^{13}C-CH_4 is getting constantly more enriched by ~2 ‰ from -50 to -48 ‰ while, both $p$$CH_4$ and δ^{18}O show little variability but remain rather constant. Despite increasing temperature and $p$$CH_4$ of ~100 ppb throughout DO-22, δ^{13}C-CH_4 continues its trend and further increases for ~1.8 ka at an even faster rate of 1 ‰ ka^{-1}. The δ^{13}C-CH_4 enrichment reaches a plateau towards the end of DO-22, while $p$$CH_4$ is still increasing towards its maximum level during DO-22. Throughout this plateau, δ^{13}C-CH_4 seems rather stable and ranges at values around -47.0 $\pm$ 0.2 ‰.

Two of the samples from ~85 ka BP recorded the pronounced DO-21 precursor event (e.g., Capron et al., 2010; Vallelonga et al., 2012) where one sample was from NGRIP and the other one from the NEEM ice core. With a growth rate of 2.5 ppb a^{-1}, this pre-DO event exhibits the fastest $p$$CH_4$ increase rate yet recorded in Greenlandic ice core (Chappellaz et al., 2013). Therefore, it is particularly exciting to analyze this section for δ^{13}C-CH_4. The strong $p$$CH_4$ variability of this event determined the highest correction for firn diffusion was required for these two samples. The corrected samples are by ~1 ‰ more depleted than the rather stable δ^{13}C-CH_4 plateau during the previous stadial from ~86-87 ka BP.

During DO-21, δ^{13}C-CH_4 slowly decreases towards a maximum depletion in δ^{13}C-CH_4 of -49.2 ‰ which is reached at ∼82.5 ka BP, approximately 2 ka after the $p$$CH_4$ maxima of DO-21. Note, DO-21 is one of the most pronounced $p$$CH_4$ variations during the last glacial period (Chappellaz et al., 2013). Over the next 5 ka, δ^{13}C-CH_4 shows a steady increasing trend by ∼0.75 ‰, which is terminated by a sudden ∼0.3 ‰ enrichment before δ^{13}C-CH_4 decreases by ∼1 ‰ over the first half of DO-20. As it was the case for DO-21, the δ^{13}C-CH_4 gets more and more depleted during DO-20 until the end of the record at 75 ka BP, which is beyond the $p$$CH_4$ maximum at 76 ka BP.

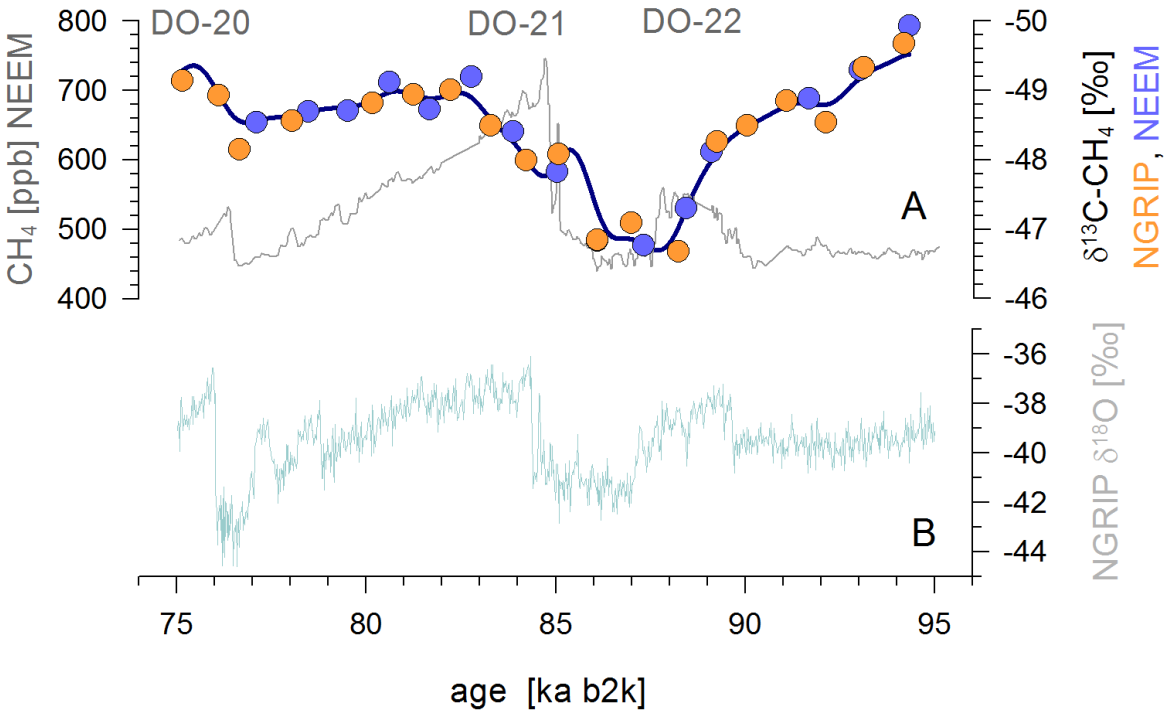

Figure 4.1: δ^{13}C-CH_4 during DO21 and DO22. Panel A shows δ^{13}C-CH_4 from NGRIP and NEEM in orange and blue circles, respectively. δ^{13}C-CH_4 date were annualized by linear interpolation and smoothed with a 1000 year window as represented by the dark blue line. CH_4 is indicated by the grey line (Baumgartner et al., 2013). The Dansgaard Oeschger events are indicated by DO-20 to DO-22. Panel B shows the NGRIP δ^{18}O (ice) record (NGRIP community members et al., 2004).

Discussion: CH_4 carbon isotopes from NGRIP and NEEM samples from 75-95 ka BP

Overall, our high resolution record confirms the finding of Möller et al. (2013), that δ^{13}C-CH_4 and CH_4 show independent variation. The results are an interesting challenge for our understanding of the atmospheric CH_4 cycle. How can extreme changes in δ^{13}C-CH_4 suggest an intensive variability in the CH_4 source and sink system at times when $p$$CH_4$ suggests the CH_4 system is in stable state? Likewise, how can rapid $p$$CH_4$ increases such as the onset of DO-21 happen and not be mirrored in the δ^{13}C-CH_4 record?

Möller et al. (2013) answer these questions by suggesting that several processes that counter balance each other in δ^{13}C-CH_4 are likely to occur simultaneously during some periods of rapid $p$$CH_4$ variation. Charcoal records from the Iberian Peninsula, suggests that fire intensity varies with DO-cyclicity and thus NH temperature (Daniau et al., 2007). Assuming that the $p$$CH_4$ variability during DO events is mostly caused by (boreal) wetland emissions (e.g., Chappellaz et al., 1993a; Brook et al., 1996b; Dällenbach et al., 2000; Bock et al., 2010a), a simultaneous increase of isotopically light wetland CH_4 and δ^{13}C enriched pyrogenic CH_4 could be a possible explanation for the $p$$CH_4$ and δ^{13}C-CH_4 variability observed during DO-21.

Möller et al. (2013) also argument that the δ^{13}C of specific CH_4 sources changes which allows for δ^{13}C-CH_4 variability and rather contsant $p$$CH_4$. They propose the mechanism that the δ^{13}C of major CH_4 source areas depends on the C3/C4 plant ratio in the respective vegetation zones, which is a function of temperature and $p$$CO_2$ (e.g., Ehleringer et al., 1997; Collatz et al., 1998). The δ^{13}C of C3 and C4 plants shows systematic differences with C3 plants being more depleted in δ^{13}C by ∼12 ‰ (e.g., Ehleringer et al., 1997). Consequently, the δ^{13}C-CH_4 that is produced from C3 and C4 plant material varies by ∼12 ‰ as well. Variability in $p$$CO_2$ and climate (represented by RSL changes) thus controls the δ^{13}C of plant material which is decomposed to CH_4 by microbes. Moreover, glacial-interglacial sea-level variability has a significant impact on the size of exposed shelf areas and inundated coastal flood plains (e.g., Montenegro et al., 2006; Weber et al., 2010; Guo et al., 2012), which are suggested to impact CH_4 emissions (Weber et al., 2010; Guo et al., 2012; Möller et al., 2013). In fact, Möller et al. (2013) found that δ^{13}C-CH_4 and $p$$CO_2$ as well as δ^{13}C-CH_4 and RSL changes show more common variance than δ^{13}C-CH_4 and $p$$CH_4$. Möller et al. (2013) suggest the control of $p$$CO_2$ on C3/C4 plant ratio (e.g., Bragg et al., 2013).

Figure 4.2 compares δ^{13}C-CH_4 to RSL and $p$$CO_2$ variability (Rohling et al., 2009a; Bereiter et al., 2012) to test the control of RSL and $p$$CO_2$ on δ^{13}C-CH_4 as suggested by Möller et al. (2013). For the time 75-95 ka BP, the curves seem to share some variation as δ^{13}C-CH_4, $p$$CO_2$ and RSL all show a pronounced minima between 85 and 88.5 ka BP. Besides of that, there are quite some differences between δ^{13}C-CH_4 on the one hand and RSL and $p$$CO_2$ variability on the other hand, which are probably the reason for the low correlation coefficients between δ^{13}C-CH_4 and $p$$CO_2$ (r = -0.33) and δ^{13}C-CH_4 and RSL (r = 0), respectively. These correlations suggest that other processes were likely in place that controlled δ^{13}C-

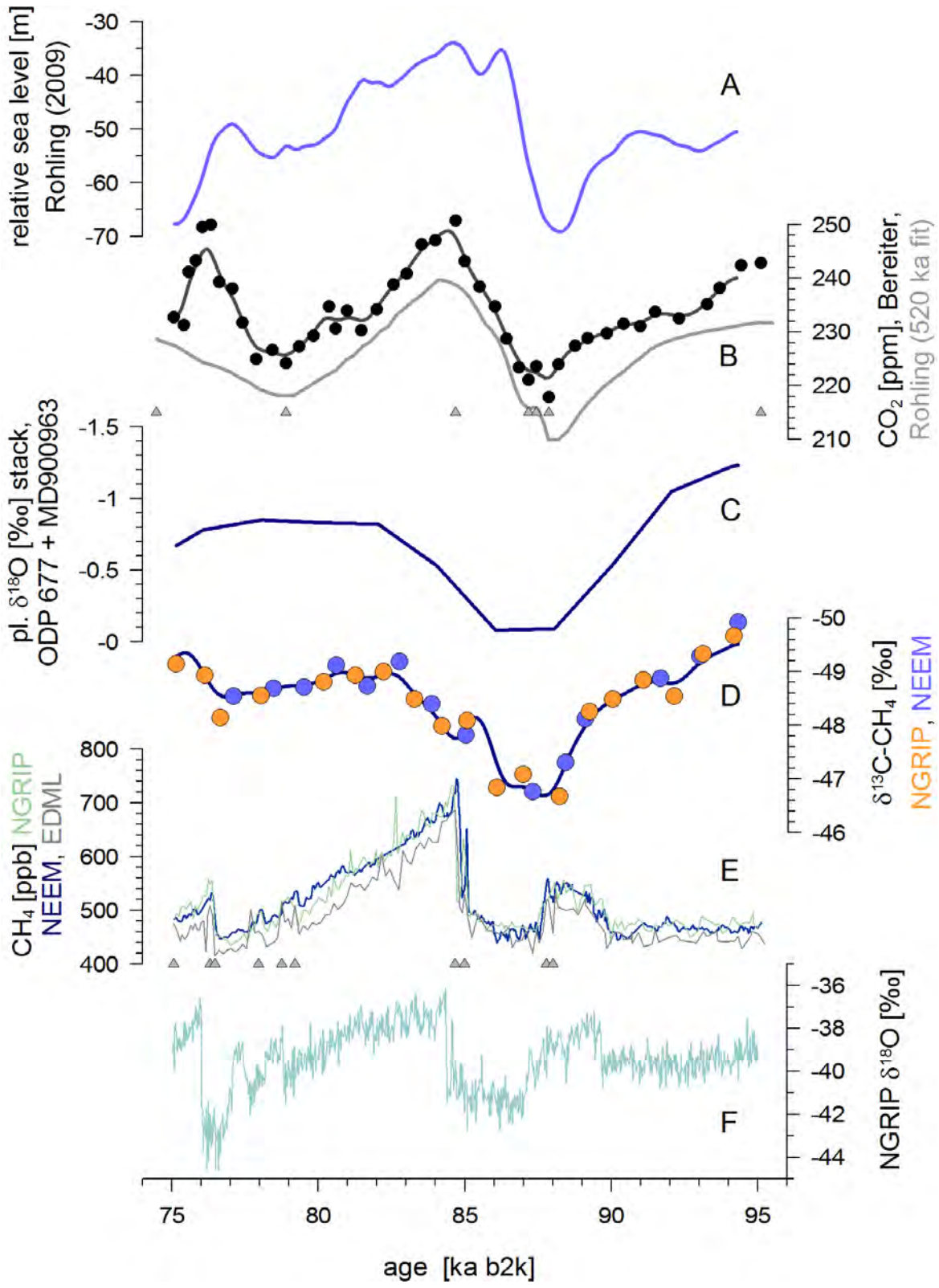

Figure 4.2: δ^{13}C-CH_4 of DO21 and DO22 in comparison to climate records. Panel A and B show RSL and pCO_2 from Rohling et al. (2009a) and Bereiter et al. (2012), respectively. Panel C presents a δ^{18}O stack from two tropical planktonic foraminifera records (Bassinot et al., 1994). Panel E shows the CH_4 concentration records from NGRIP (green) NEEM (blue) and EDML (grey) as published by Baumgartner et al. (2013), Chappellaz et al. (2013) and Schilt et al. (2010b), respectively and highlight the agreement of the time scale synchronization. Panel D and F are identical to Figure 4.1. Grey triangles in panel B and E indicate the matchpoints (table 4.2) used to synchronize all time scales to GICC05_modelext.

CH_4 between 75 and 95 ka BP. This is in strong contrast to Möller et al. (2013), who found correlation coefficients of r = 0.86 between δ^{13}C-CH_4 and pCO_2 and of r = 0.69 between δ^{13}C-CH_4 and RSL.

How can the pattern of correlation be so different on glacial-interglacial time scales Möller et al. (2013) or in the high resolution record between DO-21 and DO-22? Bereiter et al. (2012) show that pCO_2 varies by ∼30 ppm between DO-20 and DO-22 and that two pronounced pCO_2 maxima fall together with the maxima in pCH_4 of DO-20 and DO-21. As previously discussed, the maximum δ^{13}C depletions of CH_4 occur some 1.5 to 2 ka later (note that the end of the presented δ^{13}C-CH_4 record during DO-20 does not necessarily represent the maximum δ^{13}C-CH_4). At the time of maximum δ^{13}C depletion, pCO_2 has already decreased by ∼50 %. DO-22 however shows no clear signal in pCO_2 which is a feature pCO_2 has in common with δ^{13}C-CH_4, while RSL shows a variability which does not seem to unambiguously match any of the other records presented in figure 4.2. Otherwise, the comparison between δ^{13}C-CH_4 and RSL is similar to δ^{13}C-CH_4 and pCO_2.

However, the RSL maxima near DO-20 seems to lead the maxima in pCO_2 by ∼1 ka, which is somewhat unlikely (Grant et al., 2012; Foster and Rohling, 2013). Since the RSL record was transferred to GICC05_modelext via synchronizing pCO_2 of Rohling et al. (2009a) and Bereiter et al. (2012), the comparison of δ^{13}C-CH_4, pCO_2 and RSL is extremely sensitive to correct matching of the time scale. Despite greatest possible care, it cannot be excluded that the presented timing contains significant errors. In absence of another independent parameter than pCO_2 however, this seems to be the best possible solution at the current stage. However, the error in the correlations based on dating uncertainties is expected to not considerably change the conclusions.

Tropical wetlands are considered the most important CH_4 source regions during glacial period and DO-events (e.g., Chappellaz et al., 1993a; Guo et al., 2012). Thus, it seems obvious to compare the δ^{13}C-CH_4 record to a geological monsoon records. Bassinot et al. (1994) produced a δ^{18}O stack that was measured on planktonic foraminifera in two tropical marine cores. The δ^{18}O in the shells of the planktonic foraminifera recorded the δ^{18}O signal of the global ocean due to ice volume changes, but they also recorded a superimposing signal which is caused by the variability of tropical monsoon systems. The tropical δ^{18}O stack and δ^{13}C-CH_4 showed a correlation coefficient of r = 0.93. However, the δ^{18}O stack contained ∼10 data points that cover the period between 75 and 95 ka BP. If the relation between δ^{13}C-CH_4 and δ^{18}O stack was consistent, it has to be apparent and robust during periods outside of our data range as well. Therefore, the long term variability of δ^{13}C-CH_4 will be analyzed in a following chapter including the 170 ka record that was previously published by Möller et al. (2013).

Chapter 5

No bullet hole from the clathrate gun?!

Abstract

Ice core samples of the NEEM and NGRIP ice cores have been measured to produce a methane carbon isotope (δ^{13}C-CH_4) record of high temporal resolution that also covers the DO-21 precursor event ($\sim$85 ka BP). High precision/high resolution CH_4 mixing ratio measurements show this rapid event occurred within $\sim$120 years, comprising a CH_4 mixing ratio increase of $\sim$150 ppb and a variability in δ^{13}C-CH_4 of $\sim$1 ‰. A recent study on δ^{13}C-CH_4 in ice core samples highlights the uncertainty of box model calculations of CH_4 fluxes that do not consider vegetation changes on glacial-interglacial time scales (Möller et al., 2013). Since global vegetation changes in CH_4 source ecosystems are poorly constrained, we alternatively suggest to analyse δ^{13}C-CH_4 during the DO-21 precursor event by Keeling plot analysis. We find the δ^{13}C of the additional CH_4 source was -57.6$\pm$2.5 ‰. Our result suggests tropical wetlands as most probable additional CH_4 source category but it does not unambiguously rule out contributions from CH_4 hydrates and boreal wetlands. We discuss our result in a context to prevailing climate variability and the predicted impact of large CH_4 pulses in ice core records as would be expected from sudden destabilization of CH_4 hydrates. We present climatic evidence suggesting increased emissions from tropical wetlands as the major contributor to the rapid CH_4 anomaly and discuss the possibility of complementary increases from biomass burning and boreal wetland sources. Our results do not allow distinguishing between CH_4 emission from tropical wetlands or aerobically produced CH_4 by C3 plants, which has recently been proposed as significant but unaccounted CH_4 source. Due to identical δ^{13}C values, aerobic CH_4 emitted from plants could linearly substitute tropical wetland CH_4, but not change our conclusions that CH_4 release from CH_4 hydrates was probably not the main driver of DO-21 precursor event variability. Because a pCO_2 related shift of the C3/C4 plant ratio towards C4 plants in the tropical wetlands would significantly enrich δ^{13}C-CH_4 on glacial-interglacial time scales (Möller et al., 2013), the good match of our result with present day δ^{13}C of tropical wetland CH_4 emission suggest that tropical CH_4 source ecosystems were still dominated by C3 plants around the DO-21 precursor event.

Introduction

Methane (CH_4) is a strong greenhouse gas that presently contributes 20 % to the total radiactive forcing in Earth's atmosphere, thus playing a role in projections of global warming and sea-level variability (e.g., Trenberth et al., 2007; Bindoff et al., 2007). Reconstructions of atmospheric CH_4 using ice core samples show distinct variations during the last millennium (e.g., Blunier et al., 1993; Etheridge et al., 1998; MacFarling Meure et al., 2006; Mitchell et al., 2011) and on glacial-interglacial time scales (e.g., Chappellaz et al., 1990; Brook et al., 1996a; Loulergue et al., 2008). Rapid pCH_4 increases in the order of 150-300 ppb occured within decades to centuries and were most likely triggerred by sudden Northern Hemispheric warming during the so called Dansgaard-Oeschger (DO) events (e.g., Brook et al., 1996a, 2000).

Several authors showed that a few DO events were preceded by sharp precursor events of high amplitude (e.g., Capron et al., 2010; Vallelonga et al., 2012). During the DO-21 precursor event some 85.000 years ago (85 ka BP), Chappellaz et al. (2013) found a CH_4 spike of ∼150 ppb that occurred just within ∼120 years. Rapid CH_4 changes of this magnitude and time scale pose the question whether or not catastrophic release of CH_4 hydrates might have been the cause of this pCH_4 variability. Ocean sediments contain vast amounts of CH_4 that is produced by hydrogenothophic and aceticlastic methanogens. Estimations of the hydrate-bound CH_4 quantity range from 500-2500 Gt carbon (Milkov, 2004) to 3000 Gt carbon (Buffett and Archer, 2004). These numbers may be better appreciated in comparison to the estimated amount of carbon in permafrost areas that account for ∼400 Gt plus another ∼500 Gt in permanently frozen loess deposits in Siberia (Yedoma), (Zimov et al., 2006) or the CH_4 that is presently in the atmosphere (∼5 Gt after Denman et al. (2007)). The emission potential of CH_4 hydrates per °C warming is humungous (Buffett and Archer, 2004) and might impact both atmospheric pCH_4 as well as ocean chemistry (e.g., Kessler et al., 2011; Redmond and Valentine, 2012). It is thus of great interest to investigate the stability of CH_4 hydrates.

Atmospheric chemistry models suggested the pCH_4 variability during DO-events was almost entirely driven by CH_4 sources (Levine et al., 2012). The question as to which CH_4 sources accounted for rapid pCH_4 rises is a matter of controversial scientific debate. While some authors propose catastrophic CH_4 release events from marine gas hydrates as response to ocean warming (e.g., Kennett et al., 2000, 2003), others suggest enhanced CH_4 emissions of tropical and boreal wetlands have caused the pCH_4 variability (e.g., Chappellaz et al., 1993a; Brook et al., 2000; Guo et al., 2012; Baumgartner et al., 2012). Aerobic CH_4 formation in plants has been proposed as a new CH_4 source (Keppler et al., 2006, 2007, 2009) which has been supported by further authors (e.g., Bruhn et al., 2009; Vigano et al., 2008, 2009a; Qaderi and Reid, 2011). To date, the magnitude of aerobic CH_4 emission and its response to climate change is uncertain. The sources of atmospheric CH_4 comprise specific composition in $\delta^{13}C$ and $\delta^{2}H$. Observations of $\delta^{13}C$-CH_4 or $\delta^{2}H$-CH_4 constrain CH_4 source flux reconstructions using mass balance calculations in box models (e.g., Ferretti et al., 2005; Schaefer et al., 2006; Sowers, 2006; Fischer et al., 2008; Bock et al., 2010b; Sapart et al., 2012). However, Möller et al. (2013) advised of the limited accuracy when constant vegetation and C3/C4 plant ratios within typical CH_4 source ecosystems are assumed in simulations cov-

ering glacial-interglacial time scales.

Here, we propose Keeling plot analysis (KPA) (e.g., Keeling, 1958, 1961) to investigate the relative difference of δ^{13}C-CH_4 between periods of stable background and strong variability in $p$$CH_4$. By assuming both the $p$$CH_4$ and its δ^{13}C of background CH_4 are stable, KPA is independent of quantitative assumptions regarding vegetation and δ^{13}C of CH_4 sources that cause the $p$$CH_4$ backgrond. To our knowledge, this is the first time KPA is applied to studies of CH_4 in ice core samples. Therefore, we first suggest simple modifications to ice core CH_4 data that enable KPA for the analysis of rapid $p$$CH_4$ variation such as the DO-21 precursor event.

Methods

Optical measurement techniques were recently applied to measure CH_4 mixing ratios in the NEEM ice core Stowasser et al. (2012), resulting in a continuous record of unprecedented temporal resolution and precision Chappellaz et al. (2013). These data show the DO-21 precursor event in best possible detail. Discrete samples from the NEEM and NGRIP ice cores covering this DO-21 precursor event have also been measured for δ^{13}C-CH_4 (Figure 5.1), using the analytical techniques described in detail by Sperlich et al. (2013).

In short, cleaned ice core samples are melted in a vacuum system from which the liberated air sample is extracted. A helium carrier gas stream transports the sample through the analytical system to isolate CH_4 and to combust it into CO_2 before it is measured for δ^{13}C on an isotope ratio mass spectrometer. The δ^{13}C isotope ratio in each sample is reported with respect to the VPDB (Vienna Pee Dee Belemnite) isotope scale using the referencing technique described by Sperlich et al. (2012). The analytical uncertainty of the δ^{13}C-CH_4 measurements is 0.09 ‰. All δ^{13}C-CH_4 samples are corrected for firn diffusion fractionation after Buizert et al. (2013), which accounted for maximum correction of 0.35 ‰ during the DO-21 precursor event.

For KPA, the isotopic composition of a group of samples is plotted over its inverse mixing ratio, so that the intercept of the regression with the y-axis indicates the average isotopic signature of an additional local gas sources (e.g., Keeling, 1958, 1961). This technique assumes a one box model with two principal components, representing background air and one additional source of analyte gas (Pataki et al., 2003). Hitherto, KPA has been applied in ice core studies of CO_2 (e.g., Köhler et al., 2006; Lourantou et al., 2010a,b) but not ofCH_4. Pataki et al. (2003) express the global atmospheric budget as:

$$c_a = c_b + c_s \tag{5.1}$$

where c_a, c_b and c_s represents the CH_4 mixing ratios as measured in the atmosphere, the background atmosphere and the term due to the additional source, respectively. While c_a and c_b are directly measured, c_s can be calculated after equation 5.1 because we assume the background is well defined by the average of c_b.

Referring to the isotopic composition of each term by δ^{13}C, a mass-balance calculation

$$\delta^{13}C_a c_a = \delta^{13}C_b c_b + \delta^{13}C_s c_s \tag{5.2}$$

can then be re-arranged to calculate the isotopic composition of the additional CH_4 in the sample $\delta^{13}C_s$. Note, applying KPA to CH_4 ice core records does not result in the δ^{13}C of the additional CH_4 source directly as it is the case for present day atmospheric samples (e.g., Fisher et al., 2011).

The y-intercept in the KPA of CH_4 in ice core samples points to the δ^{13}C-CH_4 of the additional CH_4 source after the isotope fractionation caused by the atmospheric sink. To extract the δ^{13}C-CH_4 of the additional CH_4 source, the y-axis intercept of the Keeling plot needs to be corrected for the sink weighted fractionation ε_{tot}. The removal rate constant of each CH_4 sink (i) is expressed as α_i and determined as the ratio of the kinetic reaction rates (k) of the light and heavy isotope of CH_4 (e.g., Frey, 2006).

$$\alpha_i = \frac{^{12}k_i}{^{13}k_i} \tag{5.3}$$

With a known α_i, the fractionation factor of each individual sink ε_i (expressed in ‰) can be calculated according to:

$$\varepsilon_i = (\alpha_i - 1) \tag{5.4}$$

The sink weigthed fractionation factor ε_{tot} can then be calculated as

$$\varepsilon_{tot} = \sum_i \varepsilon_i \times {}^1/_{\tau_i} \tag{5.5}$$

where $1/\tau_i$ is the specific CH_4 removal rate of sink (i). Levine et al. (2012) found that the OH sink during DO-events remained relatively stable, which leads to the assumption that the sink weighted fractionation factor was approximately constant as well (e.g., Sapart et al., 2012). Lassey et al. (2007) account for the chlorine sink of the marine boundary layer and suggest a ε_{tot} of -7.7 ‰. However, the history of the chlorine sink is poorly constrained. We therefore follow Fischer et al. (2008); Mischler et al. (2009) and Sapart et al. (2012) and do not consider the chlorine sink. Relative sink contributions $1/\tau_i$ and sink fractionation factors used by (Sapart et al., 2012) are shown in table 5.1, which suggest an ε_{tot} of -6.3 ‰ that is added to the δ^{13}C result from the KPA.

Table 5.1: CH_4 sink categories, their relative contribution and fractionation factor

Sink category	Contribution [%]	ε_i[‰]
OH oxidation	90.5	-5.4
Soils	5.5	-18.0
Stratosphere	4.0	-12.0

Results

The rapid DO-21 precursor event lasted ∼120 years and is recorded over an ice core length of only ∼1.5 m. The number of available samples to study this event is therefore extremely limited. We have two δ^{13}C-CH_4 measurements from the precursor event and four δ^{13}C-CH_4 measurements of the preceding stadial period that we consider background (Figure 5.1). The δ^{13}C-CH_4 and corresponding CH_4 mixing ratio data are shown in table 5.2.

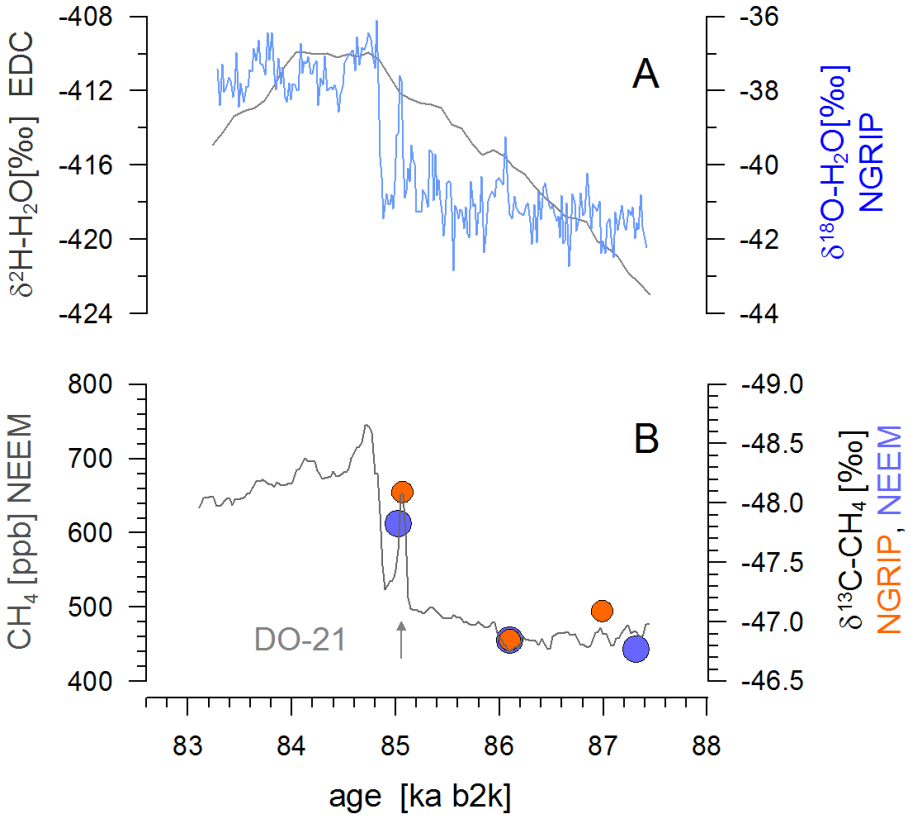

Figure 5.1: Water isotope ratios, δ^{13}C-CH_4 and pCH_4 during the DO-21 precursor event. Panel A shows δ^2H (ice) from the Antarctic EDC ice core (grey line) and δ^{18}O (ice) from the Greenlandic NGRIP ice core (blue line). The time scales of δ^2H (ice) and δ^{18}O (ice) have been shifted by a constant offset so the δ^{18}O (ice) onset of DO-21 matches the onset of pCH_4. Panel B illustrates CH_4 mixing ratios from NEEM with a grey line. Orange and blue circles indicate δ^{13}C-CH_4 from NGRIP and NEEM ice core samples, respectively. Blue circles are enlarged to visualize the NEEM sample at 86 ka BP that would otherwise be hidden under the orange circle. The arrow indicates the precursor event of the labeled DO-21 event. The time scale for the gases is GICC05_modelext (Wolff et al., 2010).

Table 5.2: δ^{13}C-CH_4 and CH_4 as used in the KPA. Column 1 shows the gas age on the GICC05_modelext time scale, (Wolff et al., 2010) corresponding to the firn-diffusion corrected δ^{13}C-CH_4 data that are displayed in column 2. Average CH_4 mixing ratios of the δ^{13}C-CH_4 samples are shown in column 3.

Age [ka BP]	δ^{13}C-CH_4 [‰]	pCH_4 [ppb]
84.974	-47.8	635
85.015	-48.1	581
86.044	-46.8	472
86.045	-46.8	444
86.934	-47.1	469
87.264	-46.8	463

The linear regression of the KPA intersects the y-axis at -51.3 ±2.5 ‰ (Figure 5.2). Considering ε_{tot} of -6.3 ‰ suggests a δ^{13}C-CH_4 of the additional source during the DO-21 precursor event in the order of -57.6 ±2.5 ‰, where the uncertainty represents the 95 % confidence interval of the least square regression (Figure 5.2). The propagation of measurement uncertainty (0.09 ‰) and of the firn diffusion correction (∼0.1 ‰, after Buizert et al. (2013)) does not increase the uncertainty of the KPA of ±2.5 ‰. The mass balance calculation based on averaged pCH_4, δ^{13}C-CH_4 (equation 5.2) reproduces the KPA results within 0.2 ‰. Note that chosing ε_{tot} after Lassey et al. (2007) would only change the result within the given uncertainty.

Discussion

Average δ^{13}C values of CH_4 sources are illustrated in table 5.3. In line with Levine et al. (2012), our results are interpreted as entirely CH_4 source driven signal. The KPA (Figure 5.2) suggests the additional CH_4 during the DO-21 precursor event was emitted from a source with δ^{13}C of -57.6 ±2.5 ‰. This result is in best agreement with the δ^{13}C of CH_4 emitted from tropical wetlands or C3 plants due to aerobic CH_4 production. However, the δ^{13}C of boreal wetland and CH_4 hydrate is isotopically close to our result (table 5.3). Considering the δ^{13}C range of CH_4 emissions in nature, it seems reasonable to discuss the potential contribution of the latter two sources as well.

With δ^{13}C-CH_4 measurements alone it is not possible to further distinct the contribution of these four CH_4 sources. Brook et al. (2000) and Bock et al. (2012) simulated how a single event that rapidly emitted a pulse of 4000 Tg CH_4 into the atmosphere would be reflected in polar ice core records. They show that the signal duration of the simulated pulse would be in the order of decades, based on the short lifetime of CH_4 in the atmosphere and the smoothing within the firn column. The CH_4 peak of the DO-21 precursor event however, occurred during a period of ∼120 years (Chappellaz et al., 2013). We take the conclusion of Brook et al. (2000) into consideration and assume it is unlikely for the DO-21 event to stem from only one single catastrophic CH_4 release event from CH_4 hydrates. A period of

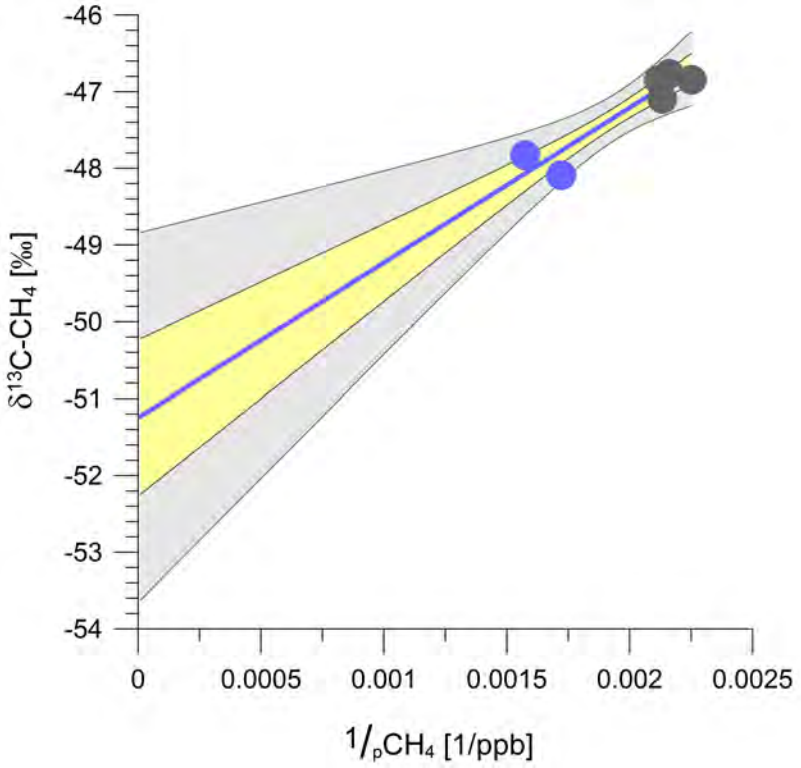

Figure 5.2: Keeling plot with two measurements from the DO-21 precursor event (blue circles) and four measurements from the stadial period preceding DO-21 (grey circles). The blue line represents the least square linear fit while the yellow and grey shading illustrate the 67 % and 95 % confidence interval of the linear fit, respectively.

multiple sudden CH_4 release events could explain both the $\delta^{13}C$ record and the duration of the precursor event. This theoretical possibility can be better tested with additional δ^2H-CH_4 measurements, which better distinct between wetland and clathrate CH_4 (e.g., Sowers, 2009; Bock et al., 2010b).

Wetland extend and CH_4 emissions are largely controlled by temperature and precipitation (e.g., Brook et al., 2000; Guo et al., 2012). The phasing of climate and CH_4 variations might therefore help to pinpoint CH_4 source variations during the DO-21 precursor event. The water isotopic composition in ice core records is a proxy for local temperature (e.g., NGRIP community members et al., 2004; Jouzel et al., 2007). One pronounced, hemispheric climate pattern recorded in both Greenland and Antarctic ice cores is coined as the "bipolar see-saw" (e.g., EPICA, 2006), where a long lasting Antarctic warming preceds a rapid temperature increase in Greenland, which again coincides with the onset of slow Antarctic cooling. This biploar see-saw pattern was very distinct during DO-21 (EPICA, 2006) and Figure 5.1.

A recent sea-level reconstruction shows the amplitude of sea-level changes is primarily controlled by Antarctic temperature and exhibits a substanical sea-level rise during DO-21 (Grant et al., 2012), thereby suggesting that the Antarcitic temperature maximum during DO-21 was relatively high. Furthermore, the NGRIP $\delta^{18}O$ (ice) record shows that the stadial temperatures in Greenland preceding DO-21 were not as low as stadial temperatures

during the full glacial periods. This scenario of relatively high Antarctic and moderate temperature in Greenland suggests relatively warm tropical latitudes. Monsoon system strength reconstructions from marine sediments of the Cariaco Basin (Peterson et al., 2000; Wang et al., 2004; Deplazes et al., 2013), the Indian Ocean (Rostek et al., 1993; Deplazes et al., 2013) and from speleothems (Wang et al., 2008) indicate warmer and wetter climate during DO-21, where both factors are likely to raise tropical wetland CH_4 emissions (e.g., Brook et al., 1996a). Peterson et al. (2000) show evidence that link Greenlandic and tropical South American climate and that remarkably indicate the highest precipitation throughout DO-21 to occur during the precursor event. It seems thus very likely that the rapid temperature increase as recorded by $\delta^{18}O$ (ice) in the NGRIP ice core (NGRIP community members et al., 2004) triggered the increase of CH_4 emission in tropical wetlands.

The variability of pCH_4 was furthermore related to northern hemisphere summer insolation (e.g., Brook et al., 1996a; Loulergue et al., 2008; Guo et al., 2012). The rise in northern hemispheric summer insolation during DO-21 (Laskar et al., 2004) likely enhanced CH_4 emissions from boreal wetlands, which are more depleted in $\delta^{13}C$ (Whiticar and Schaefer, 2007; Walter et al., 2008). Therefore, the KPA suggests that boreal wetland emissions cannot be the only additional CH_4 source during the DO-21 precursor event (table 5.3). However, the relative contribution of boreal wetlands to the total CH_4 emission might have increased. This seems plausible, as the relative sea-level reconstructions suggest the ice volume was only 50 % of its peak during the last glacial maximum (Grant et al., 2012) and the glaciation of boreal wetlands was unlikely to be full-grown. However, increased boreal CH_4 emissions would have to be in phase with enhanced pyrogenic CH_4 emissions that are more enriched in $\delta^{13}C$ to match the $\delta^{13}C$-CH_4 observations. Daniau et al. (2007) found wildfire intensity in Europe to correlate with increased Greenlandic temperature, which might have compensated enhanced boreal CH_4 emissions.

A most likely emission scenario to explain the rapid pCH_4 variability of the DO-21 precursor event comprises enhanced tropical wetland sources and possibly moderate increases of both biomass burning and boreal wetland sources. Note that the suggested scenario allows substituting tropical wetland sources for aerobic CH_4 formation from C3 plants as both sources are identical in the $\delta^{13}C$ of emitted CH_4 (Keppler et al., 2006). However, the variability of aerobic CH_4 formation in plants is not well understood and can therefore not be discussed in the context of rapid climate changes. The KPA furthermore precludes that CH_4 emitted from biomass burning and termites contributed large fractions of the additional CH_4 that caused the DO-21 precursor anomaly, which is not unexpected. Interestingly, an outstanding CH_4 emission pulse from geological mantle sources (e.g., Etiope and Lollar, 2013) can also be ruled out as these sources are significantly more enriched in $\delta^{13}C$. A recently proposed mechanism to control the $\delta^{13}C$-CH_4 on millenial to glacial-interglacial time scales includes extensive shifts in the C3/C4 plant ratio towards more C4 plants in tropical wetlands during periods of low pCO_2 (Möller et al., 2013). In fact, C4 plants are by $\sim$12 ‰ more enriched in $\delta^{13}C$ than C3 plants (Ehleringer et al., 1997) which would likely cause a linear enrichment of the CH_4 produced from C4 plants. Since the $\delta^{13}C$ of the additional CH_4 is close to the present day $\delta^{13}C$ of C3 dominated tropical wetland emissions, we interprete the good match as indication that tropical CH_4 source ecosystems were dominated by C3 plants during the DO-21 precursor event. This hypothesis is furthermore supported

by reconstructions of Australian/Asian vegetation biomes, which show relatively stable forest cover during our study period Hope et al. (2004). Furthermore, a cross over pCO_2 range of 210-220 ppm was suggested as threshold for significant C3/C4 plant ratio changes (Ehleringer et al., 1997). However, pCO_2 did not fall below this range during the DO-21 and the preceding cold period (Bereiter et al., 2012).

Table 5.3: Average $\delta^{13}C$ isotope ratios of categorized CH_4 sources. Values with indices [a,b,c,d,e] taken from Whiticar and Schaefer (2007); Mikaloff Fletcher et al. (2004a); Keppler et al. (2006); Denman et al. (2007); Walter et al. (2008), respectively. Boreal and tropical wetland values represent estimates for glacial periods (Whiticar and Schaefer, 2007). Note the data represent average values and the uncertainty is in the order of 2-5 ‰ (e.g., Quay et al., 1999).

Source	$\delta^{13}C$-CH_4 [‰]
Tropical wetlands	-58 [a]
Boreal wetlands	-63 [a]
CH_4 hydrates	-60 [b]
Aerobic C3	-58 [c]
Aerobic C4	-50 [c]
Termites	-70 [b]
Geological	-40 [d]
Biomass burning	-25 [b]
Thermokarst lakes	-70 [e]

Conclusions

High resolution δ^{13}C-CH_4 and CH_4 ice core records allow for the δ^{13}C determination of CH_4 sources by Keeling plot analysis. Our mass balance calculation reproduces the δ^{13}C-CH_4 results from the Keeling plot analysis within $\pm$0.2 ‰, which highlights the feasibility of this method for the CH_4 variability during the DO-21 precursor event. We discussed our results in consideration of prevailing climate variability and the theoretical footprint of large CH_4 emission pulses in ice core records. With this information at hand, we interprete our result to suggest the rapid CH_4 variability during the DO-21 precursor event was predominantly caused by enhanced tropical wetland sources. Minor contributions from biomass burning and boreal wetlands were only possible if their relative contribution matches the isotopic budget. The δ^{13}C-CH_4 result alone does not allow to unambiguously conclude CH_4 hydrate sources did not cause the rapid $p$$CH_4$ increase. However, that would require to assume the strongest sink fractionation found in the literature in combination with the maximum possible depletion of δ^{13}C-CH_4 within 95 % uncertainty of the Keeling plot analysis. Further measurements of δ^{2}H-CH_4 during the DO-21 precursor event would furthermore constrain our conclusions. A key question for future research is the relative contribution of aerobic CH_4 in plants and its variability during climate changes.

Chapter 6

CH_4 carbon isotopes during the last 170 ka

Abstract

Ice core records showed that for the last 800.000 years, atmospheric CH_4 mixing ratios were intimately linked to global temperature (Loulergue et al., 2008). Records of CH_4 have recently been proposed as the best proxy for global monsoon system strength (Guo et al., 2012). Here we suggest CH_4 carbon isotope ratios as monsoon controlled proxy for the variability in vegetation communities and microbial processes that dominate global CH_4 source ecosystems. The most important natural CH_4 sources during glacial and interglacial climate are tropical wetlands (e.g., Chappellaz et al., 1993b; Kirschke et al., 2013), which largely comprise of tropical rain forest during interglacial climate. However, tropical rain forest ecosystems declined and were outcompeted by C4 grasses during glacial climate, which are more competitive when atmospheric CO_2 is low (Ehleringer et al., 1997; Collatz et al., 1998) and likely cause a stronger enrichment in $\delta^{13}C$ in tropical wetland CH_4 as their relative contribution as CH_4 precursor material increases (e.g., Sowers, 2009; Möller et al., 2013).

Boreal wetlands are the second most important natural CH_4 sources (e.g., Guo et al., 2012) in which vegetation (e.g., Tarasov et al., 2007; Lozhkin et al., 2007) and possibly the ratio of methanogenic pathways (Walter et al., 2008; Holmes et al., 2013) changed with climate. Here we combine both CH_4 and $\delta^{13}C$-CH_4 with further geological records and derive important information that enable to time the fall of tropical tree cover and boreal vegetation cover in response to climate change. This allows identifying environmental thresholds, beyond which global vegetation significantly degraded on glacial-interglacial time scales. Our findings are important to further work on the global CH_4 budget and vegetation dynamics as well as for the assessment of their predicted future scenarios.

Introduction

Mixing ratios and the carbon isotopic composition of atmospheric CH_4 integrate both global sink and source processes and show large variability on decadal to orbital time scales (e.g., Kirschke et al., 2013; Loulergue et al., 2008; Quay et al., 1999; Möller et al., 2013). On glacial-interglacial time scales, the global CH_4 sink was found to be rather constant (Levine et al., 2012), suggesting the observed variability of CH_4 (Figure 6.3) is predominantly controlled by changes in CH_4 sources in response to changing climate. CH_4 is generally produced by methanogenic microbes that decompose organic material through hydrogenotrophic or acetoclastic methanogenesis (e.g., Conrad, 2005; Angel et al., 2012; Holmes et al., 2013).

The $\delta^{13}C$ of produced CH_4 depends on a complex chain of factors (Conrad, 2005). On a macroscopic level, prevailing climate and environmental parameters such as temperature, precipitation, pCO_2 control the composition of vegetation biomes (Ehleringer et al., 1997; Collatz et al., 1998). These large scale parameters control the average $\delta^{13}C$ of the organic material in CH_4 source ecosystems, which propagates through microbial decomposition processes into the produced CH_4. For example, temperature and atmospheric CO_2 mixing ratios control the fraction of C4 plants in tropical biomes on glacial-interglacial time scales. C4 plants are more enriched in $\delta^{13}C$ than C3 plants (Ehleringer et al., 1997; Collatz et al., 1998) and will therefore contribute to atmospheric $\delta^{13}C$-CH_4 enrichment (Quay et al., 1999; Conrad, 2005). Furthermore, periods of droughts decrease the primary productivity (Phillips et al., 2009, 2010; Davidson et al., 2012; Lewis et al., 2011; Chen et al., 2011; Wang et al., 2013a) and thereby microbial production of $\delta^{13}C$ depleted CH_4 while the frequency of wildfires will increase (Davidson et al., 2012; Lewis et al., 2011; Chen et al., 2011; Wang et al., 2013a) which enhances the formation of $\delta^{13}C$ enriched CH_4 (e.g., Mikaloff Fletcher et al., 2004a).

Also, mixing ratio variations of atmospheric CO_2 directly impact the $\delta^{13}C$ of C3 plants through fractionation during CO_2 uptake and assimilation, with generally higher depletion in $\delta^{13}C$ with higher CO_2 (Figure 6.1). Glacial-interglacial CO_2 approximately ranged between 180 and 280 ppm (Lüthi et al., 2008) which accounts for $\sim$2 ‰ in $\delta^{13}C$ variability in C3 plants (Schubert and Jahren, 2010). Climate variability also controls $\delta^{13}C$-CH_4 on a microscopic level. Microbial CH_4 formation occurs through the two main pathways of CO_2 reduction and acetate fermentation, which significantly differ in the resulting $\delta^{13}C$-CH_4 (Conrad, 2005). The ratio of hydrogenotrophic to acetoclastic CH_4 formation varies with microbial communities, nutrient availability and vegetation type and is thus sensitive to climate change (Conrad, 2005; Walter et al., 2008; Holmes et al., 2013).

Ice core records of $\delta^{13}C$-CH_4 (Figure 6.3) integrate the dynamics of entire CH_4 source ecosystems on a global level on millennial to glacial-interglacial time scales. As Möller et al. (2013) have pointed out, the variability of CH_4 mixing ratio has little control of $\delta^{13}C$-CH_4 on these time scales (Figure 6.3). This highlights that CH_4 emission on the one hand and CH_4 formation pathway and vegetation dynamics on the other hand change on different time scales, which reveals that different controlling mechanisms are in place (Figure 6.3).

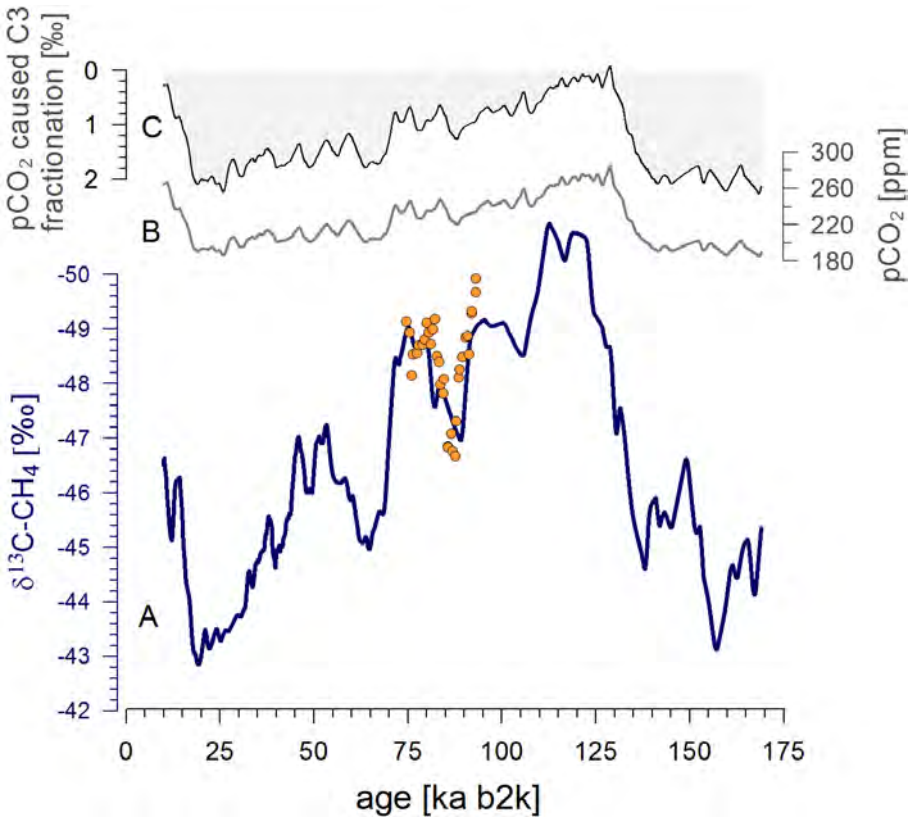

Figure 6.1: Fractionation of C3 plant material based on $p\mathrm{CO}_2$ variability. A) $\delta^{13}\mathrm{C\text{-}CH}_4$, blue line (Möller et al., 2013), orange circles this study, B) $p\mathrm{CO}_2$ composite record (as described in text), C) $\delta^{13}\mathrm{C}$ fractionation in C3 plants due to variability in $p\mathrm{CO}_2$ observations after (Schubert and Jahren, 2010). The y-axes of A) and C) are equally scaled. The grey shading indicates the fractionation by C3 plants and thus the maximum effect on $\delta^{13}\mathrm{C\text{-}CH}_4$ if all vegetation in CH_4 source ecosystems comprised C3 plants only. The calculations are based on preindustrial holocene $p\mathrm{CO}_2$ of 280 ppm (Etheridge et al., 1996) that give zero fractionation.

Unfortunately, the knowledge of hydrogenotrophic and acetoclastic CH_4 formation variability is limited (Conrad, 2005) and high resolution data on vegetation dynamics over the last 170 ka are presently not available, as would be required for CH_4 source reconstructions on glacial-interglacial time scales using CH_4 mixing and isotope ratios from ice cores (Möller et al., 2013). Here, we pool $\delta^{13}\mathrm{C\text{-}CH}_4$ and geological records that cover a range of tropical to sub-polar regions as shown in Figure 6.2. The data show glacial-interglacial changes in climate and vegetation and are compared to $\delta^{13}\mathrm{C\text{-}CH}_4$ in and Figure 6.3. We apply singular-spectrum analysis (SSA) (e.g., Golyandina and Korobeynikov, 2013; Ghil et al., 2002) to investigate the timing of gradual and abrupt changes in CH_4 formation processes. We propose $\delta^{13}\mathrm{C\text{-}CH}_4$ as unique proxy integrating the temporal variability of boreal and tropical vegetation dynamics on a global scale in addition to pollen analysis based vegetation reconstructions that are limited in spatial representativeness.

Analysed data

We present our new high resolution Greenlandic δ^{13}C-CH_4 data (Figure 6.3) that were measured using the analytical methods described by Sperlich et al. (2012, 2013). The record comprises samples from the NGRIP and NEEM ice cores that are dated between 75-95 ka b2k (ka b2k abbreviates thousand years before 2000), (Figure 6.3). The NEEM samples were transferred to the AICC time scale (Veres et al., 2013; Bazin et al., 2013) through the access of NGRIP, where high resolution pCH$_4$ data and δ^{15}N data (Kindler et al. (2013) and Myriam Guillevic pers. comm., (2013)) were used to optimize the gas age agreement between NGRIP and NEEM gas age scales. Thereby, NEEM samples could be interpolated on the NGRIP depth scale which is part of the AICC time scale.

We combine our data and the data from Möller et al. (2013) to extend the covered time period to 170 ka b2k. Möller et al. (2013) found that δ^{13}C-CH_4 and CH_4 are decoupled on millennial to glacial-interglacial time scales. Instead, Möller et al. (2013) found strong correlations between δ^{13}C-CH_4 and CO_2 (Figure 6.3) and relative sea level (RSL) variations, respectively and suggest that CO_2 and climate control atmospheric δ^{13}C-CH_4 on glacial-interglacial time scales by controlling C3/C4 plant ratios and δ^{13}C of plant material (Ehleringer et al., 1997; Collatz et al., 1998; Schubert and Jahren, 2010). Möller et al. (2013) furthermore point out that the suggested correlation with CO_2 weakens during the Dangaard-Oeschger events 17, 21 and 24, at times of rapid RSL variation. However, some variations in the δ^{13}C-CH_4 record have no clear counterpart in either CO_2 and RSL or pCH$_4$, e.g. the depletion of δ^{13}C between 155 and 150 ka b2k, which suggests further processes were in place that controlled δ^{13}C-CH_4.

In Figure 6.3, we compare the δ^{13}C-CH_4 data to solar insolation (Laskar et al., 2004) and polar temperature reconstructions (NGRIP community members et al., 2004; Jouzel et al., 2007), CH_4 (Schilt et al., 2010a) and CO_2 (Ahn and Brook, 2008; Bereiter et al., 2012; Lüthi et al., 2008) records as well as a range of proxies for monsoon strength (Rostek et al., 1993; Bassinot et al., 1994; Caley et al., 2011b), the El Nino Southern Oscillation (ENSO) (Clement et al., 1999), dust as proxy for vegetation cover and aridity (Ruth et al., 2007; EPICA, 2004; Winckler et al., 2008; Clemens et al., 1996) and biogenic productivity (Prokopenko et al., 2001). Furthermore, we include the most recent estimation of the time of the mount Toba eruption (Svensson et al., 2013) (Figure 6.3). CH_4 mixing ratios shown in Figure 6.3 combine two Southern Hemispheric datasets to cover the complete period of time (Schilt et al., 2010a; Loulergue et al., 2008). Likewise, the CO_2 composite record comprises data from Monnin et al. (2001); Bereiter et al. (2012); Ahn and Brook (2008); Lüthi et al. (2008) to cover the time period in highest resolution. δ^{13}C-CH_4, CH_4, CO_2 and EDC temperature records are interpolated to equidistant time intervals and smoothed with a 1000 year filter to account for uneven temporal sample resolution (Figure 6.3). Because the 1000 year window removed too many details from NGRIP δ^{18}O record it was thus reduced to 300 years in Figure 6.3. The calculations were done with smoothed and unsmoothed CH_4 data which showed the smoothing had no significant difference to the results. All geological records are on the time scale as published while all ice core records are shown on the recently published AICC2012 time scale (Veres et al., 2013; Bazin et al., 2013). Note, the use of the newer AICC2012 time scale as compared the scale from Lemieux-Dudon et al. (2010) which was used by Möller

et al. (2013) resulted in some changes to the timing. For example is the oldest δ^{13}C-CH_4 sample on AICC2012 dated to ∼169 ka b2k while the same sample is dated to ∼162 ka b2k on the time scale used by Möller et al. (2013), which is, however, within the uncertainty of both.

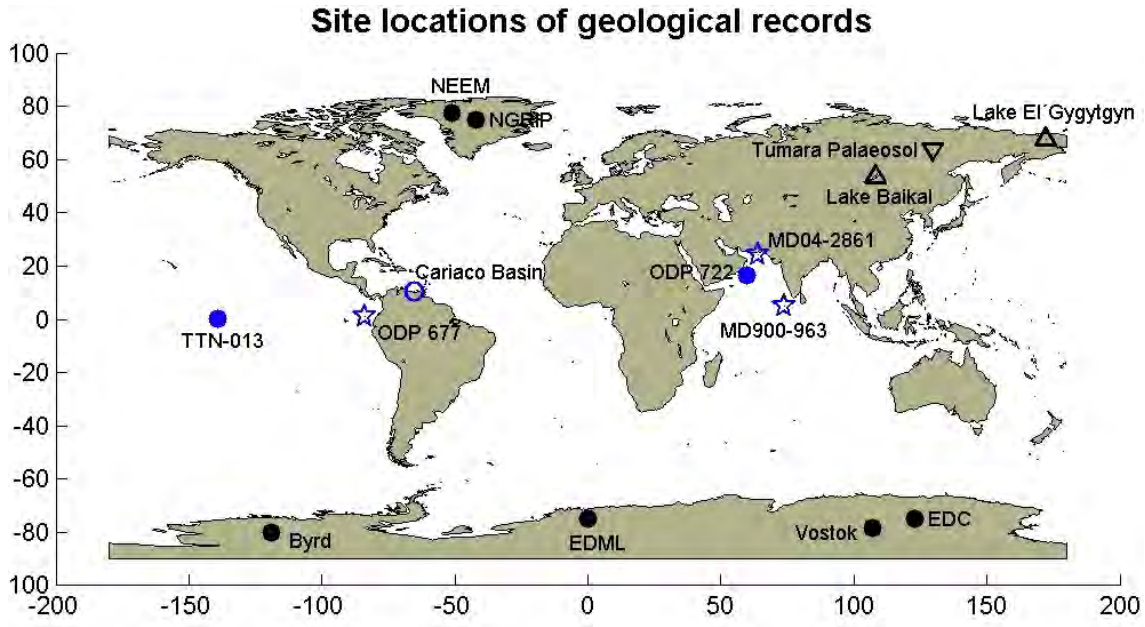

Figure 6.2: Sample sites and core names of used data. Black circles indicate ice core sites while blue filled circles mark the marine dust record sites, blue stars indicate sites of δ^{18}O measurements as marine monsoon proxies and the blue open circle shows the Cariaco Basin site from where the color reflectance data originate. Black pyraminds indicate lake sediments while the black triangle pointing downwards indicates the palaesol sequence.

There are visually convincing temporal relations between δ^{13}C-CH_4 and a range of parameters which are primarily temperature and precipitation controlled. We see correlations with records that originate from tropical, boreal and polar sites, suggesting that the δ^{13}C-CH_4 record reflects a combination of CH_4 source variations with hemispheric to global extend. However, the temporal variation in the relation suggests that CH_4 sources contributed on different spatio-temporal time scales to the δ^{13}C-CH_4 variability over the last 170 ka. We analyze the above mentioned parameters by time series analysis to investigate the temporal variability in more detail.

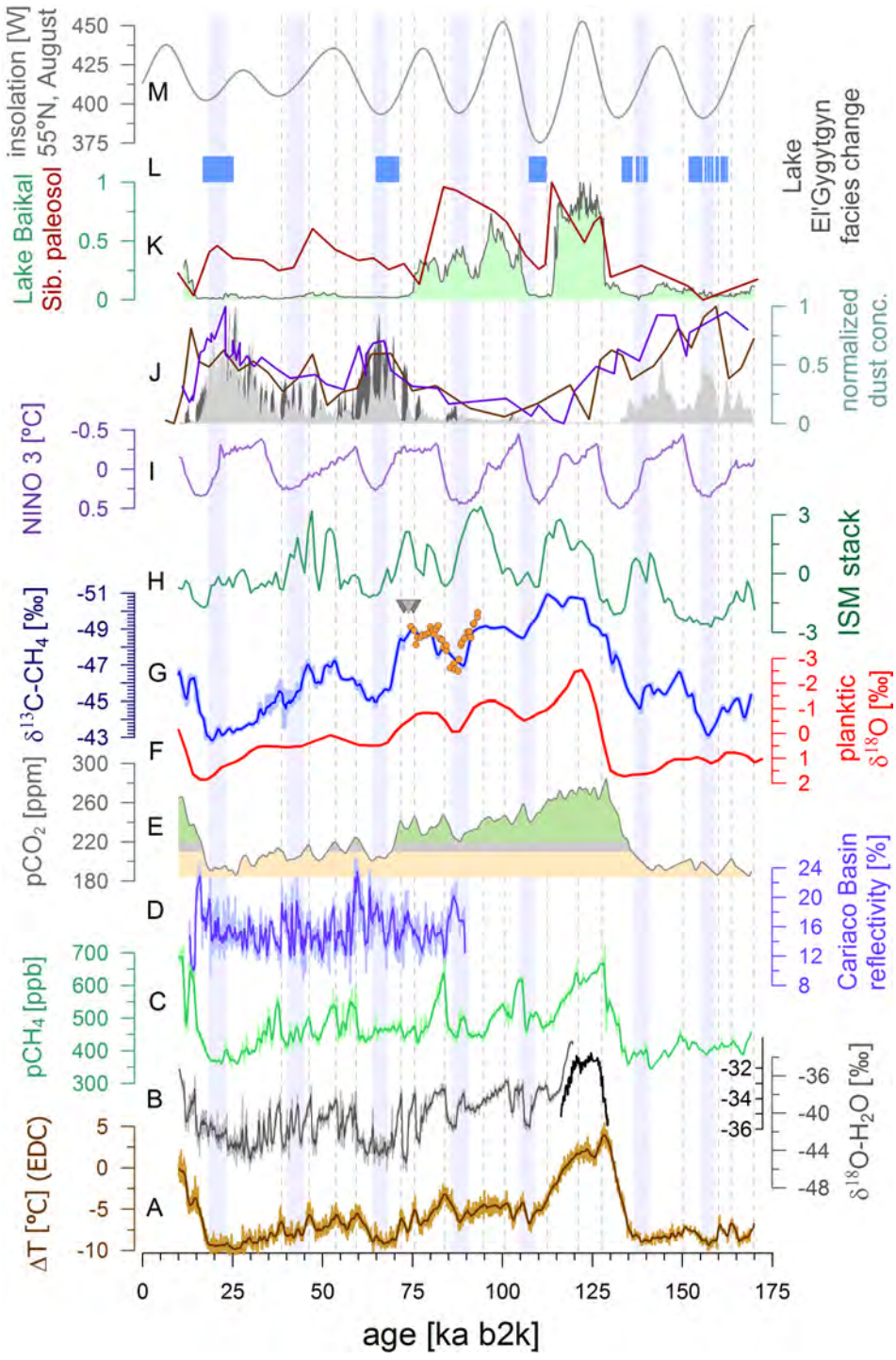

Figure 6.3: All data. A) Antarctic (EDC) temperature relative to today (Jouzel et al., 2007), B) δ^{18}O from NGRIP ice (grey) (NGRIP community members et al., 2004), Eemian section from NEEM ice core on inner y-axis (black) (NEEM community members et al., 2013), C) Antarctic pCH$_4$ stack (Loulergue et al., 2008; Schilt et al., 2010a), D) reflectivity Cariaco Basin (Peterson et al., 2000), E) pCO$_2$ stack (Monnin et al., 2001; Ahn and Brook, 2008; Bereiter et al., 2012; Lüthi et al., 2008), grey filling indicates the 210-220 ppm cross over threshold, green and grey the pCO$_2$ that favours C3 and C4 plants, respectively (Ehleringer et al., 1997), F) tropical marine δ^{18}O stack as monsoon proxy (Bassinot et al., 1994), G) Antarctic δ^{13}C-CH$_4$ (Möller et al., 2013) in blue, dots represent Greenlandic δ^{13}C-CH$_4$, this study, central triangle shows Toba eruption (Svensson et al., 2013), the darker two triangles represent the gas age uncertainty window of δ^{13}C-CH$_4$ during Toba event, H) monsoon stack (Caley et al., 2011b), I) ENSO variability (Clement et al., 1999), J) light and dark grey filling represents Antarctic (EPICA, 2004) and Greenlandic (Ruth et al., 2007) dust records, purple and brown lines represent equatorial marine dust records from Winckler et al. (2008) and Clemens et al. (1996), respectively, K) green filled line indicates biogenic silica [%] from Lake Baikal (Prokopenko et al., 2001), dark red line shows plant source water isotopic composition reconstructed from a Siberian palaeosol (Zech et al., 2013), both boreal datasets normalized to 1, L) blue indicates perennial ice coverage of Lake El'Gygytgyn (Melles et al., 2012), M) mean August solar insolation at 55° N (Laskar et al., 2004). Blue bars indicate monsoon (Bassinot et al., 1994) minima, dashed lines show peaks occuring in A), G) and B) during last glacial. Light shading in A), B), C), D) and G) represent original data, overlying darker lines are smoothed.

Singular Spectrum Analysis

Singular spectrum analysis (SSA) is a tool designed to extract subsignals of non-stationary time series (for a detailed description see e.g. (Golyandina et al., 2001; Ghil et al., 2002)). SSA is more flexible than the discrete Fourier transform as it is able to extract phase and amplitude modulated signals within a prescribed frequency windows. This makes SSA particularly useful to analyse the variability of systems that fluctuate regularly but with variable timing as frequently found in natural systems, e.g. the ENSO phenomenon. SSA was performed in the R language of scientific computing as described in Golyandina and Korobeynikov (2013) and kindly provided by Miguel Mahecha (pers. comm., 2013).

The SSA was constructed by breaking each record down into 6 frequency bands (0-14, 14-28, 28-35, 35-45, 45-95 and $\geq$ 95 ka). We found distinct signals in the frequency bands matching orbital eccentricity ($\geq$ 95 ka), obliquity (35-45 ka) and precession (14-28 ka). Figure 6.4, 6.5 and 6.6 show the variation of the records in the orbital frequency bands. We binned the residuals of all three intermediate frequency bands (0-14, 28-35 and 45-95 ka) as shown in Figure 6.7. To analyse the relevance of each parameter, we correlated both all original data as well as their respective frequency bands with those from δ^{13}C-CH_4 as shown in table 6.1. The correlations were calculated as using Spearman's rank coefficient of correlation (Spearman's ρ) to account for non-linear relations (section 6).

Results SSA

The results of the SSA are shown in Figure 6.4, 6.5, 6.6 and 6.7. The most obvious feature in the majority of the original data is the glacial-interglacial variability in the frequency band category $\geq$ 95 ka. This variability largely reflects temperature, global ice volume (hence sea-level) and hydrological oscillations (Jouzel et al., 2007; Grant et al., 2012). However, both the 14-28 and 35-45 ka frequency bands also contain significant signals.

In general, the amplitude in the $\geq$ 95 ka signal accounts for 50 % of the amplitude while the remaining 50 % are about evenly distributed between the signals within the 14-28 and 35-45 ka frequency bands. The Eemian (last interglacial period, 115-130 ka b2k) was marked by the warmest temperatures of the last 170 ka as recorded in Greenland and Antarctic ice cores (NEEM community members et al., 2013; EPICA, 2006; Jouzel et al., 2007), (Figure 6.3). Note the NGRIP δ^{18}O record only reaches back as far as $\sim$120 ka. Therefore, it does not contain a full glacial-interglacial cycle but begins with the distinct cooling at the onset of the last glaciation. However, a feature this strong at the end of an analysed record produces artefacts in the extracted frequency bands and was thus removed. Because the time covered by the NGRIP δ^{18}O record is limited to the cooling during the last glaciation and the onset of Termination 1 (Figure 6.4), the correlation as shown in table 6.1 is likely overestimated.

We display $\geq$ 95 ka signals that were meaningful extracted by SSA and excluded the ones that were dominated by artefacts. For example, the modelled ENSO index was assigned a small signal in the $\geq$ 95 frequency band even though it is entirely based on the precessional cycle (Clement et al., 1999). This indicates that additional work might optimize the SSA.

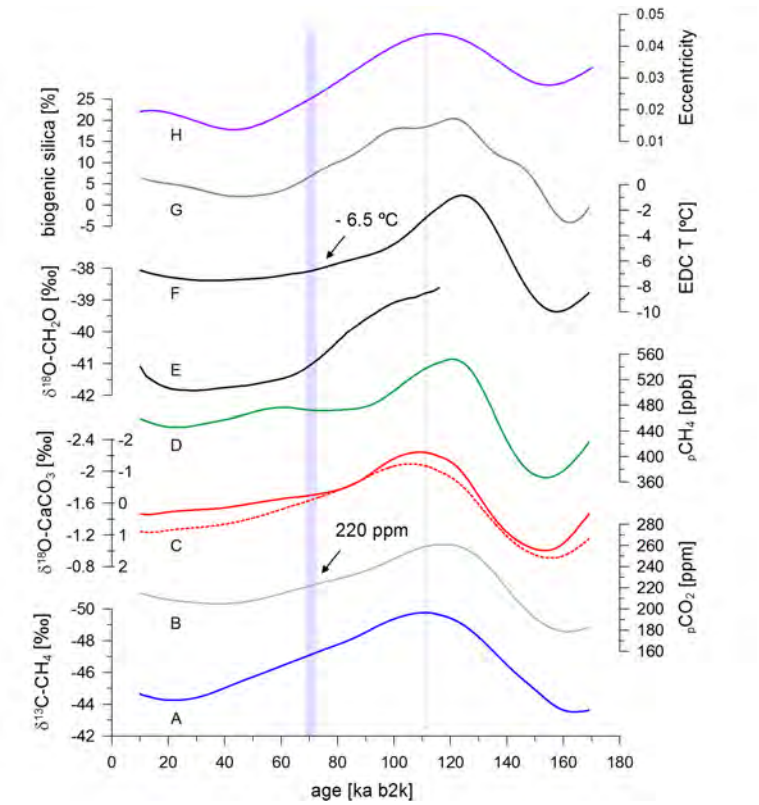

Figure 6.4: Band with $\geq$ 95 ka frequency. A) δ^{13}C-CH_4, B) $p\mathrm{CO}_2$, C) tropical marine δ^{18}O proxies, solid line (Rostek et al., 1993), dashed line (Bassinot et al., 1994), D) $p\mathrm{CH}_4$, E) NGRIP δ^{18}O, F) Antarctic (EDC) temperature relative to today, G) biogenic silica in Lake Baikal, H) orbital eccentricity (Laskar et al., 2004). The blue bar indicates the MIS 5/MIS 4 transition, when temperatures at EDC were about 6.5 colder than today (Jouzel et al., 2007) and $p\mathrm{CO}_2$ ranged about 220 ppm (Ahn and Brook, 2008; Bereiter et al., 2012). The grey dashed line indicates the maximum δ^{13}C depletion of CH_4 in the $\geq$ 95 ka band.

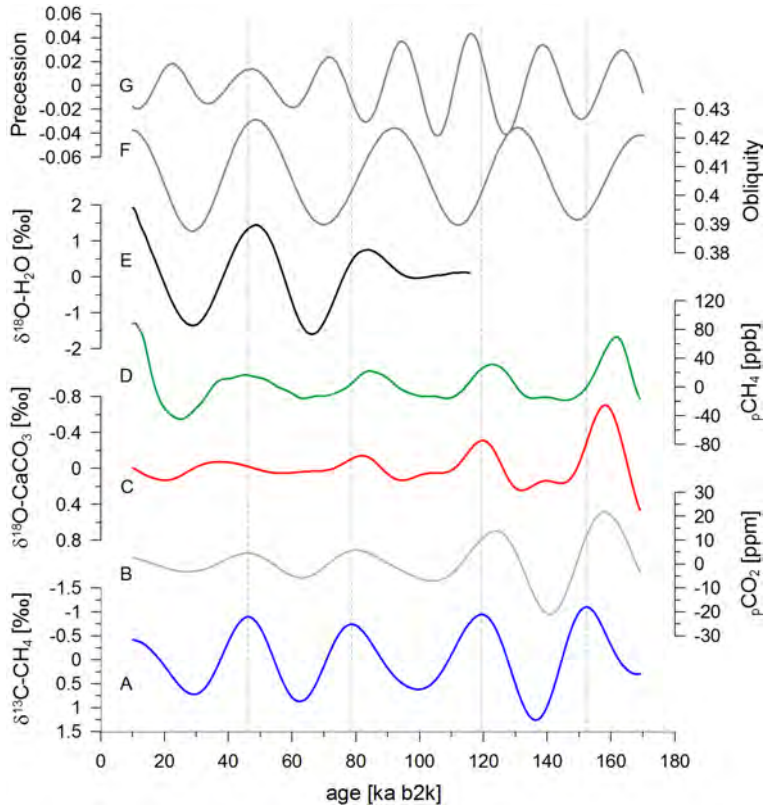

Figure 6.5: Band with 35-45 ka frequency. A) δ^{13}C-CH_4, B) pCO_2, C) tropical marine δ^{18}O proxy after Rostek et al. (1993), D) pCH_4, E) NGRIP δ^{18}O, F) orbital obliquity, G) orbital precession, F) and G) after Laskar et al. (2004). The grey dashed lines indicates the maximum δ^{13}C depletion of CH_4 in the 35-45 ka band.

The signals which were extracted in the 35-45 ka frequency band are shown in Figure 6.5. In addition, the orbital precession and obliquity cycles are also shown in Figure 6.5. While the δ^{13}C-CH_4 signal is of relatively constant amplitude, other records such as CH_4, CO_2 and the tropical monsoon proxy seem to weaken in amplitude throughout the last glacial period. Note the flat end of the NGRIP δ^{18}O signal is likely due to edge effects of the SSA (Figure 6.5). It is important to keep in mind that the signals in the 14-28 ka frequency band are likely to contain edge effects of the SSA. The high amplitude during the youngest or oldest 10-15 ka in δ^{13}C-CH_4, the monsoon signal as well as CO_2 and CH_4 are a good example. Nevertheless, the 14-28 ka frequency band highlights distinct variations in δ^{13}C-CH_4, CO_2, the monsoon and temperature proxies as well as in the dust record (Figure 6.6). For example, both CO_2 and Antarctic dust show moderately enhanced amplitudes between MIS 4 and MIS 2. In contrast, the 14-28 ka frequency band display the weakening of the monsoon proxy signal throughout the last glacial, as has been suggested in further monsoon studies (e.g., Caley et al., 2011b).

Simultaneously, the amplitude of the orbital precession dampens, as does the variability of CH_4, δ^{18}O and of the ENSO temperature anomaly. A positive precessional signal indicates less summer insolation in the Northern Hemisphere. The residuals of the three remaining frequency bands (0-14, 28-35 and 45-95 ka) are added and displayed in Figure 6.7.

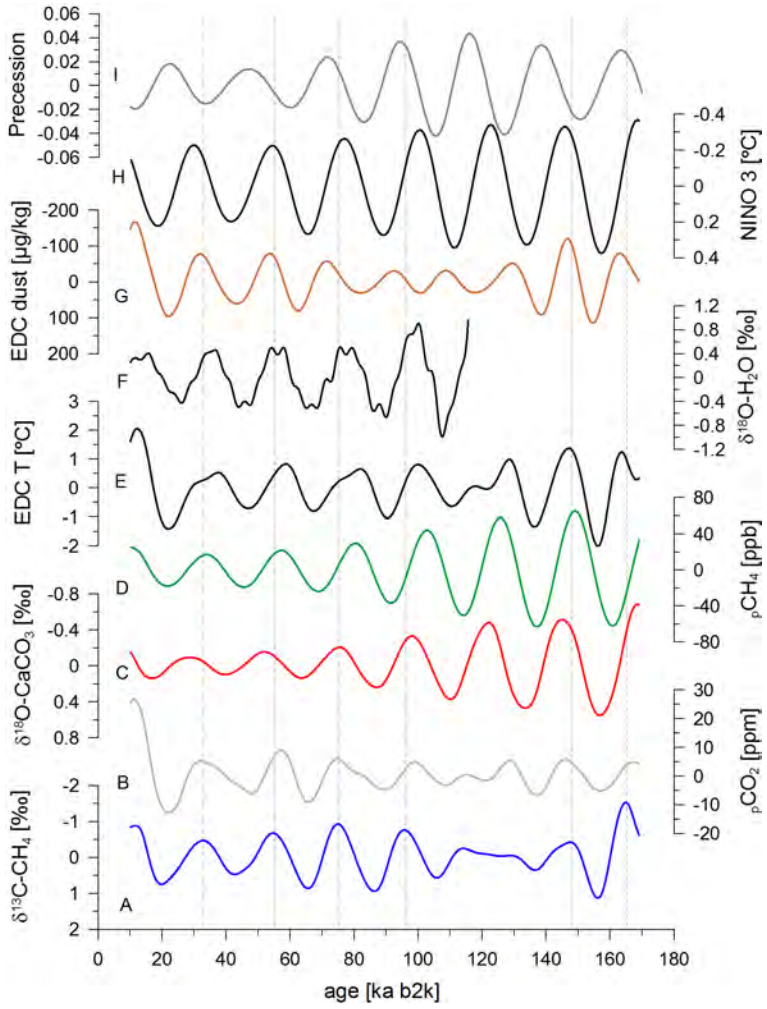

Figure 6.6: Band with 14-28 ka frequency. A) δ^{13}C-CH_4, B) pCO_2, C) tropical marine δ^{18}O proxy after Rostek et al. (1993), D) pCH_4, E) Antarctic (EDC) temperature, F) NGRIP δ^{18}O, G) Antarctic (EDC) dust , H) ENSO temperature variability I) orbital precession after Laskar et al. (2004). The grey dashed lines indicates the maximum δ^{13}C depletion of CH_4 in the 14-28 ka band.

On average, the cumulative residuals contain ∼10 % of the total variations. However, features of rapid variability within CH_4 and NGRIP $\delta^{18}O$ exceed 10 % and the residuals of the ENSO temperature anomaly index which show up to 50 % of the amplitude of its original signal.

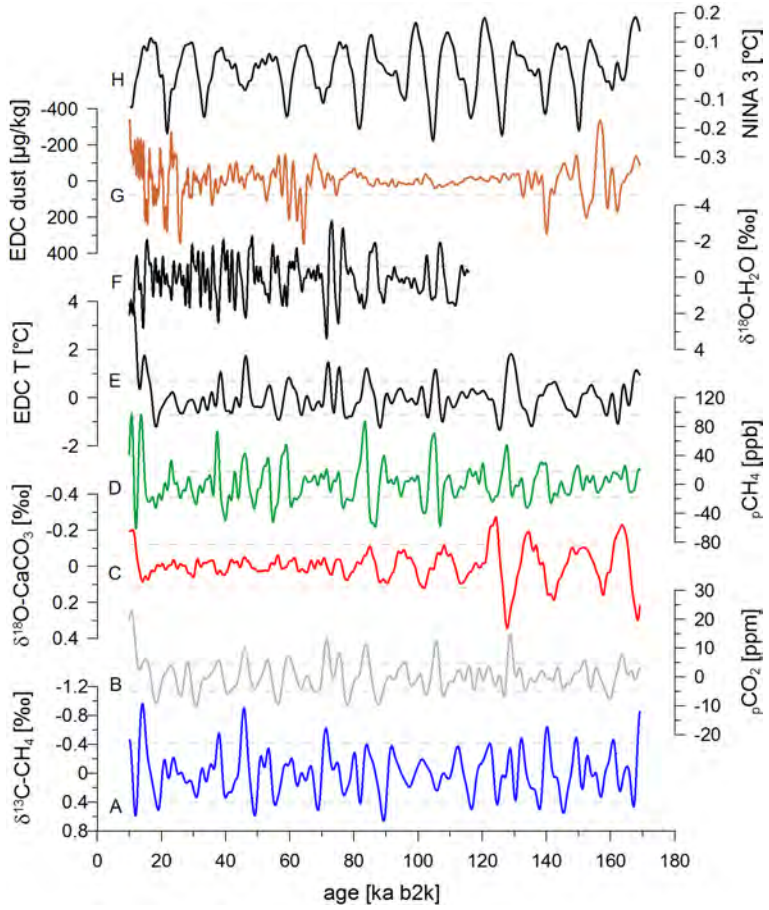

Figure 6.7: Cumulated residual frequencies of the 0-14, 28-35 and 45-95 ka bands. A) $\delta^{13}C\text{-}CH_4$, B) pCO_2, C) tropical marine $\delta^{18}O$ proxy after Rostek et al. (1993), D) pCH_4, E) Antarctic (EDC) temperature, F) NGRIP $\delta^{18}O$, G) Antarctic (EDC) dust , H) ENSO temperature variability. The band between the grey dashed lines indicates 10 % of the range of the original signal to provide an estimate about the relative extraction efficiency of the SSA method.

Results: correlation of frequency bands

Spearman's rank coefficient of correlation "ρ" is a measure of how well a statistical relation between two records can be described by a monotonic function. The results in table 6.1 show the correlation of indicated parameters with δ^{13}C-CH_4 within each of the $\geq$ 95, 35-45 and 14-28 ka frequency band, respectively. δ^{13}C-CH_4 and δ^{18}O as Greenland temperature proxy show the highest coefficient of correlation in the $\geq$ 95 ka frequency band with R=0.95. However, the Greenland record does not contain the full glacial-interglacial period, the result is thus not as robust. Besides, the strongest correlation of δ^{13}C-CH_4 in all three frequency bands is found with CO_2, thereby supporting the recent finding of Möller et al. (2013).

Möller et al. (2013) furthermore report the second highest correlation between δ^{13}C-CH_4 and RSL. Our analysis confirms this correlation in the original data. However, the SSA shows the correlation between δ^{13}C-CH_4 and RSL is mostly due to the $\geq$ 95 ka variability. In the $\geq$ 95 ka frequency band, δ^{13}C-CH_4 correlates with all data better than |R = 0.83|, except for the ENSO model that is forced by orbital precession. The Spearman's rank correlation suggests a close relation between δ^{13}C-CH_4 and CH_4 in the original data of -0.73 and even stronger in the $\geq$ 95 ka band with R = -0.89. The correlation with the two monsoon proxies (Rostek et al., 1993; Bassinot et al., 1994) is consistently high in the original data (R = 0.75 and 0.82) and in all frequency bands (R = 0.88-0.64 and 0.92-0.48) for Rostek et al. (1993); Bassinot et al. (1994), respectively. The SSA found no correlation between δ^{13}C-CH_4 and the monsoon proxy of Bassinot et al. (1994) in the 35-45 ka frequency band, which requires further investigation.

Within the 170 ka period, the global monsoon system showed the strongest amplitude between onset and end of the Eemian interglacial as is shown in the summer monsoon stack of Caley et al. (2011b). Note, that the monsoon index (Caley et al., 2011b) mimics the $\geq$ 95 ka variability in its baseline and shows the absolute minimum monsoon strength at about 155 ka b2k which remarkably reflects the variability in δ^{13}C-CH_4 (Figure 6.3). (Unfortunately, it was not possible to include the monsoon index of Caley et al. (2011b) to the SSA at the time this thesis was written, but it will be done in future work.)

The correlation with Antarctic and Greenlandic temperature proxies is very strong throughout all orbital frequency bands as well as in the original data. While the biogenic silica record from Lake Baikal correlates best on the $\geq$ 95 ka frequency, the correlation of Antarctic dust record is strong in both the $\geq$ 95 ka and 14-28 ka frequency bands. As expected, the correlation with the ENSO variability is strongest in the 14-28 frequency while it is weak in all other frequencies or suffers from an artificial signal that is likely introduced by the SSA method. Note the correlations are to be interpreted with great care as a good correlation does not necessarily identify a true controlling parameter.

Table 6.1: Spearman's rank correlation coefficients for the corelation of displayed parameters with δ^{13}C-CH_4. The headers refer to the correlation with the records of 1) data indentifyer, 2) CH_4 mixing ratios, 3) CO_2 mixing ratios, 4) the δ^{18}O monsoon proxy after Rostek et al. (1993), 5) the δ^{18}O monsoon proxy after Bassinot et al. (1994), 6) relative sea level after Grant et al. (2012), 7) biogenik silica in Lake Baikal Prokopenko et al. (2001), 8) Antarctic (EDC) dust record EPICA (2004), 9) Antarctic (EDC) temperature variability Jouzel et al. (2007), 10) δ^{18}O of NGRIP ice core, 11) ENSO temperature anomaly Clement et al. (1999). The first column indicates whether the correlations are derived from the respective frequency band or the original dataset.

Band	pCH_4	pCO_2	Mon_R	Mon_B	RSL	Silica	Dust	Temp.	δ^{18}O	ENSO
≥ 95	-0.89	-0.93	0.88	0.92	-0.83	-0.88	0.84	-0.89	-0.95	-0.47
35-45	-0.60	-0.76	0.67	NaN	-0.47	NaN	NaN	-0.59	-0.76	-0.01
14-28	-0.20	-0.76	0.64	0.48	NaN	-0.12	0.67	-0.60	-0.68	0.63
orig.	-0.73	-0.86	0.75	0.82	-0.86	-0.67	0.76	-0.82	-0.69	0.06

Discussion: correlation within frequency bands

The good correlation between δ^{13}C-CH_4 and δ^{18}O from both the Indian and Pacific Ocean suggest that the strength of monsoonal systems including the Indian summer monsoon (ISM) and the South American monsoon (SAM) impact on δ^{13}C-CH_4. Even though tropical marine δ^{18}O records global ice volume variations as well (Rostek et al., 1993; Bassinot et al., 1994), both records contain a superimposing monsoon signal which is confirmed by the high coefficients of correlation in the frequency bands where the correlation with RSL is weak or absent. Furthermore, the fact that all statistical correlations with both Antarctic and Greenlandic temperature proxies as well as the monsoon proxies are high suggests that these parameters represent climate factors that truly control δ^{13}C-CH_4. This hypothesis gets further support by the recently described interhemispheric temperature teleconnections and the role of Southern hemispheric temperatures that control Indian Ocean sea surface temperatures (Wang et al., 2013b), hence an important component of the strength of the ISM (An et al., 2011; Caley et al., 2013) and thereby δ^{13}C-CH_4.

Furthermore, the correlation between δ^{13}C-CH_4 and the ENSO signal in the 14-28 ka frequency underlines the sensitivity of δ^{13}C-CH_4 to tropical climate phenomena. On the other hand, we interpret the good correlation with both the Antarctic dust and biogenic silica from Lake Baikal record as being a consequence of common climate control. A strong linear correlation between Antarctic temperatures and CO_2 has been found for the last 800 ka (Fischer et al., 2010) where the latter is largely controlled by Southern Ocean processes. It is furthermore reported that CO_2 levels affect the δ^{13}C of plant material (Schubert and Jahren, 2010) and the biological productivity (Ehleringer et al., 1997) and thereby impact CH_4 source ecosystem (Hornibrook and Bowes, 2007; Hornibrook, 2009). However, to what extend both CO_2 and RSL are in control or in covariance with δ^{13}C-CH_4 needs to be assessed.

Discussion: The Monsoon concert and CH_4 carbon isotopes

It is currently debated whether or not the South American, African and Asian monsoon systems can be regarded as one global monsoon system (e.g., Ziegler et al., 2010; Cheng et al., 2012) and whether the different timing found in speleothem or marine records results from site specific influences (Ziegler et al., 2010). However, there seems to be a growing consensus that monsoonal systems represent individual but possibly linked climate features (e.g., Caley et al., 2011a). A good example is the monsoon variability during MIS 3 that is particularly irregular represented in different records. While the MIS 3 variability is one of the most distinct features of the last 170 ka in the summer monsoon stack of Clemens and Prell (2003), it shows moderate amplitudes in the Sanbao/Hulu cave record (Wang et al., 2008) and in the summer monsoon stack of Caley et al. (2011b) but is completely absent in the Mediterranean sapropel record (Ziegler et al., 2010).

However, we assume that an increased strength of the wet monsoon season enhances tropical wetland precipitation and the export of heat and moisture into the extra-tropics (Guo et al., 2012), which causes the correlation between δ^{13}C-CH_4, monsoon system strength and polar temperatures. Since δ^{13}C-CH_4 integrates the CH_4 signal of global sources, it cannot differentiate the temporal variability between geographically isolated monsoon systems. Therefore, it seems reasonable to proceed with the assumption of an integrative monsoon impact on δ^{13}C-CH_4, acknowledging that there is probably more internal variability than δ^{13}C-CH_4 can differentiate.

There is furthermore growing consensus that the Asian monsoon system is not only controlled by Northern Hemispheric insolation (Cheng et al., 2009) and that Southern Hemispheric temperature variations contribute significantly (Rohling et al., 2009b; An et al., 2011; Caley et al., 2013). Changes in the monsoon and climate system have strong implications for heat and moisture distribution into tropical and boreal wetlands that are likely the reason for the good correlation with δ^{13}C-CH_4. This might be the reason that millennial scale maxima in Antarctic temperatures (Jouzel et al., 2007) and Greenland temperature reconstructions (NGRIP community members et al., 2004) which characterize the bipolar seasaw variability (EPICA, 2006) have counterparts in the δ^{13}C-CH_4 record (Figure 6.3). In the following, we attempt to disentangle tropical and boreal processes that control δ^{13}C-CH_4 and begin the discussion with tropical systems and focus on the boreal wetland variability thereafter.

CH_4 carbon isotopes and tropical vegetation variability

Enhanced ISM and SAM delivered more precipitation into tropical rainforest ecosystems (Rostek et al., 1993; Bassinot et al., 1994) during periods when CH_4 was depleted in δ^{13}C and vice versa (Figure 6.3). Monsoonal precipitation controls primary productivity (Phillips et al., 2010; Davidson et al., 2012; Lewis et al., 2011; Chen et al., 2011; Wang et al., 2013a) and vegetation biomes (e.g., Hope et al., 2004; Zheng et al., 2013) and is presently the strongest control of natural CH_4 emissions from tropical wetlands (Bloom et al., 2010). Because precipitation is also in direct control of wildfire intensity on today's (Davidson et al., 2012; Lewis et al., 2011; Chen et al., 2011; Wang et al., 2013a; Worden et al., 2013) and glacial-

interglacial monsoon cycles (e.g., Beaufort et al., 2003; Thevenon et al., 2004), we suggest the monsoon system strength controls the ratio of $\delta^{13}C$ depleted microbial versus $\delta^{13}C$ enriched pyrogenic CH_4 emissions from the tropical wetlands. This hypothesis is supported by maxima in the charcoal data around ∼40 and ∼60 ka b2k (Figure 4, 2ka smoothing window in Daniau et al. (2010)), when the monsoon strength was weak (Figure 6.3). Furthermore, the ratio of microbial versus pyrogenic CH_4 emissions within tropical wetlands has recently been suggested to be controlled by ENSO, where satellite observations showed the reduced biogenic CH_4 emissions during hot and dry ENSO periods were compensated by increased pyrogenic CH_4 emissions from peat fires (Worden et al., 2013). This is in line with the correlation in the 14-28 ka frequency band which suggests $\delta^{13}C$ enrichments in CH_4 when ENSO is in hot and dry phase (Figure 6.6).

The alteration of tropical vegetation and C3/C4 plant ratio through climate and pCO_2 variability (e.g., Ehleringer et al., 1997; Collatz et al., 1998; Bragg et al., 2013) is another mechanism to control atmospheric $\delta^{13}C$-CH_4 (e.g., Sowers, 2009; Möller et al., 2013). Note, this mechanism is only relevant for for tropical wetlands as boreal vegetation predominantly comprises C3 vegetation throughout glacial-interglacial vegetation cycles (e.g., Lozhkin et al., 2007). Atmospheric CO_2 mixing ratios ranged between 180 and 280 ppm during the last 170 ka with a distinct variability on glacial and interglacial periods, respectively (Ahn and Brook, 2008; Bereiter et al., 2012; Lüthi et al., 2008). Thereby, CO_2 passed the critical cross over range of 210-220 ppm (Ehleringer et al., 1997), which decides whether C3 or C4 plants are more competitive in tropical wetlands. The CO_2 cross over range was passed during the glacial terminations, the MIS 5/MIS 4 transition and furthermore oscillated around the cross over range during MIS 3 (Figure 6.3), which resulted in significant shifts of vegetation within biomes (e.g., Ehleringer et al., 1997; Collatz et al., 1998; Bragg et al., 2013) and is most likely linked to the synchronous variability in $\delta^{13}C$-CH_4. The CO_2 variability in combination with a warmer and wetter climate (NGRIP community members et al., 2004; Jouzel et al., 2007) during the interglacial periods allows for C3 plant domination in tropical wetland vegetation during MIS 5 and MIS 1. The increased wildfire intensities following the MIS 5/MIS 4 transition (Daniau et al., 2010) likely contributed to increased tropical tree mortality and thereby increased the pace of the transition from forests into savanna (Chapin et al., 2004; Davidson et al., 2012) which promoted the expansion of C4 plants, thereby enriching the CH_4 that is emitted from tropical wetlands in $\delta^{13}C$. Note that CO_2 did not exceed the cross over threshold during the pronounced $\delta^{13}C$-CH_4 variability at 155 ka b2k at all (Figure 6.3). This indicates little vegetation changes in the tropical wetlands. In further consideration of the small variability in the monsoon records (Figure 6.3), this suggests non tropical CH_4 sources have likely caused the variability in $\delta^{13}C$-CH_4 around 155 ka b2k.

The eruption of mount Toba in Sumatra is believed to be the largest volcanic event during the last 2 million years and has recently been accurately dated to ∼74 ka b2k (Svensson et al., 2013). Zielinski et al. (1996) estimate that the eruption injected as much as 2200-4400 Mt of H2SO4 into the stratosphere and that the resulting radiative cooling of 3-5 °C (Rampino and Self, 1992) lasted for up to 200 years. Even in consideration of the uncertainty in the difference between gas age and ice age, the Tuba eruption has probably occurred before the MIS 5/MIS 4 transition occurs in the $\delta^{13}C$-CH_4 record while $\delta^{13}C$-CH_4 shows little

variability (Figure 6.3). This suggests the sudden Toba eruption event did not cause vast and sustainable changes in vegetation and microbial communities with a temporal extend exceeding firn smoothing processes, (e.g., Bock et al., 2012).

We propose that C3 plants declined in tropical vegetation between MIS 4 and MIS 2, when the climate was distinctly colder and drier (NGRIP community members et al., 2004; Jouzel et al., 2007) with CO_2 levels almost permanently below the cross over threshold for most of the time (Ahn and Brook, 2008), (Figure 6.3). This suggestion is in line with vegetation reconstructions of tropical Asia (Hope et al., 2004; Zheng et al., 2013). In support, marine dust records from the Arabian Sea (Clemens et al., 1996) and across the equatorial Pacific Ocean (Winckler et al., 2008) indicate increased aridity and receding vegetation cover in north-eastern Africa and Asia as well as northern South America during the cold phases MIS 2, MIS 4 and MIS 6, respectively. These observations are in line with modelled variations in tropical dust source areas during the last glacial period (Muhs, 2013). Both dust records also show relatively high deposits around 155 ka b2k and during MIS 3 (Figure 6.3), thereby suggesting low precipitation and that a dense vegetation cover such as tropical forest did not dominate tropical wetlands on a global scale. It is important to note, that the MIS 4/MIS 3 transition is marked by the highest reflectivity of the Cariaco Basin record (Figure 6.3), suggesting northern South America has received little precipitation (Peterson et al., 2000). This is advantageous for C4 plants, even though CO_2 moderately exceeded the cross over threshold of 220 ppm (Figure 6.3 and 6.4).

The suggested fall and rise of tropical forests considerably impacts the C3/C4 plant ratio and thus the emitted δ^{13}C-CH_4 through the change in δ^{13}C of the CH_4 precursor material (Möller et al., 2013). The forest decline and C4 expansion particularly enriches atmospheric CH_4 in δ^{13}C when the transition is accompanied by increased fire intensity, as observed during MIS 5/MIS 4 transition. Combining the information from the geological records and δ^{13}C-CH_4 we suggest that tropical forest was greatly abundant during the last interglacial periods but irrevocably declined during the MIS 5/MIS 4 transition on a global scale, when CO_2 fell below 220 ppm and Antarctic temperatures at EDC were by $\sim$6.5 degrees colder than today (Figure 6.3 and 6.4). Tropical forest was likely at minimum levels throughout the last two glacial periods, with only moderate recuperation during MIS 3, in line with tropical Asian vegetation reconstructions (e.g., Hope et al., 2004; Zheng et al., 2013). The restriction during MIS 3 is in good match with the above mentioned inconsistent variability of monsoon strength and could be explained by inhomogeneous response of individual monsoon systems to the MIS 3 warming. The ENSO variability (Clement et al., 1999) likely contributed to the δ^{13}C-CH_4 signal shown in the 14-28 ka frequency band. Whether the ratio of acetoclastic versus hydrogenotrophic CH_4 formation varied the δ^{13}C of tropical wetland CH_4 on glacial-interglacial time scales (as is probably the case in boreal wetlands) has to our knowldedge not been reported. In the light of significant variations in substrate as well as moisture and temperatures this cannot be excluded.

Hydrogenotrophic CH_4 in boreal wetlands

Acetate fermentation was thought to be the most dominant CH_4 formation process in boreal wetlands as it is the case in tropical wetlands. Therefore, similar $\delta^{13}C$ values were assumed for boreal and tropical wetland CH_4 sources (e.g., Denman et al., 2007). However, recent studies have shown that this assumption overlooks systematic variations within CH_4 sources that produce remarkably depleted $\delta^{13}C$ (e.g., Walter et al., 2007; Hornibrook and Bowes, 2007; Walter et al., 2008; Hornibrook, 2009) and would thus introduce large errors to palaeoatmospheric $\delta^{13}C$-CH_4 reconstructions if not considered (Walter et al., 2007, 2008). (Note this is the essential argument of Möller et al. (2013) and this work, suggesting ecosystem variability is significantly under constrained and leads to inaccurate CH_4 source reconstructions on glacial-interglacial time scales.) Therefore, boreal wetland CH_4 source processes are briefly discussed at this place.

Permafrost and boreal wetland soils are characterized by high peat and carbon content (Schuur et al., 2008; Hornibrook, 2009). Warmer and wetter climate initiates permafrost melt where the active layer thickness, topography, temperature and hydrology determine for thermokarst lake formation (Walter et al., 2007, 2008; Laurion et al., 2010) and vegetative succession (Hornibrook and Bowes, 2007; Hornibrook, 2009). Permafrost degradation is generally associated with the reduction of soil organic carbon to CH_4 upon thawing (Walter et al., 2007; Hornibrook and Bowes, 2007; Schuur et al., 2008; Walter et al., 2008; Hornibrook, 2009; Laurion et al., 2010). In contrast to tropical wetlands, boreal wetland CH_4 is mostly produced by CO_2 reducing microbes, where the fraction of hydrogenotrophic CH_4 is a function of pH and nutrient availability which is controlled by hydrology and vegetation (Hornibrook and Bowes, 2007; Hornibrook, 2009).

Stagnant water bodies of thermokarst systems are associated with low pH and low nutrient influx and enhanced hydrogenotrophic CH_4 formation whereas water runoff increases nutrient influx and pH and thereby acetoclastic CH_4 formation (Hornibrook and Bowes, 2007; Hornibrook, 2009). The domination of hydrogenotrophic CH_4 formation leads to emissions of extremely $\delta^{13}C$ depleted CH_4 with an average of -70 ‰ (Walter et al., 2007, 2008). Thermokarst CH_4 emissions are particularly depleted in $\delta^{13}C$ when the CH_4 stems from newly eroded thermokarst lake margins (Walter et al., 2008). This observation matches the association of thermokarst lakes in early degradation with lower pH (Manasypov et al., 2013), where the latter enhances hydrogenotrophic CH_4 formation (Hornibrook and Bowes, 2007; Hornibrook, 2009; Holmes et al., 2013).

The exact mechanisms controlling the ratio of acetoclastic to hydrogenotrophic CH_4 formation in today's ecosystems are currently poorly understood (Hornibrook, 2009) and not predictable, in particular on large temporal and spatial scales. For example, dominant hydrogenotrophic CH_4 formation has also been observed in subtropical wetlands with relatively high pH of 7-8 (Holmes et al., 2013) as well as in Siberian thermokarst lakes of similar pH range (Walter et al., 2008).

Boreal CH_4 over the last 170 ka

Reconstruction of boreal wetland extent for the LGM and the preindustrial Holocene (PIH) surprisingly suggested the wetland area was 15 % larger during the LGM than during the PIH (Kaplan, 2002). Even though much of the PIH wetland area was frozen or covered by continental ice sheets during the LGM, the reduced sea level exposed large Arctic shelf areas that accounted for an even larger boreal wetland gain (Kaplan, 2002). Reduced boreal CH_4 emissions were therefore due to a reduced CH_4 formation rate based on reduced biogenic productivity (Kaplan, 2002). One reason for low primary productivity is that plants suffer from CO_2 starvation when atmospheric pCO_2 levels are low (e.g., Cowling and Sykes, 1999), thereby limiting nutrient supply. Atmospheric pCO_2 ranged at its lowest levels during the LGM as compared to the rest of the last glacial period (Lüthi et al., 2008). Boreal vegetation is furthermore controlled by heat and moisture influxes (Chapin et al., 2004; Hornibrook and Bowes, 2007; Hornibrook, 2009) which are both regulated by solar insolation (Tarasov et al., 2007), and by convection through ocean circulation (Peterson et al., 2000; Ganopolski and Rahmstorf, 2001) and the tropical monsoon systems (Tarasov et al., 2007; Guo et al., 2012; Caley et al., 2013). Periods of weak monsoon coincided with consistent ice cover of Lake El'Gygytgyn as revealed by the deposition of a geological facie that indicates oxygen depletion and minimum biological productivity (Melles et al., 2012) (Figure 6.3). In contrast, periods of strengthened monsoon and enhanced export of heat and moisture from the tropics cause warmer and wetter boreal summers that allow for higher biological productivity as recorded in pollen records from Lake Baikal sediments (Tarasov et al., 2005, 2007).

In comparison to the Holocene, Northern Hemispheric solar insolation was significantly higher during the Eemian (Laskar et al., 2004) (Figure 6.3), whichresulted in a more favorable climate. This is reflected in higher abundance of trees in pollen reconstructions of both Lake El'Gygytgyn (Lozhkin et al., 2007) and Lake Baikal (Tarasov et al., 2007). Warmer and wetter periods in boreal ecosystems generally allow for higher boreal wetland CH_4 emissions (Christensen et al., 1996; Hornibrook and Bowes, 2007; Hornibrook, 2009), also due to permafrost degradation and thermokarst lake formation (Walter et al., 2007, 2008). Figure 6.3 shows that CH_4 was by $\sim$2 ‰ more depleted in $\delta^{13}C$ during the warmer Eemian as compared to the Holocene (Sowers, 2009; Möller et al., 2013).

Possible explanations for the Eemian-Holocene difference in atmospheric $\delta^{13}C$-CH_4 include increased CH_4 fluxes or increased $\delta^{13}C$ depletion of boreal CH_4 sources due to enhanced thermokarst lake formation. Furthermore, reduced Eemian biomass burning CH_4 emissions could have contributed to the $\delta^{13}C$ depletion of CH_4 (e.g., Beaufort et al., 2003; Thevenon et al., 2004). In fact, the summer monsoon index (Caley et al., 2011b) indicates weaker maximum monsoon strength for the Eemian than for the Holocene, which suggests reduced moisture and possibly lower boreal wetland emission potential. Unfortunately, this cannot be analyzed further and represents the limitation of the current interpretability of the $\delta^{13}C$-CH_4 signal. Using the box model with the configuration of Sapart et al. (2012) highlights the shortcoming of an inverse CH_4 budget analysis with assigning constant $\delta^{13}C$ source values over glacial-interglacial time scales. The calculations produce negative biomass burning fluxes during the Eemian which is impossible and an unambiguous proof that the average $\delta^{13}C$ of biogenic CH_4 sources had changed over time.

In the 14-28 ka band, both the monsoon strength and δ^{13}C-CH_4 varied considerably during MIS 5, while the amplitude of the monsoon proxy decreased significantly towards the LGM (Rostek et al., 1993; Bassinot et al., 1994; Caley et al., 2011b; Bolton et al., 2013) (Figure 6.6). This resulted in decreasing variations of monsoonal heat and moisture fluxes into boreal wetlands with progressing glaciations. This is reflected in three geological records, the boreal plant source water isotopic composition (Zech et al., 2013), the decreased biogenic silica in Lake Baikal sediments (Prokopenko et al., 2001) and the increased dust fluxes (EPICA, 2004) (Figure 6.3 and 6.6). We suggest that at the end of MIS 5, the reduced heat and moisture influx considerably dampened boreal productivity. In fact, the biogenic silica record exhibits a gradual decrease in its maxima throughout MIS 5 but both the plant source water isotopic composition and the biogenic silica records show rapid and seemingly irrevocable decreases during the MIS 5/MIS 4 transition. We infer from the δ^{13}C-CH_4 record that the reduction in monsoonal system strength and NH summer insolation towards the LGM (Figure 6.3) strongly reduced thermokarst formation and boreal vegetation productivity and thereby boreal CH_4 emissions. Because boreal CH_4 is strongly depleted in δ^{13}C as compared to most other CH_4 sources (e.g., Whiticar and Schaefer, 2007; Mikaloff Fletcher et al., 2004a), reduced boreal CH_4 emissions likely contributed to the δ^{13}C-CH_4 variability throughout the last 170 ka. The monsoon variability possibly modulated thermokarst formation and biogenic productivity and thereby contributed to the δ^{13}C-CH_4 variability observed in the $\geq$ 95, 35-45 and the 14-28 ka frequency bands (Figure 6.4, 6.5 and 6.6).

The severity of the changes on the vegetation is furthermore supported by global dust records (Figure 6.3) which are strong indicators for degradation of vegetation cover and to lesser extend of variations in aridity and transport (e.g., Mahowald et al., 2006). While ice core dust records from Antarctica are most representative for southern South American dust sources, Greenland ice core dust sources are discussed controversially but include Asian and possibly North American and Siberian sources as well, where the dust mostly results from loess erosion and glacial ice sheet oscillations (Muhs, 2013).

Despite the different dust source regions, both Antarctic and Greenlandic dust deposition generally increases during cold periods (Fischer et al., 2007) as it is the case for the marine dust records (Winckler et al., 2008). Here, we use this general correlation to extrapolate from both Antarctic and marine dust load to boreal vegetation cover and aridity during the penultimate glacial period, because Greenland ice core records do not reach as far back and would therefore limit our comparison. However, this is a limitation of our analysis but in the light of a lacking alternative it seems the best solution.

Boreal dust fluxes increased by one to two orders of magnitude during the glacial (Fischer et al., 2007; Muhs, 2013) (Figure 6.6). Because dust deposition increases in colder and dryer climates (Muhs, 2013), it can be interpreted as a reciprocal measure of boreal biological productivity and hence CH_4 emission potential (Guo et al., 2012). Precise age control of ice core records allows precise timing of dust events relative to the δ^{13}C-CH_4 record which suggests minimal boreal CH_4 emissions during MIS 2, MIS 4 and MIS 6 (Figure 6.3). This is in line with recent reconstructions of the interhemispheric difference (IPD) in CH_4 (Baumgartner et al., 2013), which is indicative for the ratio of tropical and boreal emission fluxes

with high IPD values suggesting high boreal CH_4 emissions. While the IPD ranged around 10 % during MIS 3 and MIS 5, values of 5-7.5 % have been found for MIS 2 and MIS 4 (Baumgartner et al., 2013). Guo et al. (2012) estimated the boreal CH_4 emissions reduced by 50 % on glacial-interglacial time scales, which means that the variability of CH_4 emissions that are potentially depleted in $\delta^{13}C$ can be timed by the dust record. Based on the common variability of $\delta^{13}C$-CH_4, plant source water and biogenic silica and dust, we suggest the boreal CH_4 emissions decreased gradually during MIS 5 and reached low values during the MIS 5/MIS 4 transition and lowest values during the LGM and about 170 ka b2k.

Dust (EPICA, 2004; Ruth et al., 2007) and biogenic silica (Prokopenko et al., 2001) records furthermore suggest that boreal vegetation has somewhat recuperated during MIS 3 and between 155 and 150 ka b2k, which was likely enhanced by the summer insolation maximum at 55° N (Laskar et al., 2004) (Figure 6.3), but was probably far from reaching the productivity of MIS 5 or MIS 1. We suggest that increasing boreal biological productivity and thermokarst formation caused the $\delta^{13}C$ depletion between 155 and 150 ka b2k and during MIS 3 (Figure 6.3), either by increased $\delta^{13}C$ depletion of boreal CH_4 sources or by relative increases of boreal CH_4 emission rates as was previously suggested for MIS 3 based on hydrogen CH_4 isotope measurements (Bock et al., 2010b).

We furthermore speculate that boreal CH_4 emissions were relatively more important for the $\delta^{13}C$-CH_4 variability between 155-150 ka b2k as compared to MIS 3. While reconstructions of western Pacific Ocean planktic assemblages reveal a pronounced variability during MIS 3 and 155-150 ka b2k in subpolar regions, the tropical assemblages remain rather constant at 155-150 ka b2k (Heusser and Morley, 1997). Tropical pollen records show a moderate increase in the tree fraction during MIS 3 (Zheng et al., 2013), suggesting increasing biological productivity and thereby that the $\delta^{13}C$-CH_4 variability during MIS 3 was caused by enhanced tropical CH_4 emissions as well.

This relatively stronger relative role of boreal wetlands for the $\delta^{13}C$-CH_4 variability during 155-150 ka b2k as compared to MIS 3 is furthermore in good agreement with higher productivity in Lake Baikal around 155 ka b2k (Prokopenko et al., 2001) as well as a smaller increase in CH_4 (Schilt et al., 2010a) and Antarctic temperature (Jouzel et al., 2007) (Figure 6.3) where the latter two suggest significant increases of tropical CH_4 emissions for MIS 3. The strongest enrichment in the $\delta^{13}C$-CH_4 record around 155 ka b2k furthermore suggests a period of minimum thermokarst lake formation and biological productivity in boreal wetlands. This hypothesis is in line with high dust deposition in both marine (Winckler et al., 2008) and Antarctic records (EPICA, 2004) and as well as lowest tree pollen in several tropical Asian ecosystems (Hope et al., 2004; Zheng et al., 2013), probably due to the low Antarctic temperatures (Jouzel et al., 2007) and stably low CO_2 mixing ratios that barely exceeded 200 ppm (Lüthi et al., 2008), (Figure 6.3).

Conclusions

We suggest that δ^{13}C-CH_4 ice core records can be used to overcome the spatial limitation of vegetation reconstructions based on regional proxy records to a global scale. We consider the δ^{13}C of CH_4 emissions from tropical wetlands as an indirect measure of biological productivity versus drought and fire, where periods of δ^{13}C-CH_4 depletion are generally associated with higher forest cover and productivity. The strong depletion of δ^{13}C-CH_4 record during the Eemian suggests that Eemian and Holocene tropical vegetation likely comprised similar C3 fractions. We suggest the MIS 5/MIS 4 transition as the most likely time of maximum tree decline and that the suppression of trees in tropical wetlands lasted until the glacial termination.

The generally low monsoon strength after the MIS 5/MIS 4 transition suggests dryer tropical climate leading to increased vulnerability of prevailing vegetation to fire. Tropical forests suffering from continuously dryer conditions are increasingly susceptible to wild fires which would increase the mortality rate and therefore promote the expansion of the more competitive C4 plants. In fact, this in line with wildfire reconstructions of Daniau et al. (2010) and Beaufort et al. (2003); Thevenon et al. (2004), where the latter two discuss the control of the monsoon system.

We furthermore attempt reconstructing the variability of boreal CH_4 sources. However, there is great uncertainty regarding the temporal variability of the isotopic composition from boreal CH_4 sources. Boreal CH_4 sources have been reported of being generally more depleted in δ^{13}C as previously assumed. To what extend simultaneous changes in both the isotopic composition and the fluxes of boreal CH_4 occurred cannot be reconstructed. However, we suggest that boreal CH_4 emissions are tightly linked to the influx of heat and moisture as mediated by monsoon system strength. The impact of monsoon system variability on boreal CH_4 emissions indicates the sensitivity of remote ecosystems such as boreal wetlands to tropical climate phenomena.

Chapter 7

Conclusions

This PhD thesis comprises a package of analytical developments to reference and measure δ^{13}C-CH_4 in ice core samples as well as two different approaches for the interpretation of data on different time scales.

1) The problem of lacking reference material has been addressed by nearly every method paper on CH_4 isotope analysis in the last 3 decades. Inaccurate referencing may lead to misinterpretation by confusing inhomogeneous referencing for atmospheric variability. This is a particularly important topic for present day observations in high spatio-temporal resolution, as has recently been discussed in a publication by Levin et al. (2012) in Nature. With our referencing method, we calibrated the isotopic composition of two CH_4 gases in high precision for both δ^{13}C-CH_4 as well as δ^{2}H-CH_4 and produced synthetic reference gases in a bottom-up fashion for internal use. The calibration of our gases was confirmed by intercomparison measurements at IMAU, Bern and most recently by MPI-BGC. However, the Centre for Ice and Climate (CIC) cannot maintain and provide isotope scale material as would be needed by the community measuring CH_4 isotopes in ice core and atmospheric samples. Nevertheless, the output of this work presented here is highly relevant for ongoing work in this field. The two CH_4 gases that were calibrated at CIC presently form the base within an international project to provide isotope reference gases for CH_4 in air to the community in future.

2) The setup that was built to measure δ^{13}C-CH_4 in ice core samples during this study is able to operate in a routine fashion on a daily base. It is fully calibrated and referenced and should allow for future measurememts of δ^{13}C-CH_4 without great preparation efforts. For example, crucial compontents of the system are either constantly flushed with ultra pure helium or permanently evacuated and are therefore always operative. A permanent oxidation system ensures high CH_4 conversion rates at all times. The system is furthermore equipped for δ^{2}H-CH_4 analysis, though this configuration has not been tested. Ironically, a source of significant analytical variability could be excluded by blinding the laboratory windows with tin foil to prevent direct sunshine from entering the laboratory. Thereafter, standard measurements bracketing the measured samples showed no significant drift throughout the measurement days (within 0.09 ‰). This could possibly allow to increase the number of measured samples by decreasing the number of measured standards per measurement day (presently 2 and 7, respectively). Further improvements involve tuning the system for

smaller sample sizes (presently 200-500 g of ice) and to analyse more parameters per sample, as done in Bern (Jochen Schmitt pers. comm. 2013).

3) A δ^{13}C-CH_4 record covering the last 170 ka with a temporal resolution between 1 sample per 200-1660 years has recently been published from Antarctic ice cores (Möller et al., 2013). Here, we present a high resolution record of DO-21 and DO-22 with 1 sample in 500 years. Datasets from several laboratories (PSU, Bern, IMAU and now CIC) measured on Antarctic and Greenlandic ice cores were found in relatively good agreement, suggesting the analytical infrastructure is fairly robust and the measured signal is accurate. However, the interpretation of δ^{13}C-CH_4 data is currently limited as the independent variability of δ^{13}C-CH_4 and $p$$CH_4$ suggest controling processes were in place that cannot be reliably reconstructed to this day, which precludes accurate calculations of CH_4 emission scenarios. In order to still extract information from measured datasets, I used different analytical approaches.

I analysed δ^{13}C-CH_4 during the rapid and pronounced DO-21 precursor event using by Keeling Plot Analysis (KPA) and found an increased tropical CH_4 emissions to be the most likely cause of the observed $p$$CH_4$ variability (Chappellaz et al., 2013). The 170 ka δ^{13}C-CH_4 record together with further geological records were analysed by singular spectrum analysis (SSA) in order to perform correlation tests on both the original data as well as the extracted bands of orbital frequency. The results reproduce the high correlation with $p$$CO_2$ and sea level variability as reported by (Möller et al., 2013) who suggest a controlling mechanism through vegetation response to $p$$CO_2$ and climate change. Based on the SSA analysis, I furthermore propose a high impact of monsoon system strength variation to δ^{13}C-CH_4 by controlling the ratio of biogenic to pyrogenic CH_4 formation in the tropics as well as the export of heat and moisture to the boreal CH_4 source ecosystems. Heat and moisture influx modulate the biogenic productivity in boreal CH_4 source ecosystems. Heat, moisture, substrate and productivity are associated with the ratio of hydrogenotrophic and acetoclastic CH_4 formation processes, which differ greatly in the isotopic composition of emitted CH_4. However, due to generally poor understanding of the variability within CH_4 formation processes, their quantification on glacial interglacial time scales is yet impossible.

Future research is needed to investigate the role of changing climate on tropical and boreal biomes and their consequences for the isotopic composition of emitted CH_4 on macro- and microscales. Further research should also include observation of all CH_4 isotopes, where the clumped isotopes of CH_4 are particularly useful to quantify pyrogenic CH_4 emissions (Eiler et al., 2013). Furthermore, the enigmatic CH_4 formation observed in plants (Keppler et al., 2006, 2009) under aerobic conditions should be in the focus of future research. Since this parameter is poorly understood, we have not included it in our analysis. The discussed variability of CH_4 sources is quite complex. However, a variability in CH_4 sinks was assumed to be negligible. Whether or not this assumption is valid requires thorough assessment in future work as well.

Chapter 8

Bibliography

Abrajano, T. A., Sturchio, N. C., Bohlke, J. K., Lyon, G. L., Poreda, R. J., and Stevens, C. M. (1988). Methane hydrogen gas seeps, Zambales Ophiolite, Philippines - deep or shallow origin. *Chemical Geology*, 71(1-3):211–222.

Ahn, J. and Brook, E. J. (2008). Atmospheric CO_2 and climate on millennial time scales during the last glacial period. *Science*, 322(5898):83–85.

An, Z. S., Clemens, S. C., Shen, J., Qiang, X. K., Jin, Z. D., Sun, Y. B., Prell, W. L., Luo, J. J., Wang, S. M., Xu, H., Cai, Y. J., Zhou, W. J., Liu, X. D., Liu, W. G., Shi, Z. G., Yan, L. B., Xiao, X. Y., Chang, H., Wu, F., Ai, L., and Lu, F. Y. (2011). Glacial-Interglacial Indian Summer Monsoon dynamics. *Science*, 333(6043):719–723.

Andersen, K. K., Svensson, A., Johnsen, S. J., Rasmussen, S. O., Bigler, M., Rothlisberger, R., Ruth, U., Siggaard-Andersen, M. L., Steffensen, J. P., Dahl-Jensen, D., Vinther, B. M., and Clausen, H. B. (2006). The Greenland Ice Core Chronology 2005, 15-42 ka. Part 1: constructing the time scale. *Quaternary Science Reviews*, 25(23-24):3246–3257.

Angel, R., Claus, P., and Conrad, R. (2012). Methanogenic archaea are globally ubiquitous in aerated soils and become active under wet anoxic conditions. *Isme Journal*, 6(4):847–862.

Aston, F. W. (1920). The constitution of atmospheric neon. *Philosophical Magazine*, 39(232):449–455.

Bassinot, F. C., Labeyrie, L. D., Vincent, E., Quidelleur, X., Shackleton, N. J., and Lancelot, Y. (1994). The astronomical theory of climate and the age of the Brunhes-Matuyama magnetic reversal. *Earth and Planetary Science Letters*, 126(1-3):91–108.

Baumgartner, M., Kindler, P., Eicher, O., Floch, G., Schilt, A., Schwander, J., Spahni, R., Capron, E., Chappellaz, J., Leuenberger, M., Fischer, H., and Stocker, T. F. (2013). NGRIP CH_4 concentration from 120 to 10 kyr before present and its relation to a temperature reconstruction from the same ice core. *Climate of the Past, Discussion*, 9:4655–4704.

Baumgartner, M., Schilt, A., Eicher, O., Schmitt, J., Schwander, J., Spahni, R., Fischer, H., and Stocker, T. F. (2012). High-resolution interpolar difference of atmospheric methane around the last glacial maximum. *Biogeosciences*, 9(10):3961–3977.

Bazin, L., Landais, A., Lemieux-Dudon, B., Kele, H. T. M., Veres, D., Parrenin, F., Martinerie, P., Ritz, C., Capron, E., Lipenkov, V., Loutre, M. F., Raynaud, D., Vinther, B., Svensson, A., Rasmussen, S. O., Severi, M., Blunier, T., Leuenberger, M., Fischer, H., Masson-Delmotte, V., Chappellaz, J., and Wolff, E. (2013). An optimized multi-proxy, multi-site Antarctic ice and gas orbital chronology (AICC2012): 120-800 ka. *Climate of the Past*, 9(4):1715–1731.

Beaufort, L., de Garidel-Thoron, T., Linsley, B., Oppo, D., and Buchet, N. (2003). Biomass burning and oceanic primary production estimates in the Sulu Sea area over the last 380 kyr and the East Asian monsoon dynamics. *Marine Geology*, 201(1-3):53–65.

Beerling, D. J., Gardiner, T., Leggett, G., McLeod, A., and Quick, W. P. (2008). Missing methane emissions from leaves of terrestrial plants. *Global Change Biology*, 14(8):1821–1826.

Behrens, M., Schmitt, J., Richter, K. U., Bock, M., Richter, U. C., Levin, I., and Fischer, H. (2008). A gas chromatography/combustion/isotope ratio mass spectrometry system for high-precision $\delta^{13}C$ measurements of atmospheric methane extracted from ice core samples. *Rapid Communications in Mass Spectrometry*, 22(20):3261–3269.

Bekker, A., Holland, H. D., Wang, P. L., Rumble, D., Stein, H. J., Hannah, J. L., Coetzee, L. L., and Beukes, N. J. (2004). Dating the rise of atmospheric oxygen. *Nature*, 427(6970):117–120.

Bereiter, B., Lüthi, D., Siegrist, M., Schüpbach, S., Stocker, T. F., and Fischer, H. (2012). Mode change of millennial CO_2 variability during the last glacial cycle associated with a bipolar marine carbon seesaw. *Proceedings of the National Academy of Sciences of the United States of America*, 109(25):9755–9760.

Bergamaschi, P., Brenninkmeijer, C. A. M., Hahn, M., Rockmann, T., Scharffe, D. H., Crutzen, P. J., Elansky, N. F., Belikov, I. B., Trivett, N. B. A., and Worthy, D. E. J. (1998). Isotope analysis based source identification for atmospheric CH_4 and co sampled across russia using the trans-siberian railroad. *Journal of Geophysical Research-Atmospheres*, 103(D7):8227–8235.

Bindoff, N.L.and Willebrand, J., Artale, V., Cazenave, A., Gregory, J., Gulev, S., Hanawa, K., Le Quéré, C., Levitus, S., Nojiri, Y., Shum, C. K., Talley, L. D., and Unnikrishnan, A. (2007). Observations: Oceanic Climate Change and Sea Level. In Solomon, S., Qin, D., Manning, M., Chen, Z., Marquis, M., Averyt, K., Tignor, M., and Miller, H., editors, *Climate Change 2007: The Physical Science Basis. Contribution of Working Group I to the Fourth Assessment Report of the Intergovernmental Panel on Climate Change*. Cambridge University Press, Cambridge, United Kingdom and New York, NY, USA.

Bloom, A. A., Palmer, P. I., Fraser, A., Reay, D. S., and Frankenberg, C. (2010). Large-scale controls of methanogenesis inferred from methane and gravity spaceborne data. *Science*, 327(5963):322–325.

Blunier, T. and Brook, E. J. (2001). Timing of millennial-scale climate change in Antarctica and Greenland during the last glacial period. *Science*, 291(5501):109–112.

Blunier, T., Chappellaz, J., Schwander, J., Dallenbach, A., Stauffer, B., Stocker, T. F., Raynaud, D., Jouzel, J., Clausen, H. B., Hammer, C. U., and Johnsen, S. J. (1998). Asynchrony of Antarctic and Greenland climate change during the last glacial period. *Nature*, 394(6695):739–743.

Blunier, T., Chappellaz, J., Schwander, J., Stauffer, B., and Raynaud, D. (1995). Variations in atmospheric methane concentration during the Holocene epoch. *Nature*, 374(6517):46–49.

Blunier, T., Chappellaz, J. A., Schwander, J., Barnola, J. M., Desperts, T., Stauffer, B., and Raynaud, D. (1993). Atmospheric methane, record from a greenland ice core over the last 1000 year. *Geophysical Research Letters*, 20(20):2219–2222.

Blunier, T., Spahni, R., Barnola, J. M., Chappellaz, J., Loulergue, L., and Schwander, J. (2007). Synchronization of ice core records via atmospheric gases. *Climate of the Past*, 3(2):325–330.

Bock, J., Martinerie, P., Witrant, E., and Chappellaz, J. (2012). Atmospheric impacts and ice core imprints of a methane pulse from clathrates. *Earth and Planetary Science Letters*, 349:98–108.

Bock, M., Schmitt, J., Behrens, M., Möller, L., Schneider, R., Sapart, C., and Fischer, H. (2010a). A gas chromatography/pyrolysis/isotope ratio mass spectrometry system for high-precision δD measurements of atmospheric methane extracted from ice cores. *Rapid Communications in Mass Spectrometry*, 24(5):621–633.

Bock, M., Schmitt, J., Möller, L., Spahni, R., Blunier, T., and Fischer, H. (2010b). Hydrogen isotopes preclude marine hydrate CH_4 emissions at the onset of Dansgaard-Oeschger events. *Science*, 328(5986):1686–1689.

Bolton, C. T., Chang, L., Clemens, S. C., Kodama, K., Ikehara, M., Medina-Elizalde, M., Paterson, G. A., Roberts, A. P., Rohling, E. J., Yamamoto, Y., and Zhao, X. (2013). A 500,000 year record of Indian summer monsoon dynamics recorded by eastern equatorial Indian Ocean upper water-column structure. *Quaternary Science Reviews*, 77:167–180.

Boone, D. R. (2000). Biological Formation and Consumption of Methane. In Khalil, M. A. K., editor, *Atmospheric Methane*, pages 42–62. Springer, Berlin, Heidelberg, Germany.

Bragg, F. J., Prentice, I. C., Harrison, S. P., Eglinton, G., Foster, P. N., Rommerskirchen, F., and Rullkotter, J. (2013). Stable isotope and modelling evidence for CO_2 as a driver of glacial-interglacial vegetation shifts in southern Africa. *Biogeosciences*, 10(3):2001–2010.

Brand, W. A. (2004). Mass spectrometer hardware for analyzing stable isotope ratios. In Groot, P. A., editor, *Handbook of Stable Isotope Analytical Techniques*, volume 1, pages 835–856. Elsevier B.V.

Breas, O., Guillou, C., Reniero, F., and Wada, E. (2002). The global methane cycle: Isotopes and mixing ratios, sources and sinks. *Isotopes in Environmental and Health Studies*, 37(4):257–379.

Breecker, D. O., Sharp, Z. D., and McFadden, L. D. (2010). Atmospheric CO_2 concentrations during ancient greenhouse climates were similar to those predicted for AD 2100. *Proceedings of the National Academy of Sciences of the United States of America*, 107(2):576–580.

Broecker, W. S. (1988). *How to Build a Habitable Planet*. Eldigio Press, Palisades, NY, New York, NY, USA.

Broecker, W. S. (1998). Paleocean circulation during the last deglaciation: A bipolar seesaw? *Paleoceanography*, 13(2):119–121.

Brook, E. J., Harder, S., Severinghaus, J., Steig, E. J., and Sucher, C. M. (2000). On the origin and timing of rapid changes in atmospheric methane during the last glacial period. *Global Biogeochemical Cycles*, 14(2):559–572.

Brook, E. J., Nesje, A., Lehman, S. J., Raisbeck, G. M., and Yiou, F. (1996a). Cosmogenic nuclide exposure ages along a vertical transect in western norway: Implications for the height of the fennoscandian ice sheet. *Geology*, 24(3):207–210.

Brook, E. J., Sowers, T., and Orchardo, J. (1996b). Rapid variations in atmospheric methane concentration during the past 110,000 years. *Science*, 273(5278):1087–1091.

Bruhn, D., Mikkelsen, T. N., Obro, J., Willats, W. G. T., and Ambus, P. (2009). Effects of temperature, ultraviolet radiation and pectin methyl esterase on aerobic methane release from plant material. *Plant Biology*, 11:43–48.

Buffett, B. and Archer, D. (2004). Global inventory of methane clathrate: sensitivity to changes in the deep ocean. *Earth and Planetary Science Letters*, 227(3-4):185–199.

Buizert, C., Sowers, T., and Blunier, T. (2013). Assessment of diffusive isotopic fractionation in polar firn, and application to ice core trace gas records. *Earth and Planetary Science Letters*, 361:110–119.

Caley, T., Malaize, B., Kageyama, M., Landais, A., and Masson-Delmotte, V. (2013). Bi-hemispheric forcing for Indo-Asian monsoon during glacial terminations. *Quaternary Science Reviews*, 59:1–4.

Caley, T., Malaize, B., Revel, M., Ducassou, E., Wainer, K., Ibrahim, M., Shoeaib, D., Migeon, S., and Marieu, V. (2011a). Orbital timing of the Indian, East Asian and African boreal monsoons and the concept of a 'global monsoon'. *Quaternary Science Reviews*, 30(25-26):3705–3715.

Caley, T., Malaize, B., Zaragosi, S., Rossignol, L., Bourget, J., Eynaud, F., Martinez, P., Giraudeau, J., Charlier, K., and Ellouz-Zimmermann, N. (2011b). New Arabian Sea records help decipher orbital timing of Indo-Asian monsoon. *Earth and Planetary Science Letters*, 308(3-4):433–444.

Came, R. E., Eiler, J. M., Veizer, J., Azmy, K., Brand, U., and Weidman, C. R. (2007). Coupling of surface temperatures and atmospheric CO_2 concentrations during the Palaeozoic era. *Nature*, 449(7159):198–U3.

Capron, E., Landais, A., Chappellaz, J., Schilt, A., Buiron, D., Dahl-Jensen, D., Johnsen, S. J., Jouzel, J., Lemieux-Dudon, B., Loulergue, L., Leuenberger, M., Masson-Delmotte, V., Meyer, H., Oerter, H., and Stenni, B. (2010). Millennial and sub-millennial scale climatic variations recorded in polar ice cores over the last glacial period. *Climate of the Past*, 6(3):345–365.

Catling, D. C. and Claire, M. W. (2005). How earth's atmosphere evolved to an oxic state: A status report. *Earth and Planetary Science Letters*, 237(1-2):1–20.

Chadwick, R., Wu, P. L., Good, P., and Andrews, T. (2013). Asymmetries in tropical rainfall and circulation patterns in idealised CO_2 removal experiments. *Climate Dynamics*, 40(1-2):295–316.

Chapin, F. S., Callaghan, T. V., Bergeron, Y., Fukuda, M., Johnstone, J. F., Juday, G., and Zimov, S. A. (2004). Global change and the boreal forest: Thresholds, shifting states or gradual change? *Ambio*, 33(6):361–365.

Chappellaz, J., Barnola, J. M., Raynaud, D., Korotkevich, Y. S., and Lorius, C. (1990). Ice-core record of atmospheric methane over the past 160,000 years. *Nature*, 345(6271):127–131.

Chappellaz, J., Blunier, T., Kints, S., Dallenbach, A., Barnola, J. M., Schwander, J., Raynaud, D., and Stauffer, B. (1997). Changes in the atmospheric CH_4 gradient between greenland and antarctica during the holocene. *Journal of Geophysical Research-Atmospheres*, 102(D13):15987–15997.

Chappellaz, J., Blunier, T., Raynaud, D., Barnola, J. M., Schwander, J., and Stauffer, B. (1993a). Synchronous changes in atmospheric CH_4 and Greenland climate between 40-kyr and 8-kyr BP. *Nature*, 366(6454):443–445.

Chappellaz, J., Stowasser, C., Blunier, T., Baslev-Clausen, D., Brook, E. J., Dallmayr, R., Faïn, X., Lee, J. E., Mitchell, L. E., Pascual, O., Romanini, D., Rosen, J., and Schüpbach, S. (2013). High-resolution glacial and deglacial record of atmospheric methane by continuous-flow and laser spectrometer analysis along the NEEM ice core. *Climate of the Past*, 9:2579–2593.

Chappellaz, J. A., Fung, I. Y., and Thompson, A. M. (1993b). The atmospheric CH_4 increase since the last glacial maximum. *Tellus Series B-Chemical and Physical Meteorology*, 45(3):228–241.

Chen, Y., Randerson, J. T., Morton, D. C., DeFries, R. S., Collatz, G. J., Kasibhatla, P. S., Giglio, L., Jin, Y. F., and Marlier, M. E. (2011). Forecasting Fire Season Severity in South America Using Sea Surface Temperature Anomalies. *Science*, 334(6057):787–791.

Cheng, H., Edwards, R. L., Broecker, W. S., Denton, G. H., Kong, X. G., Wang, Y. J., Zhang, R., and Wang, X. F. (2009). Ice Age Terminations. *Science*, 326(5950):248–252.

Cheng, H., Sinha, A., Wang, X. F., Cruz, F. W., and Edwards, R. L. (2012). The Global Paleomonsoon as seen through speleothem records from Asia and the Americas. *Climate Dynamics*, 39(5):1045–1062.

Christensen, T. R., Prentice, I. C., Kaplan, J., Haxeltine, A., and Sitch, S. (1996). Methane flux from northern wetlands and tundra - an ecosystem source modelling approach. *Tellus Series B-Chemical and Physical Meteorology*, 48(5):652–661.

Clayton, D. (2003). *Handbook of Isotopes in the Cosmos: Hydrogen to Galliumquot*. Cambridge University Press, Cambridge, United Kingdom.

Clemens, S. C., Murray, D. W., and Prell, W. L. (1996). Nonstationary phase of the plio-pleistocene Asian monsoon. *Science*, 274(5289):943–948.

Clemens, S. C. and Prell, W. L. (2003). A 350,000 year summer-monsoon multi-proxy stack from the Owen ridge, Northern Arabian sea. *Marine Geology*, 201(1-3):35–51.

Clement, A. C., Seager, R., and Cane, M. A. (1999). Orbital controls on the El Nino/Southern Oscillation and the tropical climate. *Paleoceanography*, 14(4):441–456.

Collatz, G. J., Berry, J. A., and Clark, J. S. (1998). Effects of climate and atmospheric CO_2 partial pressure on the global distribution of C-4 grasses: present, past, and future. *Oecologia*, 114(4):441–454.

Conrad, R. (2005). Quantification of methanogenic pathways using stable carbon isotopic signatures: a review and a proposal. *Organic Geochemistry*, 36(5):739–752.

Cowling, S. A. and Sykes, M. T. (1999). Physiological significance of low atmospheric CO_2 for plant-climate interactions. *Quaternary Research*, 52(2):237–242.

Craig, H., Chou, C. C., Welhan, J. A., Stevens, C. M., and Engelkemeir, A. (1988). The isotopic composition of methane in polar ice cores. *Science*, 242(4885):1535–1539.

Curl, R. F., Capasso, F., Gmachl, C., Kosterev, A. A., McManus, B., Lewicki, R., Pusharsky, M., Wysocki, G., and Tittel, F. K. (2010). Quantum cascade lasers in chemical physics. *Chemical Physics Letters*, 487(1-3):1–18.

Dällenbach, A., Blunier, T., Flückiger, J., Stauffer, B., Chappellaz, J., and Raynaud, D. (2000). Changes in the atmospheric CH_4 gradient between Greenland and Antarctica during the Last Glacial and the transition to the Holocene. *Geophysical Research Letters*, 27(7):1005–1008.

Daniau, A. L., Harrison, S. P., and Bartlein, P. J. (2010). Fire regimes during the Last Glacial. *Quaternary Science Reviews*, 29(21-22):2918–2930.

Daniau, A. L., Sanchez-Goni, M. F., Beaufort, L., Laggoun-Defarge, F., Loutre, M. F., and Duprat, J. (2007). Dansgaard-Oeschger climatic variability revealed by fire emissions in southwestern Iberia. *Quaternary Science Reviews*, 26(9-10):1369–1383.

Dansgaard, W. (1964). Stable isotopes in precipitation. *Tellus*, 16(4):436–468.

Davidson, E. A., de Araujo, A. C., Artaxo, P., Balch, J. K., Brown, I. F., Bustamante, M. M. C., Coe, M. T., DeFries, R. S., Keller, M., Longo, M., Munger, J. W., Schroeder, W., Soares, B. S., Souza, C. M., and Wofsy, S. C. (2012). The amazon basin in transition. *Nature*, 481(7381):321–328.

Denman, K., Brasseur, G., Chidthaisong, A., Ciais, P., Cox, P. M., Dickinson, R. E., Hauglustaine, D., Heinze, C., Holland, E., Jacob, D., Lohmann, U., Ramachandran, S., da Silva Dias, P. L., C., W. S., and Zhang, X. (2007). Couplings Between Changes in the Climate System and Biogeochemistry. In Solomon, S., Qin, D., Manning, M., Chen, Z., Marquis, M., Averyt, K., Tignor, M., and Miller, H., editors, *Climate Change 2007: The Physical Science Basis. Contribution of Working Group I to the Fourth Assessment Report of the Intergovernmental Panel on Climate Change*. Cambridge University Press, Cambridge, United Kingdom and New York, NY, USA.

Deplazes, G., Luckge, A., Peterson, L. C., Timmermann, A., Hamann, Y., Hughen, K. A., Rohl, U., Laj, C., Cane, M. A., Sigman, D. M., and Haug, G. H. (2013). Links between tropical rainfall and north atlantic climate during the last glacial period. *Nature Geoscience*, 6(3):213–217.

Dlugokencky, E. J., Bruhwiler, L., White, J. W. C., Emmons, L. K., Novelli, P. C., Montzka, S. A., Masarie, K. A., Lang, P. M., Crotwell, A. M., Miller, J. B., and Gatti, L. V. (2009). Observational constraints on recent increases in the atmospheric CH_4 burden. *Geophysical Research Letters*, 36.

Dueck, T. A., de Visser, R., Poorter, H., Persijn, S., Gorissen, A., de Visser, W., Schapendonk, A., Verhagen, J., Snel, J., Harren, F. J. M., Ngai, A. K. Y., Verstappen, F., Bouwmeester, H., Voesenek, L., and van der Werf, A. (2007). No evidence for substantial aerobic methane emission by terrestrial plants: a C-13-labelling approach. *New Phytologist*, 175(1):29–35.

Ehleringer, J. R., Cerling, T. E., and Helliker, B. R. (1997). C-4 photosynthesis, atmospheric CO_2 and climate. *Oecologia*, 112(3):285–299.

Eiler, J. M. (2007). "Clumped-isotope" geochemistry - The study of naturally-occurring, multiply-substituted isotopologues. *Earth and Planetary Science Letters*, 262(3-4):309–327.

Eiler, J. M., Clog, M., Magyar, P., Piasecki, A., Sessions, A., Stolper, D., Deerberg, M., Schlueter, H. J., and Schwieters, J. (2013). A high-resolution gas-source isotope ratio mass spectrometer. *International Journal of Mass Spectrometry*, 335:45–56.

Encyclopaedia, Britannica, O. (2013). Methane Cycle. Art. Website. Available online at http://www.britannica.com/EBchecked/media/141533/; last visited December 3, 2013.

EPICA (2004). Eight glacial cycles from an Antarctic ice core. *Nature*, 429(6992):623–628.

EPICA (2006). One-to-one coupling of glacial climate variability in Greenland and Antarctica. *Nature*, 444(7116):195–198.

Epstein, S., Buchsbaum, R., Lowenstam, H., and Urey, H. C. (1951). Carbonate-water isotopic temperature scale. *Geological Society of America Bulletin*, 62(4):417–426.

ESA (2013). European Space Agency, SCIAMACHY Product Control Service. Website. Available online at http://earth.eo.esa.int/pcs/envisat/sciamachy/; last visited December 3, 2013.

Etheridge, D. M., Steele, L. P., Francey, R. J., and Langenfelds, R. L. (1998). Atmospheric methane between 1000 AD and present: Evidence of anthropogenic emissions and climatic variability. *Journal of Geophysical Research-Atmospheres*, 103(D13):15979–15993.

Etheridge, D. M., Steele, L. P., Langenfelds, R. L., Francey, R. J., Barnola, J. M., and Morgan, V. I. (1996). Natural and anthropogenic changes in atmospheric CO_2 over the last 1000 years from air in Antarctic ice and firn. *Journal of Geophysical Research-Atmospheres*, 101(D2):4115–4128.

Etiope, G., Lassey, K. R., Klusman, R. W., and Boschi, E. (2008). Reappraisal of the fossil methane budget and related emission from geologic sources. *Geophysical Research Letters*, 35(9).

Etiope, G. and Lollar, B. S. (2013). Abiotic methane on earth. *Reviews of Geophysics*, 51(2):276–299.

Ferretti, D. F., Miller, J. B., White, J. W. C., Etheridge, D. M., Lassey, K. R., Lowe, D. C., Meure, C. M. M., Dreier, M. F., Trudinger, C. M., van Ommen, T. D., and Langenfelds, R. L. (2005). Unexpected changes to the global methane budget over the past 2000 years. *Science*, 309(5741):1714–1717.

Fiore, A. M., Jacob, D. J., Field, B. D., Streets, D. G., Fernandes, S. D., and Jang, C. (2002). Linking ozone pollution and climate change: The case for controlling methane. *Geophysical Research Letters*, 29(19):4.

Fischer, H., Behrens, M., Bock, M., Richter, U., Schmitt, J., Loulergue, L., Chappellaz, J., Spahni, R., Blunier, T., Leuenberger, M., and Stocker, T. F. (2008). Changing boreal methane sources and constant biomass burning during the last termination. *Nature*, 452(7189):864–867.

Fischer, H., Schmitt, J., Lüthi, D., Stocker, T. F., Tschumi, T., Parekh, P., Joos, F., Kohler, P., Volker, C., Gersonde, R., Barbante, C., Le Floch, M., Raynaud, D., and Wolff, E. (2010). The role of Southern Ocean processes in orbital and millennial CO_2 variations - A synthesis. *Quaternary Science Reviews*, 29(1-2):193–205.

Fischer, H., Siggaard-Andersen, M. L., Ruth, U., Rothlisberger, R., and Wolff, E. (2007). Glacial/interglacial changes in mineral dust and sea-salt records in polar ice cores: Sources, transport, and deposition. *Reviews of Geophysics*, 45(1):26.

Fisher, R. E., Sriskantharajah, S., Lowry, D., Lanoiselle, M., Fowler, C. M. R., James, R. H., Hermansen, O., Myhre, C. L., Stohl, A., Greinert, J., Nisbet-Jones, P. B. R., Mienert, J., and Nisbet, E. G. (2011). Arctic methane sources: Isotopic evidence for atmospheric inputs. *Geophysical Research Letters*, 38:6.

Floodgate, G. D. and Judd, A. G. (1992). The origins of shallow gas. *Continental Shelf Research*, 12(10):1145–1156.

Foster, G. L. and Rohling, E. J. (2013). Relationship between sea level and climate forcing by CO_2 on geological timescales. *Proceedings of the National Academy of Sciences of the United States of America*, 110(4):1209–1214.

Frey, B. (2006). *Stable Isotope Ecology*. Springer Science+Business Media, LLC, New York, NY, USA.

Ganopolski, A. and Rahmstorf, S. (2001). Rapid changes of glacial climate simulated in a coupled climate model. *Nature*, 409(6817):153–158.

Ghil, M., Allen, M. R., Dettinger, M. D., Ide, K., Kondrashov, D., Mann, M. E., Robertson, A. W., Saunders, A., Tian, Y., Varadi, F., and Yiou, P. (2002). Advanced spectral methods for climatic time series. *Reviews of Geophysics*, 40(1):41.

Ghosh, P. and Bhattacharya, S. K. (2001). CO_2 levels in the Late Palaeozoic and Mesozoic atmosphere from soil carbonate and organic matter, Satpura basin, Central India. *Palaeogeography Palaeoclimatology Palaeoecology*, 170(3-4):219–236.

Godwin, H. (1962). Half-life of radiocarbon. *Nature*, 195(4845):984–&.

Golyandina, N. and Korobeynikov, A. (2013). Basic Singular Spectrum Analysis and Forecasting with R. *Computational Statistics Data Analysis*, 71:934–954.

Golyandina, N., Nekrutin, V., and Zhigljavsky, A. (2001). *Analysis of Time Teries Structure: SSA and related techniques*. Chapman & Hall/CRC, Boca Raton, Fl, USA.

Grachev, A. M., Brook, E. J., and Severinghaus, J. P. (2007). Abrupt changes in atmospheric methane at the mis 5b-5a transition. *Geophysical Research Letters*, 34(20).

Grachev, A. M., Brook, E. J., Severinghaus, J. P., and Pisias, N. G. (2009). Relative timing and variability of atmospheric methane and GISP2 oxygen isotopes between 68 and 86 ka. *Global Biogeochemical Cycles*, 23:10.

Grant, K. M., Rohling, E. J., Bar-Matthews, M., Ayalon, A., Medina-Elizalde, M., Ramsey, C. B., Satow, C., and Roberts, A. P. (2012). Rapid coupling between ice volume and polar temperature over the past 150,000 years. *Nature*, 491(7426):744–747.

Guo, Z. T., Zhou, X., and Wu, H. B. (2012). Glacial-interglacial water cycle, global monsoon and atmospheric methane changes. *Climate Dynamics*, 39(5):1073–1092.

Gupta, M., Tyler, S., and Cicerone, R. (1996). Modeling atmospheric $\delta^{13}C$-CH_4 and the causes of recent changes in atmospheric CH_4 amounts. *Journal of Geophysical Research-Atmospheres*, 101(D17):22923–22932.

Hein, R., Crutzen, P. J., and Heimann, M. (1997). An inverse modeling approach to investigate the global atmospheric methane cycle. *Global Biogeochemical Cycles*, 11(1):43–76.

Heusser, L. and Morley, J. (1997). Monsoon fluctuations over the past 350 kyr: High-resolution evidence from northeast Asia northwest Pacific climate proxies (marine pollen and radiolarians). *Quaternary Science Reviews*, 16(6):565–581.

Holmes, M. E., Chanton, J. P., Bae, H. S., and Ogram, A. (2013). Effect of nutrient enrichment on δ^{13}C-CH_4 and methane production pathway in the Florida Everglades. *Journal of Geophysical Research-Biogeosciences*, 118:11.

Hope, G., Kershaw, A. P., van der Kaars, S., Xiangjun, S., Liew, P. M., Heusser, L. E., Takahara, H., McGlone, M., Miyoshi, N., and Moss, P. T. (2004). History of vegetation and habitat change in the Austral-Asian region. *Quaternary International*, 118:103–126.

Hornibrook, E. R. C. (2009). The Stable Carbon Isotope Composition of Methane Produced and Emitted From Northern Peatlands. In Baird, A. J., Belyea, L. R., Comas, X., Reeve, A. S., and Slater, L. D., editors, *Carbon Cycling in Northern Peatlands*, volume 184, pages 187–203. Amer Geophysical Union, 2000 Florida Ave Nw, Washington, Dc 20009 USA.

Hornibrook, E. R. C. and Bowes, H. L. (2007). Trophic status impacts both the magnitude and stable carbon isotope composition of methane flux from peatlands. *Geophysical Research Letters*, 34(21):5.

Houweling, S., van der Werf, G. R., Goldewijk, K. K., Röckmann, T., and Aben, I. (2008). Early anthropogenic CH_4 emissions and the variation of CH_4 and $\delta^{13}C$-CH_4 over the last millennium. *Global Biogeochemical Cycles*, 22(1).

Huber, C., Leuenberger, M., Spahni, R., Flückiger, J., Schwander, J., Stocker, T. F., Johnsen, S. J., Landais, A., and Jouzel, J. (2006). Isotope calibrated Greenland temperature record over Marine Isotope Stage 3 and its relation to CH_4. *Earth Planet. Sc. Lett.*, 243:504–519.

IUPAC (2013). Periodic table of the isotopes. Website. Available online at http://www.ciaaw.org/; last visited December 3, 2013.

Johnsen, S. J., Clausen, H. B., Dansgaar.W, and Langway, C. C. (1972). Oxygen isotope profiles through antarctic and greenland ice sheets. *Nature*, 235(5339):429–434.

Johnsen, S. J., DahlJensen, D., Gundestrup, N., Steffensen, J. P., Clausen, H. B., Miller, H., Masson-Delmotte, V., Sveinbjornsdottir, A. E., and White, J. (2001). Oxygen isotope and palaeotemperature records from six greenland ice-core stations: Camp century, dye-3, grip, gisp2, renland and northgrip. *Journal of Quaternary Science*, 16(4):299–307.

Jouzel, J., Masson-Delmotte, V., Cattani, O., Dreyfus, G., Falourd, S., Hoffmann, G., Minster, B., Nouet, J., Barnola, J. M., Chappellaz, J., Fischer, H., Gallet, J. C., Johnsen, S., Leuenberger, M., Loulergue, L., Lüthi, D., Oerter, H., Parrenin, F., Raisbeck, G., Raynaud, D., Schilt, A., Schwander, J., Selmo, E., Souchez, R., Spahni, R., Stauffer, B., Steffensen, J. P., Stenni, B., Stocker, T. F., Tison, J. L., Werner, M., and Wolff, E. W. (2007). Orbital and millennial Antarctic climate variability over the past 800,000 years. *Science*, 317(5839):793–796.

Kaplan, J. O. (2002). Wetlands at the last glacial maximum: Distribution and methane emissions. *Geophysical Research Letters*, 29(6):4.

Kaplan, J. O., Folberth, G., and Hauglustaine, D. A. (2006). Role of methane and biogenic volatile organic compound sources in late glacial and holocene fluctuations of atmospheric methane concentrations. *Global Biogeochemical Cycles*, 20(2):16.

Karion, A., Sweeney, C., Tans, P., and Newberger, T. (2010). Aircore: An innovative atmospheric sampling system. *Journal of Atmospheric and Oceanic Technology*, 27(11):1839–1853.

Keeling, C. D. (1958). The concentration and isotopic abundances of atmospheric carbon dioxide in rural areas. *Geochimica Et Cosmochimica Acta*, 13(4):322–334.

Keeling, C. D. (1961). The concentration and isotopic abundances of carbon dioxide in rural and marine air. *Geochimica Et Cosmochimica Acta*, 24(3-4):277–298.

Kennett, J. P., Cannariato, K. G., Hendy, I. L., and Behl, R. J. (2000). Carbon isotopic evidence for methane hydrate instability during quaternary interstadials. *Science*, 288(5463):128–133.

Kennett, J. P., Cannariato, K. G., Hendy, I. L., and Behl, R. J. (2003). *Methane Hydrates in Quaternary Climate Change: The Clathrate Gun Hypothesis*. American Geophysical Union, Special Publications Series, Washington, DC, USA.

Keppler, F., Boros, M., Frankenberg, C., Lelieveld, J., McLeod, A., Pirttila, A. M., Röckmann, T., and Schnitzler, J. P. (2009). Methane formation in aerobic environments. *Environmental Chemistry*, 6(6):459–465.

Keppler, F., Hamilton, J. T. G., Brass, M., and Röckmann, T. (2006). Methane emissions from terrestrial plants under aerobic conditions. *Nature*, 439(7073):187–191.

Keppler, F., Harper, D. B., Kalin, R. M., Meier-Augenstein, W., Farmer, N., Davis, S., Schmidt, H. L., Brown, D. M., and Hamilton, J. T. G. (2007). Stable hydrogen isotope ratios of lignin methoxyl groups as a paleoclimate proxy and constraint of the geographical origin of wood. *New Phytologist*, 176(3):600–609.

Kessler, J. D., Valentine, D. L., Redmond, M. C., Du, M. R., Chan, E. W., Mendes, S. D., Quiroz, E. W., Villanueva, C. J., Shusta, S. S., Werra, L. M., Yvon-Lewis, S. A., and Weber, T. C. (2011). A persistent oxygen anomaly reveals the fate of spilled methane in the deep gulf of mexico. *Science*, 331(6015):312–315.

Khalil, M. A. K., Shearer, M. J., and Rasmussen, R. A. (2000). Methane sinks, Distribution and Trends. In Khalil, M. A. K., editor, *Atmospheric Methane*, pages 86–97. Springer, Berlin, Heidelberg, Germany.

Kindler, P., Guillevic, M., Baumgartner, M., Schwander, J., Landais, A., and Leuenberger, M. (2013). NGRIP temperature reconstruction from 10 to 120 kyr b2k. *Climate of the Past, Discussion*, 9:4099–4143.

Kirschke, S., Bousquet, P., Ciais, P., Saunois, M., Canadell, J. G., Dlugokencky, E. J., Bergamaschi, P., Bergmann, D., Blake, D. R., Bruhwiler, L., Cameron-Smith, P., Castaldi, S., Chevallier, F., Feng, L., Fraser, A., Heimann, M., Hodson, E. L., Houweling, S., Josse, B., Fraser, P. J., Krummel, P. B., Lamarque, J.-F., Langenfelds, R. L., Le Quéré, C., Naik, V., O'Doherty, S., Palmer, P. I., Pison, I., Plummer, D., Poulter, B., Prinn, R. G., Rigby, M., Ringeval, B., Santini, M., Schmidt, M., Shindell, D. T., Simpson, I. J., Spahni, R., Steele, L. P., Strode, S. A., Sudo, K., Szopa, S., van der Werf, G. R., Voulgarakis, A., van Weele, M., Weiss, R. F., Williams, J. E., and Zeng, G. (2013). Three decades of global methane sources and sinks. *Nature Geoscience*, 6:813–823.

Köhler, P., Fischer, H., Schmitt, J., and Munhoven, G. (2006). On the application and interpretation of keeling plots in paleo climate research - deciphering $\delta^{13}C$ of atmospheric CO_2 measured in ice cores. *Biogeosciences*, 3(4):539–556.

Laskar, J., Robutel, P., Joutel, F., Gastineau, M., Correia, A. C. M., and Levrard, B. (2004). A long-term numerical solution for the insolation quantities of the Earth. *Astronomy & Astrophysics*, 428(1):261–285.

Lassey, K. R. (2007). Livestock methane emission: From the individual grazing animal through national inventories to the global methane cycle. *Agricultural and Forest Meteorology*, 142(2-4):120–132.

Lassey, K. R., Etheridge, D. M., Lowe, D. C., Smith, A. M., and Ferretti, D. F. (2007). Centennial evolution of the atmospheric methane budget: what do the carbon isotopes tell us? *Atmospheric Chemistry and Physics*, 7(8):2119–2139.

Laurion, I., Vincent, W. F., MacIntyre, S., Retamal, L., Dupont, C., Francus, P., and Pienitz, R. (2010). Variability in greenhouse gas emissions from permafrost thaw ponds. *Limnology and Oceanography*, 55(1):115–133.

Le Treut, H., Somerville, R.and Cubasch, U. D. Y., Mauritzen, C., Mokssit, A., Peterson, T., and Prather, M. (2007). Historical Overview of Climate Change. In Solomon, S., Qin, D., Manning, M., Chen, Z., Marquis, M., Averyt, K., Tignor, M., and Miller, H., editors, *Climate Change 2007: The Physical Science Basis. Contribution of Working Group I to the Fourth Assessment Report of the Intergovernmental Panel on Climate Change*. Cambridge University Press, Cambridge, United Kingdom and New York, NY, USA.

Lemaitre, G. (1931). The expanding universe. *Monthly Notices of the Royal Astronomical Society*, 91:490–501.

Lemieux-Dudon, B., Blayo, E., Petit, J. R., Waelbroeck, C., Svensson, A., Ritz, C., Barnola, J. M., Narcisi, B. M., and Parrenin, F. (2010). Consistent dating for Antarctic and Greenland ice cores. *Quaternary Science Reviews*, 29(1-2):8–20.

Levin, I., Veidt, C., Vaughn, B. H., Brailsford, G., Bromley, T., Heinz, R., Lowe, D., Miller, J. B., Poss, C., and White, J. W. C. (2012). No inter-hemispheric delta(ch4)-c-13 trend observed. *Nature*, 486(7404):E3–E4.

Levine, J. G., Wolff, E. W., Hopcroft, P. O., and Valdes, P. J. (2012). Controls on the tropospheric oxidizing capacity during an idealized Dansgaard-Oeschger event, and their implications for the rapid rises in atmospheric methane during the last glacial period. *Geophysical Research Letters*, 39:7.

Levine, J. G., Wolff, E. W., Jones, A. E., Hutterli, M. A., Wild, O., Carver, G. D., and Pyle, J. A. (2011a). In search of an ice core signal to differentiate between source-driven and sink-driven changes in atmospheric methane. *Journal of Geophysical Research-Atmospheres*, 116:15.

Levine, J. G., Wolff, E. W., Jones, A. E., Sime, L. C., Valdes, P. J., Archibald, A. T., Carver, G. D., Warwick, N. J., and Pyle, J. A. (2011b). Reconciling the changes in atmospheric methane sources and sinks between the Last Glacial Maximum and the pre-industrial era. *Geophysical Research Letters*, 38:6.

Lewis, S. L., Brando, P. M., Phillips, O. L., van der Heijden, G. M. F., and Nepstad, D. (2011). The 2010 Amazon Drought. *Science*, 331(6017):554–554.

Lipp, J. S., Morono, Y., Inagaki, F., and Hinrichs, K. U. (2008). Significant contribution of archaea to extant biomass in marine subsurface sediments. *Nature*, 454(7207):991–994.

Loulergue, L., Schilt, A., Spahni, R., Masson-Delmotte, V., Blunier, T., Lemieux, B., Barnola, J. M., Raynaud, D., Stocker, T. F., and Chappellaz, J. (2008). Orbital and millennial-scale features of atmospheric CH_4 over the past 800,000 years. *Nature*, 453(7193):383–386.

Lourantou, A., Chappellaz, J., Barnola, J. M., Masson-Delmotte, V., and Raynaud, D. (2010a). Changes in atmospheric CO_2 and its carbon isotopic ratio during the penultimate deglaciation. *Quaternary Science Reviews*, 29(17-18):1983–1992.

Lourantou, A., Lavric, J. V., Kohler, P., Barnola, J. M., Paillard, D., Michel, E., Raynaud, D., and Chappellaz, J. (2010b). Constraint of the CO_2 rise by new atmospheric carbon isotopic measurements during the last deglaciation. *Global Biogeochemical Cycles*, 24.

Lowe, D. C., Brenninkmeijer, C. A. M., Brailsford, G. W., Lassey, K. R., Gomez, A. J., and Nisbet, E. G. (1994). Concentration and ^{13}C records of atmospheric methane in new-zealand and antarctica - evidence for changes in methane sources. *Journal of Geophysical Research-Atmospheres*, 99(D8):16913–16925.

Lozhkin, A. V., Anderson, P. M., Matrosova, T. V., and Minyuk, P. S. (2007). The pollen record from El'Gygytgyn Lake: implications for vegetation and climate histories of northern Chukotka since the late middle Pleistocene. *Journal of Paleolimnology*, 37(1):135–153.

Lüthi, D., Le Floch, M., Bereiter, B., Blunier, T., Barnola, J. M., Siegenthaler, U., Raynaud, D., Jouzel, J., Fischer, H., Kawamura, K., and Stocker, T. F. (2008). High-resolution carbon dioxide concentration record 650,000-800,000 years before present. *Nature*, 453(7193):379–382.

MacFarling Meure, C. M., Etheridge, D., Trudinger, C., Steele, P., Langenfelds, R., van Ommen, T., Smith, A., and Elkins, J. (2006). Law dome CO_2, CH_4 and N_2O ice core records extended to 2000 years bp. *Geophysical Research Letters*, 33(14).

Mahowald, N. M., Muhs, D. R., Levis, S., Rasch, P. J., Yoshioka, M., Zender, C. S., and Luo, C. (2006). Change in atmospheric mineral aerosols in response to climate: last glacial period, preindustrial, modern, and doubled carbon dioxide climate. *Journal of Geophysical Research-Part D-Atmospheres*, 111(D10):22 pp.–22 pp.

Manasypov, R. M., Pokrovski, O. S., Kirpotin, S. N., and Shirokova, L. S. (2013). Hydrochemical composition of thermokarst lake waters in the permafrost zone of western Siberia within the context of climate change. *The Cryosphere Discussions*, 7:5333–5387.

Manhes, G., Allegre, C. J., Dupre, B., and Hamelin, B. (1980). Lead isotope study of basic-ultrabasic layered complexes - speculations about the age of the earth and primitive mantle characteristics. *Earth and Planetary Science Letters*, 47(3):370–382.

Martinerie, P., Brasseur, G. P., and Granier, C. (1995). The chemical-composition of ancient atmospheres - a model study constrained by ice core data. *Journal of Geophysical Research-Atmospheres*, 100(D7):14291–14304.

McLeod, A. R., Fry, S. C., Loake, G. J., Messenger, D. J., Reay, D. S., Smith, K. A., and Yun, B. W. (2008). Ultraviolet radiation drives methane emissions from terrestrial plant pectins. *New Phytologist*, 180(1):124–132.

McManus, J. B., Zahniser, M. S., Nelson, D. D., Shorter, J. H., Herndon, S., Wood, E., and Wehr, R. (2010). Application of quantum cascade lasers to high-precision atmospheric trace gas measurements. *Optical Engineering*, 49(11):11.

Melles, M., Brigham-Grette, J., Minyuk, P. S., Nowaczyk, N. R., Wennrich, V., DeConto, R. M., Anderson, P. M., Andreev, A. A., Coletti, A., Cook, T. L., Haltia-Hovi, E., Kukkonen, M., Lozhkin, A. V., Rosen, P., Tarasov, P., Vogel, H., and Wagner, B. (2012). 2.8

Million Years of Arctic Climate Change from Lake El'Gygytgyn, NE Russia. *Science*, 337(6092):315–320.

Melton, J. R., Schaefer, H., and Whiticar, M. J. (2011a). Enrichment in ^{13}C of atmospheric CH_4 during the younger dryas termination. *Climate of the Past*, 8(4):1177–1197.

Melton, J. R., Wania, R., Hodson, E. L., Poulter, B., Ringeval, B., Spahni, R., Bohn, T., Avis, C. A., Beerling, D. J., Chen, G., Eliseev, A. V., Denisov, S. N., Hopcroft, P. O., Lettenmaier, D. P., Riley, W. J., Singarayer, J. S., Subin, Z. M., Tian, H., Zurcher, S., Brovkin, V., van Bodegom, P. M., Kleinen, T., Yu, Z. C., and Kaplan, J. O. (2013). Present state of global wetland extent and wetland methane modelling: conclusions from a model intercomparison project (wetchimp). *Biogeosciences*, 10(2):753–788.

Melton, J. R., Whiticar, M. J., and Eby, P. (2011b). Stable carbon isotope ratio analyses on trace methane from ice samples. *Chemical Geology*, 288(3-4):88–96.

Mikaloff Fletcher, S. E., Tans, P. P., Bruhwiler, L. M., Miller, J. B., and Heimann, M. (2004a). CH_4 sources estimated from atmospheric observations of CH_4 and its $^{13}C/^{12}C$ isotopic ratios: 1. inverse modeling of source processes. *Global Biogeochemical Cycles*, 18(4):17.

Mikaloff Fletcher, S. E., Tans, P. P., Bruhwiler, L. M., Miller, J. B., and Heimann, M. (2004b). CH_4 sources estimated from atmospheric observations of CH_4 and its $^{13}C/^{12}C$ isotopic ratios: 2. inverse modeling of ch(4) fluxes from geographical regions. *Global Biogeochemical Cycles*, 18(4):15.

Milkov, A. V. (2004). Global estimates of hydrate-bound gas in marine sediments: how much is really out there? *Earth-Science Reviews*, 66(3-4):183–197.

Mischler, J. A., Sowers, T. A., Alley, R. B., Battle, M., McConnell, J. R., Mitchell, L., Popp, T., Sofen, E., and Spencer, M. K. (2009). Carbon and hydrogen isotopic composition of methane over the last 1000 years. *Global Biogeochemical Cycles*, 23.

Mitchell, L. E., Brook, E. J., Sowers, T., McConnell, J. R., and Taylor, K. (2011). Multidecadal variability of atmospheric methane, 1000-1800 ce. *Journal of Geophysical Research-Biogeosciences*, 116:16.

Mohn, J., Guggenheim, C., Tuzson, B., Vollmer, M. K., Toyoda, S., Yoshida, N., and Emmenegger, L. (2010). A liquid nitrogen-free preconcentration unit for measurements of ambient N_2O isotopomers by QCLAS. *Atmospheric Measurement Techniques*, 3(3):609–618.

Möller, L., Sowers, T., Bock, M., Spahni, R., Behrens, M., Schmitt, J., Miller, H., and Fischer, H. (2013). Independent variations of CH_4 emissions and isotopic composition over the past 160,000 years. *Nature Geoscience*, 6(10):885–890.

Monnin, E., Indermuhle, A., Dällenbach, A., Fluckiger, J., Stauffer, B., Stocker, T. F., Raynaud, D., and Barnola, J. M. (2001). Atmospheric CO_2 concentrations over the last glacial termination. *Science*, 291(5501):112–114.

Montenegro, A., Eby, M., Kaplan, J. O., Meissner, K. J., and Weaver, A. J. (2006). Carbon storage on exposed continental shelves during the glacial-interglacial transition. *Geophysical Research Letters*, 33(8):3.

MPI-BGC (2013). Max-Planck-Institute for Biogeochemistry, MPI-BGC, Zotino Tall Tower Observatory, (ZOTTO). Website. Available online at http://www.bgc-jena.mpg.de/bgc-systems/pmwiki2/pmwiki.php/TAG/Facilities; last visited December 3, 2013.

MPI-C (2013). Max-Planck-Institute for Chemistry, MPI-C, Civil Aircraft for the Regular Investigation of the atmosphere Based on an Instrument Container, (CARIBIC). Website. Available online at http://www.mpg.de/5012675/CARIBIC?c=5732389; last visited December 3, 2013.

Muhs, D. R. (2013). The geologic records of dust in the Quaternary. *Aeolian Research*, 9:3–48.

NEEM community members, Dahl-Jensen, D., Albert, M. R., Aldahan, A., Azuma, N., Balslev-Clausen, D., Baumgartner, M., Berggren, A. M., Bigler, M., Binder, T., Blunier, T., Bourgeois, J. C., Brook, E. J., Buchardt, S. L., Buizert, C., Capron, E., Chappellaz, J., Chung, J., Clausen, H. B., Cvijanovic, I., Davies, S. M., Ditlevsen, P., Eicher, O., Fischer, H., Fisher, D. A., Fleet, L. G., Gfeller, G., Gkinis, V., Gogineni, S., Goto-Azuma, K., Grinsted, A., Gudlaugsdottir, H., Guillevic, M., Hansen, S. B., Hansson, M., Hirabayashi, M., Hong, S., Hur, S. D., Huybrechts, P., Hvidberg, C. S., Iizuka, Y., Jenk, T., Johnsen, S. J., Jones, T. R., Jouzel, J., Karlsson, N. B., Kawamura, K., Keegan, K., Kettner, E., Kipfstuhl, S., Kjaer, H. A., Koutnik, M., Kuramoto, T., Kohler, P., Laepple, T., Landais, A., Langen, P. L., Larsen, L. B., Leuenberger, D., Leuenberger, M., Leuschen, C., Li, J., Lipenkov, V., Martinerie, P., Maselli, O. J., Masson-Delmotte, V., McConnell, J. R., Miller, H., Mini, O., Miyamoto, A., Montagnat-Rentier, M., Mulvaney, R., Muscheler, R., Orsi, A. J., Paden, J., Panton, C., Pattyn, F., Petit, J. R., Pol, K., Popp, T., Possnert, G., Prie, F., Prokopiou, M., Quiquet, A., Rasmussen, S. O., Raynaud, D., Ren, J., Reutenauer, C., Ritz, C., Rockmann, T., Rosen, J. L., Rubino, M., Rybak, O., Samyn, D., Sapart, C. J., Schilt, A., Schmidt, A. M. Z., Schwander, J., Schupbach, S., Seierstad, I., et al. (2013). Eemian interglacial reconstructed from a Greenland folded ice core. *Nature*, 493(7433):489–494.

NGRIP community members, Andersen, K. K., Azuma, N., Barnola, J. M., Bigler, M., Biscaye, P., Caillon, N., Chappellaz, J., Clausen, H. B., DahlJensen, D., Fischer, H., Fluckiger, J., Fritzsche, D., Fujii, Y., Goto-Azuma, K., Gronvold, K., Gundestrup, N. S., Hansson, M., Huber, C., Hvidberg, C. S., Johnsen, S. J., Jonsell, U., Jouzel, J., Kipfstuhl, S., Landais, A., Leuenberger, M., Lorrain, R., Masson-Delmotte, V., Miller, H., Motoyama, H., Narita, H., Popp, T., Rasmussen, S. O., Raynaud, D., Rothlisberger, R., Ruth, U., Samyn, D., Schwander, J., Shoji, H., Siggard-Andersen, M. L., Steffensen, J. P., Stocker, T., Sveinbjornsdottir, A. E., Svensson, A., Takata, M., Tison, J. L., Thorsteinsson, T., Watanabe, O., Wilhelms, F., White, J. W. C., and Project, N. G. I. C. (2004). High-resolution record of Northern Hemisphere climate extending into the last interglacial period. *Nature*, 431(7005):147–151.

Nisbet, R. E. R., Fisher, R., Nimmo, R. H., Bendall, D. S., Crill, P. M., Gallego-Sala, A. V., Hornibrook, E. R. C., Lopez-Juez, E., Lowry, D., Nisbet, P. B. R., Shuckburgh, E. F., Sriskantharajah, S., Howe, C. J., and Nisbet, E. G. (2009). Emission of methane from plants. *Proceedings of the Royal Society B-Biological Sciences*, 276(1660):1347–1354.

NIWA (2013). National Institute of Water and Atmospheric Reseach Ltd, NIWA, Baring Head monitoring station, (BHD). Website. Available online at http://www.niwa.co.nz/our-science/atmosphere/baring; last visited December 3, 2013.

NOAA (2013). National Oceanic & Atmospheric Administration, Global Monitoring Devision Observatory Operations (OBOP). Website. Available online at http://www.esrl.noaa.gov/gmd/obop/; last visited December 3, 2013.

Nobelprize (2013). Nobel Prize Laureates in Chemistry. Website. Available online at http://www.nobelprize.org/nobel_prizes/chemistry/laureates/; last visited December 3, 2013.

Olivier, J. and Berdowski, J. J. M. (2001). Global emissions sources and sinks. In Berdowski, J., Guicherit, R., and Heij, B., editors, *The Climate System*, pages 33–78. A.A. Balkema Publishers/Swets & Zeitlinger Publishers, Lisse, The Netherlands.

Paldus, B. A. and Kachanov, A. A. (2005). An historical overview of cavity-enhanced methods. *Canadian Journal of Physics*, 83(10):975–999.

Pataki, D. E., Ehleringer, J. R., Flanagan, L. B., Yakir, D., Bowling, D. R., Still, C. J., Buchmann, N., Kaplan, J. O., and Berry, J. A. (2003). The application and interpretation of keeling plots in terrestrial carbon cycle research. *Global Biogeochemical Cycles*, 17(1):15.

Peterson, L. C., Haug, G. H., Hughen, K. A., and Rohl, U. (2000). Rapid changes in the hydrologic cycle of the tropical Atlantic during the last glacial. *Science*, 290(5498):1947–1951.

Petrenko, V. V., Smith, A. M., Brook, E. J., Lowe, D., Riedel, K., Brailsford, G., Hua, Q., Schaefer, H., Reeh, N., Weiss, R. F., Etheridge, D., and Severinghaus, J. P. (2009). CH_4-c-14 Measurements in Greenland Ice: Investigating Last Glacial Termination CH_4 sources. *Science*, 324(5926):506–508.

Phillips, O. L., Aragao, L., Lewis, S. L., Fisher, J. B., Lloyd, J., Lopez-Gonzalez, G., Malhi, Y., Monteagudo, A., Peacock, J., Quesada, C. A., van der Heijden, G., Almeida, S., Amaral, I., Arroyo, L., Aymard, G., Baker, T. R., Banki, O., Blanc, L., Bonal, D., Brando, P., Chave, J., de Oliveira, A. C. A., Cardozo, N. D., Czimczik, C. I., Feldpausch, T. R., Freitas, M. A., Gloor, E., Higuchi, N., Jimenez, E., Lloyd, G., Meir, P., Mendoza, C., Morel, A., Neill, D. A., Nepstad, D., Patino, S., Penuela, M. C., Prieto, A., Ramirez, F., Schwarz, M., Silva, J., Silveira, M., Thomas, A. S., ter Steege, H., Stropp, J., Vasquez, R., Zelazowski, P., Davila, E. A., Andelman, S., Andrade, A., Chao, K. J., Erwin, T., Di Fiore, A., Honorio, E., Keeling, H., Killeen, T. J., Laurance, W. F., Cruz, A. P., Pitman, N. C. A., Vargas, P. N., Ramirez-Angulo, H., Rudas, A., Salamao, R., Silva, N., Terborgh, J., and Torres-Lezama, A. (2009). Drought Sensitivity of the Amazon Rainforest. *Science*, 323(5919):1344–1347.

Phillips, O. L., van der Heijden, G., Lewis, S. L., Lopez-Gonzalez, G., Aragao, L., Lloyd, J., Malhi, Y., Monteagudo, A., Almeida, S., Davila, E. A., Amaral, I., Andelman, S., Andrade, A., Arroyo, L., Aymard, G., Baker, T. R., Blanc, L., Bonal, D., de Oliveira, A. C. A., Chao, K. J., Cardozo, N. D., da Costa, L., Feldpausch, T. R., Fisher, J. B., Fyllas, N. M., Freitas, M. A., Galbraith, D., Gloor, E., Higuchi, N., Honorio, E., Jimenez, E., Keeling, H., Killeen, T. J., Lovett, J. C., Meir, P., Mendoza, C., Morel, A., Vargas, P. N., Patino, S., Peh, K. S. H., Cruz, A. P., Prieto, A., Quesada, C. A., Ramirez, F., Ramirez, H., Rudas, A., Salamao, R., Schwarz, M., Silva, J., Silveira, M., Slik, J. W. F., Sonke, B., Thomas, A. S., Stropp, J., Taplin, J. R. D., Vasquez, R., and Vilanova, E. (2010). Drought-mortality relationships for tropical forests. *New Phytologist*, 187(3):631–646.

Picarro (2013a). Datasheet Picarro G2131-i Analyzer for δ^{13}C-CO_2. Website. Available online at http://www.picarro.com/products_solutions/isotope_analyzers/13c_for_co2; last visited December 3, 2013.

Picarro (2013b). Datasheet Picarro G2132-i Analyzer for δ^{13}C-CH_4. Website. Available online at http://www.picarro.com/products_solutions/isotope_analyzers/13c_for_ch4; last visited December 3, 2013.

Prokopenko, A. A., Karabanov, E. B., Williams, D. F., Kuzmin, M. I., Shackleton, N. J., Crowhurst, S. J., Peck, J. A., Gvozdkov, A. N., and King, J. W. (2001). Biogenic silica record of the Lake Baikal response to climatic forcing during the Brunhes. *Quaternary Research*, 55(2):123–132.

Qaderi, M. M. and Reid, D. M. (2011). Stressed crops emit more methane despite the mitigating effects of elevated carbon dioxide. *Functional Plant Biology*, 38(2):97–105.

Quay, P., Stutsman, J., Wilbur, D., Snover, A., Dlugokencky, E., and Brown, T. (1999). The isotopic composition of atmospheric methane. *Global Biogeochemical Cycles*, 13(2):445–461.

Rampino, M. R. and Self, S. (1992). Volcanic winter and accelerated glaciation following the Toba super-eruption. *Nature*, 359(6390):50–52.

Rasmussen, S. O., Abbott, P., Blunier, T., Bourne, A., Brook, E., Buchardt, S. L., Buizert, C., Chappellaz, J., Clausen, H. B., Cook, E., Dahl-Jensen, D., Davies, S., Guillevic, M., Kipfstuhl, S., Laepple, T., Seierstad, I. K., Severinghaus, J. P., Steffensen, J. P., Stowasser, C., Svensson, A., Vallelonga, P., Vinther, B. M., Wilhelms, F., and M., W. (2013). A first chronology for the NEEM ice core. *Climate of the Past, Discussion*, 9:2967–3013.

Redmond, M. C. and Valentine, D. L. (2012). Natural gas and temperature structured a microbial community response to the deepwater horizon oil spill. *Proceedings of the National Academy of Sciences of the United States of America*, 109(50):20292–20297.

Retallack, G. J. (2009). Refining a pedogenic-carbonate CO_2 paleobarometer to quantify a middle Miocene greenhouse spike. *Palaeogeography Palaeoclimatology Palaeoecology*, 281(1-2):57–65.

Robbins, R. C., Cavanagh, L. A., Salas, L. J., and Robinson, E. (1973). Analysis of ancient atmospheres. *Journal of Geophysical Research*, 78(24):5341–5344.

Röckmann, T., Brass, M., Borchers, R., and Engel, A. (2011). The isotopic composition of methane in the stratosphere: high-altitude balloon sample measurements. *Atmospheric Chemistry and Physics*, 11(24):13287–13304.

Rohling, E. J., Grant, K., Bolshaw, M., Roberts, A. P., Siddall, M., Hemleben, C., and Kucera, M. (2009a). Antarctic temperature and global sea level closely coupled over the past five glacial cycles. *Nature Geoscience*, 2(7):500–504.

Rohling, E. J., Liu, Q. S., Roberts, A. P., Stanford, J. D., Rasmussen, S. O., Langen, P. L., and Siddall, M. (2009b). Controls on the East Asian monsoon during the last glacial cycle, based on comparison between Hulu Cave and polar ice-core records. *Quaternary Sci. Rev.*, 28(27-28):3291–3302.

Rosenfeld, W. D. and Silverman, S. R. (1959). Carbon isotope fractionation in bacterial production of methane. *Science*, 130(3389):1658–1659.

Ross, A. N., Wooster, M. J., Boesch, H., and Parker, R. (2013). First satellite measurements of carbon dioxide and methane emission ratios in wildfire plumes. *Geophysical Research Letters*, 40(15):4098–4102.

Rostek, F., Ruhland, G., Bassinot, F. C., Muller, P. J., Labeyrie, L. D., Lancelot, Y., and Bard, E. (1993). Reconstructing sea-surface temperature and salinity using $\delta^{18}O$ and alkenone records. *Nature*, 364(6435):319–321.

Ruddiman, W. F. (2001). *Earth's Climate: Past and Future*. W. H. Freeman and Company, NY, New York, NY, USA.

Ruddiman, W. F. (2003). The anthropogenic greenhouse era began thousands of years ago. *Climatic Change*, 61(3):261–293.

Ruth, U., Bigler, M., Rothlisberger, R., Siggaard-Andersen, M. L., Kipfstuhl, S., Goto-Azuma, K., Hansson, M. E., Johnsen, S. J., Lu, H. Y., and Steffensen, J. P. (2007). Ice core evidence for a very tight link between North Atlantic and east Asian glacial climate. *Geophysical Research Letters*, 34(3):5.

Sapart, C. J., Monteil, G., Prokopiou, M., van de Wal, R. S. W., Kaplan, J. O., Sperlich, P., Krumhardt, K. M., van der Veen, C., Houweling, S., Krol, M. C., Blunier, T., Sowers, T., Martinerie, P., Witrant, E., Dahl-Jensen, D., and Röckmann, T. (2012). Natural and anthropogenic variations in methane sources during the past two millennia. *Nature*, 490(7418):85–88.

Sapart, C. J., van der Veen, C., Vigano, I., Brass, M., van de Wal, R. S. W., Bock, M., Fischer, H., Sowers, T., Buizert, C., Sperlich, P., Blunier, T., Behrens, M., Schmitt, J., Seth, B., and Röckmann, T. (2011). Simultaneous stable isotope analysis of methane and nitrous oxide on ice core samples. *Atmospheric Measurement Techniques*, 4(12):2607–2618.

Schaefer, H. and Whiticar, M. J. (2007). Measurement of stable carbon isotope ratios of methane in ice samples. *Organic Geochemistry*, 38(2):216–226.

Schaefer, H., Whiticar, M. J., Brook, E. J., Petrenko, V. V., Ferretti, D. F., and Severinghaus, J. P. (2006). Ice record of $\delta^{13}C$ for atmospheric CH_4 across the younger dryas-preboreal transition. *Science*, 313(5790):1109–1112.

Schilt, A., Baumgartner, M., Blunier, T., Schwander, J., Spahni, R., Fischer, H., and Stocker, T. F. (2010a). Glacial-interglacial and millennial-scale variations in the atmospheric nitrous oxide concentration during the last 800,000 years. *Quaternary Science Reviews*, 29(1-2):182–192.

Schilt, A., Baumgartner, M., Schwander, J., Buiron, D., Capron, E., Chappellaz, J., Loulergue, L., Schupbach, S., Spahni, R., Fischer, H., and Stocker, T. F. (2010b). Atmospheric nitrous oxide during the last 140,000 years. *Earth and Planetary Science Letters*, 300(1-2):33–43.

Schoell, M. (1988). Multiple origins of methane in the earth. *Chemical Geology*, 71(1-3):1–10.

Schubert, B. A. and Jahren, A. H. (2010). The effect of atmospheric CO_2 concentration on carbon isotope fractionation in C-3 land plants. *Geochimica Et Cosmochimica Acta*, 96:29–43.

Schüpbach, S., Federer, U., Bigler, M., Fischer, H., and Stocker, T. F. (2011). A refined TALDICE-1a age scale from 55 to 112 ka before present for the Talos Dome ice core based on high-resolution methane measurements. *Climate of the Past*, 7(3):1001–1009.

Schuur, E. A. G., Bockheim, J., Canadell, J. G., Euskirchen, E., Field, C. B., Goryachkin, S. V., Hagemann, S., Kuhry, P., Lafleur, P. M., Lee, H., Mazhitova, G., Nelson, F. E., Rinke, A., Romanovsky, V. E., Shiklomanov, N., Tarnocai, C., Venevsky, S., Vogel, J. G., and Zimov, S. A. (2008). Vulnerability of permafrost carbon to climate change: Implications for the global carbon cycle. *Bioscience*, 58(8):701–714.

Schwander, J., Barnola, J. M., Andrie, C., Leuenberger, M., Ludin, A., Raynaud, D., and Stauffer, B. (1993). The age of the air in the firn and the ice at summit, Greenland. *Journal of Geophysical Research-Atmospheres*, 98(D2):2831–2838.

Schwander, J., Jouzel, J., Hammer, C. U., Petit, J. R., Udisti, R., and Wolff, E. (2001). A tentative chronology for the EPICA Dome Concordia ice core. *Geophysical Research Letters*, 28(22):4243–4246.

Schwander, J. and Stauffer, B. (1984). Age difference between polar ice and the air trapped in its bubbles. *Nature*, 311:45–47.

Seidel, D. J., Ross, R. J., Angell, J. K., and Reid, G. C. (2001). Climatological characteristics of the tropical tropopause as revealed by radiosondes. *Journal of Geophysical Research-Atmospheres*, 106(D8):7857–7878.

Severinghaus, J. P. and Brook, E. J. (1999). Abrupt climate change at the end of the last glacial period inferred from trapped air in polar ice. *Science*, 286(5441):930–934.

Severinghaus, J. P., Sowers, T., Brook, E. J., Alley, R. B., and Bender, M. L. (1998). Timing of abrupt climate change at the end of the Younger Dryas interval from thermally fractionated gases in polar ice. *Nature*, 391(6663):141–146.

Singarayer, J. S., Valdes, P. J., Friedlingstein, P., Nelson, S., and Beerling, D. J. (2011). Late Holocene methane rise caused by orbitally controlled increase in tropical sources. *Nature*, 470(7332):82–U91.

Sowers, T. (2006). Late quaternary atmospheric CH_4 isotope record suggests marine clathrates are stable. *Science*, 311(5762):838–840.

Sowers, T. (2009). Atmospheric methane isotope records covering the Holocene period. *Quaternary Science Reviews*, 29(1-2):213–221.

Sowers, T., Bender, M., Raynaud, D., and Korotkevich, Y. S. (1992). $\delta^{15}N$ of N_2 in air trapped in polar ice - a tracer of gas-transport in the firn and a possible constraint on ice age-gas age-differences. *Journal of Geophysical Research-Atmospheres*, 97(D14):15683–15697.

Sowers, T., Bernard, S., Aballain, O., Chappellaz, J., Barnola, J. M., and Marik, T. (2005). Records of the $\delta^{13}C$ of atmospheric CH_4 over the last 2 centuries as recorded in Antarctic snow and ice. *Global Biogeochemical Cycles*, 19(2).

Sperlich, P., Buizert, C., Jenk, T. M., Sapart, C. J., Prokopiou, M., Röckmann, T., and Blunier, T. (2013). An automated GC-C-GC-IRMS setup to measure paleoatmospheric $\delta^{13}C$-CH_4, $\delta^{15}N$-N_2O and $\delta^{18}O$-N_2O in one ice core sample. *Atmospheric Measurement Techniques*, 6(8):2027–2041.

Sperlich, P., Guillevic, M., Buizert, C., Jenk, T. M., Sapart, C. J., Schaefer, H., Popp, T. J., and Blunier, T. (2012). A combustion setup to precisely reference $\delta^{13}C$ and $\delta^{2}H$ isotope ratios of pure CH_4 to produce isotope reference gases of $\delta^{13}C$-CH_4 in synthetic air. *Atmospheric Measurement Techniques*, 5(9):2227–2236.

Steen-Larsen, H. C., Johnsen, S. J., Masson-Delmotte, V., Stenni, B., Risi, C., Sodemann, H., Balslev-Clausen, D., Blunier, T., Dahl-Jensen, D., Ellehoj, M. D., Falourd, S., Grindsted, A., Gkinis, V., Jouzel, J., Popp, T., Sheldon, S., Simonsen, S. B., Sjolte, J., Steffensen, J. P., Sperlich, P., Sveinbjornsdottir, A. E., Vinther, B. M., and White, J. W. C. (2013). Continuous monitoring of summer surface water vapor isotopic composition above the Greenland Ice Sheet. *Atmospheric Chemistry and Physics*, 13(9):4815–4828.

Stocker, T. F. and Johnsen, S. J. (2003). A minimum thermodynamic model for the bipolar seesaw. *Paleoceanography*, 18(4):9.

Stowasser, C., Buizert, C., Gkinis, V., Chappellaz, J., Schupbach, S., Bigler, M., Fain, X., Sperlich, P., Baumgartner, M., Schilt, A., and Blunier, T. (2012). Continuous measurements of methane mixing ratios from ice cores. *Atmospheric Measurement Techniques*, 5(5):999–1013.

Svensson, A., Bigler, M., Blunier, T., Clausen, H. B., Dahl-Jensen, D., Fischer, H., Fujita, S., Goto-Azuma, K., Johnsen, S. J., Kawamura, K., Kipfstuhl, S., Kohno, M., Parrenin, F., Popp, T., Rasmussen, S. O., Schwander, J., Seierstad, I., Severi, M., Steffensen, J. P., Udisti, R., Uemura, R., Vallelonga, P., Vinther, B. M., Wegner, A., Wilhelms, F., and Winstrup, M. (2013). Direct linking of Greenland and Antarctic ice cores at the Toba eruption (74 ka bp). *Climate of the Past*, 9(2):749–766.

Tans, P. P. (1997). A note on isotopic ratios and the global atmospheric methane budget. *Global Biogeochemical Cycles*, 11(1):77–81.

Tarasov, P., Bezrukova, E., Karabanov, E., Nakagawa, T., Wagner, M., Kulagina, N., Letunova, P., Abzaeva, A., Granoszewski, W., and Riedel, F. (2007). Vegetation and climate dynamics during the Holocene and Eemian interglacials derived from Lake Baikal pollen records. *Palaeogeography Palaeoclimatology Palaeoecology*, 252(3-4):440–457.

Tarasov, P., Granoszewski, W., Bezrukova, E., Brewer, S., Nita, M., Abzaeva, A., and Oberhansli, H. (2005). Quantitative reconstruction of the last interglacial vegetation and climate based on the pollen record from Lake Baikal, Russia. *Climate Dynamics*, 25(6):625–637.

Thevenon, F., Bard, E., Williamson, D., and Beaufort, L. (2004). A biomass burning record from the West Equatorial Pacific over the last 360 ky: methodological, climatic and anthropic implications. *Palaeogeography Palaeoclimatology Palaeoecology*, 213(1-2):83–99.

Trenberth, K., Jones, P., Ambenje, P., Bojariu, R., Easterling, D., Klein Tank, A., Parker, D., Rahimzadeh, F., Renwick, J., Rusticucci, M., Soden, B., and Zhai, P. (2007). Observations: Surface and Atmospheric Climate Change. In Solomon, S., Qin, D., Manning, M., Chen, Z., Marquis, M., Averyt, K., Tignor, M., and Miller, H., editors, *Climate Change 2007: The Physical Science Basis. Contribution of Working Group I to the Fourth Assessment Report of the Intergovernmental Panel on Climate Change*. Cambridge University Press, Cambridge, United Kingdom and New York, NY, USA.

Trolier, M., White, J. W. C., Tans, P. P., Masarie, K. A., and Gemery, P. A. (1996). Monitoring the isotopic composition of atmospheric CO_2: Measurements from the NOAA Global Air Sampling Network. *Journal of Geophysical Research-Atmospheres*, 101(D20):25897–25916.

Trudinger, C. M., Enting, I. G., Etheridge, D. M., Francey, R. J., Levchenko, V. A., Steele, L. P., Raynaud, D., and Arnaud, L. (1997). Modeling air movement and bubble trapping in firn. *Journal of Geophysical Research-Atmospheres*, 102(D6):6747–6763.

Umezawa, T., Aoki, S., Nakazawa, T., and Morimoto, S. (2009). A high-precision measurement system for carbon and hydrogen isotopic ratios of atmospheric methane and its application to air samples collected in the western pacific region. *Journal of the Meteorological Society of Japan*, 87(3):365–379.

Urey, H. C., Lowenstam, H. A., Epstein, S., and McKinney, C. R. (1951). Measurement of paleotemperatures and temperatures of the upper Cretaceous of England, Denmark, and the southeastern United-States. *Geological Society of America Bulletin*, 62(4):399–&.

Vallelonga, P., Bertagna, G., Blunier, T., Kjaer, H. A., Popp, T. J., Rasmussen, S. O., Steffensen, J. P., Stowasser, C., Svensson, A. S., Warming, E., Winstrup, M., Bigler, M., and Kipfstuhl, S. (2012). Duration of Greenland Stadial 22 and ice-gas Delta age from counting of annual layers in Greenland NGRIP ice core. *Climate of the Past*, 8(6):1839–1847.

van Aardenne, J. A., Dentener, F. J., Olivier, J. G. J., Goldewijk, C. G. M. K., and Lelieveld, J. (2001). A 1 degrees x 1 degrees resolution data set of historical anthropogenic trace gas emissions for the period 1890-1990. *Global Biogeochemical Cycles*, 15(4):909–928.

van der Werf, G. R., Randerson, J. T., Giglio, L., Collatz, G. J., Mu, M., Kasibhatla, P. S., Morton, D. C., DeFries, R. S., Jin, Y., and van Leeuwen, T. T. (2010). Global fire emissions and the contribution of deforestation, savanna, forest, agricultural, and peat fires (1997-2009). *Atmospheric Chemistry and Physics*, 10(23):11707–11735.

van Leeuwen, T. T. and van der Werf, G. R. (2011). Spatial and temporal variability in the ratio of trace gases emitted from biomass burning. *Atmospheric Chemistry and Physics*, 11(8):3611–3629.

Veres, D., Bazin, L., Landais, A., Kele, H. T. M., Lemieux-Dudon, B., Parrenin, F., Martinerie, P., Blayo, E., Blunier, T., Capron, E., Chappellaz, J., Rasmussen, S. O., Severi, M., Svensson, A., Vinther, B., and Wolff, E. W. (2013). The Antarctic ice core chronology (AICC2012):

an optimized multi-parameter and multi-site dating approach for the last 120 thousand years. *Climate of the Past*, 9(4):1733–1748.

Vigano, I., Holzinger, R., Röckmann, T., van Dijk, A., Keppler, F., Greule, M., Brand, W. A., van Weelden, H., and van Dongen, J. (2009a). *UV* light induces methane emission from plant biomass: Mechanism and isotope studies. *Geochimica Et Cosmochimica Acta*, 73(13):A1382–A1382.

Vigano, I., Röckmann, T., Holzinger, R., van Dijk, A., Keppler, F., Greule, M., Brand, W. A., Geilmann, H., and van Weelden, H. (2009b). The stable isotope signature of methane emitted from plant material under *UV* irradiation. *Atmospheric Environment*, 43(35):5637–5646.

Vigano, I., van Weelden, H., Holzinger, R., Keppler, F., McLeod, A., and Röckmann, T. (2008). Effect of *UV* radiation and temperature on the emission of methane from plant biomass and structural components. *Biogeosciences*, 5(3):937–947.

Walter, B. P., Heimann, M., and Matthews, E. (2001). Modeling modern methane emissions from natural wetlands 2. interannual variations 1982-1993. *Journal of Geophysical Research-Atmospheres*, 106(D24):34207–34219.

Walter, K. M., Chanton, J. P., Chapin, F. S., Schuur, E. A. G., and Zimov, S. A. (2008). Methane production and bubble emissions from arctic lakes: Isotopic implications for source pathways and ages. *Journal of Geophysical Research-Biogeosciences*, 113:16.

Walter, K. M., Edwards, M. E., Grosse, G., Zimov, S. A., and Chapin, F. S. (2007). Thermokarst lakes as a source of atmospheric CH_4 during the last deglaciation. *Science*, 318(5850):633–636.

Walter, K. M., Zimov, S. A., Chanton, J. P., Verbyla, D., and Chapin, F. S. (2006). Methane bubbling from Siberian thaw lakes as a positive feedback to climate warming. *Nature*, 443(7107):71–75.

Wang, W. L., Ciais, P., Nemani, R. R., Canadell, J. G., Piao, S. L., Sitch, S., White, M. A., Hashimoto, H., Milesi, C., and Myneni, R. B. (2013a). Variations in atmospheric CO_2 growth rates coupled with tropical temperature. *Proceedings of the National Academy of Sciences of the United States of America*, 110(32):13061–13066.

Wang, X. F., Auler, A. S., Edwards, R. L., Cheng, H., Cristalli, P. S., Smart, P. L., Richards, D. A., and Shen, C. C. (2004). Wet periods in northeastern Brazil over the past 210 kyr linked to distant climate anomalies. *Nature*, 432(7018):740–743.

Wang, Y. J., Cheng, H., Edwards, R. L., Kong, X. G., Shao, X. H., Chen, S. T., Wu, J. Y., Jiang, X. Y., Wang, X. F., and An, Z. S. (2008). Millennial- and orbital-scale changes in the East Asian monsoon over the past 224,000 years. *Nature*, 451(7182):1090–1093.

Wang, Y. V., Leduc, G., regenberg, M., Andersen, N., Larsen, T., Blanz, T., and Schneider, R. R. (2013b). Northern and Southern Hemisphere controls on seasonal sea surface temperatures in the Indian Ocean during the last deglaciation. *PALEOCEANOGRAPHY*, 28:1–14.

Wayne, R. (2009). Chemical evolution of the atmosphere. In Hewitt, C. N. and Jackson, A. V., editors, *Atmospheric Science for Environmental Scientists*, pages 26–53. Wiley-Blackwell Ltd., Oxford, United Kingdom.

Weber, S. L., Drury, A. J., Toonen, W. H. J., and van Weele, M. (2010). Wetland methane emissions during the last glacial maximum estimated from pmip2 simulations: Climate, vegetation, and geographic controls. *Journal of Geophysical Research-Atmospheres*, 115:13.

Whiticar, M. and Schaefer, H. (2007). Constraining past global tropospheric methane budgets with carbon and hydrogen isotope ratios in ice. *Philosophical Transactions of the Royal Society a-Mathematical Physical and Engineering Sciences*, 365(1856):1793–1828.

Whiticar, M. J. (2000). Can Stable Isotopes and Global Budgets Be Used to Constrain Atmospheric Methane Budgets? In Khalil, M. A. K., editor, *Atmospheric Methane*, pages 63–85. Springer, Berlin, Heidelberg, Germany.

Winckler, G., Anderson, R. F., Fleisher, M. Q., McGee, D., and Mahowald, N. (2008). Covariant glacial-interglacial dust fluxes in the equatorial Pacific and Antarctica. *Science*, 320(5872):93–96.

Witinski, M. F., Sayres, D. S., and Anderson, J. G. (2011). High precision methane isotopologue ratio measurements at ambient mixing ratios using integrated cavity output spectroscopy. *Applied Physics B-Lasers and Optics*, 102(2):375–380.

Wolff, E. W., Chappellaz, J., Blunier, T., Rasmussen, S. O., and Svensson, A. (2010). Millennial-scale variability during the last glacial: The ice core record. *Quaternary Science Reviews*, 29(21-22):2828–2838.

Worden, J., Jiang, Z., Jones, D. B. A., Alvarado, M., Bowman, K., Frankenberg, C., Kort, E. A., Kulawik, S. S., Lee, M., Liu, J. J., Payne, V., Wecht, K., and Worden, H. (2013). El Nino, the 2006 Indonesian peat fires, and the distribution of atmospheric methane. *Geophysical Research Letters*, 40(18):4938–4943.

Yokelson, R. J., Susott, R., Ward, D. E., Reardon, J., and Griffith, D. W. T. (1997). Emissions from smoldering combustion of biomass measured by open-path fourier transform infrared spectroscopy. *Journal of Geophysical Research-Atmospheres*, 102(D15):18865–18877.

Zech, M., Tuthorn, M., Detsch, F., Rozanski, K., Zech, R., Zöller, L., Zech, W., and Glaser, B. (2013). A 220 ka terrestrial δ^{18}O and deuterium excess biomarker record from an eolian permafrost paleosol sequence, NE-Siberia. *Chemical Geology*, 360-361:220–230.

Zheng, Z., Huang, K. Y., Deng, Y., Cao, L. L., Yu, S. H., Suc, J. P., Berne, S., and Guichard, F. (2013). A similar to 200 ka pollen record from Okinawa Trough: Paleoenvironment reconstruction of glacial-interglacial cycles. *Science China-Earth Sciences*, 56(10):1731–1747.

Ziegler, M., Tuenter, E., and Lourens, L. J. (2010). The precession phase of the boreal summer monsoon as viewed from the eastern Mediterranean (ODP Site 968). *Quaternary Science Reviews*, 29(11-12):1481–1490.

Zielinski, G. A., Mayewski, P. A., Meeker, L. D., Whitlow, S., Twickler, M. S., and Taylor, K. (1996). Potential atmospheric impact of the Toba mega-eruption similar to 71,000 years ago. *Geophysical Research Letters*, 23(8):837–840.

Zimov, S. A., Schuur, E. A. G., and Chapin, F. S. (2006). Permafrost and the global carbon budget. *Science*, 312(5780):1612–1613.

Chapter 9

List of publications

Sperlich, P.,C. Buizert, T. M. Jenk, C. J. Sapart, M. Prokopiou, T. Röckmann, and T. Blunier. (2013) An automated GC-C-GC-IRMS setup to measure paleoatmospheric δ^{13}C-CH_4, δ^{15}N-N_2O and δ^{18}O-N_2O in one ice core sample, Atmospheric Measurement Techniques, 6, 2027-2041.

NEEM ice core community members. (2013). Eemian interglacial reconstructed from a Greenland folded ice core, Nature, 493, 489-494.

H. C. Steen-Larsen, S. J. Johnsen, V. Masson-Delmotte, B. Stenni, D. Balslev-Clausen, D. Dahl-Jensen, M. D. Ellehøj, S. Falourd, V. Gkinis, A. Grindsted, T. Popp, S. Sheldon, S. B. Simonsen, J. Sjolte, P. Sperlich, B. M. Vinther. (2013) Continuous monitoring of summer surface water vapor isotopic composition above the Greenland Ice Sheet, Atmospheric Chemistry and Physics, 13, 4815-4828.

Sperlich, P., M. Guillevic, C. Buizert, T. Jenk, H. Schaefer, T. Blunier. (2012) A combustion setup to precisely reference δ^{13}C and δ^{2}H isotope ratios of pure CH_4 to produce isotope reference gases of δ^{13}C-CH_4 in synthetic air, Atmospheric Measurements Techniques, 9, 2227-2236.

Stowasser, C., C. Buizert, V. Gkinis, J. Chappellaz, S. Schüpbach, M. Bigler, X. Faïn, P. Sperlich, M. Baumgartner, A. Schilt, and T. Blunier. (2012) Continuous measurements of methane mixing ratios from ice cores. Atmospheric Measurements Techniques, 5, 999-1013.

Sapart, C.J., M. Prokopiou, , G. Monteil, C. van der Veen, S. Houweling, R.S.W. van de Wal, P. Sperlich, T. Blunier, T. Sowers, J. Chappellaz, P. Martinierie, K.M. Krumhardt and T. Röckmann. (2012) Natural and anthropogenic variations in methane sources over the last 2 millennia, Nature. 490, 85-88.

Sapart, C. J., P. Martinerie, J. Chappellaz, P. Sperlich, C. van der Veen, R.S.W. van de Wal, W.T. Sturges, T. Blunier, E. Witrant, J. Schwander, D. Etheridge and T. Röckman. (2012) Can the carbon isotopic composition of methane be reconstructed from multi-site firn air measurements?, Atmospheric Chemistry and Physics, 13, 6993-7005.

Sapart, C.J., C. van der Veen, I. Vigano, M. Brass, R.S.W. van de Wal, M. Bock, H. Fischer, T. Sowers, C. Buizert, P. Sperlich, T. Blunier, M. Behrens, J. Schmitt, B. Seth and T. Röckmann (2011) Simultaneous stable isotope analysis of methane and nitrous oxide on ice core samples, Atmospheric Measurements Techniques, 4, 2607-2618.

Chapter 10

Acknowledgements

This thesis is one of the very final steps of my Ph.D. journey through ice and isotopes as well as many other wonderful things that came into my life during this time.

First of all, I would like to thank my supervisor Thomas Blunier for providing me with the topic and an excellent balance of freedom and support that helped me to find my way through the experimental path of science. I am grateful to have had this opportunity, which would not have been the case if it wasn't for Dorthe, Sigfus, J.P., Sune and probably many more to start the Centre for Ice and Climate. Furthermore, I am very appreciative that Ed Brook, Martin Heimann and Anders Svensson agreed to be part of the assessment committee. I do understand this is not necessarily lightening up the christmas break.

There are so many wonderful people that I am grateful to have met during my time in Copenhagen and at the Centre for Ice and Climate. When I first came to Copenhagen, I subletted Sunes brother's flat with Christo, Mauro and Trevor. Those were awesome times that involved a couch and a lot of family guy (who started it?) while hanging out with friends and neighbours from all over the place. This was probably the best time one could have while moving into a new country to start a PhD in a place like the newly born first Centre. It was great to be part of such a fun place and team!

I particularly appreciated the time I shared with Myriam. Our little dutch oven project was a lot of fun and worked out well. I will always remember our travels with empty methane tanks and also the time we spend on our virtual stage to shake hands, successful one day. Thanks also for all the lovely secret baking recipies. I am happy to be good friends with Ernesto, Jesper, Corentin and Paul, who were a lot of fun to share office, all sorts of lab experiences or crazy stories on wild guitarrs and after work dinner with. I was furthermore happy to have met Alex, Christopher, Theo, Henning, Steff, Ellen, Ivana, Mads, HC, Michelle, Mai, Olivia at the Centre. Lone and Lars, you were always in a happy mood and cheerful which was a true pleasure despite the little overlaps we had. Furthermore, I am happy to have met Kirstin, who continues caring for the CH_4 isotope machine. I cross my fingers, some say it is a beast. I am grateful for the support by Simon, Christian from CIC as well as Carsten and Dennis from the workshop, that helped getting/keeping the machine going. I am grateful and happy to spend time with Palla and Sigfus at their summer house, which was always a lot of fun. I hope the flower boxes are still as straight as they have ever been.

During my "stay abroad" I was lucky to go to New Zealand, where I was happy to join the TROPAC group at NIWA. Thanks a lot for the good and helpful times to all of you, Hinrich, Gordon, Sara, Peter, Katja... and see you soon! Furthermore, I really enjoyed the "greater" gaslab group and the people I met through collaborations and NEEM. In particular, I would like to thank the groups in Bern and at IMAU. Our discussions and good exchange helped me a lot and was a lot of fun for me, special thanks to Célia Julia, Thomas Röckmann, Michael Bock, Jochen Schmitt und Hubertus Fischer.

Since a bit more than a year, I am in Willi Brand's group at the MPI-BGC. I remember that I finished my last ice core measurements six days befor I started my new job with Willi, which means it was not exactly a relaxed period with finishing up, moving and starting a new job. Thank you all very much ISOLAB'ers for a wonderful landing and the really good times we had, including the support during the final period of writing this thesis.

Finally, I would like to thank my family, my parents Barbara and Walter, my brother Axel, and my sister in law Birgit. I am very greateful and happy for your endless love and support and look forward to finally hanging out with you again, with a free mind. The very final words, however, are for the most wonderful person in my world. Colleen, thank you so much for everything. For all your support, smiles and laughs, for being such a wonderful wife and mother to our baby girl. The two of you mean the world to me. I will be home in a minute.